MICROCOPY RESOLUTION TEST CHART

NATIONAL BUREAU OF STANDARDS-1963-A

AFFDL-TR-76-96

FLUID DYNAMIC ENERGY CONVERSION AND TRANSFER PROCESSES

UNIVERSAL ENERGY SYSTEMS, INC.
3195 PLAINFIELD ROAD
DAYTON, OHIO 45432

OCTOBER 1976
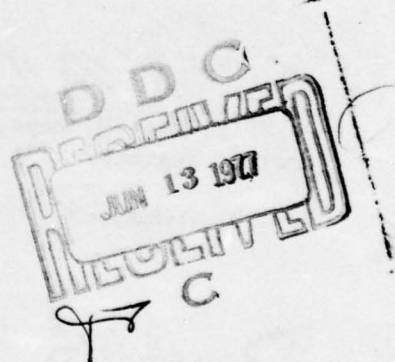
TECHNICAL REPORT AFFDL-TR-76-96
FINAL REPORT FOR PERIOD 18 MARCH 1973 - 30 JUNE 1976

AIR FORCE FLIGHT DYNAMICS LABORATORY
AIR FORCE WRIGHT AERONAUTICAL LABORATORIES
AIR FORCE SYSTEMS COMMAND
WRIGHT-PATTERSON AIR FORCE BASE, OHIO 45433

NOTICE

When Government drawings, specifications, or other data are used for any purpose other than in connection with a definitely related Government procurement operation, the United States Government thereby incurs no responsibility nor any obligation whatsoever; and the fact that the government may have formulated, furnished, or in any way supplied the said drawings, specifications, or other data, is not to be regarded by implication or otherwise as in any manner licensing the holder or any other person or corporation, or conveying any rights or permission to manufacture, use, or sell any patented invention that may in any way be related thereto.

This report has been reviewed by the Information Office (IO) and is releasable to the National Technical Information Service (NTIS). At NTIS, it will be available to the general public, including foreign nations.

This technical report has been reviewed and is approved for publication.

DAVID K. MILLER, Capt, USAF
Project Engineer
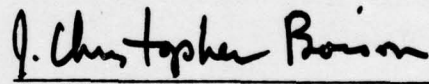
J. CHRISTOPHER BOISON
Chief, Thermomechanics Branch

FOR THE COMMANDER
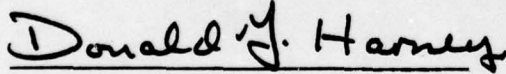
DONALD J. HARNEY
Asst for Experimental Simulation
Aeromechanics Division

Copies of this report should not be returned unless return is required by security considerations, contractual obligations, or notice on a specific document.

SECURITY CLASSIFICATION OF THIS PAGE (When Data Entered)

REPORT DOCUMENTATION PAGE

READ INSTRUCTIONS
BEFORE COMPLETING FORM

1. REPORT NUMBER AFFDL-TR-76-96	2. GOVT ACCESSION NO.	3. RECIPIENT'S CATALOG NUMBER

4. TITLE (and Subtitle)

FLUID DYNAMIC ENERGY CONVERSION AND TRANSFER PROCESSES

5. TYPE OF REPORT & PERIOD COVERED
Final Report,
18 March 1973-30 June 1976

6. PERFORMING ORG. REPORT NUMBER

7. AUTHOR(s) Ernest F. Fretter Krishan K. Joshi Russell W. Griffith	8. CONTRACT OR GRANT NUMBER(s) F33615-73-C-4053

9. PERFORMING ORGANIZATION NAME AND ADDRESS
Universal Energy Systems, Inc.
3195 Plainfield Road
Dayton, Ohio 45432

10. PROGRAM ELEMENT, PROJECT, TASK
AREA & WORK UNIT NUMBERS
Project No. 1929
Task No. 192904
Work Unit No. 19290421

11. CONTROLLING OFFICE NAME AND ADDRESS

12. REPORT DATE
October 1976

13. NUMBER OF PAGES
240

14. MONITORING AGENCY NAME & ADDRESS(if different from Controlling Office)

15. SECURITY CLASS. (of this report)

UNCLASSIFIED

15a. DECLASSIFICATION/DOWNGRADING
SCHEDULE

16. DISTRIBUTION STATEMENT (of this Report)

Approved for public release; distribution unlimited

17. DISTRIBUTION STATEMENT (of the abstract entered in Block 20, if different from Report)

D D C
JUN 13 1977
C

18. SUPPLEMENTARY NOTES

19. KEY WORDS (Continue on reverse side if necessary and identify by block number)

Energy Conversion	Electric Field
Electrofluid Dynamic Energy Conversion	High Voltage
Injector	Multi-component flow
Electrohydrodynamic Spraying	Erosion
	Swirl flow (over)

20. ABSTRACT (Continue on reverse side if necessary and identify by block number)

This is the final report of research performed on Contract F33615-73-C-4053. The research included three different work areas, Electrofluid Dynamics (EFD), Multi Component Flows (MCF), and Thrust Augmentation (TA), and was performed during the period 17 March 1973 through 30 June 1976. This report presents the experimental rigs designed and built, experiments performed, and the results of the experiments during the contract period.

DD FORM 1473 EDITION OF 1 NOV 65 IS OBSOLETE
1 JAN 73

SECURITY CLASSIFICATION OF THIS PAGE (When Data Entered)

Block 19 (continued)

Prandtl-Meyer Expansion
Mixing
Supersonic diffuser
Radial outflow diffusion
Ejector
Energy exchange
Momentum exchange
Mass augmentation
Thrust augmentation
Boundary layer
Normal Shocks
Two dimensional flow

SUMMARY

"Fluid Dynamic Energy Conversion Processes", Contract F33615-73-C-4053, was substantially performed in the facilities of Bldg. 450, Wright-Patterson Air Force Base, Ohio, during the period of 17 March 1973 through 30 June 1976. The work done under the contract involved three main area which are discussed briefly below.

Electrofluid Dynamics (EFD) is a method of direct energy conversion in which the energy contained in a flowing gas is converted directly into electrical energy. Research during the contract period involved experimental verification of a new approach to scaling EFD generators, testing of various designs for electrode configurations, performing injector tests to improve efficiency, and investigating fluids other than air as a working fluid.

Multi-component flow (MCF) research involved examining the interactions of flows containing entrained particles. In particular, the experimental work during the contract included swirl flow, erosion, high pressure swirl flow particle containment, hot particle erosion, Prandtl-Meyer expansion, helium-air mixing, pressure recovery studies for gas dynamic and chemical lasers, supersonic diffusers, radial outflow diffusers, and ejector pumps.

The Thrust Augmentation (TA) research involved investigation of energy and momentum exchange processes between flows. Specifically, the investigations involved both mass and thrust augmentation for hypermixing flow nozzles, oscillating flow nozzles, and a study of the characteristics of an entire family of nozzles. Also, a complete Nozzle Test Facility was set up and calibrated during the contract period.

All of these research activities are presented in greater detail in the three parts of this report.

TABLE OF CONTENTS

PART II

MULTI-COMPONENT FLOW (MCF)

TABLE OF CONTENTS (CONT'D)

TABLE OF CONTENTS (CONT'D)

LIST OF ILLUSTRATIONS

LIST OF ILLUSTRATIONS (CONT'D)

LIST OF ILLUSTRATIONS (CONT'D)

LIST OF ILLUSTRATIONS (CONT'D)

LIST OF TABLES

LIST OF SYMBOLS

A	Flow cross-sectional area
C	Loss coefficient, friction factor, or length
C_p	Specific heat at constant pressure
D	Diameter
E	Electric field magnitude
H	Enthalpy or distance (with Subscript)
I	Current
L	Length
M	Mach number
P	Pressure or applied load
R	Gas constant
R_e	Reynolds number
T	Temperature or thrust
$\overline{U}$	Average velocity
V	Velocity or voltage
W	Width or weight
d	Diameter
f	Friction factor
h	Height
$\dot{m}$	Mass flow rate
p	Pressure
r	Radius
t	Thickness, temperature, or area ratio
u	Velocity, x-component
v	Velocity, y-component

w   Velocity, z-component

x   Axial dimension

β Skewness factor

γ Ratio of specific heats

δ Kinetic energy ratio

ε Deflection factor or diaelectric constant

η Efficiency

θ Included angle

μ Viscosity

ξ Pressure loss coefficient

ρ Mass density

ϕ EFD potential function

χ Perimeter

Subscripts:

b	Breakdown value	noz	Nozzle
ch	Channel	opt	Optimum value
d	Diffuser	p	Primary working fluid
eff	Effective value	s	Secondary working fluid
el	Electric	sp	Sparkover value
f	Flow value	t, o	Stagnation condition
g	Gas	uf	Uniform field value
inj	Injector	x	Value in axial direction
isen	Isentropic	*	Throat
i	Ideal value		
j	Jet		

PART I

ELECTROFLUID DYNAMICS (EFD)

SECTION I

INTRODUCTION

Electrofluid Dynamics (EFD) is a method of direct energy conversion in which the energy contained in a flowing gas is converted directly into electrical energy. This is generally accomplished by seeding the flowing gas with unipolar charged ions produced by a corona discharge from a sharp grounded electrode. The unipolar ions typically are deposited on particles usually produced by condensation of either a minor component (such as water vapor) of the flowing gas or by condensation of the flowing gas itself. The charged particles are then transported by viscous interaction with the flowing gas to the collector electrode of the generator where at high potential the particles release their charge to the collector. The current thus generated travels through a load to ground. Many references can be cited which describe the basic operation of various EFD generators; several are listed in the References.

SECTION II
BACKGROUND

Considerable EFD research, both theoretical and experimental, has been performed in the past. The work reported here involves research performed since 19 March 1973 under Contract F33615-73-C-4053. Past work included the development of scaling laws for EFD processes, geometry design and analysis, electric field and flow field analysis, cycle analysis, choice of gas composition and operating points for various applications of EFD generators, as well as considerable experimentation with axisymmetric geometries, two dimensional (slab-type flow) geometries, charged colloid production, flow losses minimization, and electric field scheduling. This work has been reported previously and references are included in the Bibliography at the end of this report.

Prior to 1973, when work on this present contract was initiated, the basic approach by researchers at ARL to the scaling of EFD generators was based upon the principle that the breakdown strength of the gas varies linearly with the gas density (at constant temperature) over a relatively large range of pressures.[1] Utilization of this approach led to the design of generators which could be scaled up in power and efficiency simply by scaling up the level of operating pressure That this approach succeeded at least up to certain pressure levels for specific geometries was demonstrated in several

3

experiments. Beyond this limiting pressure level the power
did not continue to scale with pressure to the second power
and eventually remained constant with increasing pressure.
Another problem, potentially even more troublesome than the
failure of the scaling laws at high pressure, involved the
scaling of the output voltage of the generator with pressure.
The output voltage of the generator is proportional to:

$$V_{output} \simeq \rho_g \times L \qquad \text{where: } \rho_g = \text{gas density}$$
$$L = \text{channel length}$$

This scaling law, which leads to increased power and
efficiency through pressure, resulted in powers at voltages
which were also scaled upward. The result was that high
power and high efficiency generators might have collector
potentials of several million volts. In practice, these
voltages are very difficult to handle and, for practical reasons,
the actual output voltage should be limited to a few hundred
thousand volts. This voltage limitation, however, would greatly
lower the potential output power and efficiency levels of a
given generator.

Approximately one year before the start of this contract,
Mr. M.O. Lawson and his group working in EFD at the Aerospace
Research Laboratories developed a new approach to the scaling
of EFD generators. This new approach would result in increased
efficiency of operation for a given generator design while all

4

other generator electrical characteristics remained constant.
The principle of this new scaling technique is to keep:

$$\rho_g \times d = const \qquad \text{where:} \quad \rho_g = \text{gas density}$$

$$d = \text{significant dimension of the generator}$$

Thus, for a given generator design, scaling with this new
approach consists of decreasing the generator dimensions
inversely with increasing gas pressure. The result is that
constant generator electrical performance is achieved at
increased efficiency levels.

A much more detailed and formal presentation of this
theory of scaling along with a description of the results of
extensive experiments which verified this scaling law was
presented in a paper given at the 1974 Intersociety Energy
(2)
Conversion Engineering Converence.

SECTION III

EXPERIMENTAL PROGRAM

The experimental program covered by this contract involved several research areas. The major areas included verifying the new approach to the scaling laws and achieving a high degree of conversion efficiency using this scaling approach. Several less important areas of research involved conducting experiments to determine the effects of the slopes of the attractor and collector electrodes on the electric field structures of the generators, determining the effects of various additives and different working fluids on generator performance, establishing a facility for the use of hydrogen as the EFD generator working fluid, and determining the optimum p x d value for a given generator geometry and working fluid. Electrohydrodynamic spraying for the production of charged particles and experimental analysis of ejector principles as applied to EFD generators were also studied. These various aspects of the experimental program will be presented as they are listed above.

SECTION IV

EXPERIMENTAL FACILITIES

A.   High Bay Area

Experimental facilities in the High Bay Area of Building
450 consisted primarily of two test stands for large scale
EFD generator tests. These test stands included: (1) an air
supply system capable of supplying two different streams of
air to each stand, each stream being completely conditioned
with regard to pressure, temperature, and humidity; (2) a
large high pressure chamber (approximately 18"ID x 30" high)
for containing a test rig, and a high voltage lead out assembly
for transmitting the high voltage (300 KV) power out of the
tank to the load system; and (3) a high voltage load system
for dissipating the power produced in the generators. Numerous
additions and modifications were made to the systems over the
course of the research and these will be discussed briefly.

1.   Air Supply System

The air supply system in High Bay consists of a source
of 3000 psi (maximum) air which can be applied to each of two
supply lines, ("A" and "B"). Each supply line has two stages
of pressure regulation insuring accurate control of the
final pressure. Each line then passes through three 80 KW
heaters which are capable of heating the pressurized air to
nearly 1000°F if required. "A" line has automatic temperature
control while "B" line has a manual temperature control. After

passing through the heaters the air lines enter humidification
tubes where water is injected until the desired humidity
level is achieved. Here, water measured through a calibrated
orifice is sprayed through a fuel oil nozzle to produce a fine
mist of water droplets. These droplets evaporate before
reaching the end of the spray tube which is approximately 100
diameters beyond the spray nozzle. Condensate is flushed
from the line by a valve located in a trap. After leaving the
humidity tube the air passes through a chamber in which
there are humidity and temperature sensing elements. From
here, the conditioned air can be directed to either test
stand. At each stand there are pressure, temperature, and
humidity measuring instruments for determining the thermodynamic
state of the air (pressure, temperature, and humidity)
immediately before it enters the test rig. This facility has
been well described in a report listed in the Bibliography of
this paper.[3]

2.   Test Stands and High Voltage Leadouts

Two large test stands were used in the High Bay area. The
stands held 30" long, 18" diameter high pressure stainless
steel tanks. The tanks were fitted with appropriate end caps
and flanged ports for instrument sensors, for voltage input
and output leads, for air supply and exhaust lines and for
visual inspection. The lead outs were high voltage (300 KV)
coaxial cable held in a suitable clamping arrangement for about

8

10 inches of the cable length. "O" rings sealed the cable against the clamp and the leadout proved to work very well at the high voltages of the collector. Every few months an electrical breakthrough of the cable insulator would occur and the cable would have to be replaced. The breakthrough was caused by abnormally high collector voltages or by the rapid aging of the insulator subjected to rapidly collapsing high electric fields. This leadout design by Mr. M.O. Lawson proved, however, to be very effective and practical.

3. High Voltage Load System

During the experiments discussed in this report the only type of load system used in the High Bay Area was of the carbon film ceramic resistor type arranged in series. Each individual resistor is typically 20" long and 2" in diameter, with a maximum power dissipation of 100 watts and a maximum voltage drop of 125 KV. Knowing the problems associated with accurately measuring high voltages (several hundred kilovolts) and relatively low currents (millamperes) the load was purposefully designed so that each resistor was not stressed electrically to more than 25% of it maximum voltage rating. Initially the high voltage load consisted of eight 100 megohm ceramic film resistors mounted in series on a long wooden support with wooden legs. In periods of high humidity leakage current along the wooden supports was found to be excessive and these supports were replaced with plexiglass supports which

effectively stopped the leakage current. Eventually the resistors were mounted along polyvinyl chloride tubes supported by plexiglass. This resulted in insignificant current loss.

Two methods were used simultaneously to measure the voltage drop along the load bank. First, the voltage-current characteristics of the load were determined independent of the generator by using a high voltage power supply and measuring the voltage at the high voltage terminal with a precision electrostatic voltmeter and a precision generating voltmeter. During a test run, the current through the load was measured and the voltage on the high voltage termination was measured using the precision generating voltmeter. Thus, two separate measurements provided the voltage developed by the generator, and agreement between the two was always very good (within 5%).

4. Small Volume EFD Facility

During this contract a new EFD facility was established in the High Bay Area especially for use with the small (1/6", 1/12", 1/24") geometry EFD rigs. Due to the high pressures of these experiments ($P_{os} \geq 48$ atmospheres for the 1/24" channel) a much smaller volume high pressure tank was utilized. This tank was modified to accept a conventional high voltage lead-out (as described earlier) and had four windows for viewing the EFD channel. As the system evolved, it became quite versatile. The system could provide two independently

conditioned air supplies. Each supply could be treated with
additives other than water for humidification of the separate
flows. The secondary flow could be recirculated external to
the tank and thus cooled and conditioned independently. Fluids
such as carbon tetrachloride or a halocarbon could be used as
the primary input taken directly from a temperature regulated
boiler. Many variations were made possible. A small orifice
made to ASME specifications was included in the exhaust line
of the test facility in order to accurately determine mass flows
and the primary nozzle flow diameters. A diagram of the facility
is included as Figure 1.

B.   EFD Test Pit Facility

     In addition to the High Bay area, a new test facility
was constructed in the Pit adjacent to the High Bay. The
principle working fluid for use in EFD generators has been
high pressure, humidified air, warmed to slightly above room
temperature. The Pit facility was designed to condition and
control not only air but nitrogen and hydrogen gases as well.
The overall schematic of the facility is presented in Figure 2.
The following is a description of the facility and its capabilities.

     1. Working Fluid Supply and Control System

     Air is supplied to the test pit from the ARL bottle farm
storage tanks at approximately 2700 psia and with a dew point
temperature of 290° R. The high pressure air enters the Pit from
a 1/4" tube supply line. Portions of the air are directed

11
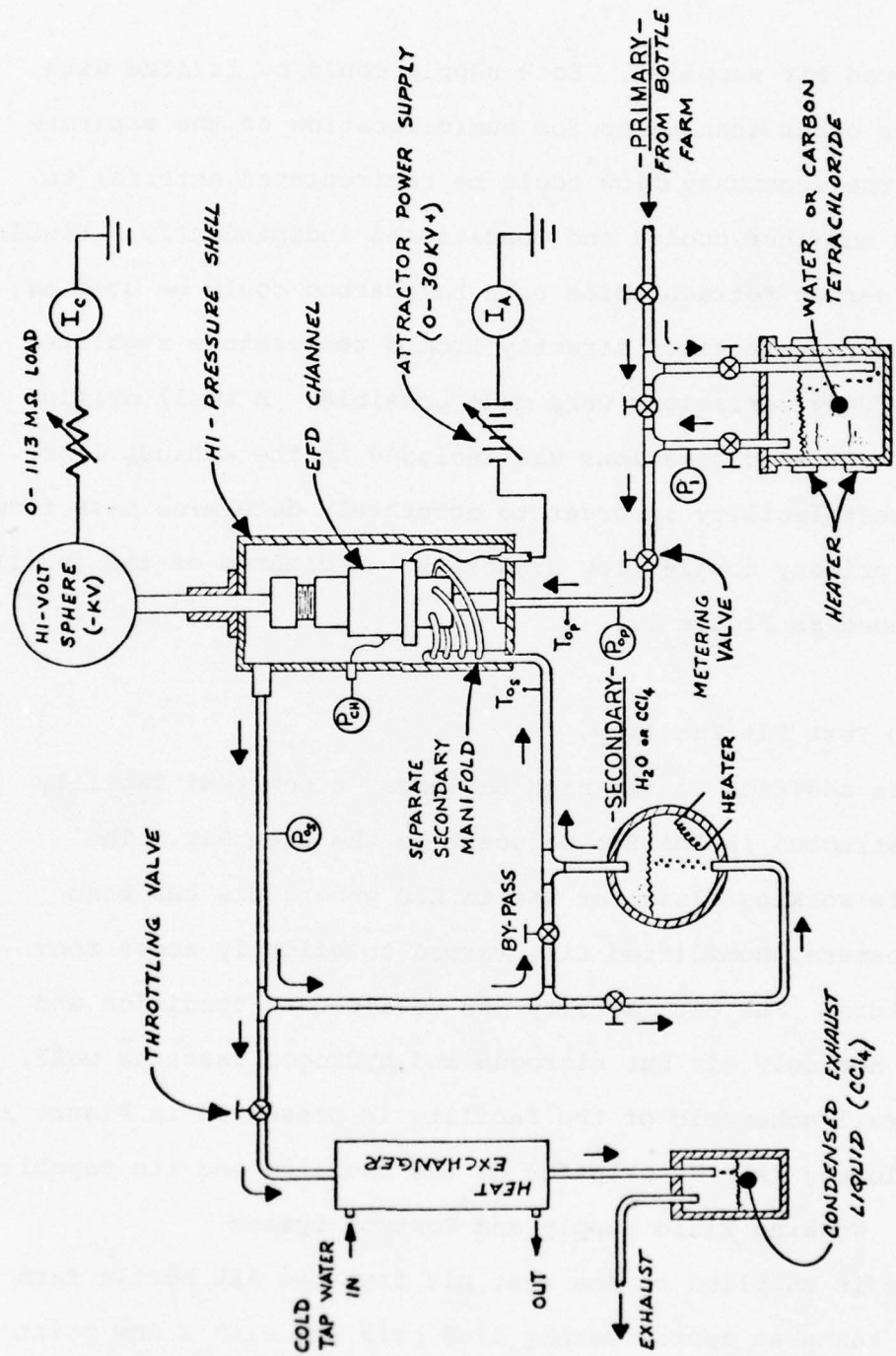
Figure 1. EFD – Carbon Tetrachloride additive system.
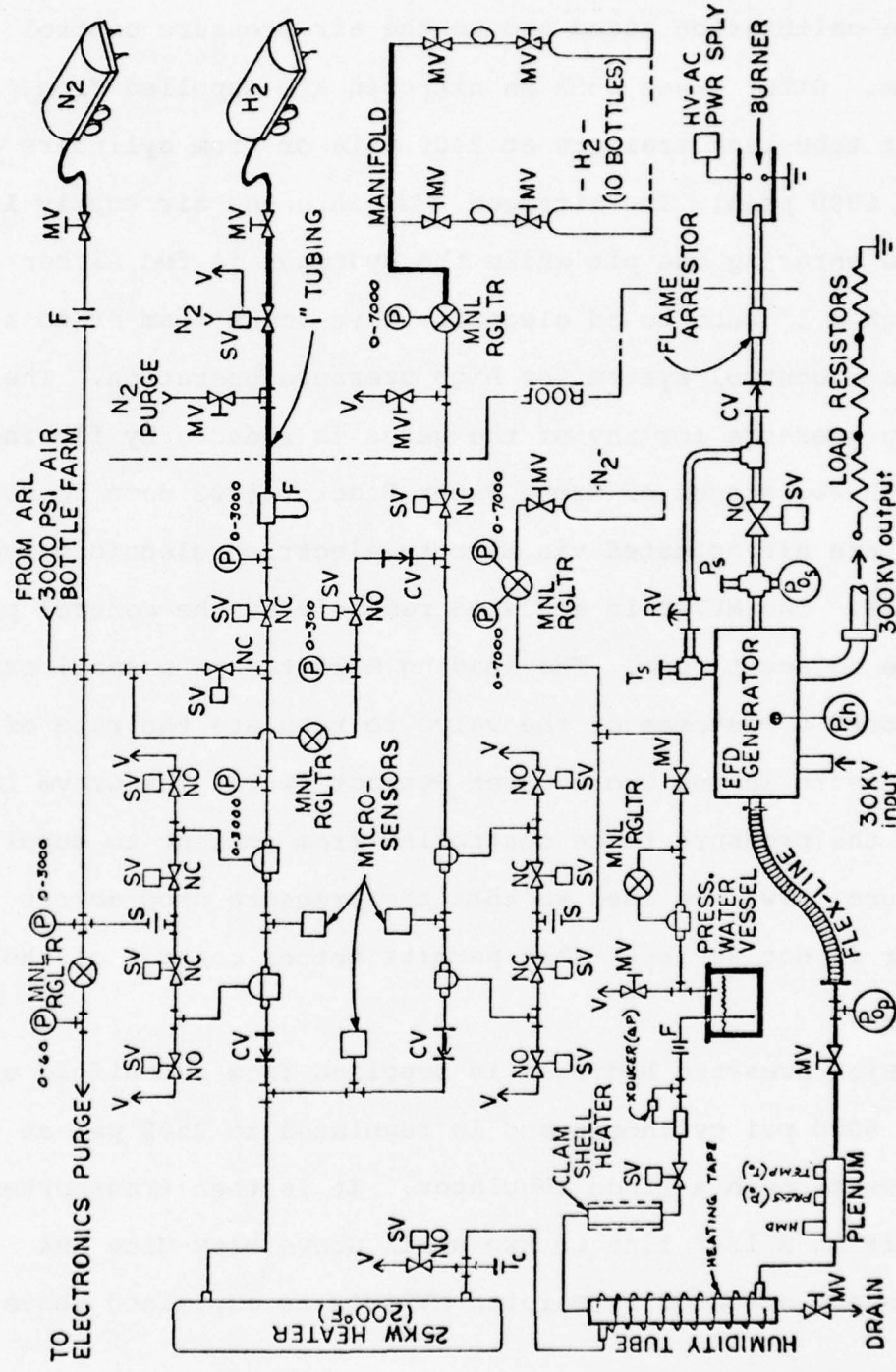
Figure 2. Gas supply/control schematic, Pit Facility.

13

to the calibration stand and to the air pressure control
system. Other gases such as nitrogen are supplied from
either tube-tank trailers at 2400 psia or from cylinders at
up to 6000 psia. The nitrogen T's into the air supply line
before entering the pit while the hydrogen is fed either
through a 1" tube to an electric valve downstream or to a
separate control system for high pressure operation. The
supply pressure for any of the gases is reduced by flowing
through two stages of Grove Power Reactor #202 dome loaders.
These are air actuated via Marotta electric solenoid valves
(MV74B). The MV74B is actuated remotely at the control panel
in the adjacent room. The loading Marotta has a small orifice
"snubber" downstream of the valve to regulate the rate of increase
of pressure in the Grove Power Reactor #202. The Grove loaders
allow the pressure to be controlled from ambient to supply
pressure. Two are used so that the pressure drop across
either is not severe. This permits better control of the
pressure.

High pressure hydrogen is supplied from a manifold of
eight 6000 psi cylinders and is regulated to 3500 psi at the
bottles through a Linde regulator. It is then transported into
the pit in a 1/4" line to two small Grove Mity-Mite M94
regulators actuated by Marotta MV74B's as explained above.

The secondary gas pressure is adjusted by a back pressure valve downstream from the rig. The original installation used a 1/2" Annin Model 3460 pneumatic control needle valve to remotely adjust the tank pressure. However, this proved to be unsatisfactory for keeping a constant secondary pressure and lacked fine adjustment control for accurate measurements. It was replaced with a simple Dragon 1/2" needle valve and the pressure was adjusted manually at the rig.

2. Gas Conditioning (Temperature and Humidity)

Downstream from the regulators the gas flows into a 25 KW Hex Industries heater (rod type immersion heater with 3000 psia shell) where the temperature of the gas can be raised to 500°F if desired. Ordinarily this heater was used to keep the gas at 72°F, and occasionally as high as 120°F. At the exit of the heater is a dump solenoid valve (Marotta 1/2" valve) to quickly empty the heater volume and depressurize the lines upstream from the rig in an emergency situation. Further heating of the gas can be accomplished by either two clam shell heaters (1-1/4" clam shells over a 1-1/4" OD copper rod over the 1/4" stainless steel gas tubing) or by heating tapes wrapped over the tubing and thermally insulated; both shells and tapes may be used in combination.

The secondary air line can also be heated by heating tapes if a separate temperature control on the secondary flow is desired. In addition, the entire test rig can be heated either

15

from external heating tapes or from internal clam shell heaters.

Humidification of the working fluid was originally accomplished by spraying water through an oil burner-type Deleval nozzle into a 1" mixing tube. This method, however, injected too much water and was not adjustable to the precision required for the experiments. The modified system still uses an atomizing spray for mixing of water and gas. However, the spray nozzle is .004" diameter and is located in a 1/4" tee in such a way as to produce a venturi effect (see Figure 3). The water is injected by a differential pressure between gas upstream from a valve and a low pressure area of the venturi (typically this driving pressure is between five and ten psid). Gas enters the mixing tube perpendicular to the water spray and mixes in the tube. Excess water is collected in a trap at the bottom of the tube where it can be removed from the line.

A further modification to the humidification system was made by installing a Hoke Milli-Mite valve before the water nozzle (See Figure 3). The valve helped control the water flow rate and Δp to the nozzle. It could be remotely actuated from the main control panel.

3. Electrical

The electrical schematic of the EFD test rig is shown in Figure 4. Input voltage to the attractor circuit is supplied by a 0-60 KV Universal Voltronics D.C. Power Supply.

16
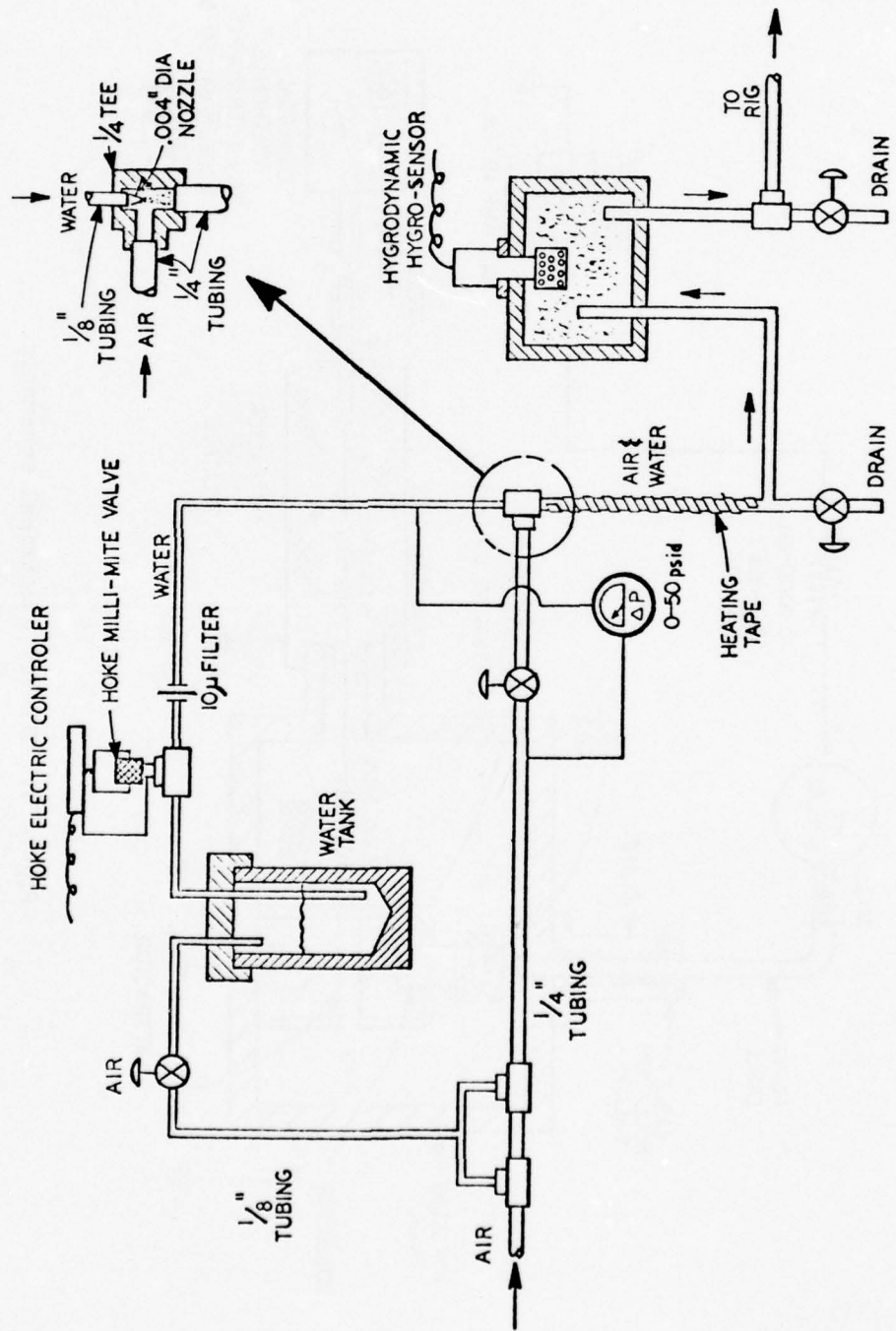
Figure 3. Pit humidification system.
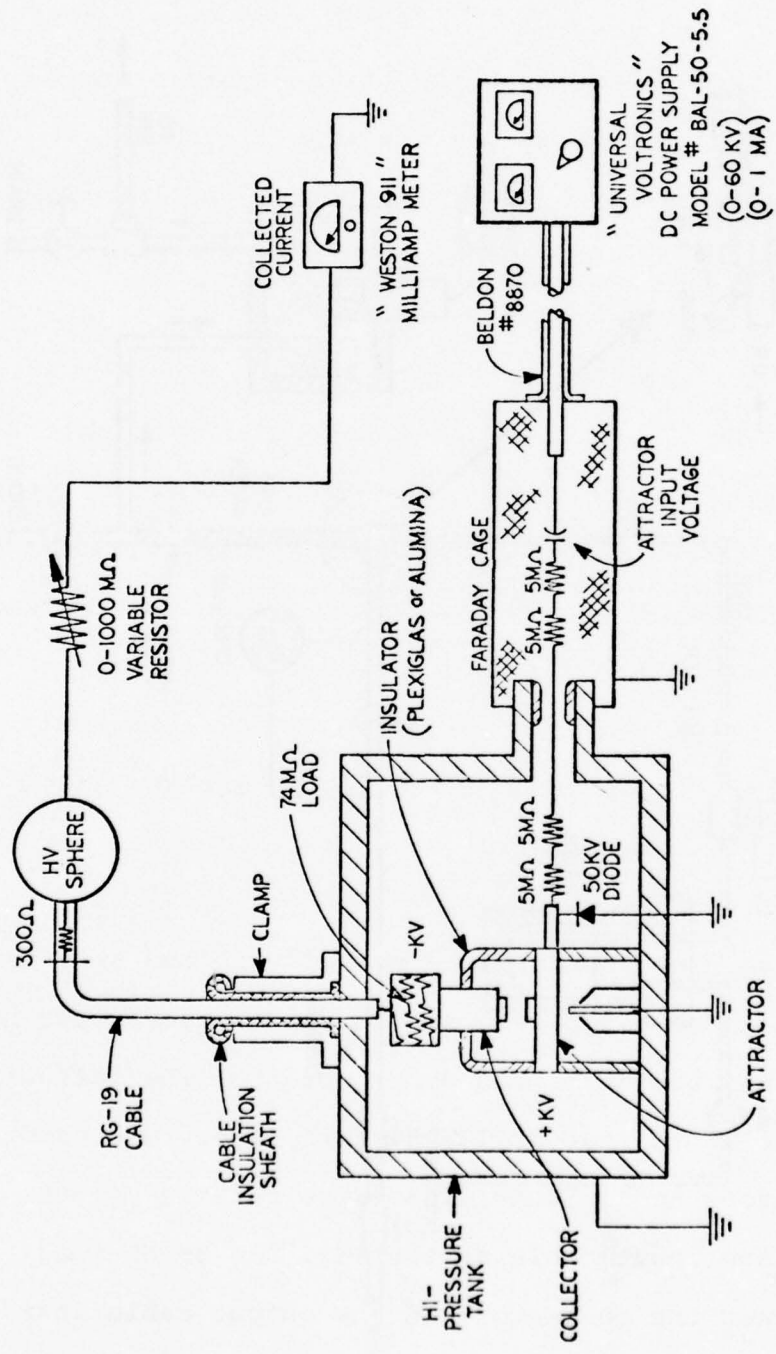
Figure 4. EFD-Pit electrical schematic.

18

Attractor voltage is recorded on the power supply meter to within ± 1 KV. Attractor current is measured on a Weston 911 milliamp meter connected to the power supply circuit. Because of the peculiar design of the test rig shell, it is not possible to measure the needle current directly. This value must be inferred as the sum of collector and attractor currents.

Generated current (collected current) is fed to a 20" diameter sphere external to the high pressure rig by a Beldon RG19U cable and an ARL designed feed through. A variable load is provided by six to ten 100 MΩ, 100 watt, 150 KV resistors (RPI type DZZ-1) mounted to PVC tubing and suspended from the pit ceiling by nylon rope. An electrical connector runs from the grounded end of the load to a Weston 911 milliamp meter in the control panel and then to ground. The resistors are calibrated using the power supply, milliamp meters, and an electrostatic voltmeter and are periodically checked for their resistance values.

As the experiments progressed both at ARL and at TRW Systems, Inc. (under a separate Air Force Contract), the need (4) for RF noise suppression became more evident. The following technique, similar to that at TRW Systems, Inc., was used. Two 5 MΩ resistors and a 50 KV diode were attached to the attractor voltage input cable at the rig. An 89 MΩ load was added between the collector and the output cable inside the high pressure rig to further reduce noise. The grounding

19

shield around the high voltage leadout was stripped back to the clamp end to reduce capacitance of the cable. Finally, a Faraday cage was placed around the input cable to eliminate the effect of breakdown noise on other instruments.

4. Instrumentation

Pressure measurements are made at the regulators, at the entrance to the primary nozzle, on the exhaust line, and at the channel cavity. Microsens pressure transducers are used to sense the interstage and final stage pressures which are recorded on meters on the control panel. These are used to give an approximate pressure reading of primary gas pressure. The primary total pressure is measured by a Validyne pressure transducer (Model 15) at the base of the test rig, and is read on a meter (Model CD 12) on the control panel. The secondary total pressure (or tank pressure) is measured by a Statham pressure transducer (0-500 psi) and fed through a Sterling amplifier and recorder console to a Texas Instruments strip chart recorder. The channel pressure is made accessible by a pressure tap on the side of the test generator that is fed through a fitting in the high pressure shell to an Ashcroft test gauge at the rig. In addition, the primary and secondary pressures are also measured on Ashcroft gauges at the rig.

All temperatures are measured with iron-constantan thermocouples located at the heater outlet, at the primary

stagnation area before the nozzle, in the tank exhaust (secondary total temperature) and on the internal heater shell shield.

The primary humidity is measured in the primary line after the humidity mixing tube. The original system used a Thunder Scientific Corp.'s TB-1001 probe with a Brady Array Model BR101R sensor and signal conditioner. However, these units did not withstand extraneous RF noises from the rig and were replaced with a Hygrodynamics Hygro-sensor installed in a special high pressure chamber. Output from this sensor is read on a Hygrodynamics Model 15-3001 Electrical Hygrometer indicator as percent relative humidity. Total temperature at the sensing unit is also recorded on the indicator. Temperature and pressure corrections to the relative humidity can be made by using calibration curves supplied by the Hygrodynamics Company. Secondary humidity was either measured directly on the exhaust line or calculated from pressure data and primary relative humidity.

Mass flow measurements were made using an ASME design venturi on the primary line. Most calculations were performed using isentropic flow data and the known nozzle area rather than by direct pressure differentials across the venturi.

Auxiliary pressure gauges are located at various parts of the system to give a gross reading of the local pressure at those locations and are shown in Figure 2.

Additional instrumentation includes a pressure calibration stand with two 12" Heise gauges, one for low pressure calibration (0-300±.25 psi) and one for high pressure calibration (0-3000 ± 2.5 psi). These are used to calibrate the pressure transducers and for setting the alignment of the needle/nozzle assembly with the attractor/collector assembly in the test rig. Mercury and water manometers are used in this alignment procedure as well.

Electrical instrumentation includes two Weston 911 milliamp meters (1 microampere to 10 milliamperes ± 5%) to read collector and attractor currents, a Universal Voltronics power supply (0-60 KV) model BAL-50-5.5, and electrostatic voltmeters to calibrate the resistor load system.

5. EFD Rig Mounting System & Pressure Vessel.

The Pit Facility uses a specially designed high pressure shell to contain the EFD test generators. An assembled view of the shell with a pit-style generator enclosed is shown in Figure 5. The shell was designed for 100 atmosphere pressures and 200°F temperatures. As used, the test generators are mounted from the bottom of the shell. The high voltage attractor cable from the power supply is affixed to the side through a special teflon feed-through. Ports are provided at the topside of the shell (1) for Conax fittings to supply power to the internal clam-shell heaters, (2) for the exhaust line, and (3) for an emergency 2000 psi pop-off valve dump line. At

22
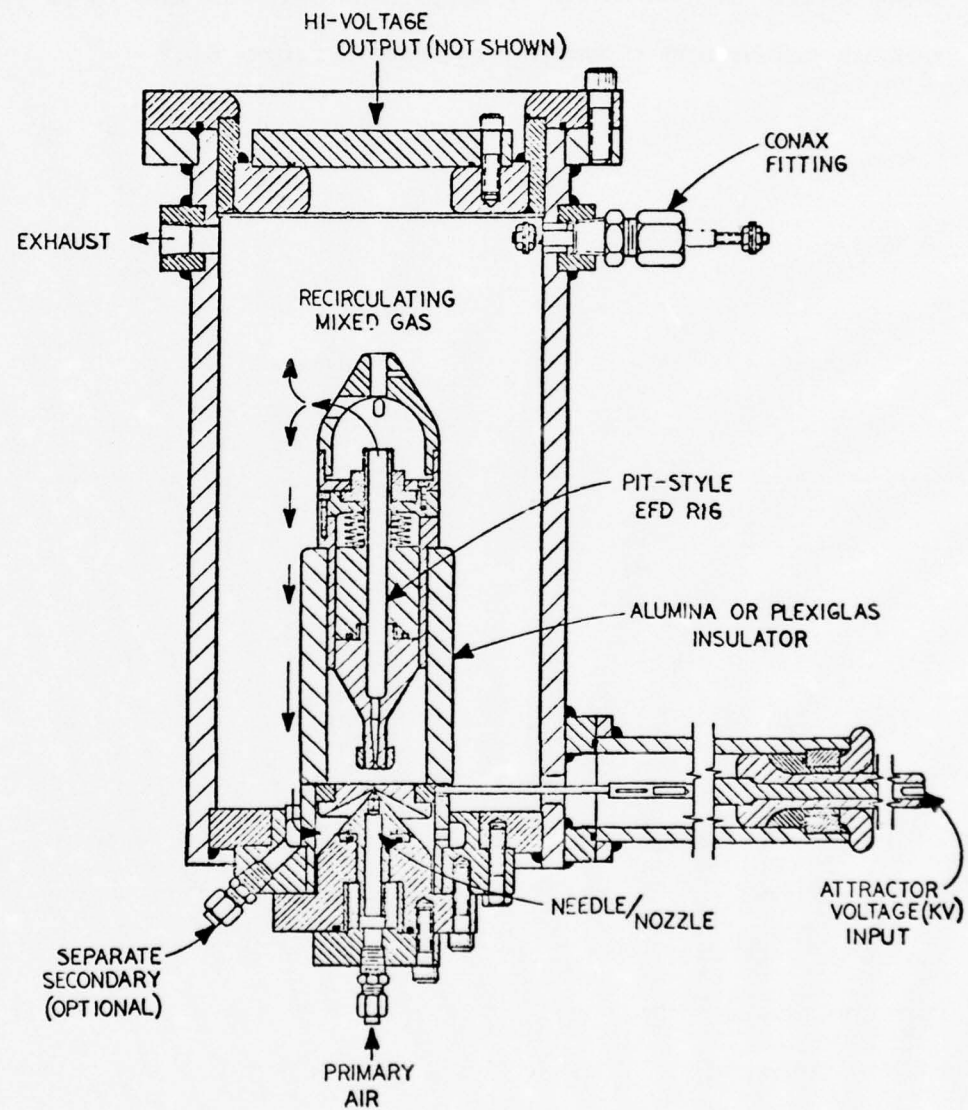
Figure 5. Pit-style EFD generator and high pressure vessel.

the top of the shell are two flanges: one large flange for easy access to the inside of the shell, and a small cap that bolts to the large flange and carries the high voltage output cable and clamping system (Figure 6).
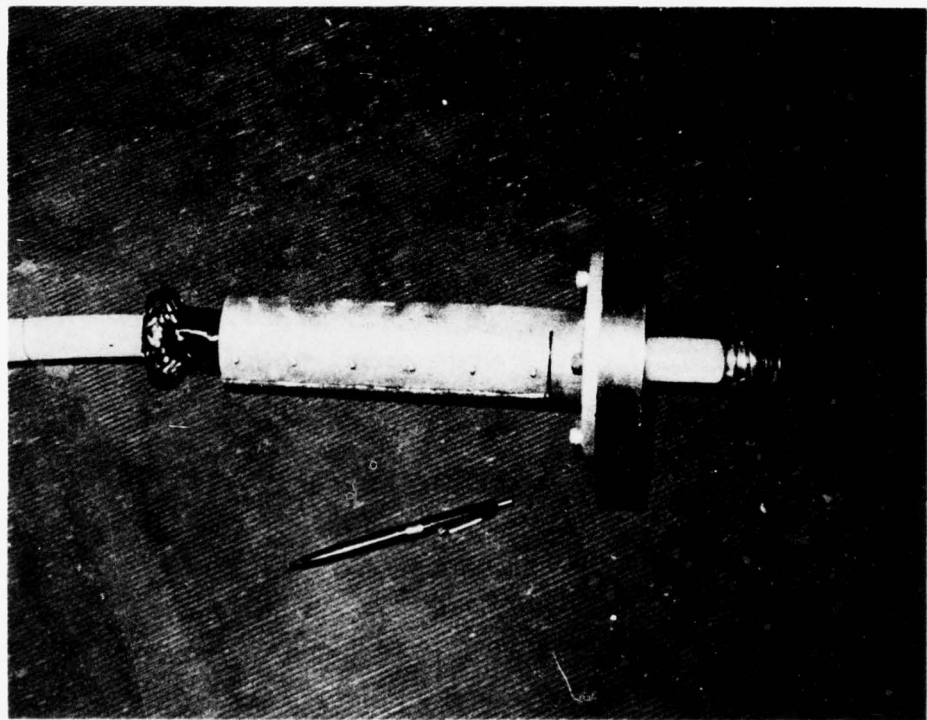
Figure 6. High-voltage lead-out cable and clamp assembly.

SECTION V

EFD TEST GENERATOR

Three separate test generators were used in the Pit
Facility. Two are basically the same ARL pit-type generators
as shown in Figure 5, one with a plexiglass insulator, the
other with a unglazed alumina insulator. The plexiglass
insulated channel holder was epoxied to the base mount and the
collector housing while the alumina piece was cemented in place
with Sauereisen High-temperature cement (see Figure 7). A
third pit-type channel was fabricated with an alumina insulator
which was hydrogen brazed to the base mount and collector holder.
This channel broke in half upon final machining of the metal
pieces.

The third functional generator was a modification of a
High-Bay style generator (Figure 8). The original High-Bay
style channel was greater in diameter than the insert opening
at the base of the High-pressure shell; consequently, the
channel had to be mated to the base mount from the upper
opening (see Figures 9 & 10).

Since spacings for the new channel were different from
the original design, a modification of the nozzle/needle holder
had to be made for the High-Bay channel (see Figure 11). This
combination allowed nozzles, needle holders, attractors and
collector pieces tested in the High-Bay Facilities to be used

26
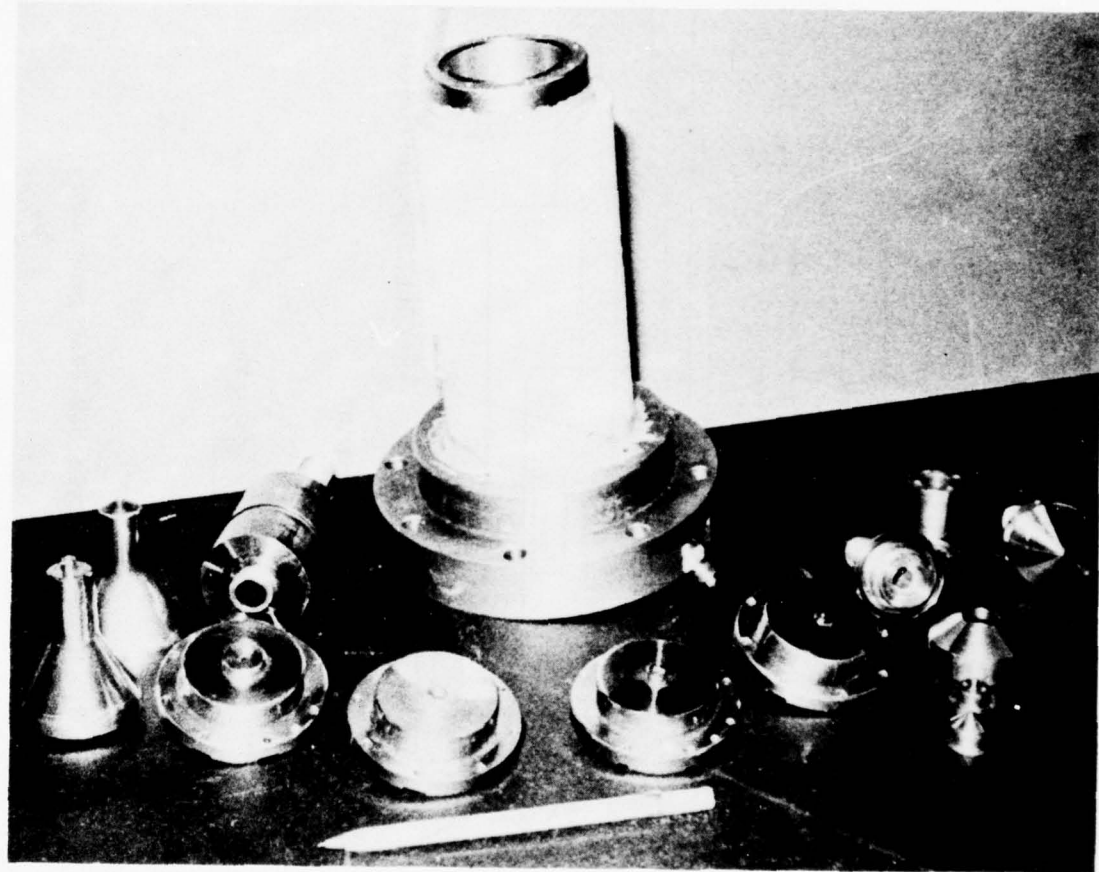
Figure 7.   Alumina Pit-style channel with various
attractor and collector inserts.

27
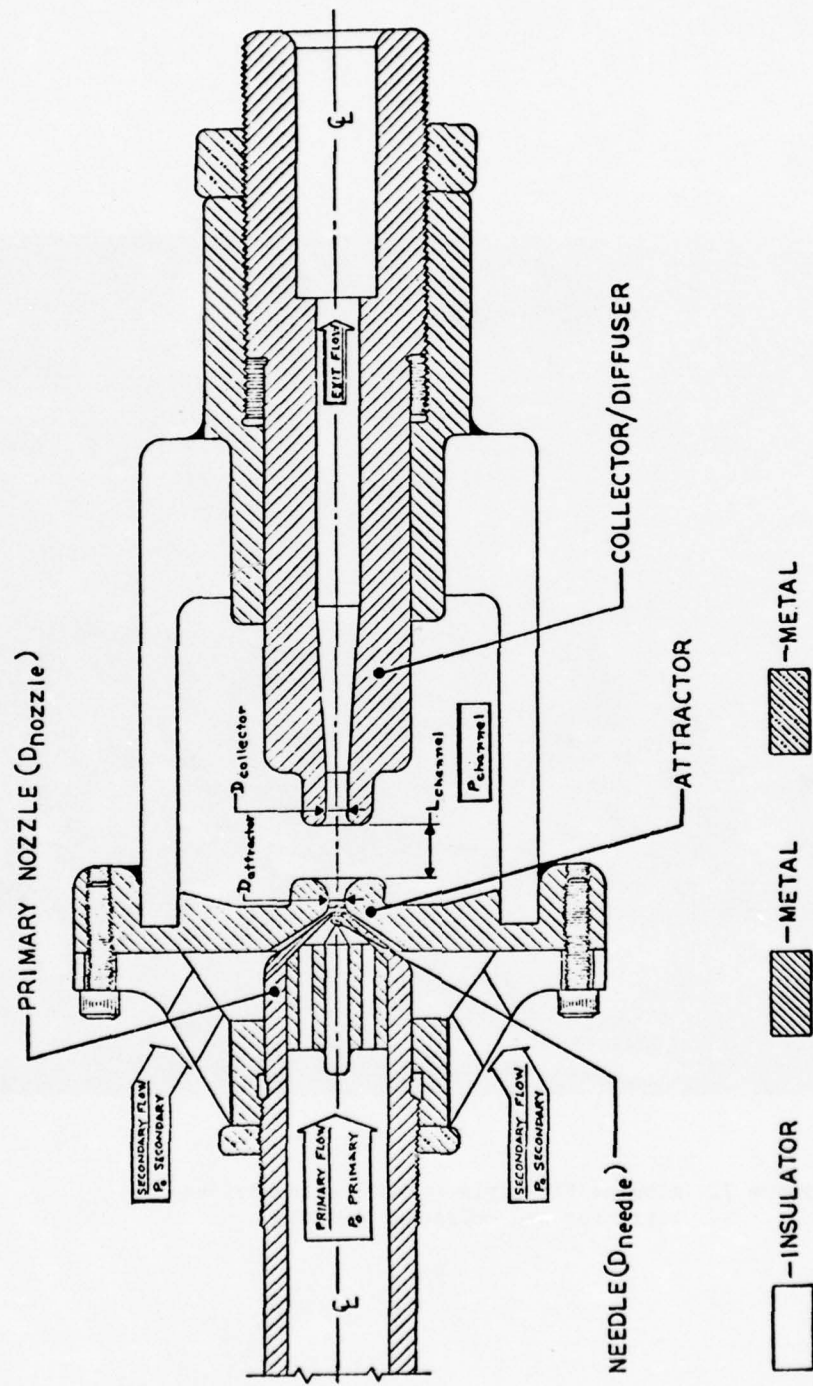
Figure 8. High-Bay style EFD test generator.

28
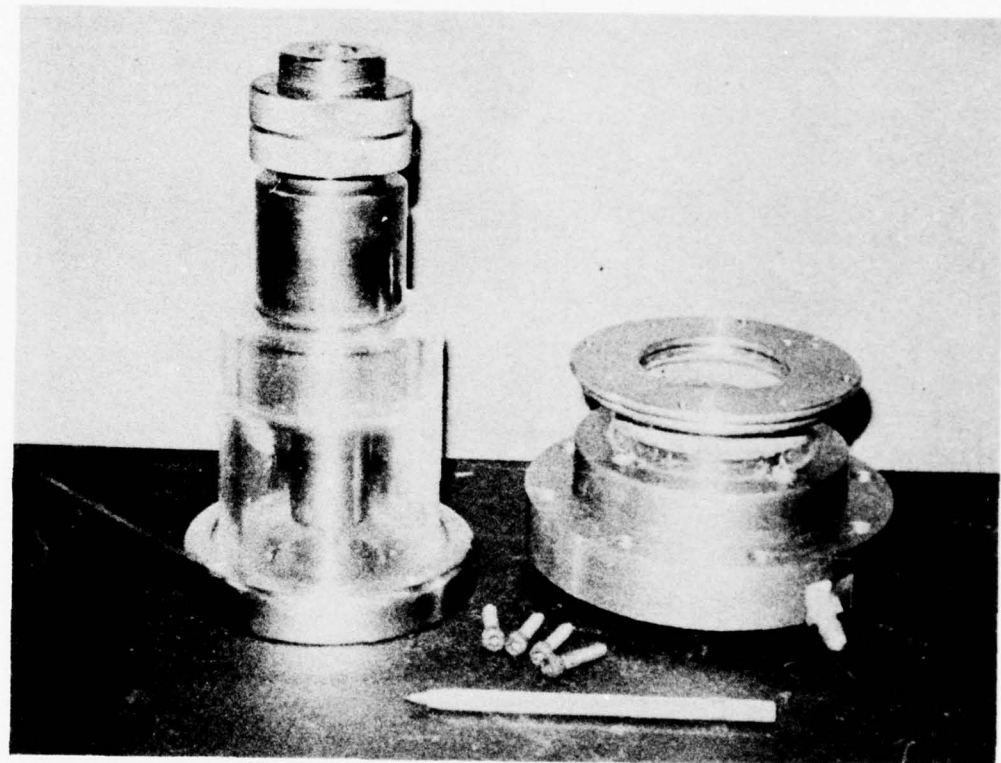
Figure 9. High-Bay generator and Pit mount assembly.
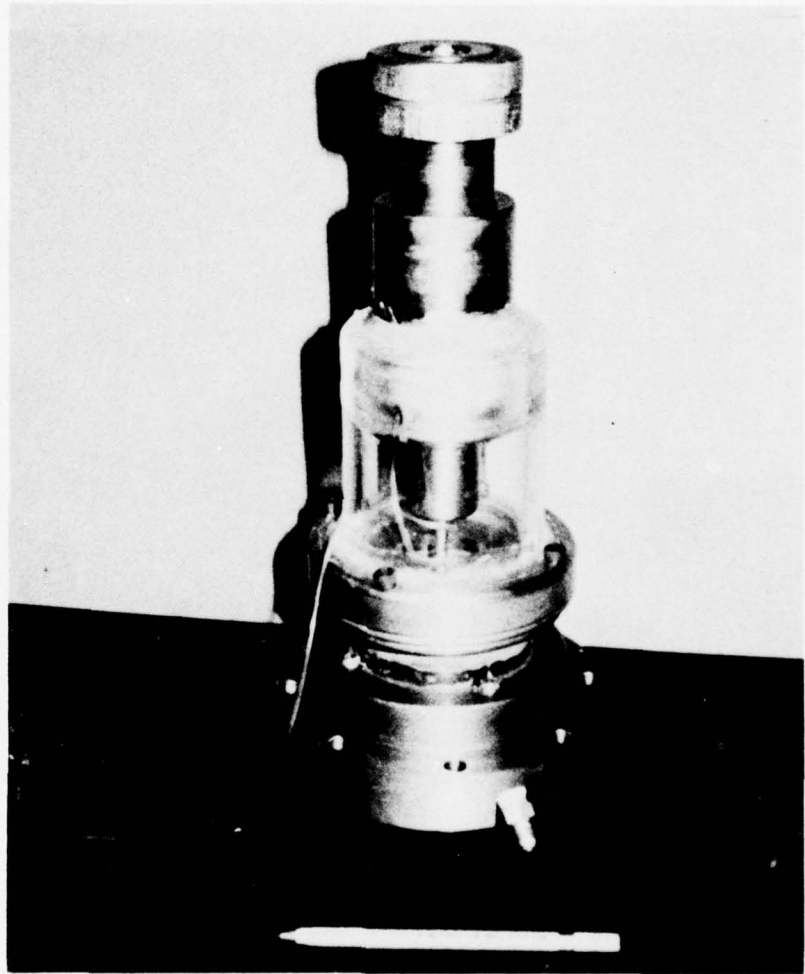
Figure 10.   Assembled view of High-Bay style generator and
mounting flange for Pit Facility.

30
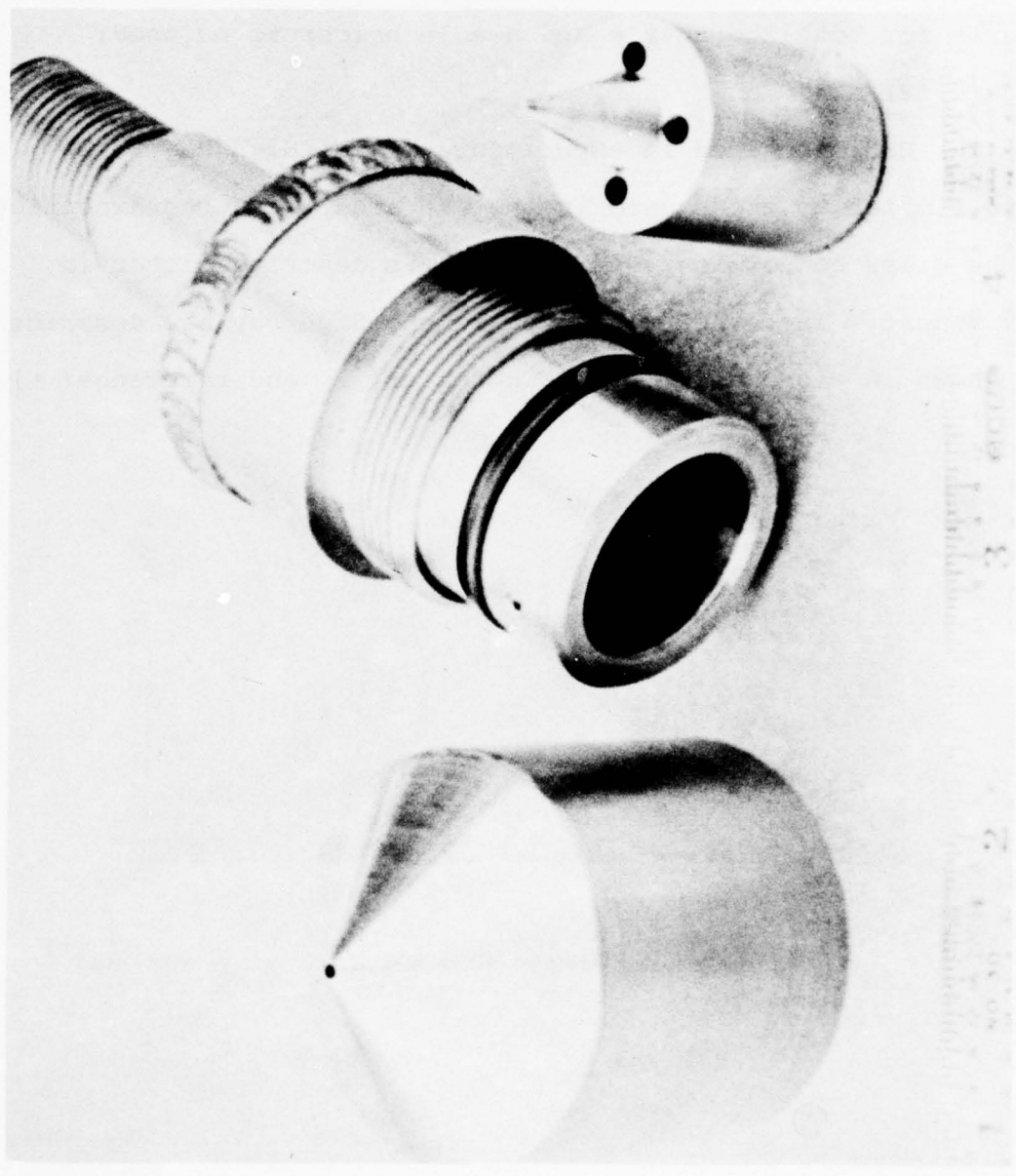
Figure 11. Adaptor for Pit to High-Bay needle/nozzle pieces

in the Pit facility. Early in the testing of the plexiglass
and alumina channels it became apparent that the original
nozzle/needle alignment system was unacceptable. A new align-
ment and holder system was fabricated which allowed changeable
inserts for both the nozzle and needle holder to be used.
(Figure 12).

   The EFD rigs used in experiments in the High Bay were
quite similar to those used in the Pit area, with the exception
of the glass conversion section which is described later in
this report. The other rigs used in the High Bay are described
and shown in pictures in the IECEC paper [2] and reference [3].
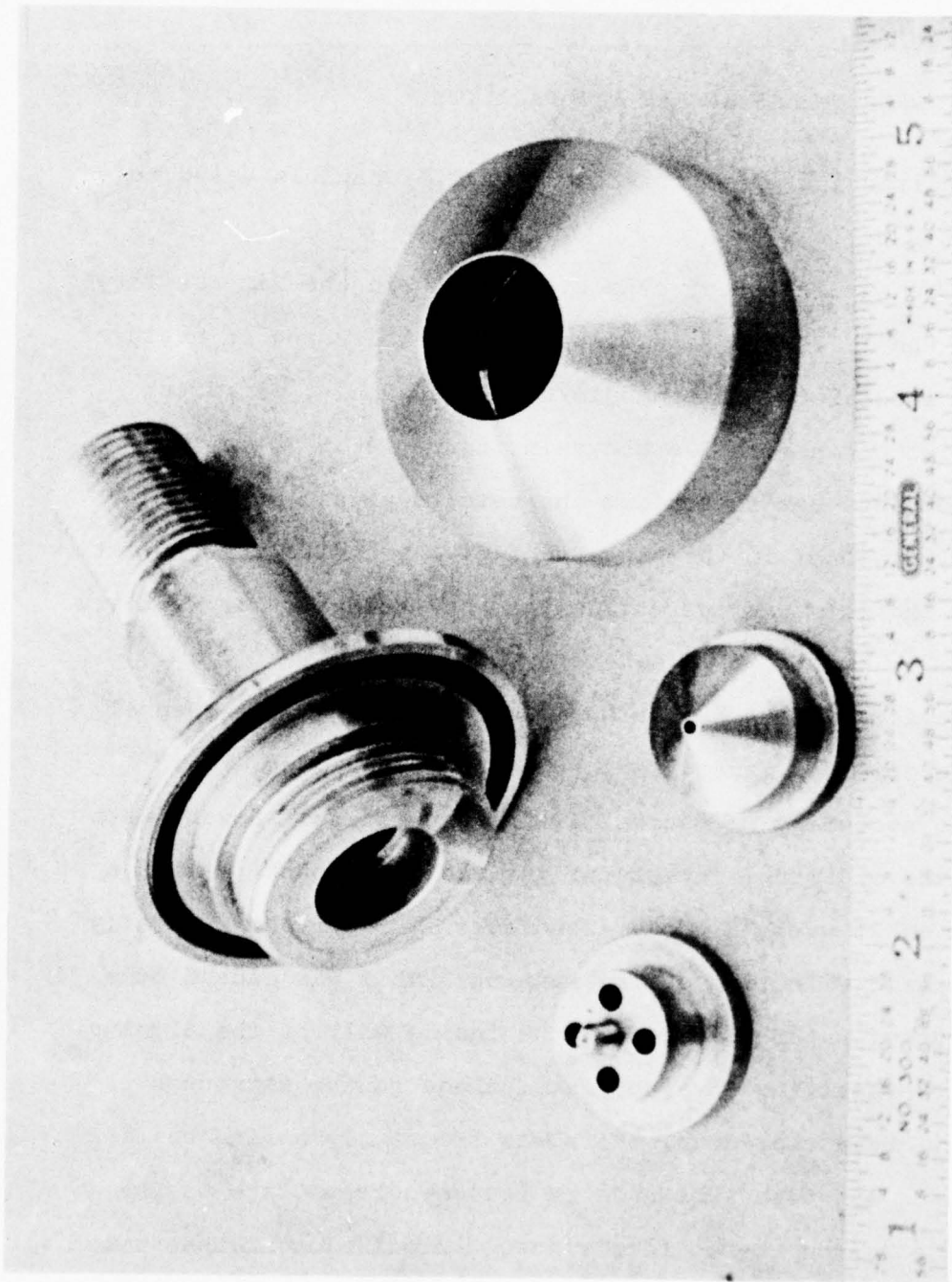
Figure 12. Interchangable nozzle/needle pieces and alignment collar for Pit style channels.

SECTION VI

EXPERIMENTS IN THE PIT FACILITY

A.   Confirmation of Performance of 1/12" Channels Using the
     Pit Facility

     The earliest test conducted by UES in the Pit Facility
were on the 1/12" standard electrode channel using an unglazed
alumina insulator. (The needle/nozzle assembly, attractor
and collector inserts are shown in figure 13.) The purpose
of these tests was to confirm the results obtained by ARL
and UES personnel in the High Bay facility and to verify that
the Pit Facility was operational and suitable for future tests
in EFD.

     The first tests on the unglazed alumina (Al_2O_3) channel
produced grounded currents of 400μA at 860 psig primary,
345 psig secondary pressures, 120°F temperature. Power tests
(using the old model 3-resistor vertical load bank) netted a
maximum of 21 watts @ 62 KV (see Table 1). Current typically
deteriorated with time during running. This was caused by a
monolayer of water absorbed on the inside wall of the alumina
insulator resulting in a current leakage to the attractor
circuit. Upon tear-down, there was frequently a fine coating
of a white ash-type substance on the downstream face of the
attractor and on the collector nose. Similar occurances with
unglazed alumina had been reported by TRW Systems, Inc. [4] scientists.
They believed that the ash was caused by surface sparks vaporizing

34
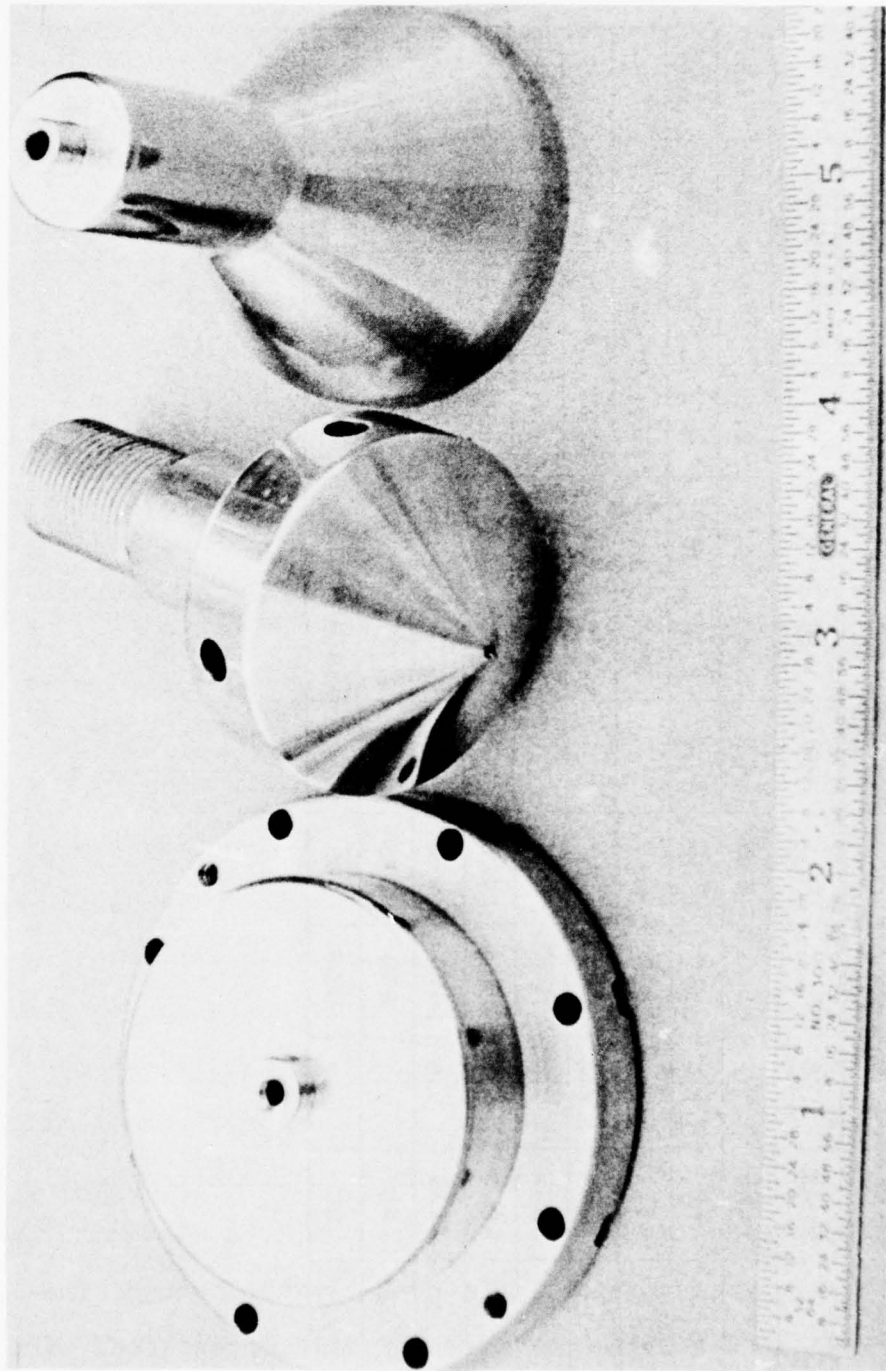
Figure 13. Standard 1/12" geometry attractor, nozzle/needle and collector inserts for Pit-style channels.

TABLE 1. EARLY PIT-FACILITY TEST RESULTS

ELCTD	CHANNEL		PSIG.		MACH NO.		L/D	$I_{coll.}$ (μamp)	OUTPUT		η%
	INSUL	SIZE (inches)	P_{pri}	P_{sec}	PRI	SEC			POWER (watts)	VOLTAGE (kv max.)	
STD	PLXG	1/12	860	345	1.2	.763	9.12	250	27.6	110.5	3.2
STD	AL	1/12	860	349	1.2	.773	9.12	210	30.25	.144	3.58
STD	AL	1/12	860	345	1.2	.745	9.12	370	67.62	182.7	7.88
STD	AL	1/12	765	345	1.11	.676	9.12	300	44.46	148.2	6.4
STD	PLXG	1/12	1050	425	1.2	.826	8.16	390	57.4	147.4	5.54
90°/90°	PLXG	1/15	1058	425	1.2	.826	9.1	430	69.8	162.5	6.65
90°/90°	PLXG	1/15	895	420	1.08	.709	9.1	350	60.5	173	7.83
80°/60°	AL	1/12	860	345	1.2	.763	9.72	400	79	197.6	9.28
80°/60°	AL	1/12	1003	405	1.2	.853	9.72	400	79	197.6	7.9

Al_2O_3 and this smoke was charged and precipitated out on the electrodes.

To help eliminate water absorption and possible sparking along the insulator surface, the inside wall of alumina was coated with a fine layer of silicone grease. Grounded current was 430µA, similar to previous results in the High Bay, but the maximum power was only 38 watts at 162 KV at a p x d = 2 atm. -in. (secondary total pressure in atmospheres times attractor or channel diameter in inches).

The Pit-style plexiglass insulator channel was tested to eliminate the effect of the alumina on test results. Generally, the results with this channel were identical to those using the alumina insulator. The maximum grounded current was 430µA, with maximum power of 26 watts at 105 KV. Again, the plexiglass channel produced good grounded results but had a low power output.

Because of the good agreement at ground and poor agreement with High Bay results under load, it was felt that the resistor load may be faulty. A new horizontal resistor bank was installed (see description in the Pit Facility section of this report). This allowed a variable load from 74 MΩ to 718 MΩ.

Other important factors for good performance became apparent at this time. Needle centering in the primary nozzle was critical for maximum power and needle life. Alignment had

to be accomplished either by using a jig designed for this purpose or by visually centering the needle under a stereo microscope. Primary humidity and secondary temperature control were also critical to produce uniform droplets and to prevent condensation inside the channel and on insulator surfaces.

With these refinements, the coated alumina channel produced results similar to the High Bay rig at a primary Mach number of 1.2 (see Table 1). The current-voltage characteristics are shown in Figure 14. UES was confident that the rig and facility were working up to expectations.

B.   Test of Flat Plate Electrodes (90°-90°) with the Alumina Insulator Channel

A short investigation into the effect of flat, parallel plate type electrodes was undertaken, using the Pit-style alumina channel. The electrodes used were the early model attractor/collector pieces, approximately a 1/15" geometry. The primary flow was 1/24" in diameter and running conditions were based on a p x d - 2 atm.-in. Results were 70 watts at 163 KV at M_p = 1.2, and 60.5 watts at M_p = 1.08 for 7.8% efficiency. Although the primary was overpowered; that is, the primary flow diameter should have been scaled down to 1/30" to match the small channel size and hold to the strict p x d scaling laws, the results showed that flat electrodes,

38

67.75 watts
7.6 % Electrical Efficiency

$\frac{1}{12}$" CHANNEL, STANDARD ELECTRODES

Pp = 860 psig   Ps = 345 psig

Top = 120° F.   65° Humidity

Copper needle , Alumina channel

9 Oct. 74

OUTPUT VOLTAGE (kilovolts)

200

150

100

50

0

0   100   200   300   400   500

COLLECTOR CURRENT (microamps)
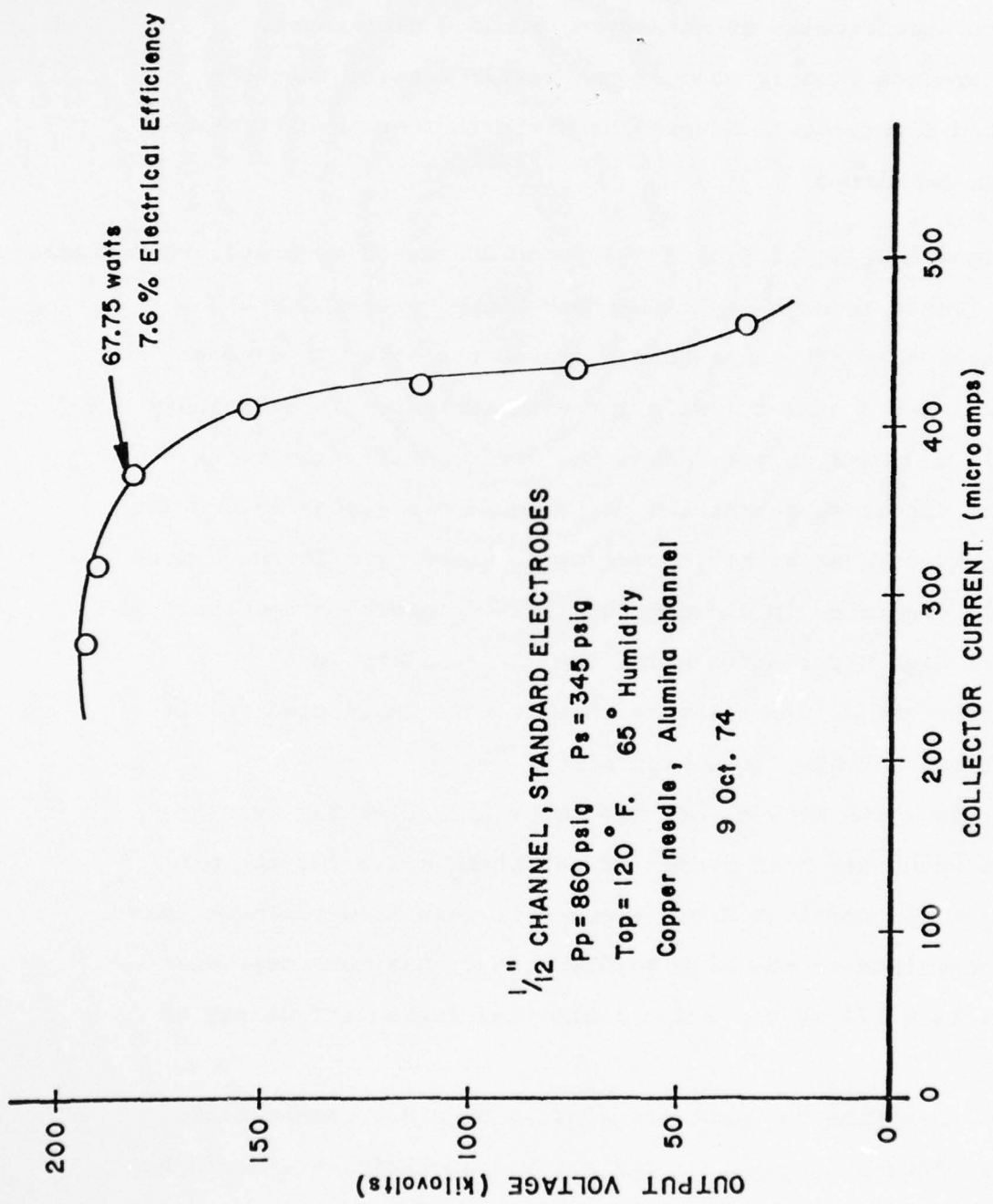
Figure 14. Current-voltage characteristics of 1/12" stand-
ard and EFD channel run in the Pit Facility.

or more specifically non-standard, rounded electrodes,
could produce equally good if not better results than the
standard electrodes and would be worth further investigation
if time permitted.

C.   Confirmation of Sloped Electrode Shapes on Generator Performance

Tests in High Bay with these sloped electrodes had
indicated that EFD generators could be run at a p x d value
greater than 2 atm.-in. with air with increases in efficiency
as well as power output. Also the good results from tests
on flat electrode geometries described above demonstrated that
sloped electrodes might improve performance by offering a more
uniform electric field condition in the conversion section. To
confirm High Bay results using the Pit facility an 80°
attractor and a 60° collector inserts were fabricated to fit
the alumina channel (see figure 15).

Flow tests showed good agreement with High Bay results,
with a secondary Mach number of .80 at M_p = 1.2 for the pit
and M_s = .89 for High Bay. Electrical results were lower than
those obtained in the High Bay facility. Maximum power was
100 watts @ 222 KV @ p x d = 3 atm.-in. for an efficiency of
8%.

At this time the parts to adapt a High Bay channel into
the Pit high-pressure tank had arrived so that tests could be
continued using a geometry as similar to High Bay's as possible.
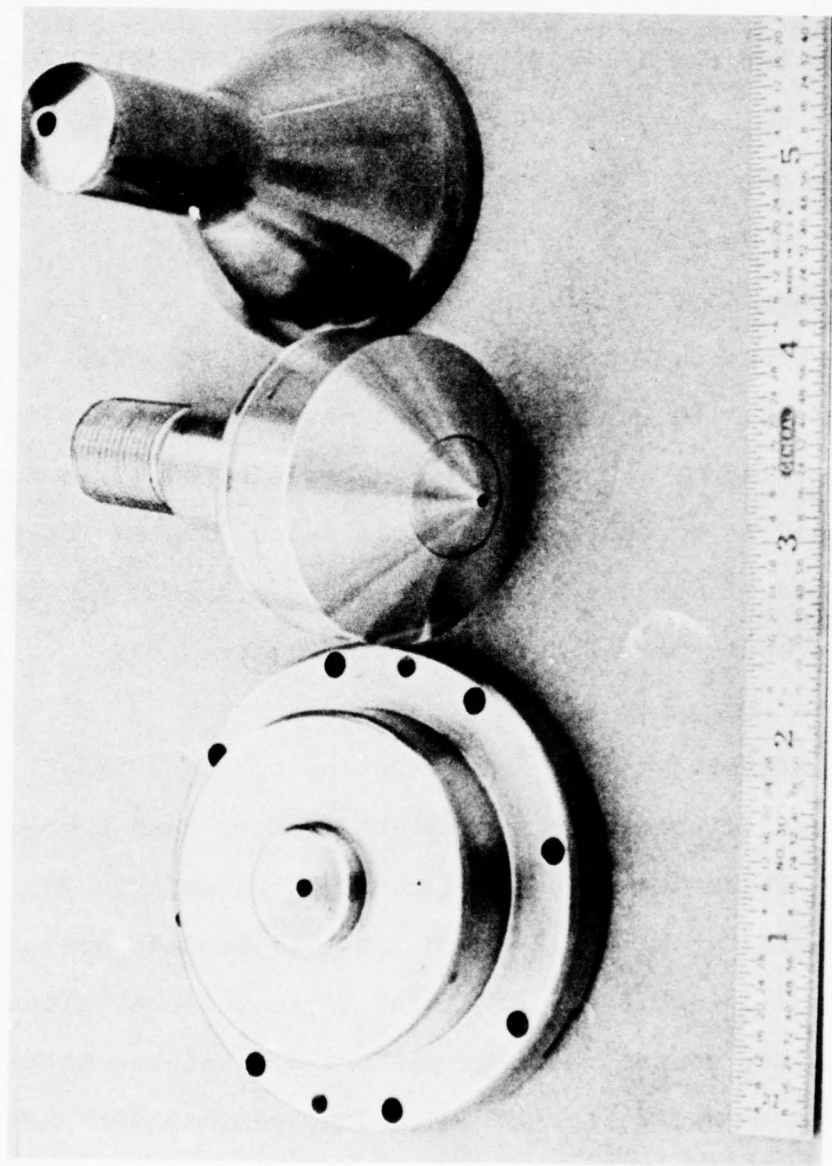
Figure 15. 1/12" 80° attractor, nozzle, and 60° collector inserts for Pit-style generator.

Both the standard geometry and 80°/60° geometry pieces from High Bay were used in this channel. Tests were conducted under normal p x d values of 2 atm.-in. and for various primary Mach numbers.

Results for the 1/12" Pit tests are presented in Table 2 for both standard and 80°/60° electrodes. Agreement between results from the Pit generator and from the High Bay generator are within 20% depending on primary Mach number.

As a comparison to High Bay, the results @ M_p - 1.2 were 460μA grounded current, 93 watts maximum and 10.6% efficiency. For some reason, the Pit facility was never able to obtain a 12 or 13% efficiency and M_p = 1.05 as was obtained in High Bay with standard geometries, and fell below High Bay output for the sloped electrodes as well. Possible causes for the lower values could be the humidification system, the heating system or sizes of the pressure tanks.

In an extension of the investigation of the 80°/60° geometry, scaling work at p x d values greater than 2 were undertaken. These tests involved the 1/12" geometry, 7° diffuser and ran at M_p = 1.2 and M - 1.15. Results are presented in Figures 16 and 17. Also presented are values for the High Bay tests. Maximum performance was 150 watts @ 261 KV, p x d -= 3-1/3 atm.-in. High Bay results were also 150 watts but at lower p x d value, yielding a larger efficiency (12.5% vs 10.6%).

TABLE 2. HIGH-BAY STYLE GENERATOR RESULTS AS RUN IN THE PIT FACILITY

Standard Electrodes (24 ATM SECONDARY TOTAL PRESSURE)

Mach # OF PRIM.	MAX. CURRENT @ GROUND	MAX. POWER	EFFICIENCY
1.2	450 μA	65.1 watts	7.4%
1.15	430 μA	69.5 watts	8.95%
1.1	405 μA	62.5 watts	9.1%
1.05	325 μA	43.1 watts	7.2%

80° Attractor/60° Collector Electrodes

1.2	445 μA	72.6 watts	8.8%
1.15	390 μA	51 watts	6.5%
1.1	390 μA	57.5 watts	8.4%
1.05	380 μA	45 watts	7.5%
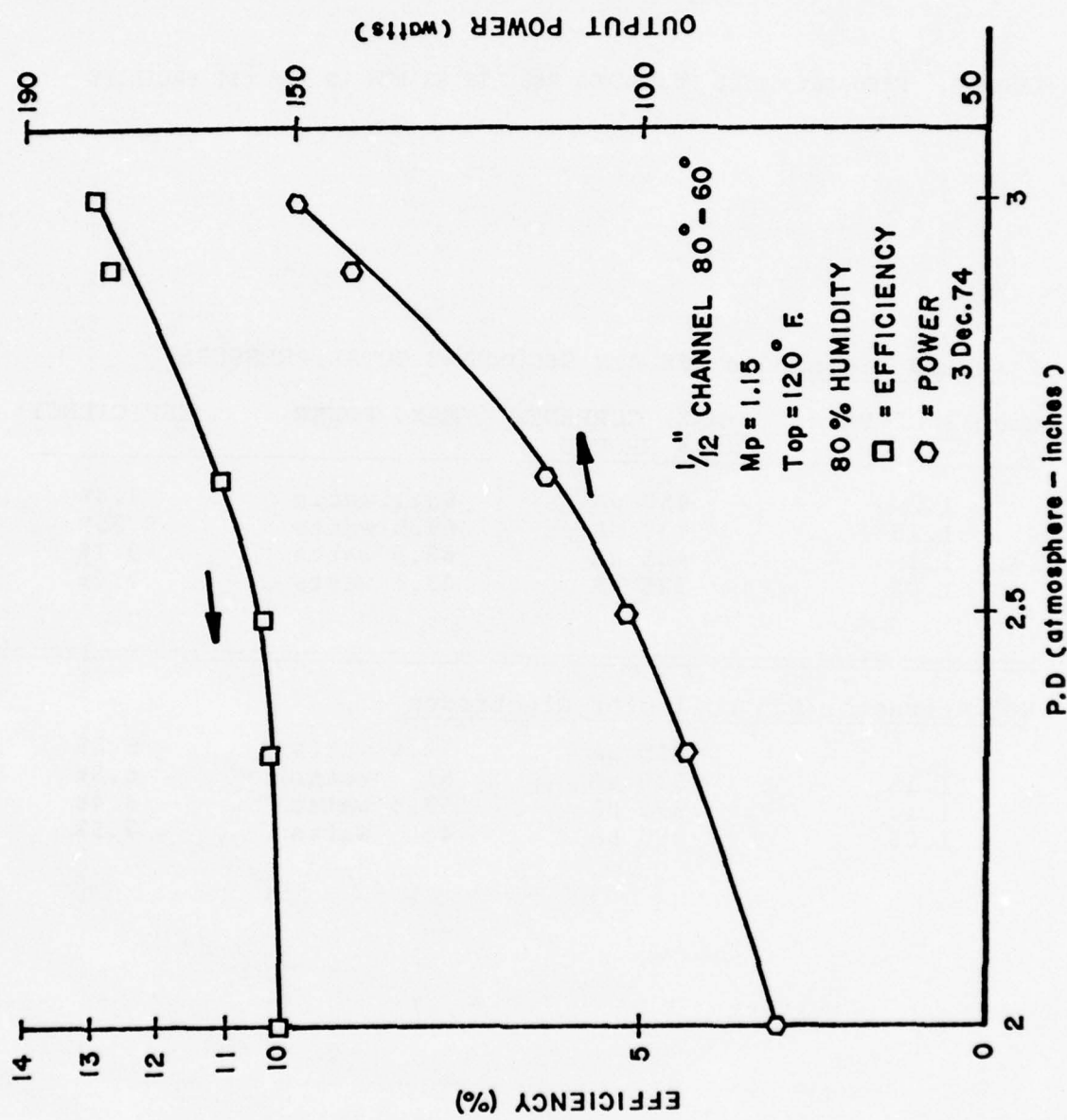
Figure 16.   1/12" channel 80°-60° electrode performance
with p x d, $M_p \approx 1.15$.
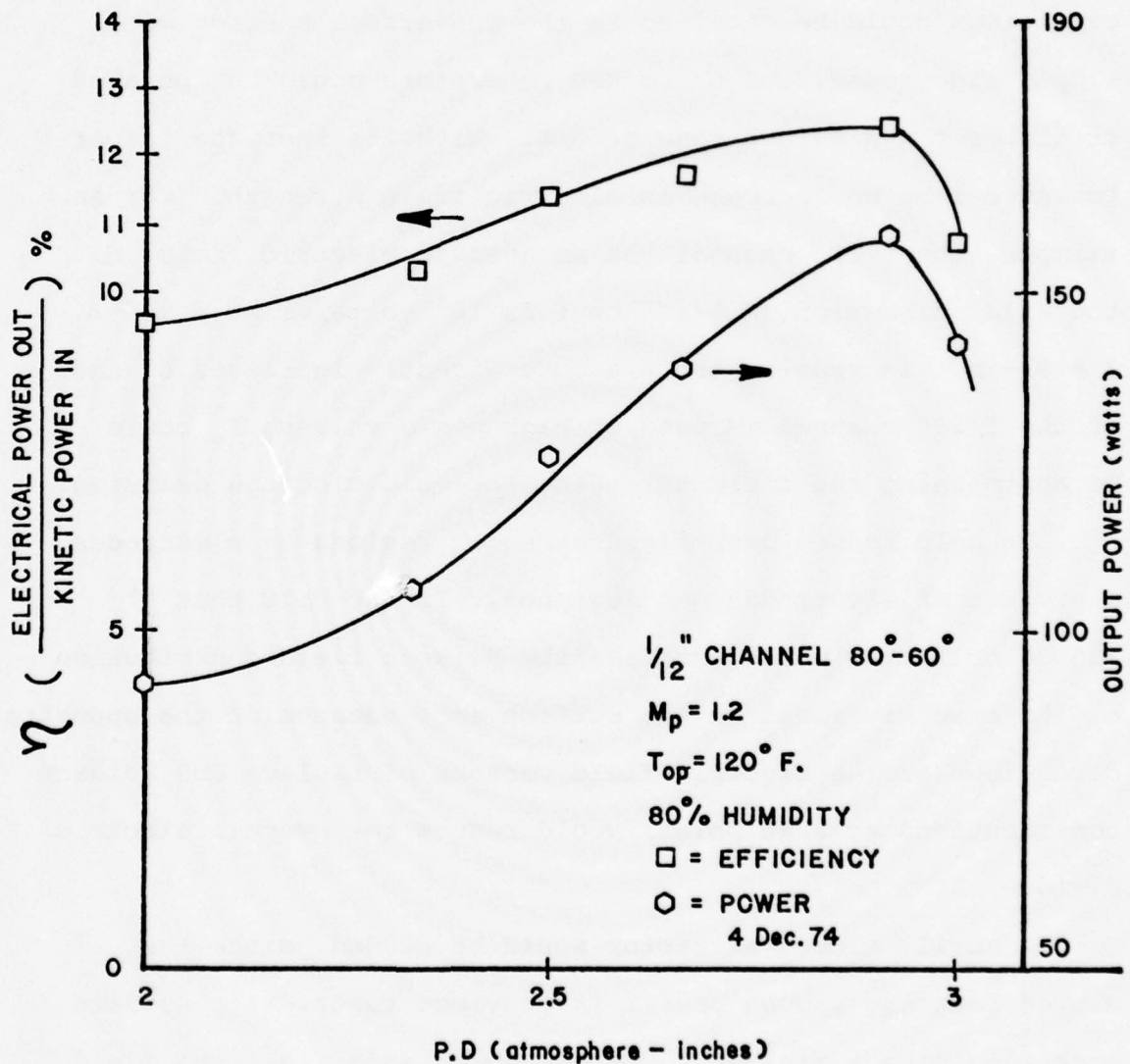
Figure 17. 1/12" channel 80°-60° electrode performance
with p x d, M_p = 1.2.

D.   Test with 0° collector and 80° Attractor of Diminished Area

Past experience with sloped electrode geometries had
proved that superior performance could be obtained using sloped
electrodes instead of curved electrodes. $^{(5)}$ More uniform field
conditions could be obtained in the conversion section with
sloped electrodes, and hence EFD generators could be operated
at higher p x d values than before. With the increase in per-
formance came an increase in electric field strength. For an
example, the 1/12" channel has an average electric field in
the axial direction (E_x) of about 2x 10^5 volts/cm at p x d =
2 atm.-in. Increasing the pressure directly increases E_x and
if the 1/24" channel is used at high p x d values, E_x could
be approaching the field strengths for cold electron emission.

To help reduce over-field strength regions on electrodes,
a new set of electrodes was designed. It was felt that 0°
sloped collector would increase the Poisson field contribution
of the electric field on the surface and, because of the opposite
directions of the electric field vectors of Laplace and Poisson
contributions at that point, would reduce the overall electric
field.

A small, sloped attractor would be needed, since the
sloped idea has proven useful in previous tests. Its surface
area should be a minimum, just enough to anchor all the field
lines from the surface of the charge cloud and the overall
Laplace field. The resulting attractor used in the tests

46

is shown in Figure 18, and has a diameter of .250" in the
1/12" geometry. This corresponds to a 32:1 attractor area to
primary area ratio for channels with L/D_{ch} on the order of 6.
The previous ratio for the 80° collector was 251:1.

The collector used is also shown in Figure 18. It
has a wall thickness of .006" and an inlet diameter of .102".
It was made as an insert for the High Bay style generator.

Experiments conducted in the Pit Facility on the 1/12"
80°/0° geometry varied primary Mach number, p x d value, and
channel length in an effort to find the optimum combination
of variables for maximum efficiency and power. Mach numbers
varied from 1.2 to 1.05, p x d values from 2 to 3.33 atm.-in.,
and channel lengths from .25 to .35 inch (L/D from 5.15 to 6.35).

Flow tests of secondary Mach number versus collector
distance were first undertaken at atmospheric conditions. The
80°/0° combination gave a better secondary Mach number than
the 80°/60° at short collector distances for both 1.2 and 1.05
primary Mach numbers. The difference was less significant
at longer collector distances of between 5 and 7 turns.
The better flow conditions in the 80°/0° case may be because of
the longer straight section (for mixing) before the 7° diffuser.

Electrical tests were undertaken next. Electrical
efficiency and power output for varying collector gaps are
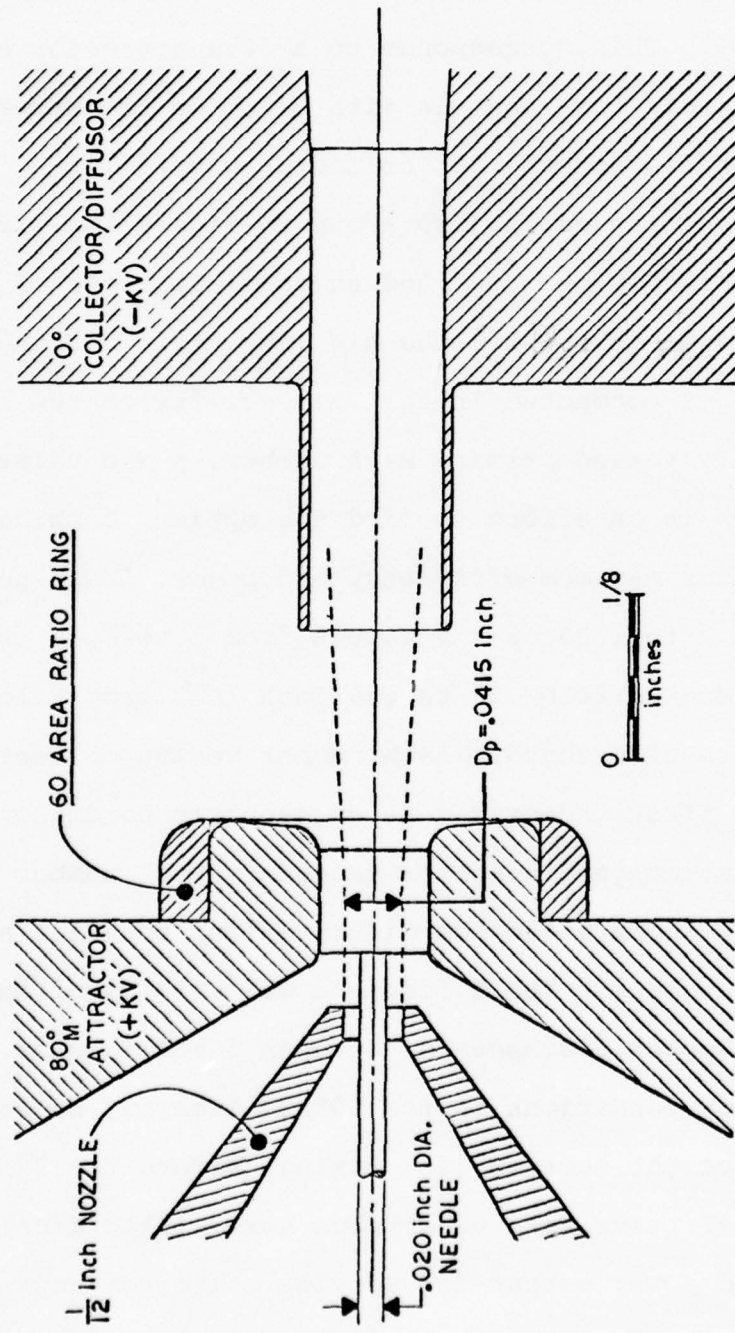
Figure 18. 1/12" 80°-0° minimum area channel

presented in Figure 19. The highly peaked characteristic results from a very sensitive matching of attractor area to charged cloud area. Since the cloud radius is roughly constant the attractor area is sensitive to charge cloud length. The initial size of the 80° attractor was chosen to match a gap of L/D=6. With expansion of the flow to a slightly larger radius than predicted from geometry alone, this would alter the optimum gap to attractor area ratio and hence the attractor under consideration would probably perform better at longer gaps than first predicted. In fact, the maximum efficiency was 8% for M_p = 1.2 and p x d = 3.33 atm.-in., at an L/D = 6.21. Also a maximum efficiency of 9.86% for M_p = 1.05 was obtained at L/D = 6.03. This value of 6.03 was closer to the L/D initially chosen for matching areas of attractor to charge cloud.

Comparison to performance of the 80°/60° geometry shows that the 80°/0° geometry is lower in both efficiency and power. The 80°/60° electrodes produced η = 10.6% at p x d = 3 atm.-in. at M_p = 1.2 and L/D = 5.88, while the 80° minimum area/0° electrodes yielded only 8% at M_p = 1.2.

A larger attractor ring was added to increase the area ratio of attractor to primary to 56.1. Flow tests results remained essentially the same as results without the ring. Electrical performance was 7.25% efficiency, 102 watts at 6.2 turns, M_p = 1.2 and p x d = 3.33 atm.-in., higher than the

49
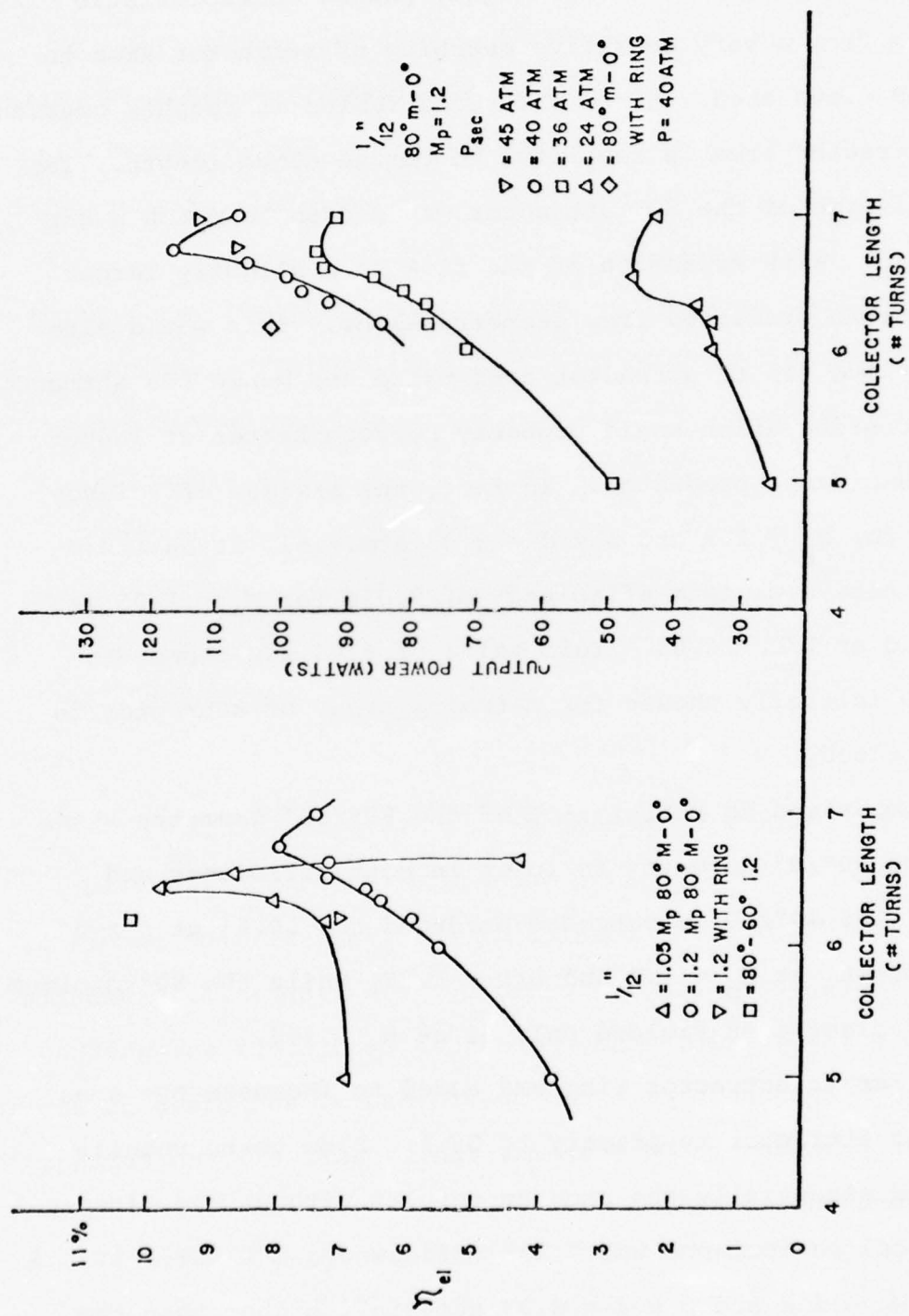
Figure 19. Performance results of 1/12" 80°-0° minimum area channel tests.

results without the ring for the identical conditions. At M_p = 1.05, however, performance was lower, η = 8.4%, 94 watts @ 6.45 turns and p x d = 3.67 atm.-in. vs 9.8% under similar circumstances. Optimization was not completed for tests with the ring and at various other collector distances.

Tests at area ratios smaller than 32:1 were not conducted because of re-direction of the research effort. Generally, however, the fluid dynamic perofrmance of the 80°/0° electrode channel was better than the 80°/60° case, with electrical performance slightly poorer in comparison. This geometry looks promising and should be tested against other electrode shapes in even higher electric fields, perhaps in a 1/17" or 1/24" geometry. Further optimization of attractor area to flow diameter could be done as well.

E.   1/24" Geometry Experiments

Only one test was conducted in the Pit facility to extend the EFD scaling results of the 1/12" 80°/60° generator to a 1/24" size to boost efficiency (see figure 20). Results were very low currents under grounded conditions and unsteady readings. Because of the poor performance, and based on similar poor performance by TRW Systems, Inc., (Ref. 6), no further tests were undertaken.
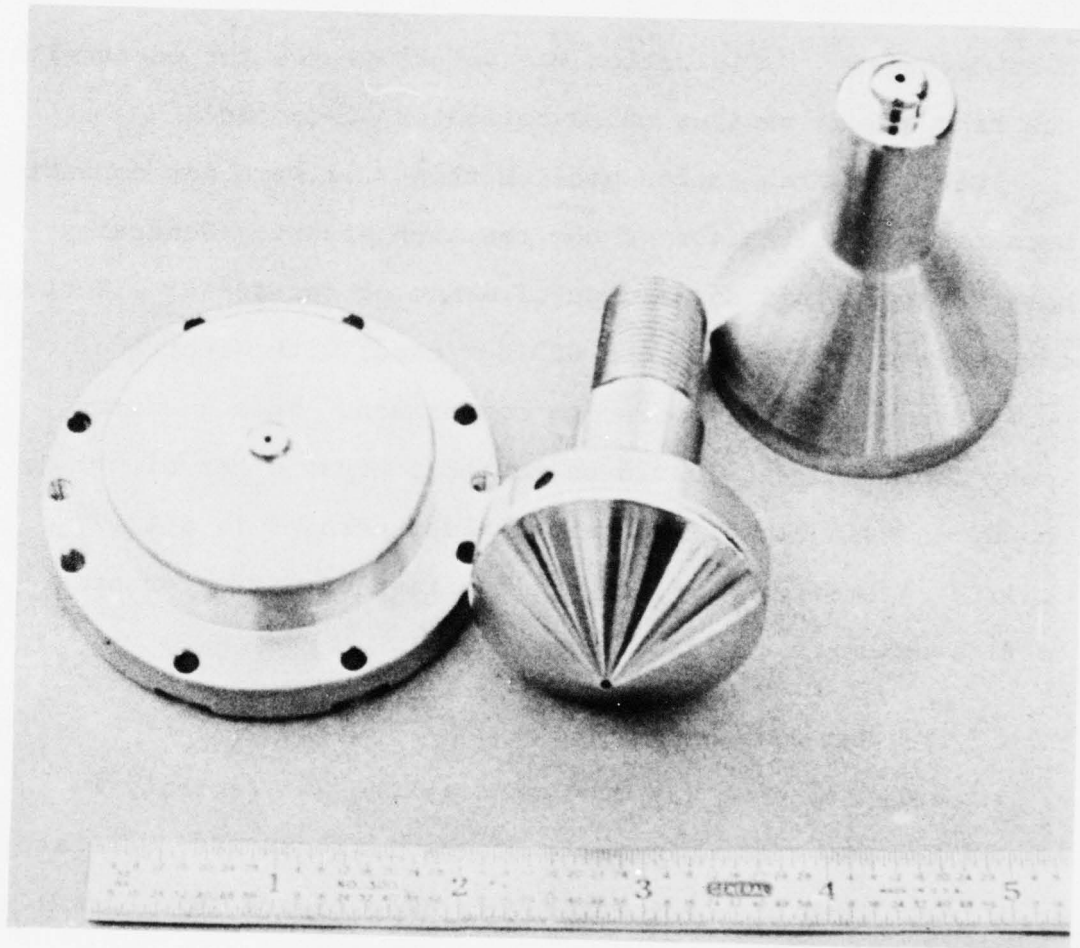
Figure 20. Photograph of 1/24" channel attractor, nozzle, and collector inserts for the Pit style generator.

F. Performance Characteristics of Small Diameter Primary
    Flows ($\overline{A} < .3$)

Recent analysis by Mr. M.O. Lawson, formerly with the
Air Force's Aerospace Research Laboratories, and now with the
Air Force Aero Propulsion Laboratory, WPAFB, on EFD injector
performance characteristics has shown that small high speed
primary flows could theoretically produce higher efficiencies
than previous generators by better optimum matching of the
driving flow to the secondary insulating flow.

According to Lawson's theory, for a given primary velocity,
channel potential function ϕ $(=1/2\epsilon\{V_{sp}/\rho L\}_{uf}E_b L/R\ 1/C_L)$,
diffuser efficiency, η_d, and channel loss characteristic, C_L,
there is an optimum secondary velocity and efficiency given by
the following equations:

$$v_{s_{opt}} = \frac{\phi}{v_p}(\eta_d-2) + \left[\frac{\phi^2}{v_p^2}(2-\eta_d)^2 + 2\phi\right]^{1/2} \tag{1}$$

$$\eta_{opt} = \frac{2/v_p v_{s_{opt}} - (2-\eta_d)/v_p^2}{1/2\phi + 1/v_{s_{opt}}^2} \tag{2}$$

and consequently an optimum primary flow diameter for a given
channel size as

$$d_p = \frac{d\ \text{channel}}{\left[1 + \eta_{el}\dfrac{v_p^{3/2}}{C_L\,\phi\,v_{s_{opt}}}\right]1/2} \tag{3}$$

53

For example, a 1/6" EFD channel operating at a primary Mach number of 1.5 and 12 atmospheres secondary total pressure would theoretically yield 13% efficiency, an optimum secondary velocity of 60 m/sec and a nozzle flow diameter of .0206", assuming ϕ = 2100 joule/kg, η_d = 85% and C_L = 0.7.

The scope of work was changed at this time to include experimental tests to confirm Lawson's ideas of small area ratio channels (A_p to A_s less than 0.3) and high Mach number primary flows. UES conducted three experiments, on the 1/6" size, on the 1/12" size, and on a multi-flow nozzle in a 1/12" size. These tests were conducted both in the High Bay and Pit facility. The High Bay results are presented in detail in Section VII, E.

The Pit facility was modified to allow separate humidification of the secondary recirculating flow (see Figure 21). The mixed exhaust flow was partially routed into a high pressure sphere where the gas bubbled through water to reach saturation conditions. By mixing the dry secondary with the saturated gas, the relative humidity of the secondary could be controlled between 10% dry to 95% relative humidity.

Table 4 gives the theoretical values of secondary velocity and efficiency based on equation 1 and 2. Also presented in Table 4 are the values of achieved secondary velocity and efficiency as well optimum efficiency calculated from the actual secondary velocity.

54
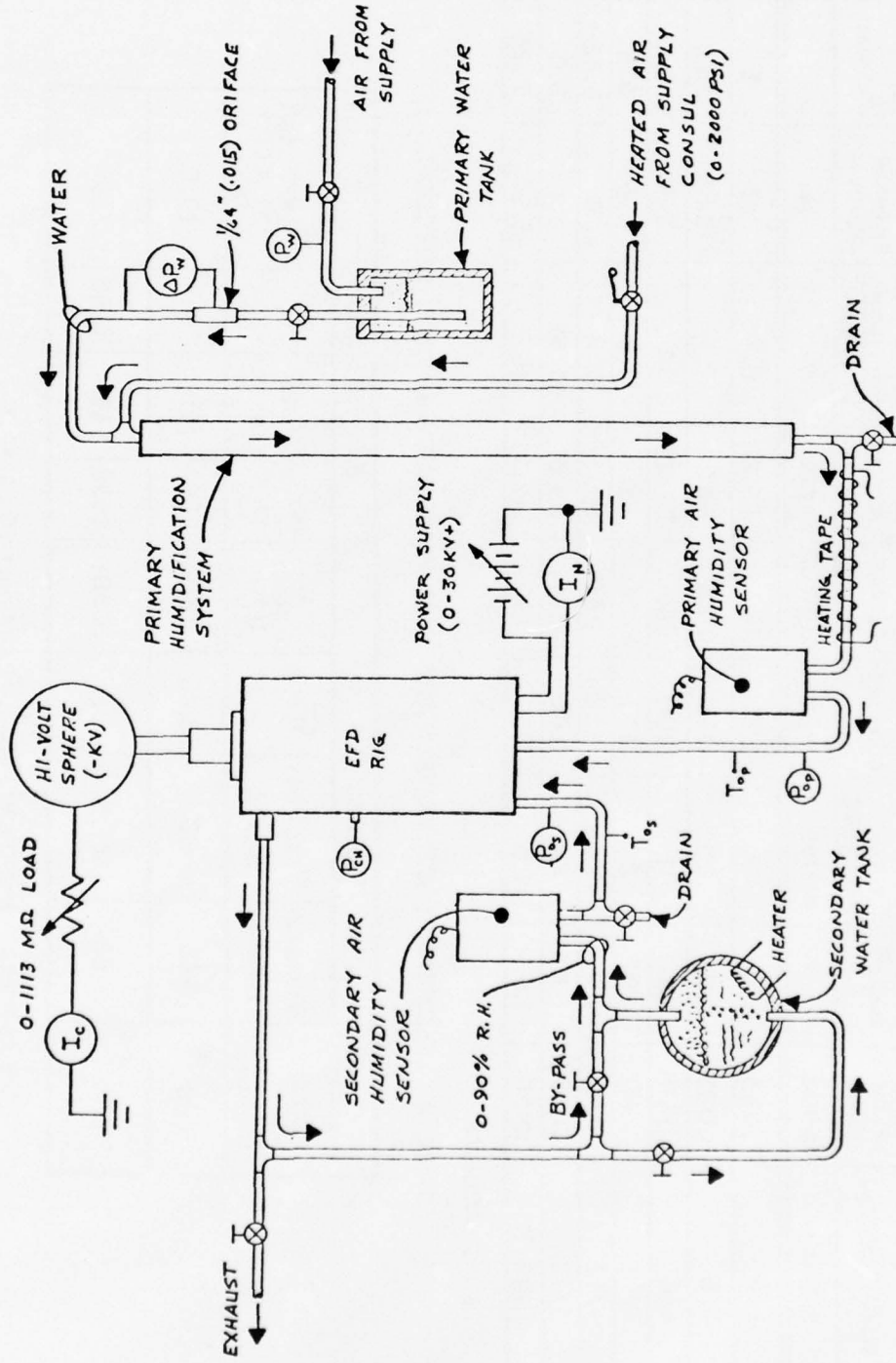
Figure 21. Separate secondary humidification system for the Pit Facility.

TABLE 3. RESULTS OF TESTS RUN WITH SMALL PRIMARY FLOWS

CHANNEL SIZE (ATTRACTOR DIA.) INCHES	PRIMARY FLOW DIA. INCHES	PRIMARY MACH #	SECONDARY TOTAL PRESSURE ATMOS.	OUTPUT CURRENT µA	OUTPUT VOLTAGE KILOVOLTs	OUTPUT POWER WATTS	EFFICIENCY $\left(\frac{\text{electric power}}{\text{kinetic power}}\right)$ %	TOTAL ENTHALPY REMOVAL %	$\frac{L}{D}$ channel	$\frac{L}{D}$ primary
1/6	.083	1.01	12	375	182	69.2	6.73	1.2	3	6
1/6	.083	1.2	20	680	263	180	7.1	1.58	3.72	7.44
1/6	.0315	1.5	12	206	190	39.25	9	2.8	3	15.7
1/12	.042	1.01	24	370	176	65	11.8	2.31	3.3	6.6
1/12	.042	1.2	36	620	250	155	13.4	3	3.72	7.44
1/12	.01975	1.5	24	260	214	55.5	16.45	5.1	5.3	13.9
1/12 *	.0156	1.5	28	214	196	42.1	16.3	5.05	2.25	12

* PIT FACILITY

TABLE 4. THEORETICAL AND EXPERIMENTAL TEST RESULTS FOR OPTIMUM EFFICIENCY

CHANNEL SIZE INCHES	THEORY				EXPERIMENT			
	V PRIMARY M/SEC	V SEC-OPT M/SEC	η OPT %	DIA. PRIMARY (opt.) CM	DIA. CM	V SEC M/SEC	η %	η WITH EXP. VELOCITY %
1/6 *	443	60	13.45	.053	.08	120	9	10.5
1/12 **	450	81.5	18.1	.0381	.0398	145	16.45	15

* ASSUMES $\phi = 2100 \text{ M}^2/\text{SEC}^2$, $\eta_{\text{diffusor}} = .85$, $C_L = 0.7$

** ASSUMES $\phi = 4200 \text{ M}^2/\text{SEC}^2$, $\eta_{\text{diffusor}} = .85$, $C_L = 0.7$

56

Table 3 presents experimental results for tests conducted in both the High Bay and the Pit. Previous test results of the 1/6" and 1/12" channels are included for comparison. Note that the small, .015" diameter primary nozzle run in the Pit produced similar results to tests conducted in the High Bay. Maximum efficiency was 16.3%, 42.1 watts at 28 atmospheres secondary total pressure.

Almost as important as the increase in efficiency was the increase in total enthalpy removal by electro-fluid dynamic forces. The percentage removal is calculated from

$$(H_O - H_p)\eta_{el}/H_O \quad \text{or} \quad (1 - T/T_t)\eta_{el}$$

Based on the primary Mach number calculated from total pressure ratios of secondary to primary, the increase in enthalpy removal was from 1.2% to 5.05%.

Tests with the eight-hole nozzles, (one with .01" dia. holes and the other with .007" dia. holes, see Figure 22) were also conducted. It was hoped that this design would provide a charge cloud diameter equal to one-half the channel diameter and power the secondary with a reduced primary diameter flow. As it turned out, neither the .01" nor the .007" size nozzles worked well at all. Distances between attractor and nozzle were critical and optimum spacing was never achieved in the limited number of tests run in the Pit. Maximum grounded current was 125 μA with 160 μA loss to the attractor. Maximum power was only 4.1 watts and $\eta = 1.6\%$.
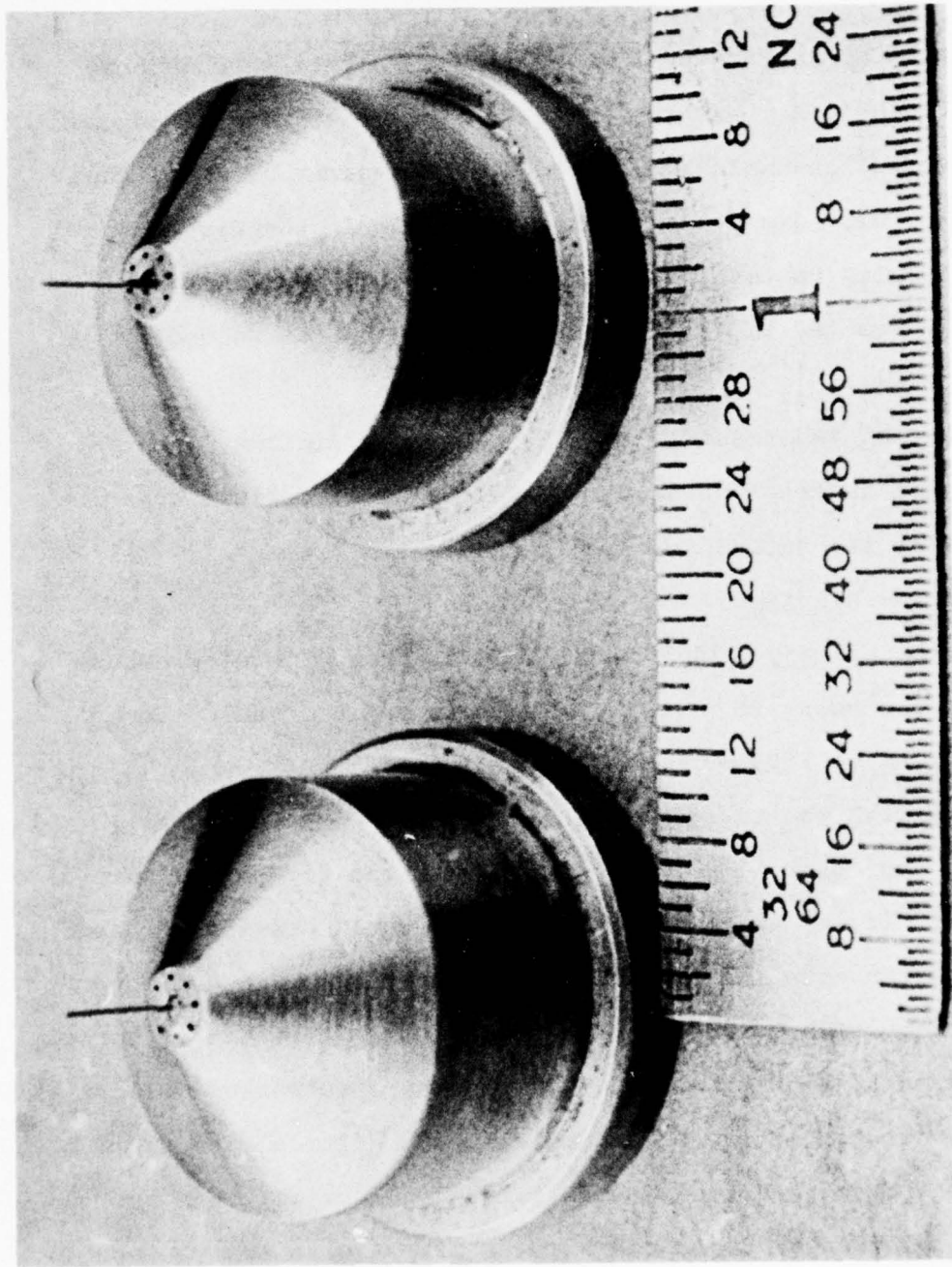
Figure 22. Photograph of eight-hole small primary flow
diameter nozzle/needle inserts for Pit Facility.

This style nozzle appears too lossy for small flow applications and further tests were dropped in favor of the more conventional nozzle/needle arrangement.

Theory indicates that with still smaller nozzles designed for supersonic flow, say M_p = 1.7 or 2, further increases in enthalpy removal could be accomplished. This is one area of future study that might increase performance in EFD power generation.

G.   EFD - Injector Flow Tests

The good results produced by tests of small primary diameter high velocity nozzles led to interest in the injector process itself. Good electrical performance depends on matching the generator EFD capacity to the injector process. The injector thus supplies the exact total pressure rise which the EFD process then extracts in terms of direct electrical power. In terms of efficiencies, for matching conditions:

$$\frac{\eta_{electric}}{\eta_{stages}} = \eta_{injector}$$

where

$$\eta_{electric} = I \cdot V / \dot{m} \; v_p^2/2$$

$$\eta_{stage} = \frac{\Delta P_{electric}}{\Delta P_{electric} + \Delta P_{drag}}$$

59

Through the work of Mr. Lawson an expression for the
injector efficiency for constant area injectors was developed.
His analysis assumes incompressible flow with uniform entrance
and exit flows. All losses are lumped into the diffuser loss
coefficient. Although the analysis uses incompressible flow
assumptions it can be applied to sonic and supersonic injectors
with reasonably good results. Using the momentum law, Mr. Lawson
defines an injector efficiency as:

$$\eta_{inj} = \frac{(P_{0_3} - P_{0_s})v_2 A_2}{\dot{m}_p v_p \dfrac{}{2} - (P_{0_s} - P_1)v_p A_p} \qquad (6)$$

where v = velocity, A = area, $\dot{m}_p$ = mass flow rate of primary
gas, P_0 = total pressure, and subscript station numbers are defined
in Figure 23. The quantity $(P_{0_s} - P_1)v_p A_p$ is the power the pri-
mary must retain to raise itself from the local pressure inside
the channel (near the primary nozzle) back to the secondary
total pressure conditions and is therefore not available for
the injector process.

Solving equation 6 in terms of dimensionless quantities
(defined as their primary value divided by their secondary
value and designated as a bar quantity), the expression becomes:

$$\eta inj = \frac{(1 + \overline{vA})}{\overline{vA}(\overline{\rho v^2}-1)} \left[\frac{2(\overline{\rho vA} + 1)}{(1 + \overline{A})} - (2 - \eta_d)\frac{(\overline{\rho vA} + 1)(1+\overline{vA})}{(1 + \overline{A})^2} - 1 \right] \quad (7)$$

Plots of η_{inj} vs $\overline{v}$ can be generated from equation 7 with
given values of $\overline{\rho},\overline{A}$, and diffuser efficiency, η_d.

(7)

60
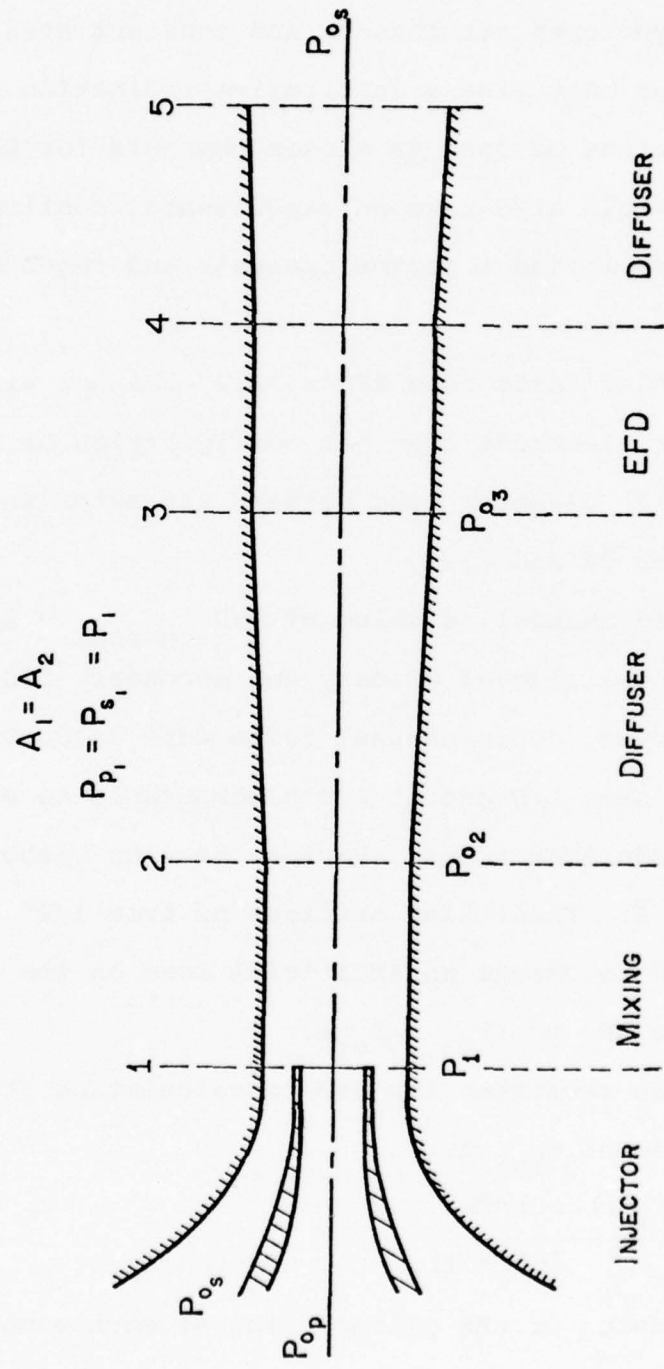
Figure 23. Injector driven EFD generator schematic.

UES undertook tests to determine the injector efficiency
of both the EFD-type open jet channel and constant area channels.
The tests would not only give a qualitative indication of the
losses and limitations of open vs closed channels for EFD con-
siderations, but would also give an experimental confirmation
of Mr. Lawson's simplified injector analysis and injector-EFD
matching theory.

The experimental tests used EFD's 1/12" channel with
either the 80°/60° electrode open jet configuration or a
constant area, 1/12" diameter tube between attractor and diffuser
as shown in Figures 24 and 25.

For the closed channel, a value of L/D $_{\text{channel}}$ = 12
was chosen for good mixing of primary and secondary flows before
entering the diffuser. Open channel tests were conducted at
approximately the same L/D and at L/D's comparable to electric
power generation configurations. Various nozzles without needle
were used to vary $\bar{A}$. Throttling orifices of from 1/2" to .042"
diameter were used to create an artificial load on the channel;
i.e., to produce a ΔP_O of $(P_{O_3} - P_{O_5})$.

Equation 6 was rewritten for use in calculating the
experimental values of η_{inj} as:

$$\eta_{\text{inj}} = \frac{\Delta P_O \ (1 + 1/\bar{v}\bar{A})}{\rho_p \ \dfrac{v_s^2}{2} \ (\bar{\rho}\bar{v}^2 - 1)} \tag{8}$$

The overexpansion of the primary flow at Mach numbers

62
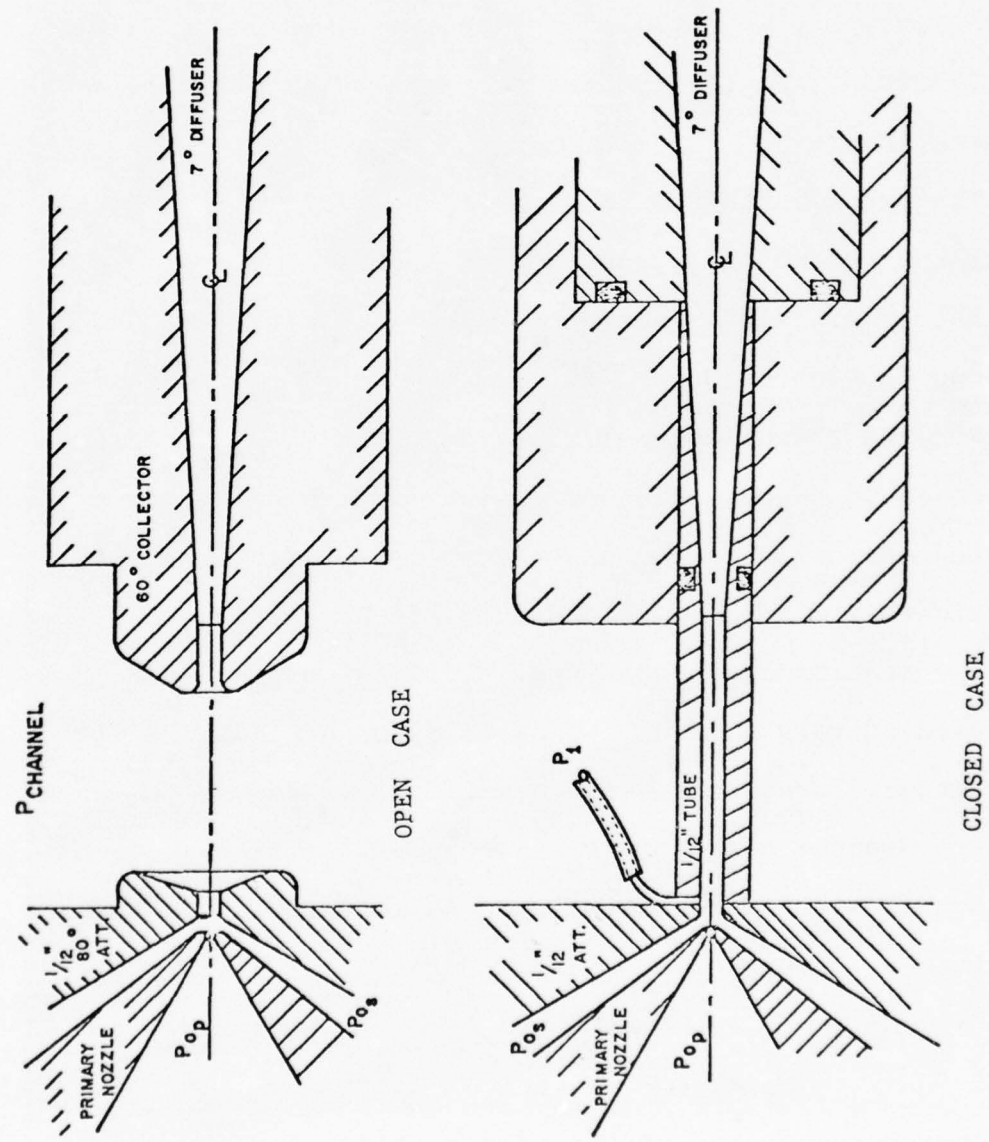
Figure 24. Diagram of open and closed channel configuration used in the injector tests.

63
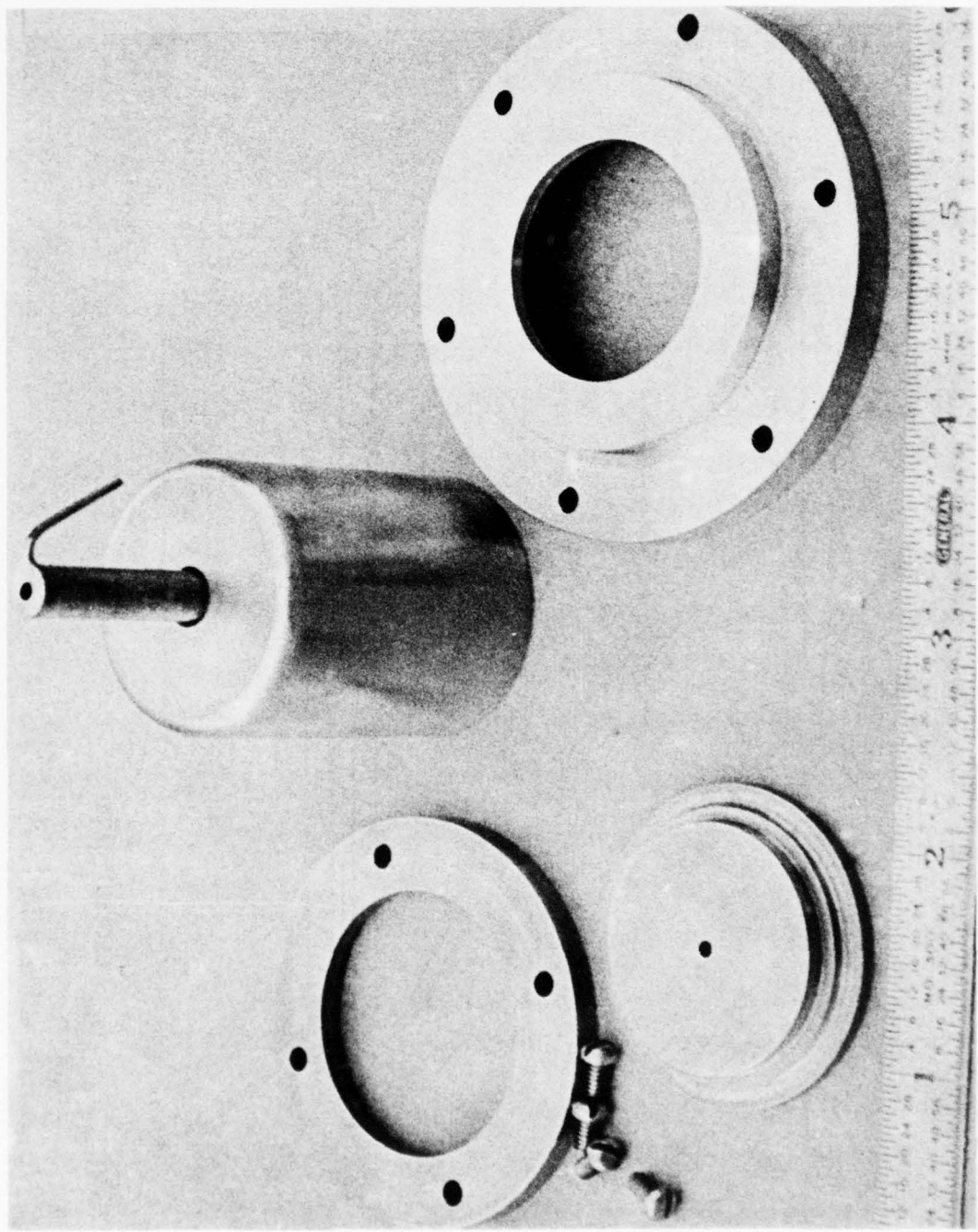
Figure 25.   Photograph of attractor and collector inserts for closed channel injector tests.

64

greater than $M_p = 1$ was considered in evaluating $\overline{A}$, and the change in density at the injector exit was considered in calculating $\overline{\rho}$. The values of local primary Mach number are based on the pressure ratio of p_1 to P_{O_p} rather than the usual ratio of total pressures between primary and secondary flows.

Results of the investigation on open channels are shown in Figure 26. A complete check of the theory was not possible before the expiration of experimental testing under this contract. A closed channel test with a .024" diameter nozzle (Figure 27) shows good agreement with Lawson's theory. Also, a comparison of Figure 26 for open channel and Figure 27 for a closed channel shows that, indeed, the open jet process is more lossy.
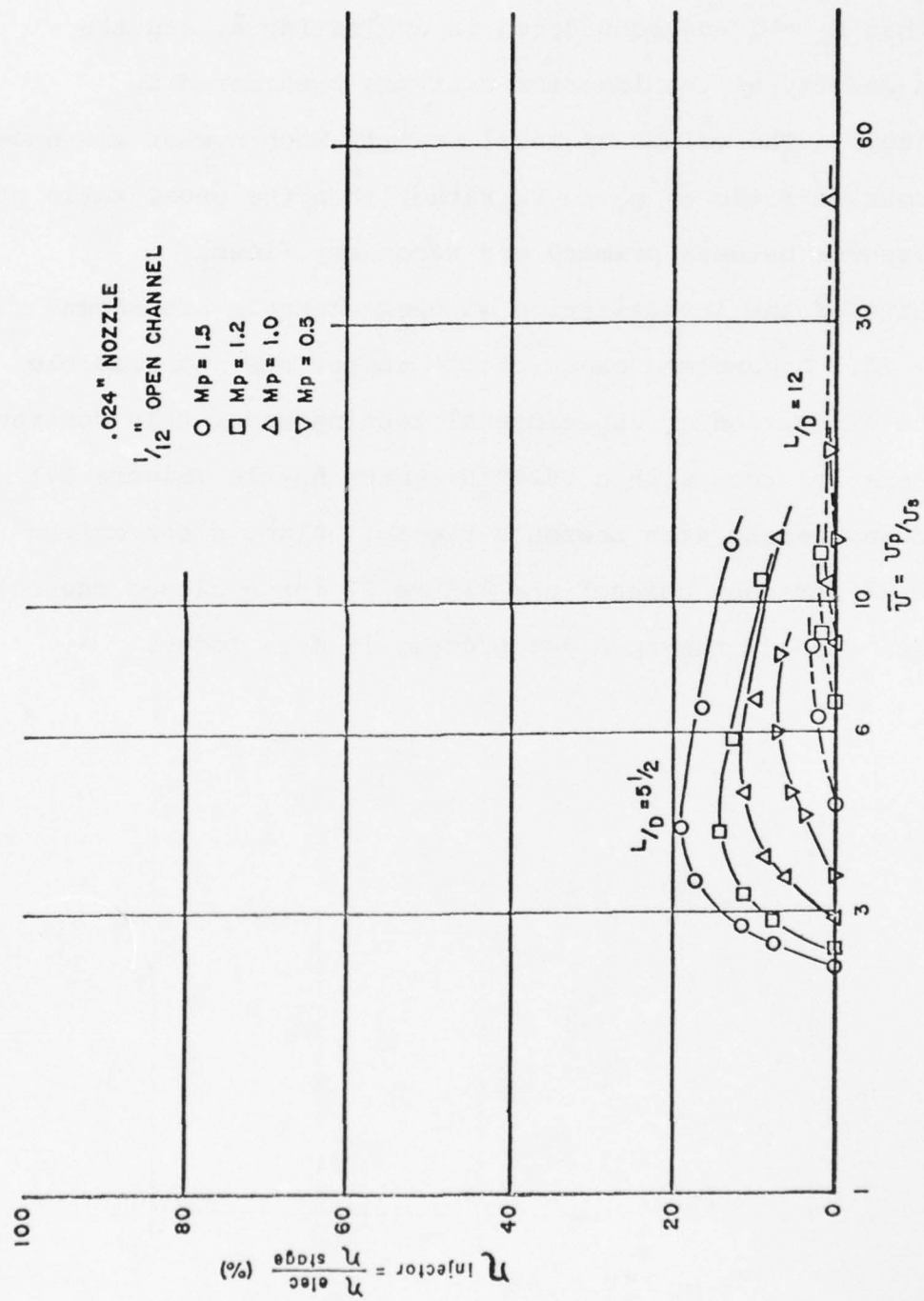
Figure 26. Injector efficiency for open channel studies.

66
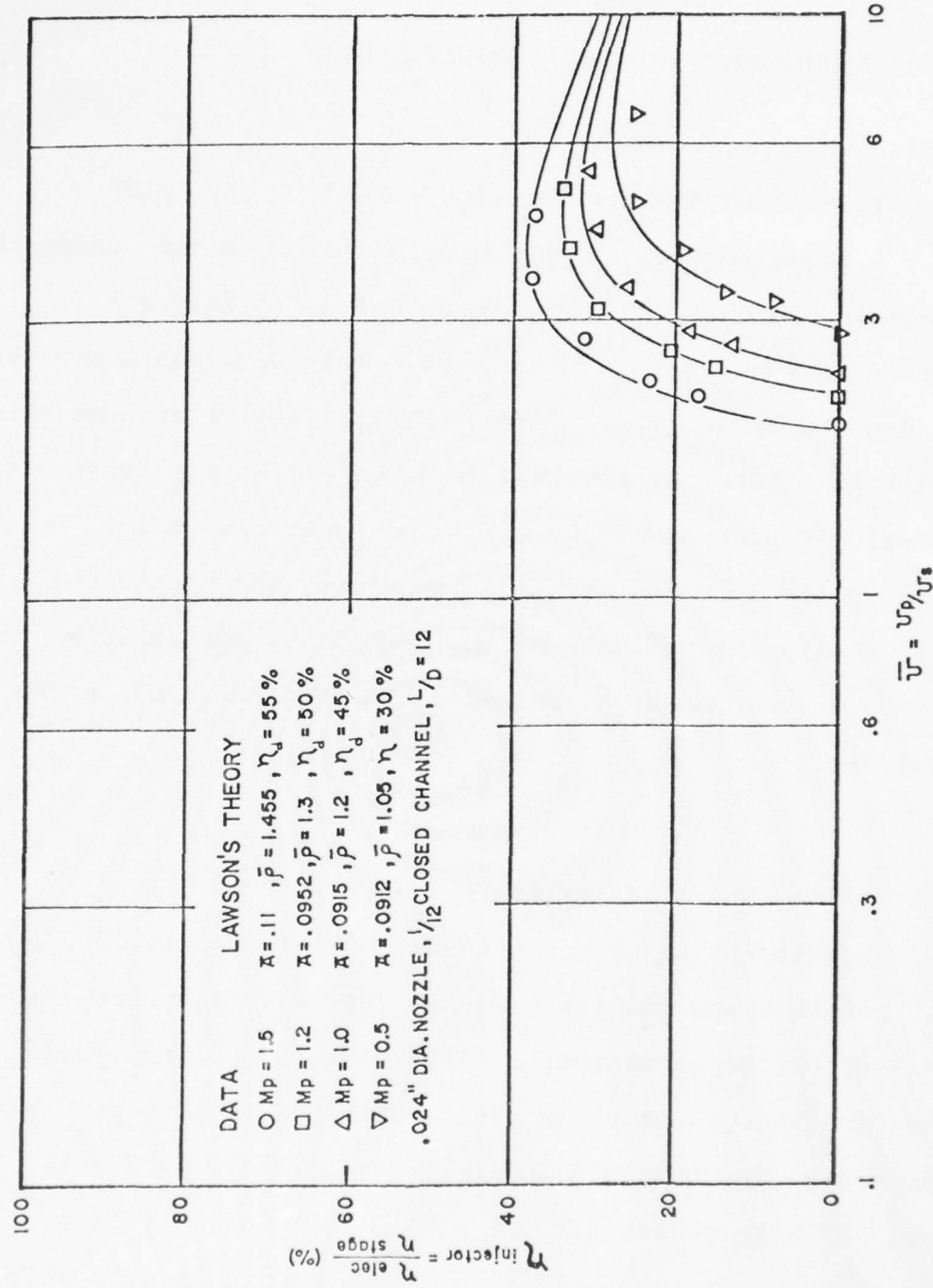
Figure 27. Injector efficiency for closed channel studies.

SECTION VII

EXPERIMENTS IN THE HIGH BAY AREA

A.   Scaling Experiments

1. Scaling Law Verification - 1/2", 1/6", 1/12"

A major portion of the experimental work done under this
contract involved verifying the new scaling technique as
discussed in section 2 of the report. This work was summarized
and presented by Mr. M. O. Lawson, Ernest Fretter and Russell
Griffith in a paper at the 1974 Intersociety Energy Conversion
Engineering Conference (Ref. 2). The paper covers in
detail the theory of the scaling technique, the approach
used to verify the validity of the technique, the experimental
rigs used in the research, and also the data obtained in the
experiments.

2. 1/24" Channel Experiments

In an attempt to extend the scaling data points to a
higher pressure and smaller geometry (and also increase the
efficiency of the generator) a 1/24" diameter channel, based
on the "scaling geometry" as reported in the IECEC paper in
the Appendix, was designed and fabricated (see Figure 28).
The primary nozzle diameter was scaled for a primary Mach
number of 1.2.   Set up and alignment proved to be extremely
tedious and difficult due to the small distances between
needle, nozzle, and attractor. Also, the needles demonstrated
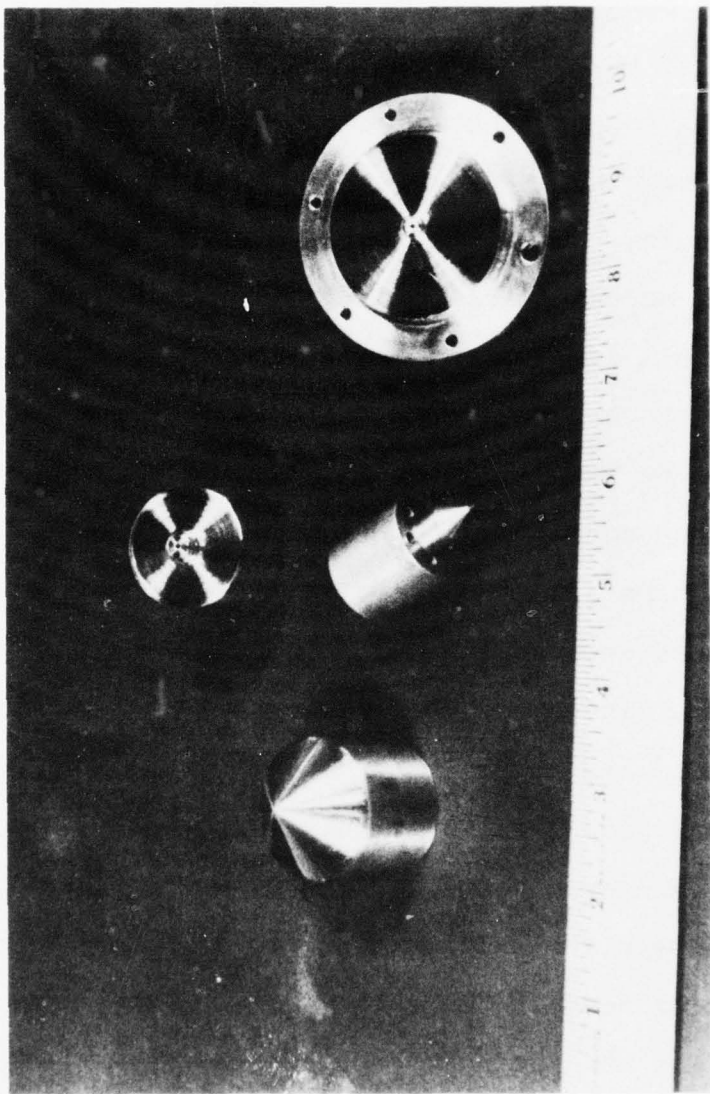
Figure 28.   1/24" nozzle, needle, collector and attractor inserts for High-Bay EFD generator.

to be very fragile, sometimes breaking off apparently due to aerodynamic stresses, and also eroding rapidly under current generation conditions.

Theoretical analysis based on Lawson's work (Section VI,F) has shown that the maximum expected efficiency for a 1/24" channel operating at 40 atmospheres secondary total pressure with a Mach 1.2 primary flow velocity is 17% (Figure 29). At half design pressure, the theoretical efficiency is 8.3%, and an expected power output on the order of 15 watts. UES's experimental results at half design conditions were below this expected value; only 70% of the expected current level was obtained. An independent test run by TRW engineers produced 9.4% efficiency, 17 watts at half design conditions. [6] It is believed that the 1/24" channel performs as expected if extreme care is taken to align the channel and adjust operating conditions exactly. However, under full design pressure, neigher UES nor TRW was able to obtain 17%.

There appears to be three problem areas that may be responsible for the poor results at full pressure; 1) the mobility of the charge carriers is too high, 2) there is excessive needle errosion under all operating conditions, and 3) the entrance collector area needs to be enlarged from its present 1.5:1 ratio to account for the increased spreading of the charge cloud at the collector. Further work by UES was stopped in order to direct effort to the use of other additives and working fluids.

$\overline{\rho} = 1.24$

$\eta_{el} = .38$

$$\Phi = \frac{v_p{}^2/2}{\phi} \; ; \; \eta = \frac{(1 + \overline{v}\,\overline{A})\,\overline{v}}{(\overline{\rho}\,\overline{v}^2 - 1)\overline{A}\,\Phi} \quad \text{(REF. 63)}$$

η_{el}

(%)

$.5 = \overline{A}$

$.356 =$

$.2 =$

$.1 =$

$.05 =$

$\Phi = 6$

$\Phi = 14$

$\Phi = 38$

$\overline{v} \; (v_p/v_s)$
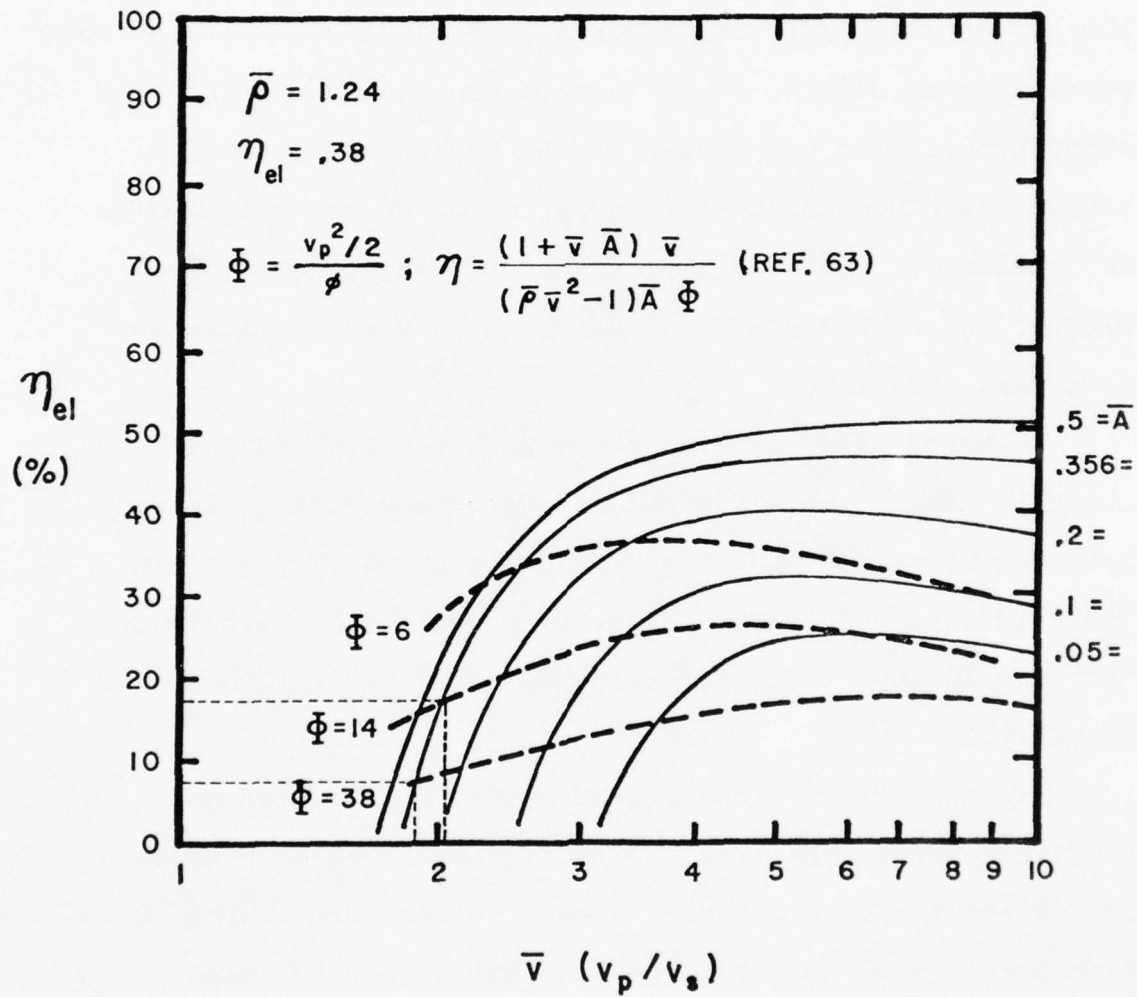
Figure 29. Theoretical performance of 1/24" EFD generator.

71

3. Pressure - Distance Scaling, 1/6" and 1/12"

In an effort to effect a more uniform field condition in the EFD channel, several electrode geometries were considered. The geometry producing the highest power and efficiency was the 80° attractor/60° collector sloped electrodes as mentioned previously in Section VI-C. A pressure-distance value of 2 atmosphere-inches was chosen at the beginning of scaling studies as a nominal operating parameter on which to design EFD channels. With the improvement brought on by sloped electrodes, higher p x d values could be used to increase power and efficiency.

In March 1974, ARL ran tests with the 1/6" 80°/60° channel. These tests yielded 168 watts and 6.8% efficiency for a primary Mach number of 1.2 and a p x d of 3 atm.-in. These results led to an attempt to produce a proportional increase in power and efficiency by using the 1/12" channel geometry.

Experiments were undertaken by UES in the High Bay Facility to test the 1/12" 80°/60° geometry at Mach numbers of 1.2 and 1.15. Pressure-distance values were increased from 2 to 3 atm.-in. by increasing the secondary total pressure from 24 atmospheres to 40 atmospheres. The $L/D_{channel}$ value was held constant at 5. Results are presented in Figures 16 and 17. Maximum performance was 13% efficiency at p x d = 3 atm.-in., 151 watts and M_p = 1.15 and 12.5%, 158 watts for M_p = 1.2 at 2.91 atm.-in.

These results indicated that the 1/12" 80°/60° channel,

72

like the 1/6" channel, could be scaled in accordance with EFD
scaling laws. Higher Mach numbers of 1.15 or 1.2 yielded
equally high efficiency at sonic conditions; that is, efficiency
at M_p = 1.15 or 1.2, p x d = 3 atm.-in., was equal to efficiency
at M_p = 1, p x d = x atm.-in. This may allow future designers
the option to use supersonic primary flow to produce condensation
in the primary flow while still obtaining efficiency levels
comparable to those of sonic conditions. Of major consideration
is the fact that an increase in total enthalpy extraction
can be obtained by using supersonic flow at high p x d
values. This was outlined in section VI F of this report.

B.   Design Consideration for High and Medium Temperature EFD Rigs

Past EFD research has primarily used air conditioned
with water as the condensing medium. Reasons other than the
convenience of these two materials include the fact that at
(nearly) ambient temperatures the amount of water vapor that
can be put into the flow is appropriate for the size channels
that have historically been used and the fact that water
and air are very compatible with many common engineering
materials such as plexiglass and stainless steel.

As one strives to improve the conversion efficiency
and/or output power of an EFD generator above that already
achieved with water and air in present generators, one can

readily see advantages to increasing the temperature level
of operation. With present geometries, and with air and water
and the EFD fluids, the new approach to scaling indicates
that as a generator is scaled down in size and up in pressure,
one needs to keep the same number of water droplets in the
channel, since the amount of current stays the same. Thus,
since the volume flow of the channel decreases with decreasing
size, while the pressure increases, it is necessary to increase
the specific humidity of the air in the channel to keep the
relative humidity of the flow constant. This can only be
done by increasing the temperature of the air and water to
increase the vapor pressure of the water. By looking at
Figure 30 which shows specific humidity as a function of temperature
(for saturated conditions) one can see that a doubling of
pressure requires approximately a 20°F. increase in tempera-
ture just to keep the same specific humidity. Thus, using
such materials as plexiglass places an upper limit of about
150°F on the operating temperature and with present geometries
and p x d values, this limits the size of the channel to 1/24".
Thus employing a different material than plexiglass would be
attractive to increase the efficiency level when air and water
are the EFD fluids. With this thought in mind a significant
effort during this contract was directed to building a
generator conversion section which would withstand significantly
higher temperatures than the plexiglass conversion section
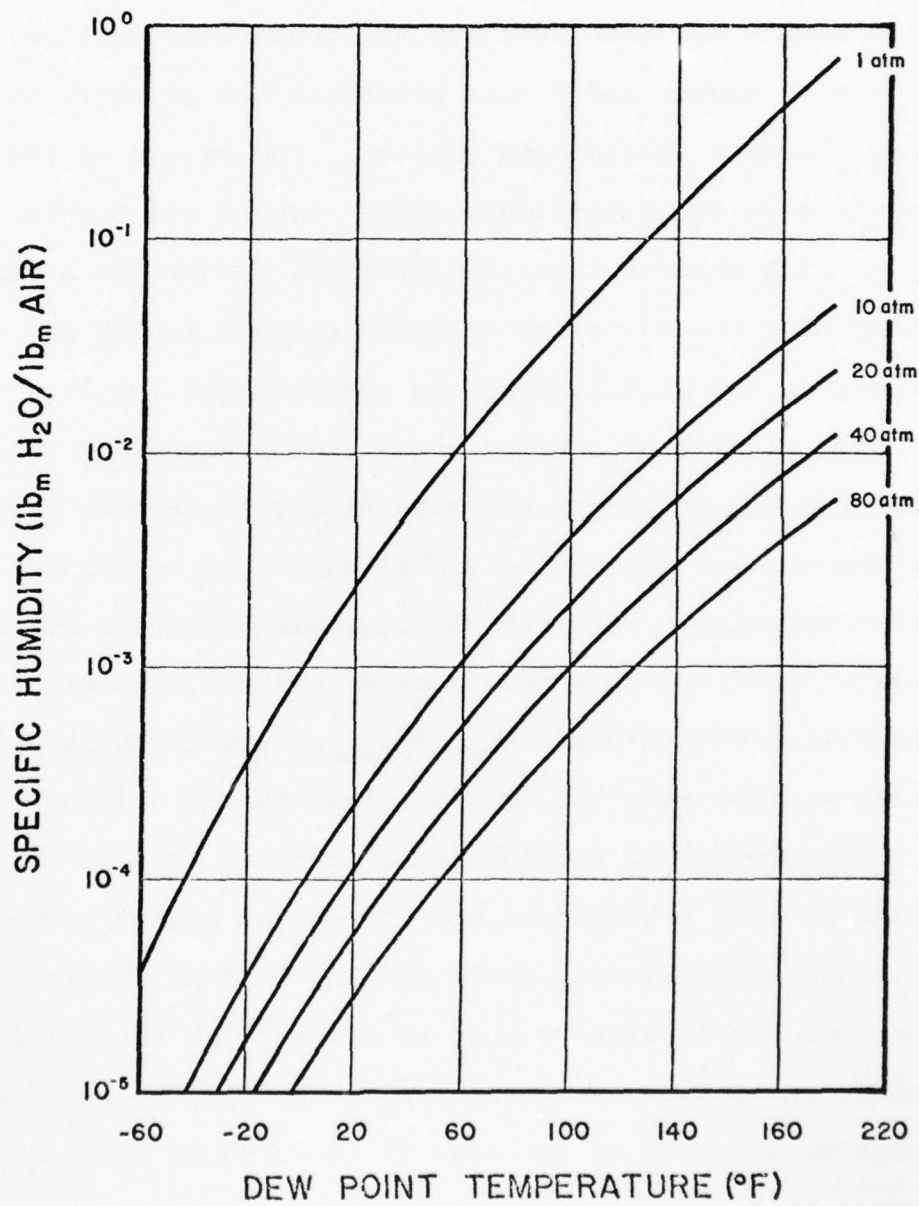
Figure 30. Specific humidity variation with dew point
temperature for water-air mixtures.

already used.

Several problems become apparent as one attempts to design such a new insulator for the conversion section. As one goes to higher and higher pressures the geometry of the channel becomes smaller and smaller. The result is that tolerances on the dimensions become tighter and tighter and, coupled with thermal expansion effects, results in a serious problem of maintaining the required channel length and symmetry at the high temperature and pressure levels.

The problem of sealing an internal chamber of this type from the total secondary pressure also becomes more severe with the smaller geometries. Sealing of the conversion section has always required considerable attention due to the sensitivity of the injector process to leaks, but with reduced volume flows with higher $Po_{sec}/P_{channel}$ levels the sealing problem against even very minute leaks become critical.

Resistivity of the insulator material also begins to take on very significant proportions at higher temperatures. Due to the high voltage levels and low current levels of EFD generators the insulators must be of very low resistivity. However, at elevated temperatures, especially in the region of 1200°R. which is of interest in the case of water at the critical point, there are very few insulators available with resistivity in the range of 10^{12} ohm-cm, which is required in order to keep electrical losses through the insulator low.

Other problems involve possible condensation of constituents of the flow on the surface of the insulator resulting in surface breakdown or even actual chemical reaction with the insulator.

The final design of the medium temperature conversion section is as shown in Figures 31 and 32. The insulator chosen for the conversion section insulator and also the nozzle/attractor insulator was Pyrex 1240 glass tubing, as it has satisfactory thermal expansion properties and electrical properties in the temperature range of interest (up to 300° F) for these experiments. Sealing the glass to the metal was most problematical, with the final design incorporating Kovar (a nickel alloy) cylinders heliarced to the stainless steel parts. The glass tubes were then epoxied with Armstrong high temperature epoxy (for use up to 350°F.) resulting in a good, relatively leaktight seal, with rigid mechanical strength for alignment of the electrodes. This design, which is compatible with all of the nozzles, attractors, and collector electrodes for the High Bay style generator, was used for the carbon tetrachloride tests and high temperature water tests discussed elsewhere in this report.

C.   Carbon Tetrachloride Tests

Carbon Tetrachloride was perceived to be a favorable fluid for use in EFD generators because of its high breakdown
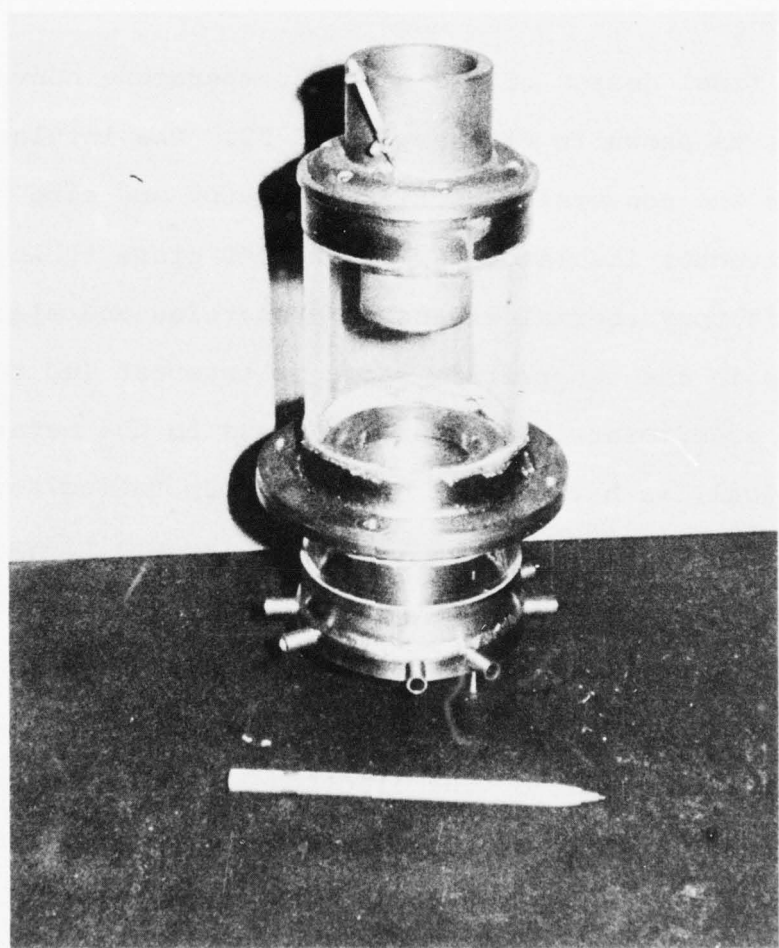
Figure 31. Assembled view of glass EFD conversion section
as used in High-Bay experiments.
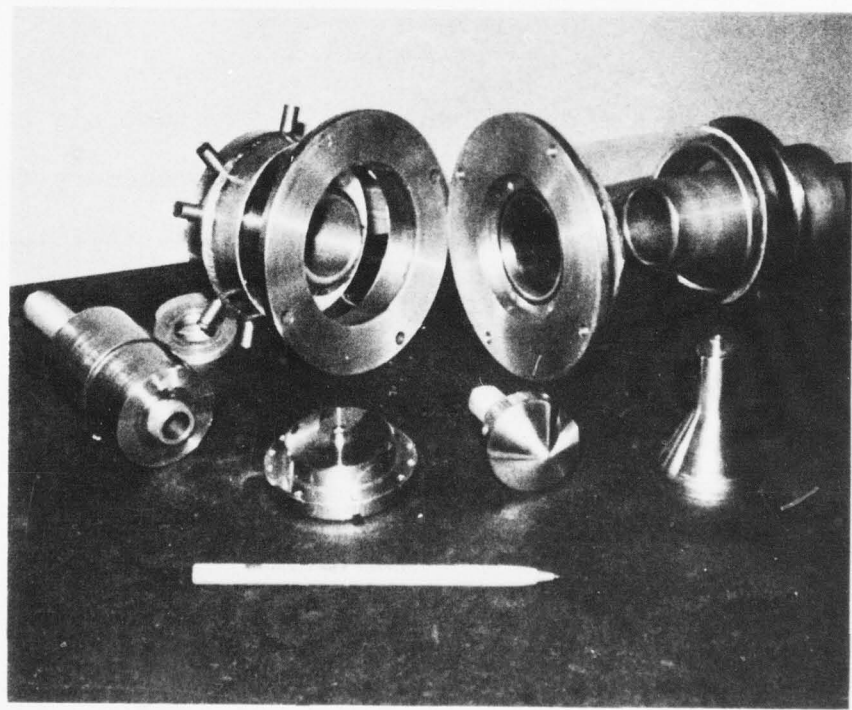
Figure 32. Exploded view of glass EFD channel with related parts.

strength ($E_{bCCl_4} \simeq 6xE_{b_{air}}$), nonflammability, and reasonably
attractive thermodynamic properties. Attempts were made to
use CCL_4 both as an additive to air as the working fluid and
as the pure working fluid.

1. CCL_4 Additive Tests

In the CCL_4 additive tests, experiments were conducted
both with water as the additive and with CCL_4 as the additive.
These experiments are described below. The test rig had
been modified to permit the passage of all secondary flow
entering the conversion section through an external tank
so that the secondary flow could be saturated with the additive.
See Figure 1. To keep the ratio of CCL_4 to air as large as
possible, and thus determine the effects of the additive,
the tests were conducted in the 1/6" diameter channel using
the M_{pri} = 1.5 nozzle and the 60° collector/80° attractor
geometry. The tests involved using the secondary flow bypass
system which permits all or part of the secondary flow going
into the conversion section to pass through a high pressure
tank which contains another agent (in this case water or
carbon tetrachloride) for conditioning of the secondary flow
with additives. This was done to increase the relative
humidity of the flow or to increase the breakdown strength
of the secondary flow or both. Initially, water was used in
the conditioning tank in order to determine the effect of

80

MICROCOPY RESOLUTION TEST CHART

NATIONAL BUREAU OF STANDARDS-1963-A
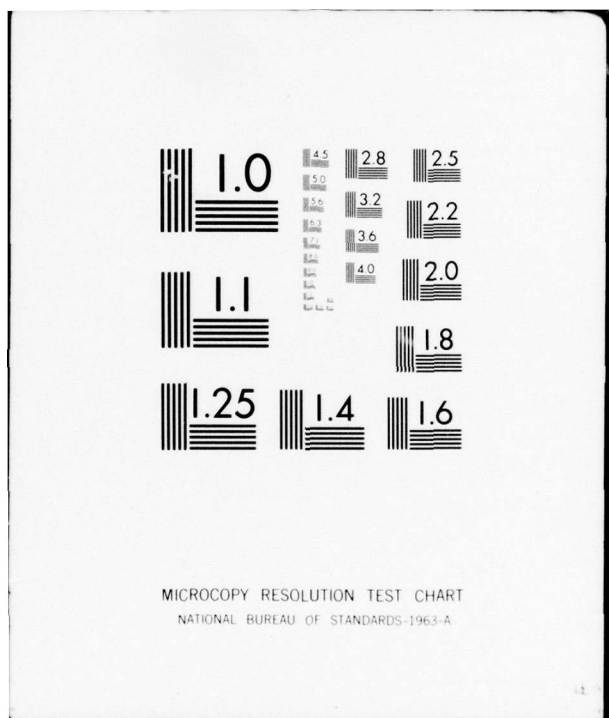
very high secondary flow relative humidity (approximately 100%) on the collected current. The effect appeared to be substantial. For example, operating with a P_{os} = 126 psia and a primary Mach number of 1.5, the grounded and 6 resistor (532 megohms) collector current levels were 190 and 140 microamperes, respectively. When the secondary flow was recirculated through the water tank resulting in a secondary flow relative humidity of about 97% the collected current increased to 250 and 218 microamperes under grounded and 6 resistor load conditions, respectively. Additional tests indicated similar favorable results. Visual observation of the channel operation did not show any noticeable secondary flow condensation phenomenon occuring.

After the favorable results of the increased secondary flow relative humidity was observed, the additive fluid was changed from water to carbon tetrachloride. Carbon tetrachloride has a vapor pressure of about .14 atmosphere at ambient temperature, resulting in a percentage (by weight) of about 5.8% when the secondary flow is saturated at 180 psia (12 atmospheres). According to the literature, this should result in a dielectric strength increase of 25% over that of air. In order not to overstress the high voltage lead out of the high pressure rig (due to excess collector voltage) the operating pressure level was reduced to P_{os} = 126 psia.

Experimental results with the CCL_4 were quite favorable. Observation of the channel showed a very distinct region of

81

secondary flow condensation along the surface between the secondary and primary flows. Collected current increased dramatically under grounded conditions as did the needle current, with the needle current increases reflecting the increased dielectric strength of the secondary flow and the collected current showing the effects of both the increased dielectric strength and the effects of secondary flow condensation. An example of the change in results with the added carbon tetrachloride in the secondary flow is shown in Table 5.

As with the water humidified secondary flow, several additional test runs indicated similarly good results.

2. CCL_4 Working Fluid Tests

Several tests were made utilizing pure carbon tetrachloride as the EFD fluid. In the first two cases the geometry was similar to that employed in the tests where air with water was used as the condensing medium. The 1/6" diameter scaling geometry was installed, with the needle to nozzle length set at .080", nozzle attractor length set at .065", and the collector turned out 11 turns (.55"). Since the high voltage lead out cable was not suitable for use with hot CCL_4, a Teflon Conax feedthrough was used with the collector grounded through a milli-ammeter.

The operating procedure was to heat up the rig and tubing to about 225°F in order to prevent condensation of the

82

TABLE 5. CARBON TETRACHLORIDE ADDITIVE TEST RESULTS

$Po_{pri} = 463$ psia

$Po_{sec} = 126$ psia

$To_{pri} = 115°F.$

$S_{pri} = 78\%$

1/6" channel, 60° collector, 80° attractor, $M_{pri} = 1.5$

Operation with no CCL_4 in secondary flow:

KV_{att}	I_{att}	I_{needle}	$I_{collector}$	$KV_{collector}$
(KV)	(UA)	(UA)	(UA)	(KV)
31.8	145	431	270	0
33.1	180	425	230	19.1
33.0	180	418	220	37.5
33.6	190	420	215	56.7
32.3	180	400	208	74.0
33.0	185	406	205	91.0
32.0	170	390	205	108.0

Operation with CCL_4 in secondary flow:

46.6	295	740	435	0
45.2	285	730	375	31.1
45.8	305	670	345	59.0
47.0	320	670	335	88.5
45.5	305	650	320	114.0
44.2	295	620	300	133.0
44.5	290	615	275	147.0

83

carbon tetrachloride vapor, to heat up the CCL_4 liquid in the boiler to the temperature corresponding to the vapor pressure needed for the primary Mach number desired, and to then run the test. The hot rig chamber was evacuated and purged with nitrogen several times just prior to the run in order to greatly reduce any oxygen which might react with CCL_4 in the presence of an electric discharge (corona) and thus produce undesirable products. The experiment was started with a partially evacuated chamber (about 1/3 of an atmosphere) in order to achieve a high Mach number primary flow (which would be advantageous for condensation) initially and then to approach a steady state condition with primary pressure corresponding to the design Mach number and the secondary pressure set to slightly above 1 atmosphere.

In the first experiment CCL_4 vapor at 205°F. (11 psig) was expanded into a total secondary pressure ranging from about 5 psia up to 16 psia. Initially, the secondary flow was nitrogen gas but as the secondary pressure rose to one atmosphere the partial pressure of the CCL_4 increased. At first, with the secondary gas predominately nitrogen, condensation in the channel was observed, but it appeared to be only in the secondary flow and was probably caused by the expansion of the nitrogen (with a higher γ than CCL_4) resulting in condensation of the CCL_4 vapor in the secondary flow, a phenomenon observed in previous experiments. However, electrical tests at several pressure ratios corresponding to

84

primary Mach numbers from about 1.8 down to less than 1.0
resulted in adequate needle current (over 100μA) but with
maximum collector current of only 2 to 3μA. This indicated
that no condensation was occuring in the primary flow. This
is predicted for fluids with very low gamma values that are
expanded to such low Mach numbers.

A second test was run with a somewhat lower initial
Mach number (1.4) and a somewhat higher final Mach number (1.15)
but starting this time with pure CCL_4 vapor as the secondary
fluid instead of nitrogen. No visual evidence of condensa-
tion was observed and again only 2 or 3 micro-amperes of
current were collected in spite of more than 100 micro-amperes
of needle current. Thus, these experimental results indicate
that using such fluids as pure CCL_4 and the Freons which also
have low γ values will require methods (such as electro-hydro-
dynamic spraying) for producing charged droplets.

3. Carbon Tetrochloride Humidification Tests

An additional investigation of channels using CCL_4 instead
of water as the additive to the primary and secondary flows
was undertaken. The High Bay Facility was modified as shown
in Figure 1. For this series of tests, the 1/12" channel was
used with the 80°/60° electrodes.

The results of this investigation are presented in Table
6 for both air/water and air/carbon tetrachloride runs. Notice
that the air/water results were lower than previous tests with

TABLE 6. TEST RESULTS WITH AIR/WATER AND AIR/CARBON TETRACHLORIDE
WORKING FLUIDS

AIR / WATER

MACH	PRESSURE		CURRENT	POWER	EFFICIENCY
prim.	prim.	sec.	@ ground	watts	%
	psia	psia	μ A		
1.2	435	180	235	11.9	2.82
1.1	385	"	235	16	4.79
1.0	340	"	205	16	6.24
1.0 *	340	"	220	17.9	6.98
0.9	305	"	136	10	5.29
0.9 *	305	"	122	10.7	5.66

P x D = 2 ATM- IN. :

1.2	875	360	340	41.8	4.86
1.1	770	"	340	53.2	7.94
1.0	723	"	345	49.5	8.43
0.9	610	"	210	28.8	7.55
0.9 *	610	"	234	29.9	7.84

AIR / CARBON TETRACHLORIDE

1.2	435	180	240	15	3.66
1.1	384	"	234	18.7	5.83
1.0	339	"	250	22.8	9.26
0.9	304	"	140	12.4	6.84

1.0	723	360	300	43	7.32
1.0	520	275	150	—	—
1.1	770	360	260	37.6	5.61

* WITH SECONDARY HUMIDITY

the same working fluids. For example, with the 80°/60°
geometry at a p x d = 2 atm.-in., at a primary Mach number
of one, the present generator produced only 8.43% efficiency
whereas this configuration was formerly 12 to 13% efficient.
Because of scheduling and deadlines. it was decided to use
these lower results as a basis of comparison for the CCL_4
additive. It was felt that a relative comparison of the worth
of CCL_4 as a humidification-additive agent could still be
made.

It is apparent from Table 6 that at a p x d = 1 atm.-in.
(1/2 design pressure), the air/CCL_4 system is superior to
air/H_2O. A maximum of 9.26% efficiency at M_p = 1 was obtained,
versus 7% with water. At a p x d = 2 atm.-in., the CCL_4
additive was inferior to water, even with the CCL_4 added to
the secondary. Perhaps the optimum for air/CCL_4 is only
at p x d = 1 rather than 2 or 3 atm.-in. as with air and
water. The optimum p x d value for other working fluids is
one area that has not been covered by any researchers in EFD
and would be valuable research area in the future.

Further tests toward optimization of the air/CCL_4
system were curtailed on 30 June at the end of the experimental
research program.

D. Vena Contracta Electrodes

It was postulated that a sharp separation of the

87

secondary flow in the secondary (attractor) nozzle would lower the loss coefficient in the channel. This effect would be demonstrated by producing a higher secondary Mach number upstream from the channel than would have been produced by a normal attractor. A vena contracta electrode was chosen to create the sharp separation and was designed to be tested in the 1/6" channel. Three electrodes were fabricated. All had a sharp 90° entrance radius on the .216" diameter throat. This diameter was chosen to yield an effective vena contracta diameter of 1/6". Electrodes VC_1, VC_2, and VC_3 are shown in Figure 33. Electrode VC_1 resulted in a slightly lower secondary Mach number than the conventional 1/6" attractor, $M_S = .59$ vs $M_S = .74$ @ $M_p = 1.2$. This test used the conventional 1.5:1 area ratio, 60° collector inlet at 11 turns separation from attractor. By using a 1.7:1 area ratio, 60° collector, M_S was improved to .69. Electrical performance was impaired with only 34 watts vs. 75 watts with the conventional electrodes for the same flow conditions.

Electrode VC_2 produced a good secondary Mach number, .79, with a 1.5:1 collector. This was comparable to the standard attractor; however, here also, the electrical performance was substandard, netting only 26.5 watts. Electrode VC_3 also required the 1.7:1 to provide a satisfactory Mach number of .63. Electrical power was 38 watts.

From the need for a large area ratio (>1.5:1) collector
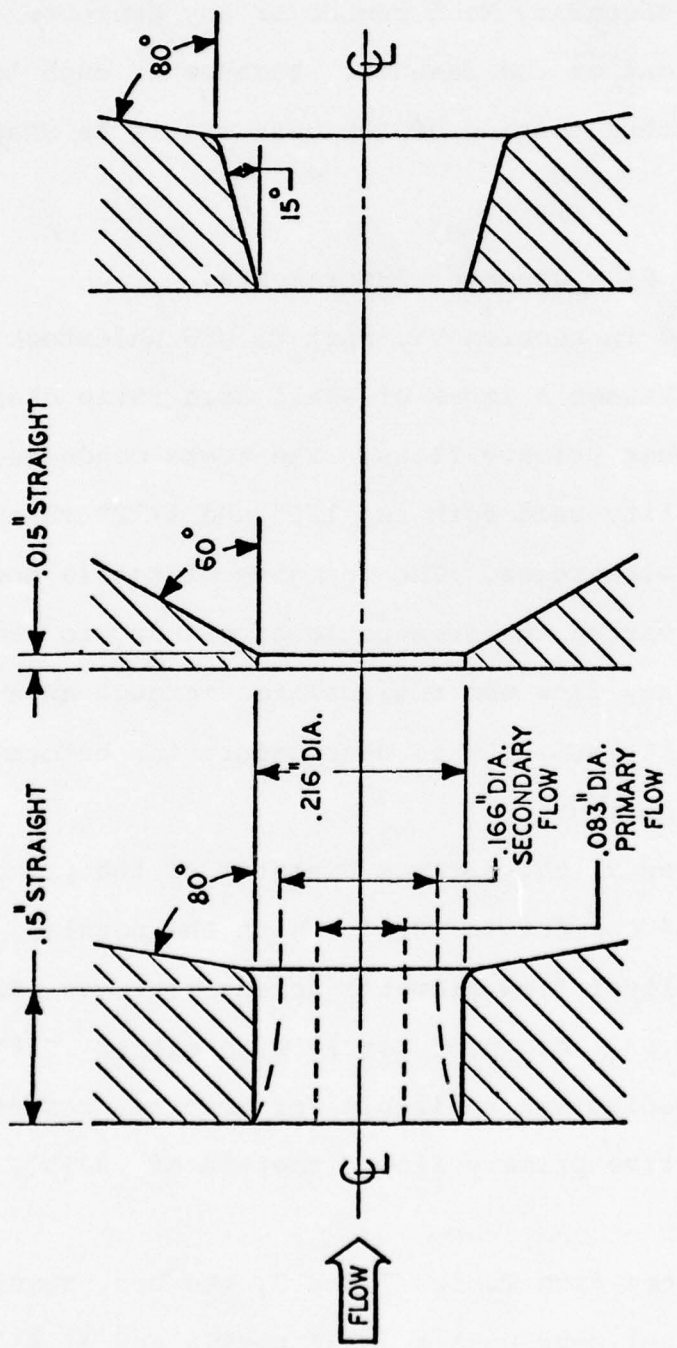
Figure 33. Vena-contracta electrodes.

it was concluded that the flow was not being contracted to
0.167" as expected. The tests also indicated little, if
any, increase in secondary Mach number or any decrease of
the loss coefficient of the channel. Because of such low
power output, further testing of the vena contracta shapes
was cancelled.

E.   Small Primary Flow Diameter Experiments.

As mentioned in section VI, part F, UES undertook
tests to confirm Lawson's ideas of small area ratio channels
and high Mach number primary flows. The tests conducted in
the High Bay Facility used both the 1/6" and 1/12" channels
with the 80°/60° electrodes. The changing of nozzle and
needle diameters varied the area ratio of primary to secondary
flow. The secondary flow was recirculated through an external
loop to increase its humidity to near saturation before it
was returned to the rig.

From equation 3, the optimum diameter of the primary
orifice for a 1/6" channel is .021". With the nozzles
available the smallest flow diameter arrangement was .026".
A combination of .033" or .039" nozzle with either .010" or
.020" diameter needles was available for testing presenting
a choice of effective primary flow diameters of .0315", .0262",
and .0335".

As can be seen from Tables 7 and 3, the best results
for the 1/6" channel were with a .033" nozzle and a .01"

90

needle for an effective flow diameter of .0315". Maximum power was 40 watts with 9% efficiency at M_p = 1.5. Without the extra secondary humidification the maximum current was only 58μA and the power was decreased to 2 watts. Thus, with a low secondary Mach number of .3 it is necessary to humidify the secondary gas separately.

The same reasoning applies to the 1/12" geometry. Most secondary Mach numbers were on the order of .45, depending on primary flow diameters and Mach numbers. From Tables 7 and 3, optimum results were 16.4% efficiency and 55.5 watts with a .0195" diameter flow and approximately 75% secondary relative humidity. With a dry recirculating secondary the power was 42 watts at M_p = 1.5. With decreasing primary flow diameter, the humidity level of the secondary flow became an increasingly important factor. With primary flow diameter = .015", 72μA were collected at ground for 0% secondary humidity and 150 μA for 75%.

A typical current voltage characteristic for the small flow channel is shown in Figure 34. Low current-high voltage operation was common. Frequently the maximum power was at 1000 MΩ resistance, the largest resistance available in the High Bay Facility. Many tests resulted in a loud electrical discharge along the external output cable. When the secondary humidity was greater than 90% surface sparks were observed on the inside of the plexiglass insulator between collector and attractor. Table 7 includes results

91
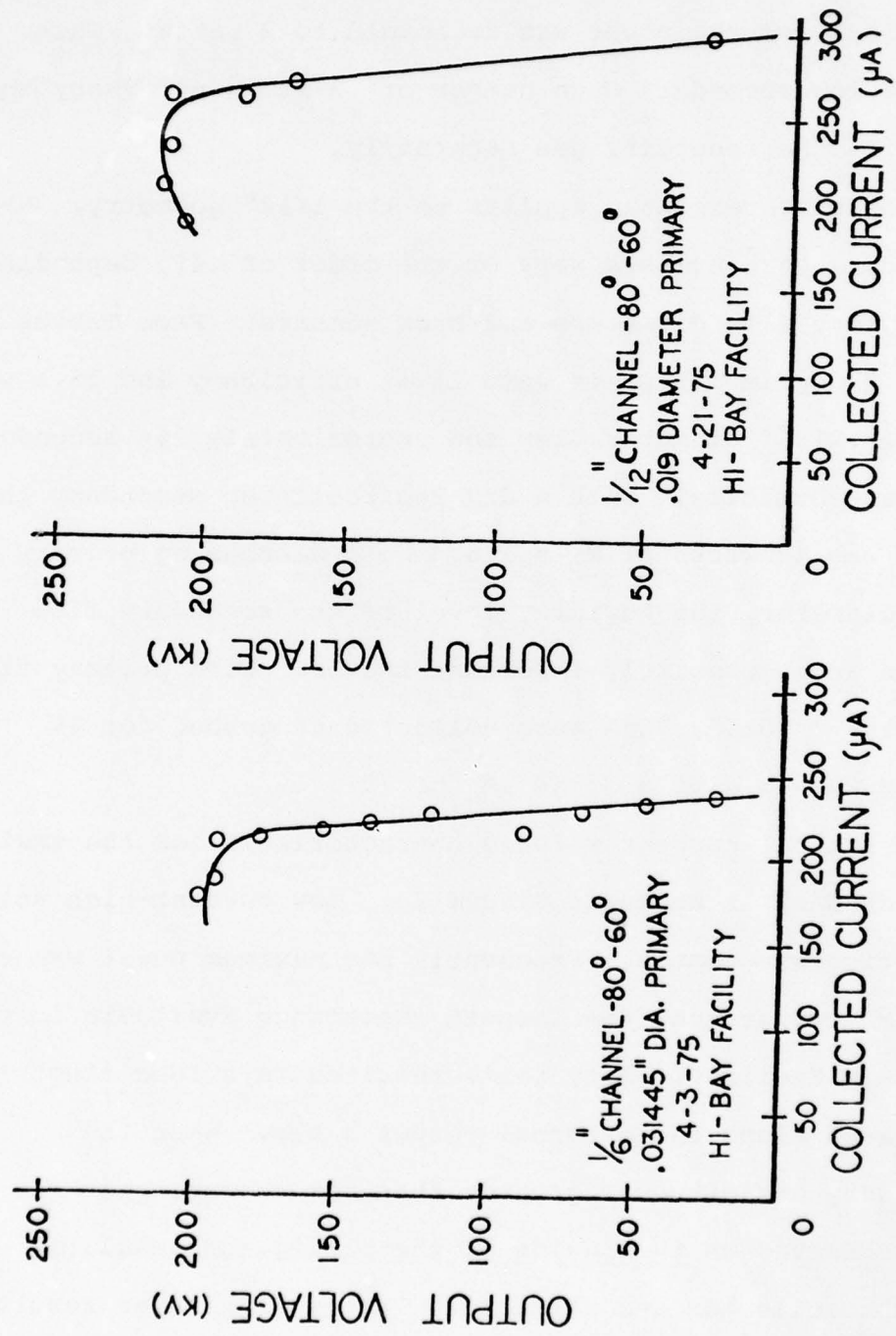
Figure 34. Typical voltage-current characteristic for small primary flow diameter tests.

TABLE 7. SMALL DIAMETER PRIMARY TEST RESULTS

ATT. SIZE	NOZ. DIA. (inches)	NDL. (inches)	$Dp_{eff.}$ (inches)	L/D	PSIG Ppri.	PSIG Psec.	RH % PRI	RH % SEC	MACH NO. PRI	MACH NO. SEC	I coll. (μ amp)	OUTPUT VOLTS (kvmax.)	OUTPUT POWER (watts)	η %	ΔHo %
1/12	1/12	.02	.0425	4.2	597	345	74	0	.9	.632	260	24	6.24	1.59	0.22
1/12	1/12	.02	.0425	4.2	562	345	73	73	.85	.6056	235	21.7	5.09	1.56	0.2
1/12	.0185	.01	.01556	4.2	1400	345	84	81	1.55	.462	162	180.3	29.16	12.49	4.05
1/12	.0185	.01	.01556	3.9	1400	345	83	83	1.55	.462	165	169.6	27.98	11.9	3.86
1/6	.033	.01	.03145	4.2	646	165	63	85	1.5	.342	237	21.9	5.19	1.2	0.37
1/6	.033	.01	.03145	4.2	646	166	70	85	1.5	.353	206	190.6	39.14	9.0	2.8
1/12	1/24	.01	.01951	4.2	1305	345	75	75	1.5	.531	285	179.3	51	15.26	4.74
1/12	1/24	.01	.01951	4.2	860	345	75	80	1.2	.3547	128	142.5	18.24	9.8	2.1
1/12	1/24	.01	.01951	4.2	1135	345	68	74	1.4	.4515	212	196.1	41.57	14.8	4.16
1/12	1/24	.01	.01951	4.2	1425	345	65	75	1.56	.536	300	188.7	56.61	15.18	4.97
1/12	1/24	.01	.01951	4.2	1305	345	66	70	1.5	.517	260	213.46	55.49	16.45	5.1

of tests at Mach numbers other than 1.2 or 1.5. Maximum efficiency was at M_p = 1.5 in most cases.

In addition to the increase in operational efficiency from a nominal 12% for sonic flow is a 1/12" channel to 16-1/2% at M_p = 1.5, there was a considerable increase in enthalpy removal. Table 7 **shows** that the enthalpy extraction increased from 2.3% to 5.1% by using small diameter-high velocity primary flows. Indeed, the use of properly designed nozzles and matched primary flow diameters and primary to secondary velocity ratios proved to be one of the most significant contributions to EFD progress during this contract. This is one of the most interesting areas for future research on improvement of efficiency and energy removal for EFD channels.

F. Electrohydrodynamic Spraying

During this contract an effort was made to produce charged droplets in a flow through the application of electro-hydrodynamic spraying. In this process a low conductivity fluid emerges from the tip of a capillary tube in the presence of a very high electric field. The field induces large forces on the surface of the liquid resulting in the rupture of the liquid surface and the subsequent spraying of extremely small charged droplets into the gas flow.

Electrohydrodynamic spraying can be employed to ensure

94

that sufficient moisture enters the flow so that enough droplets are provided to carry the charge down the channel. The problem of too many charge carriers of too small a size, as mentioned in section VII B of this report, becomes increasingly critical with smaller geometries and higher pressures. With the trend toward small size and high pressure, electrohydrodynamic spraying becomes an attractive alternative to a corona process for producing charge carriers at moderate temperatures.

Present EFD geometries are reasonably well suited for adaption to EHD spraying. The attractor electrode can apply a high field to the needle (capillary tube) which would transport the liquid to the region of the primary flow nozzle. The 1/6" test rig nozzle/needle configuration was modified to handle a .020"OD/.010 ID stainless steel tube for use in place of the solid .020" diameter needle electrode. See Figure 35. Experiments were conducted with the spraying tube position variable from a point several tube diameters inside the nozzle to a point several tube diameters outside.

High voltage could be applied to both the nozzle and the attractor independently to obtain very high field strengths at the tube tip. The edge of the tip of the tube was rounded to minimize corona effects. The liquid flow rate was controlled with a micro metering valve located at the liquid supply line. Pressure, independent of primary and secondary

95
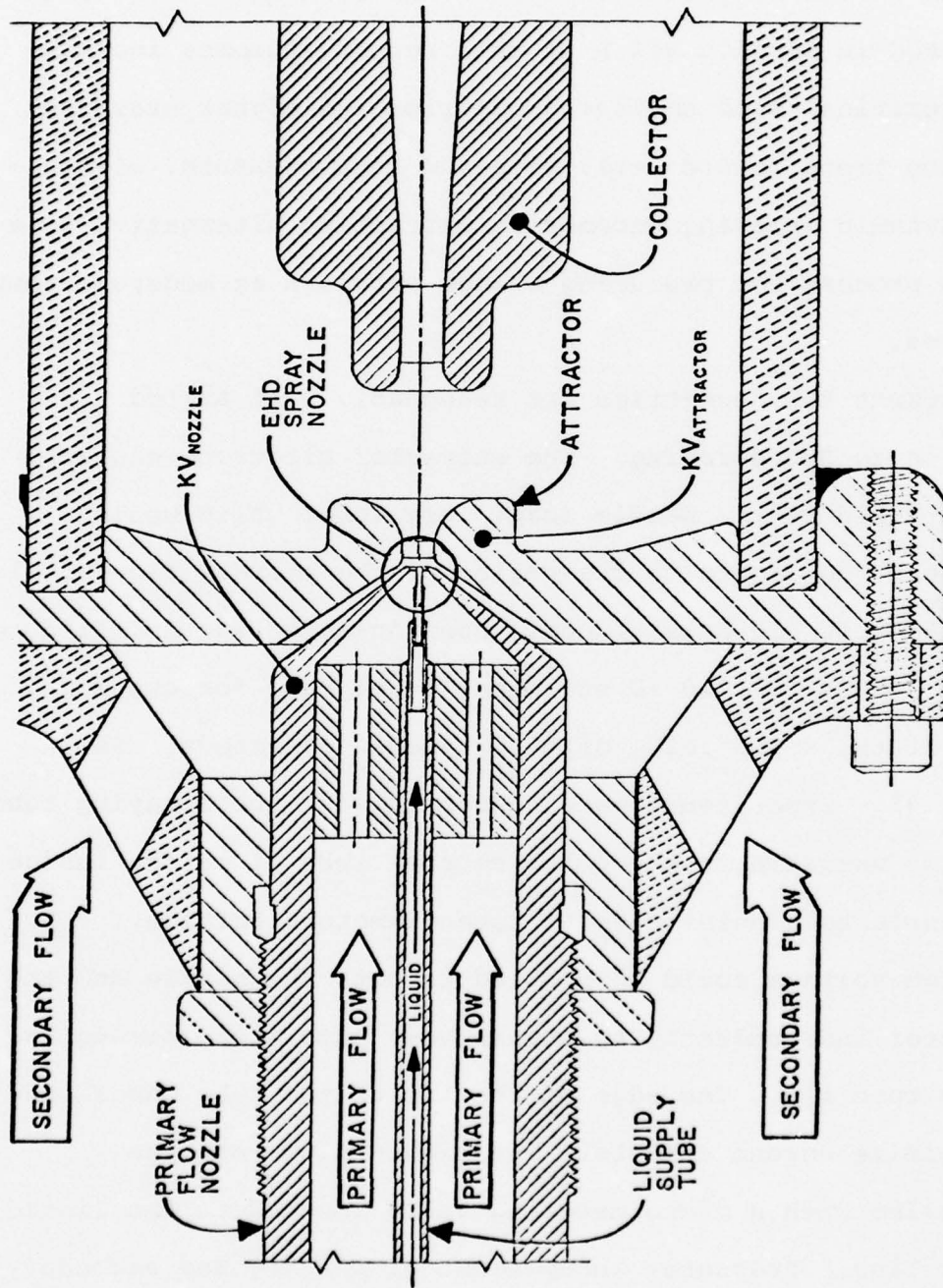
Figure 35. Electrohydrodynamic spraying EFD configuration.

gas pressure levels, could be applied to the EHD liquid. The liquid volume flow was measured with a calibrated orifice.

This system was tested at various pressure levels, flow rates and tube positions. Under no operating condition did collector current exceed levels expected from dry (ion only) operation. This result can be explained if the droplets produced were large and highly charged thus having a mobility similar to that of ions. The current from the EHD spray tube went directly to the attractor instead of the collector.

Under conditions of low attractor voltage (less than the voltage required for corona current was detected in the tube-attractor circuit indicating that charge was being transported by the droplets. Increasing the flow rate, the applied voltage or the pressure level, or varying the spray tube position did not appreciably alter the collector current level.

At higher wet flow rates (near levels required for flow saturation) EHD spraying produced a visible stream of droplets which wetted the channel and insulators causing current shorts.

In an effort to achieve larger volume flows without wetting, CCL_4 as the EHD medium was tested. Since CCL_4 has a higher vapor pressure than water, a larger volume flow is possible at the same operating temperature. At the increased volume flow rates, however, collected current levels were still only a few microamperes, again showing that large ion-behaving droplets were being produced.

SECTION VIII

CONCLUSIONS

1. A new approach to scaling which is based on the laws of similitude for electrical discharges suggests that the product of the gas density and characteristic channel dimension be kept constant, resulting in constant electrical performance for EFD generators but increasing efficiency at high gas pressure levels. Experiments by UES verify this scaling approach when applied to a 1/2", 1/6", and 1/12" EFD test generators. A conversion efficiency of 12% of kinetic power of a sonic flow into electrical power was achieved for a 1/12" EFD channel. The further application of the scaling technique to a 1/24" channel did not produce the desired efficiency. The 1/24" channel may be the smallest EFD channel useful with air and may still perform as expected if the three problem areas outlined in Section VII,A,2 can be overcome.

2. An improvement in EFD generator performance was obtained by using sloped electrodes. It was found that one could extend the operating range of EFD generators by increasing the pressure level for a fixed size channel if sloped electrodes were used. The electrodes yielded a more uniform electric field in the channel, resulting in a pressure squared effect on the output power. The best results were 7.1% efficiency, 174 watts for the 80° attractor-60° collector combination in the 1/6" diameter channel at a p x d value of 3 atm.-in.

98

Scaling to the 1/12" channel with the 80°/60° electrodes was successful, with the 1/12" channel producing 155 watts and 12.5% efficiency. This corresponds to a 2.75% total enthalpy removal by electrofluid-dynamic forces.

3. The optimum p x d parameter for EFD channels using air as both the primary and secondary working fluid and humidified with water was 3 atm.-in. This value was obtained from tests on channels with sloped electrodes and may be extended beyond 3 atm.-in. if electrode shapes can be designed to produce a more uniform electric field in the channel.

Tests on similar channels using carbon tetrachloride as the additive to air showed an optimum p x d of 1 atm.-in. The p x d parameter depends not only on electrode shapes but also on the working fluid.

4. A properly matched primary injection flow to secondary flow produced the highest efficiency of all the test runs on EFD channels under this contract. A maximum of 16 1/2% efficiency and 5% total enthalpy removal was achieved using a .02" primary flow at Mach 1.5 to power a 1.12" channel. Still further increases in efficiency may be gained with more optimum matching of the primary injector to the secondary EFD flow as outlined in this report.

5. Tests with carbon tetrachloride as a primary working fluid under grounded collector runs showed that the corona charging

process could provide adequate needle current. However, only 3% of the generated current was collected, indicating large droplet sizes or a high charge to mass ratio droplet. Fluids with low γ values require other methods for producing charged droplets of the proper low mobility for EFD applications.

6. Electrohydrodynamic spraying experiments failed to provide low mobility charged droplets with either water of CCL_4 as the working fluid. Current from the EHD spray tube went directly to the attractor instead of the collector. Since the EHD tests were of a limited scope, EHD charging of the primary flow should not be ruled out as a means of providing charged colloids for EFD generators.

PART II

MULTI-COMPONENT FLOW (MCF)

SECTION I

INTRODUCTION

During the first half of this contract, the research
under multi-component flow included experiments principally
on swirl flow erosion, high pressure swirl flow particle
containment, hot particle erosion, Prandtl-Meyer expansion
and helium-air mixing. In the latter half of the contract
emphasis was shifted to pressure recovery studies connected
with gas dynamic and chemical lasers. These included studies
in supersonic diffusers, radial outflow diffusers, and ejector
pumps, where most of the effort was concentrated in the last
year of the contract.

SECTION II

SWIRL FLOW

Experimentation on advanced swirl chamber designs and characteristics had been nearing completion at the start of this contract. These tests had been conducted to determine the properties of highly loaded particulate swirl flows for applications in colloidal core nuclear rocket concepts. The efforts at the start of this research were directed toward achieving stable, highly loaded swirl flows and studying particle loss rates, swirl stability and container wall erosion by particles.

A.   Swirl Flow Vane Erosion Experiments

Tests were conducted to determine an optimum angle at which the inlet swirl-driving gas can be injected into the particle-containing chamber to maintain a stable vortex while providing at the same time a gas shield for the chamber walls against erosion by the particles. Experiments were conducted to determine vane erosion rates as a function of vane injection angle. These tests consisted of weighing each individual vane before and after a timed test run. Injection angles up to 80° were found to provide a stable swirl and minimum erosion rates.

B.   High Pressure Swirl Flow Particle Containment Experiment

This work consisted of setting up and instrumenting a

specially designed high pressure swirl chamber. The chamber
was operated with six pounds of powder in swirl containment
with an inlet gas pressure of 450 psi and a gas mass flow of
four pounds per second. Experiments confirmed a low particu-
late loss rate through the chamber which infers a stable swirl
flow.

C.   Hot Particle Erosion Experiment

This experimental test program was designed by Capt.
Bobby Turman, formerly with the Air Force's Aerospace Research
Laboratories, to determine the erosion rate of materials sub-
jected to a high temperature jet of particle laden gas. The
important parameters for analysis in this work were the temper-
ature and velocity of the multicomponent jet and the temperature
of the sample in the jet stream. Particles were fed into a
stream of nitrogen and mixed in a long tube. The gas particle
(Zirconium Carbide) mixture was heated by passing through an
oxy-acetylene flame. The heated mixture was directed by a noz-
zle onto a sample (Tungsten Carbide) inside the test chamber.
The test chamber was purged with nitrogen during the test run.
By timing the particle injection and using a predetermined mass
of mesh-sized powder and gas flow rate the particle number den-
sity was computed. The temperature was monitored using thermo-
couples. The sample was precisely weighed before and after
each test run.

Particle velocity was measured as a function of temperature using a laser doppler velocimeter operated by Capt. Charles Miller of ARL. Tests were conducted over a temperature range of 20° to 900°C.

A detailed description of the apparatus, procedure, and results is given in ref. 8 . The data showed good correlation between particle temperature, velocity and sample erosion rate.

SECTION III

PRANDTL-MEYER EXPANSION EXPERIMENTS

This program was one of a series of programs by many investigators to study the feasibility of applying multicomponent flow processes to the design of aerodynamic and erosion test facilities, as outlined as "Reentry Heating Energies Analyzer (RHEA)", (ref. 9). The concept calls for a series of particle-gas stages to impart to air a very high enthalpy for wind tunnel applications. Separation of the particles from the gas flow would be necessary before the first stage. The experiments reported here were designed to study particle separation efficiency from a flowing gas-particle mixture by a Prandtl-Meyer expansion of the gas. The test program was conceived by Capt. Bobby Turman of ARL.

The design of the apparatus is shown in figure 36 . The experiment consisted of an air supply, a powder injection mechanism, the Prandtl-Meyer Expansion flow chamber, a powder weighing balance and associated pressure regulators, transducers, and electronic equipment. Shadowgraph and schlerien visualization of the shock waves were made.

Johnson's Baby Powder (a mixture of talc, asbestos and perfumes) was initially used as the particulate load material. Because of the health hazards of talc from the powder that escapes into the testing area, calcium carbonate ($CaCO_3$) was used in the latter half of the tests.

106
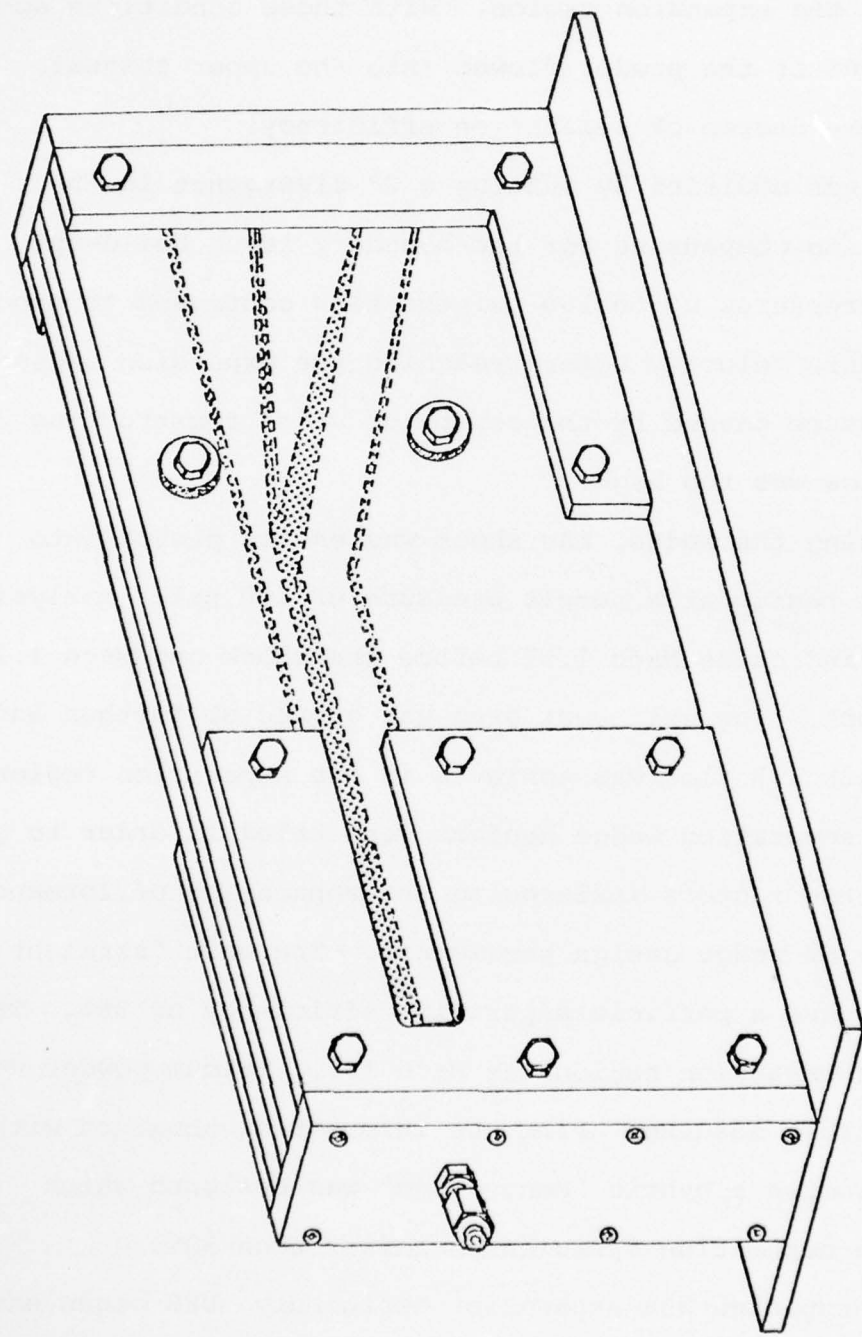
Figure 36. Prandtl-Myer expansion rig.

The first testing series with the apparatus showed subsonic conditions in the expansion region. With these conditions approximately 60% of the powder flowed into the upper channel, indicating some degree of separation efficiency.

The rig was modified by putting a 2° divergence in the channel walls to compensate for the boundary layer build-up. With nozzle pressures up to 160 psi the flow continued to shock down to subsonic velocity before reaching the expansion region. The back pressure caused by the separator wedge constructing the outlet flow was too high.

By removing the wedge, the shock was easily pushed into the expansion region at a nozzle pressure of 100 psi. Analysis of the shock indicates Mach 1.57 before the shock and Mach 1.15 after the shock. The exit duct area was opened up further and supersonic Mach 1.5 flow was achieved in the separation region.

Various separation wedge designs were tried in order to get a measure of the factors influencing the separation performance as a function of wedge design parameters. The best "straight" wedge design gave a particle separation efficiency of 86%. The flow into the expansion region was Mach 1.5. Talcum powder was used for particle loading. From the information obtained with the various wedges a hybrid "bent wedge" was designed which should show a separation efficiency greater than 90%.

With an expected 90% separation efficiency, UES began experimentation with methods to recirculate the recovered powder

back into the flow stream. One should be able to re-entrain the powder collected in the separator section and collect the powder at the exhaust duct. Also, by measuring the initial powder mass and timing the experimental run a more accurate measure of powder loss rate can be obtained.

A tube from the exit region of the flow channel which led back to the entrance of the flow channel was installed. The particles which were separated in the expansion region were re-entrained in the primary flow by an ejector-driver nozzle. However, a high percentage of particles remained in the flow indefinitely. It is believed that the particles which remained in the flow were of such a size and mass that their trajectories in the separator region kept them continuously in the flow.

Further tests on the Prandtl-Meyer (P-M) rig showed the expansion region of the P-M rig appeared to be too great of an expansion. We have observed flow separation in this region by the Schlerien system and also by the stagnant particles which appeared to collect in the separated region. This indicates that a smaller expansion angle was necessary. At the pressure and flow conditions of operation and due to the limitations on size and channel length caused by particle trajectory consider- ations a smaller expansion angle was unacceptable. At the ideal fluiddynamic expansion angle the particle separation wedge would have to be located so far downstream that the particles would re-enter the primary flow stream before reaching the wedge. In

addition, the present P-M rig was constructed of aluminum and plexiglass and has eroded to the extent that supersonic conditions cannot be maintained at previously used pressure levels.

For these reasons, thought was given to applying a different principle to the particle separation problem. Experiments were performed to determine the minimum radius of curvature that a Mach 1.5 flow would follow through the Coanda effect around a curved surface. A surface with a three inch radius of curvature was placed at the exit of a Mach 1.5 flow channel. The flow was diverted 90° by a quarter circular section. This would represent an extremely rapid change in direction of flow acceleration which would have the effect of centrifuging the particles out of the flow. Further studies needed to be conducted to determine optimum conditions of flow and particle characteristics.

Calculations of particle trajectories were completed in conjunction with the design of a new experimental apparatus. It was determined that for 10 micron diameter particles in a Mach 1.5 flow a 30 centimeter acceleration channel would accelerate the particles to 77% of the gas velocity. A new flow channel would thus need to be designed. The new rig would be of a modular construction permitting a great deal more versatility. It would also be constructed of hardened steel and glass for better erosion characteristics.

An analysis of particle acceleration and trajectory as functions of particle size and mass showed later that the separ-

ation efficiency of any separation device based on rapid accel-
eration (i.e. changes in direction) of the carrier gas is highly
sensitive to particle size for a particular particle mass den-
sity. If a separator designed for a specific particle mass and
size were to be built, it was determined that the effects of
particle erosion and break-up would result in a continuous deg-
radation of pump and separator performance.

SECTION IV

SUPERSONIC DIFFUSER STUDY

This effort was directed toward studying the means by which supersonic wind tunnel diffuser lengths could be shortened and efficiency could be improved. A series of cascade blades was installed in a Mach 3 wind tunnel for initial testing. With encouraging results, a large scale design program was undertaken to design a test model for the Mach 6, high Reynolds number wind tunnel.

The model study required an extensive look into the positioning of a cobra pressure probe and valves for closing the flow channels. The requirements dictated that the valves rotate through an area of 90° in 10 seconds with an accuracy of ±.05°. The exact position of a probe was to be remotely controllable either by an operator or a remote controller.

It was decided to position the probes or valves by a gear track and servo motor with feedback being used to establish the correct position.

An analog servo system was designed using a miniature potentiometer as feedback. The drive mechanism (gears and bearing, potentiometer and wafer)become prohibitively large to obtain the required speed and accuracy.

Several ideas were investigated. For the remote positioning of the motor and potentiometer, a digital encoder and a standard planetary speed reducer could be used instead of a gear

112

train. The remote positioning of the motor and potentiometer involved leaking at flexible drive cables. A flexible wire through a (.060") OD stainless tube was tried. Test samples were evaluated for flexibility, fatigue, and torque wind-up. Excessive torque wind-up is a limiting factor for small loads with low interia; this appeared to be a good solution. However, in most of the designs evaluated, the loads were typically low with high relative inertias (see Table 8). Direct motor drive was determined the best approach.

The optical encoder design consisted of a photo transmitter (LED), receiver (transistor) and rotating disc, the disc being driven at 1 revolution equal to 1/10 the minimum resolution of the positioned device. The optical encoder required a counter to keep track of the position. A sensor for backward of forward motion required a digital-to-analog converter.

A total digital control was evaluated and the results were that it could be built using standard TTL Logic integrated circuits, all being commonly available at a low cost. This digital control technique has several advantages. The output can easily be used to interface a printer of a computer for automatic data acquisition. Position control of the model by a programmable calculator or a computer is also possible with digital feedback and control. Also, the interface would be relatively easy and straightforward compared to an analog system.

113

TABLE 8.   EVALUATION OF TORQUE WIND UP FOR FLEXIBLE DRIVE CABLES

Test #1 - wire .015
4-9-74

Weight	Arm Length	Dyn-cm	in-oz	Degrees Deflection
1 gram	8.4	8.4	.1059	150°
2 gram	8.4	16.8	.2115	200°
3 gram	8.4	25.2	.3174	270°

Test #2 - wire .015
4-9-74

	8.4			100°
1 gram	8.4	8.4	.1059	150°
2 gram	8.4	16.8	.2115	200°
3 gram	8.4	25.2	.3174	270°
4 gram	8.4	33.6	.4233	315°
5 gram	8.4	42.0	.5292	380°

Test #3 - wire .030
4-9-74

	8.4			0
5 gram	8.4	42	.5292	110°
10 gram	8.4	89	1.0581	125°
15 gram	8.4	100	1.5873	145°
20 gram	8.4	168	2.1162	165°
50 gram	8.4	420	5.292	260°

114

Methods and components to control the diffuser blockage model damper position and movement remotely during a test were investigated extensively. A stepping motor system was considered the best method in a high temperature, low pressure environment. DC servo motors were found to have problems of brush arcing at pressures less that 1 psia and AC motors were not available with the starting torque and detent torque in the required small physical size.

Model damper position would be read out in 0.1 degree increments by using a single turn precision potentiometer. The potentiometer element, according to the manufacturer, is suitable for use up to 160°C.

A Duetch connector featuring sealed pins and having a standard military mating connector was used for electrical connection to the motor gear box. A second set of connectors were used in the chamber bulkhead for the control and instrumentation cables. This will be a permanent add-on to the chamber to facilitate wiring up to the test specimen.

The design drawings for the slated cascade wind tunnel model were completed and turned over to the Government for approval. Fabrication of the model was awarded to Systems Research Laboratories. SRL delivered the model to UES which in turn delivered it to AFFDL to be tested by Dr. A. Fiorie, AFFDL in Bldg. 450's Mach 6 tunnel after the end of this contract.

SECTION V

FLUID EJECTOR SYSTEM

One application of powder ejectors was in laser pump systems. Previous sections of this report summarized work on cascade diffusers for laser application. This section presents the work done on powder ejectors, oscillating nozzles, and air-air ejector pumps.

A.   Powder Ejectors-fluid Pump Nozzles

An experiment was conducted to test the effectiveness of an oscillating ejector as a fluid pump ejector nozzle. An oscillating nozzle was fabricated and installed in a plenum which injects flow into a mixing duct exhausting to atmosphere. The entrained air from the plenum entered the plenum through a duct with a flow orifice mounted in it. The ΔP across the flow orifice, the static pressure in the plenum, the total pressure in the ejector nozzle and the mixing duct static pressure were recorded. It was found that if the mixing duct is sufficiently long there is no difference in entrainment between straight flow and oscillating flow. The vacuum pressure in the plenum did not change. The ejector nozzle pressure was the same for the oscillating case as the straight flow condition. As the mixing duct was shortened a significant difference appeared in the plenum vacuum pressure between the oscillating and straight flow. The results indicate that the oscillating ejector nozzle can effectively shorten the required mixing duct length but has no effect

116

on the total entrainment flow with a long mixing duct. The frequency of the oscillating nozzle is an important parameter to the nozzle performance. We obtained optimum plenum vacuum pressure at a frequency of about 50 cycles per second using short mixing ducts. Above or below this frequency the plenum pressure and entrainment fell off.

Some basic experiments were conducted using a Mach 1.5 powder ejector nozzle in an axisymmetric configuration coaxial with a plexiglass tube. The plenum pressure and mass flow (entrained flow) through the plenum was measured in order to observe the effects of powder loading. A Schlieren system was used to observe mixing boundary before powder was introduced into the driver nozzle. A constant problem has been in obtaining good control over powder feed rate in these experiments. Ovservation of the plenum mass flow and pressure as powder is fed into the driver gas indicates very little effect until very high powder mass flow rates are used.

Another observation which may present very serious difficulties in the application of powder ejectors to laser pump systems was that in the mixing section and downstream where the powder driver and entrained flow is fully mixed some powder enters the wall boundary layer and appears to reverse direction and move upstream toward the plenum and ejector. This explains why just before the ejector a cloud of particles is always observed which appears to be stagnant. When the pump section (driver

117

nozzle) is shut off, this cloud of particles is deposited all over the inside of the apparatus. The problem appears to be that the powder separation efficiency is a very critical function of particle velocity and mass. Those particles trapped in the boundary layer are not effectively separated in either the start-up or shut-down of the system and therefore escape.

For these reasons and others, work on powder ejectors for pump applications was discontinued. It was felt that further research into the mechanisms and properties of gas-gas ejectors would be more promising.

B. Gas-Gas Ejectors

   1. TRW Model

      Previous work on gas-gas ejector pumps had been done for the Air Force by TRW, Inc. under Contract AF F33615-73-C-4079. The ejector pump of TRW was delivered to the Air Force and set up in a facility in T-31, Bldg. 450 by UES to re-evaluate the primary characteristics reported by TRW.

This ejector pump was designed as a one dimensional, rectangular converging duct with supersonic and subsonic diffusers, powered by a multi-nozzle array of Mach 3 nozzles using hydrazine at elevated gas temperatures as the driving gas.

UES made several runs with this rig at maximum operating pressure (300 psig using air at room temperature. With a 1" and 8" converging section a compression ratio of 2 was observed. This compression ratio remained constant over a range of simula-

118

ted laser mass flow rates of 5 to 80 grams/second.

Comparison of the TRW ejector pump with theoretical performance and geometric consideration indicated that for operation with air as the pumping fluid the geometry of the TRW rig (i.e., primary to secondary area ratios, inlet to exit area ratios and diffuser geometry) would not be suitable for further experimentation. The apparatus could be modified; however it was not considered economically feasible to do so at the time.

2. UES/AFFDL Ejector

a) Introduction

An ejector pump is a simple, non-mechanical means of exchanging driver fluid power into a pressure rise in the driven flow. An ejector pump can be used in many applications, from steam engines to laser pumping. The present interest under this contract was to test the ejector pump to provide a pressure rise of 5 times with a minimum of driver mass flow.

Mr. Siegfried Hasinger of the Air Force's Flight Dynamics Laboratory has published an analytical study of ejector devices which, in simple, compressible, one-dimensional terms, describes the performance of constant area, constant pressure, or given pressure distribution ejectors (ref. 10). The experiments undertaken by UES were designed to check the validity of the ejector analysis, and to design and test an ejector pump with a total pressure ratio of 5 and a mass flow ratio of driver to driven flow of 5. This performance is considered typical of high Mach

119

number ejectors.

b) Outline of Experiments

An ejector was designed to give a total ejector pressure ratio of 5 (total exit pressure to secondary plenum pressure) at a mass ratio of 5, in accordance with the systemization procedure given in ref. 10 . A schematic of the ejector is shown in figure 37 .

A set of experiments was then carried out with a constant area ejector. It was felt that this basic ejector geometry would allow a check on the suitability of the one-dimensional assumptions for highly compressible conditions. Most of the work done under this contract was to obtain a good understanding of this basic ejector layout. Once this simple geometry was understood, proceeding to a tapered cross-sectional ejector to achieve the first objective above would be more successful.

Besides the original primary nozzle designed for Mach 3.2, a Mach 2.7 nozzle was also used in a large part of the tests. Special investigations were made on the effect of a primary injection system consisting of 9 single nozzles. A mixing section with a square cross section was also investigated.

c) Experiments With Constant Area Cross Section

The ejector used in these series of tests is shown in figure 38 . It has a constant area mixing section and no diffuser. The mixing section was made long enough to always assure complete mixing of primary and secondary flow. With a mixing
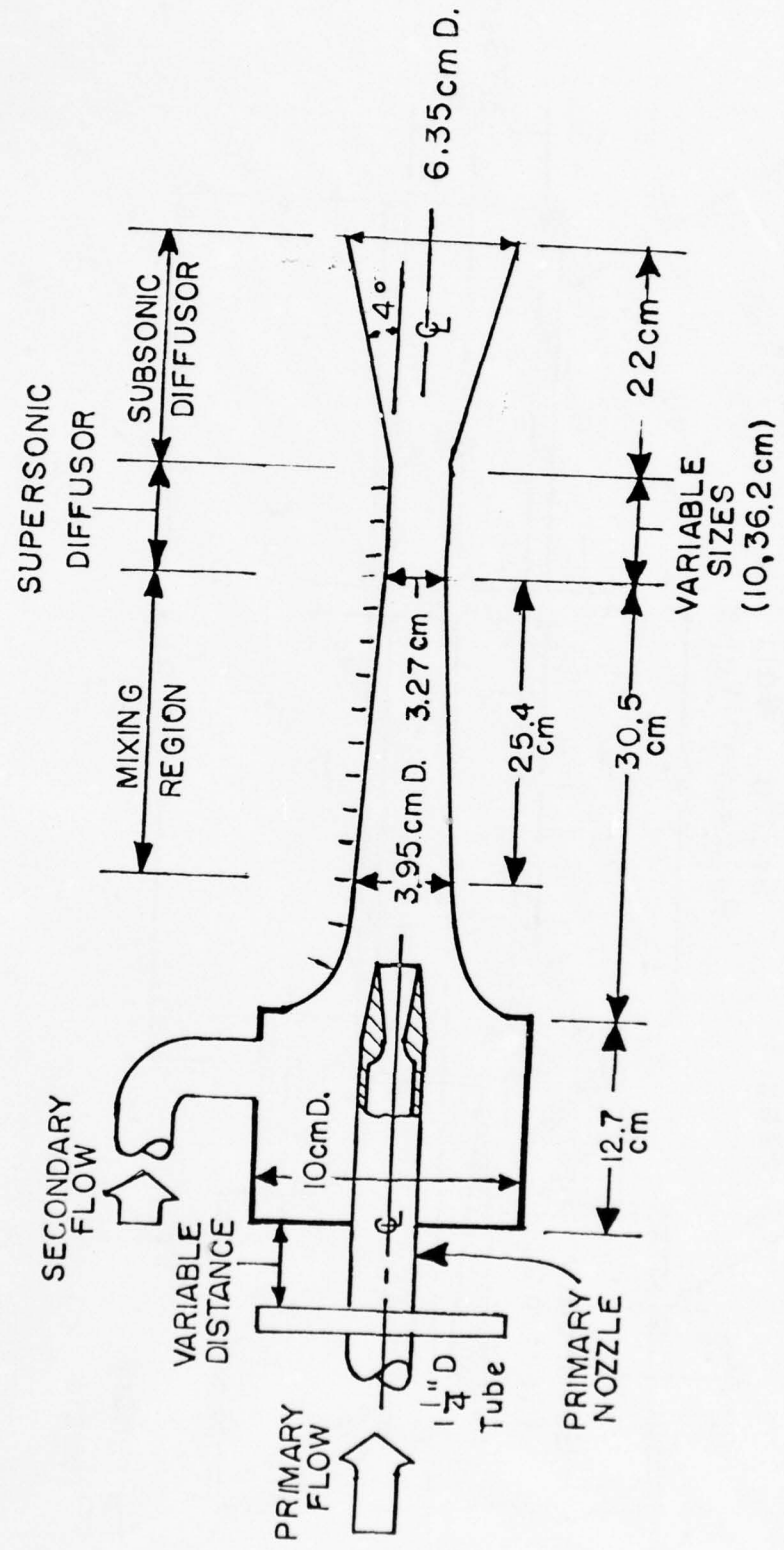
Figure 37. Layout of the optimized air/air ejector pump.

121
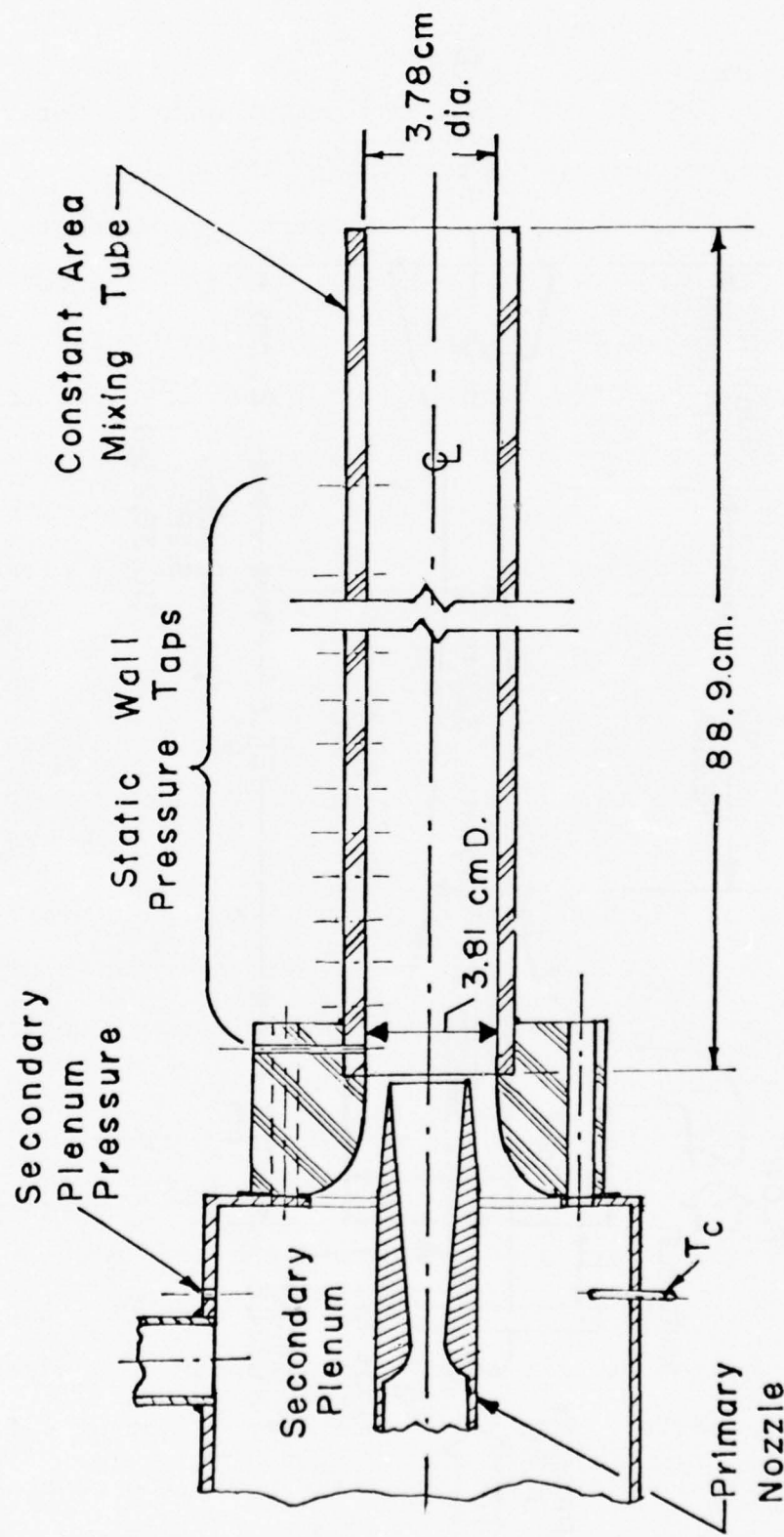
Figure 38.   Layout of the ejector used in the basic ejector experiments featuring a constant area mixing section.

section this long and no diffuser, the performance is derived from the static pressure peak occurring in the mixing section.

The ejector studied was an axisymmetric plexiglass tube with an inlet diameter of 1.501"(3.81cm) and exit diameter of 1.484"(3.77cm). The upstream end had a bell mouth inlet geometry of approximately 1"(2.54cm) radius. Pressure taps of .0625"(.159cm) were drilled into the tube at every 1/2"(1.27cm) from the end of the bell mouth to 17"(43.2cm) downstream, then every inch (2.54cm) thereafter to 30"(76.2cm) from the plenum chamber.

The nozzles used for the experiments are shown in figure 39 . They are identified as the Mach 2.7 and Mach 3.2 case, with actual exit Mach numbers of 2.70 and 3.28 respectively. The supersonic nozzles were not designed for providing a true parallel exit flow and had instead a simple conical contour for the expanded portion of the nozzle. However, the cone angle was kept at 10°, small enough to minimize the effects of deviations from a perfect nozzle.

The position of the nozzle exit plane could be varied from 1-1/2"(3.81cm) inside the mixing tube to 3-1/2"(8.9cm) upstream inside the secondary plenum. Tests proved that the ejector performance was, within certain limits, not very sensitive to the axial position of the primary nozzle with respect to the secondary bell mouth nozzle. Most tests were carried out at a fixed position 3/4"(1.9cm) upstream of the point where the constant

123

1.79 cm dia.

15°

C̶L

1 cm. dia.

2.67 cm. I.D.

1.9 cm. R

5°

M 2.7 NOZZLE

1 cm. R

5°

C̶L

1 cm. dia.

7°

2.36 cm. dia.
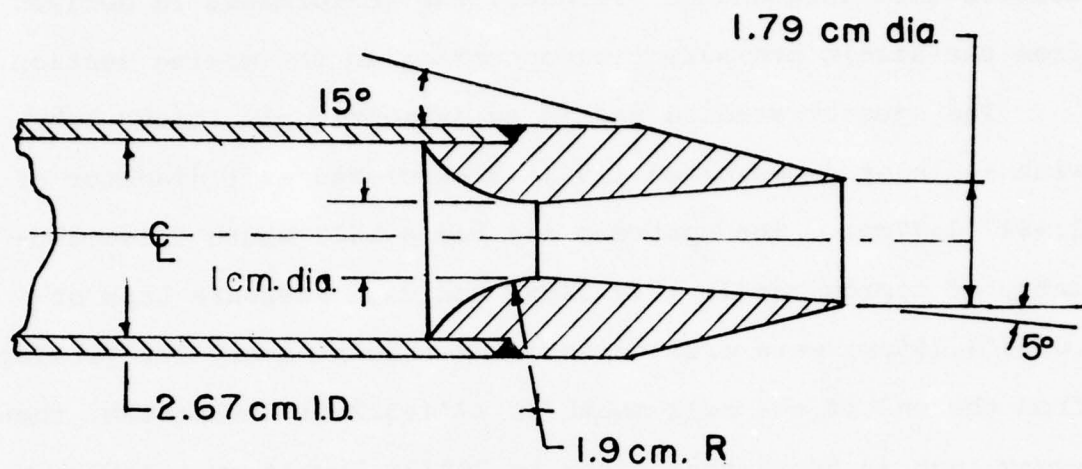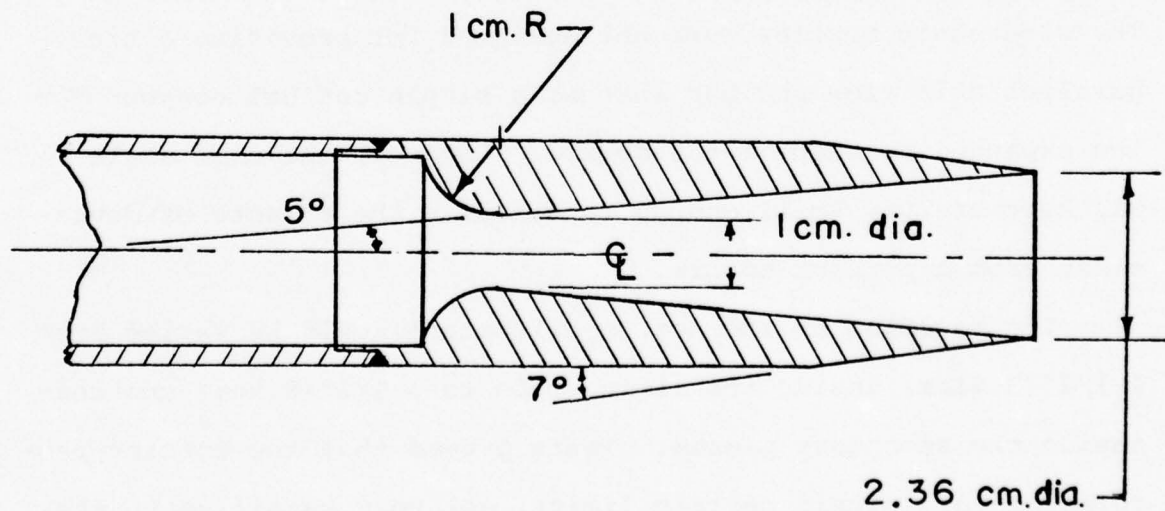
M 3.2 NOZZLE

Figure 39. Primary nozzles used in experiments.

area cross section begins. This position was also far enough
upstream with respect to the bell mouth inlet to assure an un-
restricted and continuously accelerating secondary flow. The
position was also close enough to the entrance of the actual
mixing tube to allow a proper identification of the primary and
secondary inlet area ratio as derived from the primary jet dia-
meter and mixing section diameter.

A special effort was made to align the primary nozzle coax-
ially with the mixing section. This was done purely geometrical-
ly, and then checked by observing the uniformity of the static
pressure taps located near the bell mouth - mixing section junc-
tion and spaced 120° apart around the circumference of the tube.
It was never possible to obtain a complete uniformity of the
static wall pressures at this position. The degree of uniform-
ity depended also on the operating conditions for a particular
test. Since the performance was not very sensitive to this sta-
tic pressure uniformity, deviations of 10% were tolerated at
higher secondary flow rates. At very low secondary flow rates,
approaching zero secondary flow, the non-uniformity of the sta-
tic wall pressure at the inlet could be considerable. Dynamic
pressure measurement showed that in this case the non-uniformity
is caused by unsymmetric flow re-circulations in the inlet area.

Figure 40 schematically illustrates the general arrange-
ment of the experimental apparatus. The air supply was from the
Building 450 bottle farm, reduced to 500 psig working pressure

125
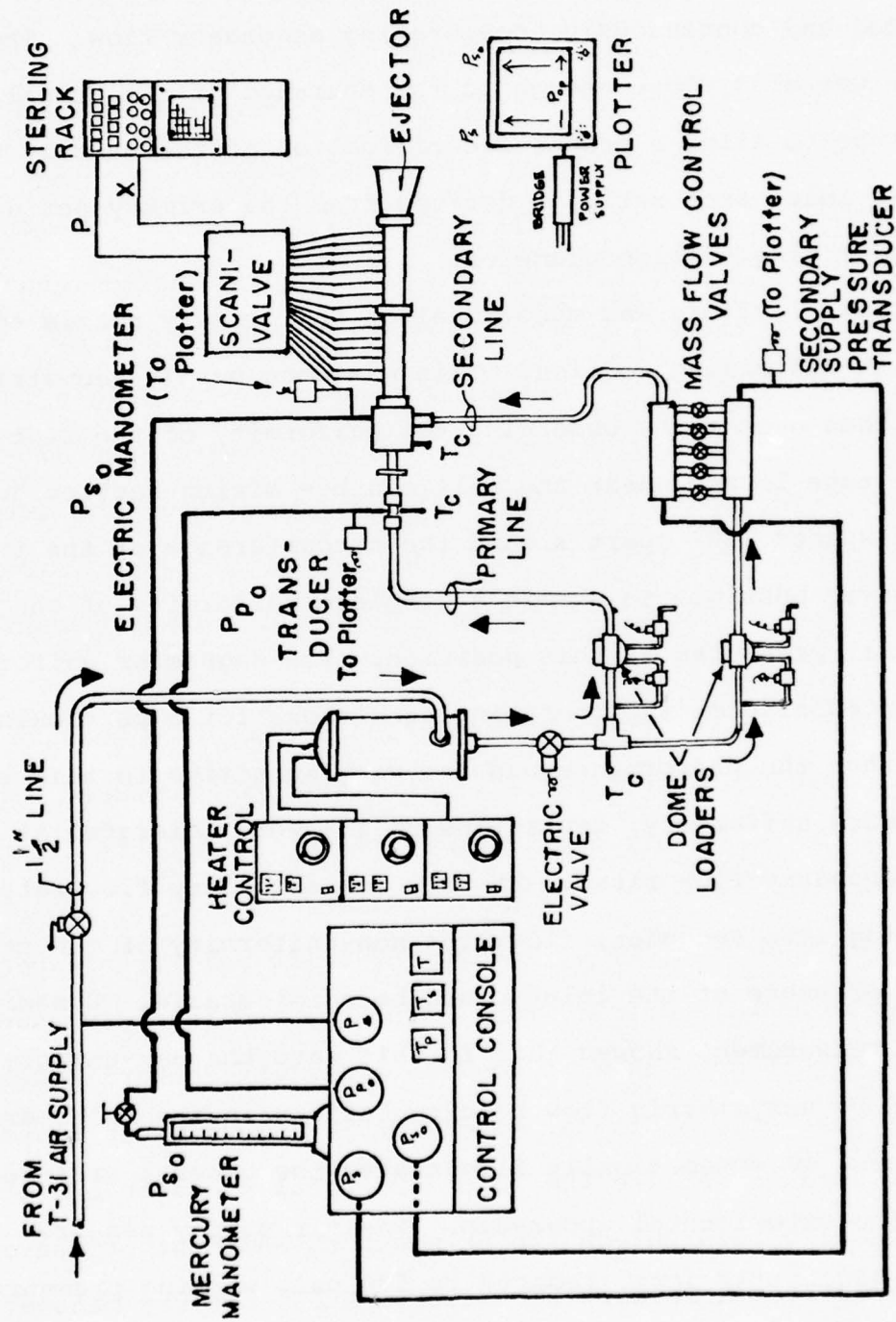
Figure 40. Layout of the ejector test stand and associated instrumentation

126

at the test site and heated typically to 70°F(21°C) before the test rig. The primary supply pressure was regulated from 0 to 200 psig for typical test conditions.

The secondary mass flow could be selected from five separate sonic orifices upstream of the plenum chamber. Either one or any number of mass flow orifices could be used to give any desired secondary mass flow, from zero to 100 g/sec, depending on the valve(s) chosen and the secondary supply pressure.

Typical pressures for a data run would be 150 psig primary total pressure, 80 psig, secondary supply pressure, -20"Hg(-500 mmHg) secondary plenum pressure, ambient pressure at the exit of the tube, 70°F(21°C) primary and secondary total temperatures, primary mass flow of .5 lbm/sec(227g/sec) and secondary mass flow of 0.1 lbm/sec(45.4g/sec).

Standard laboratory instrumentation was used to measure total temperature, supply pressure, primary and secondary total pressures, and secondary supply pressure to the mass flow control valves.

Two Statham Model PG769, 0-200 and 0-100 psig transducers were used to measure primary total pressure and secondary supply pressure. Their outputs were read on a Hewlett-Packard Model 2FA X,Y,Y plotter. A Statham Model PM397C I 300" water transducer was used to measure the secondary total pressure and its output was also read out on the HP plotter. Ambient pressure was measured from a mercury barometer. A 30" mercury manometer

was used to measure the secondary total pressure at the control console. The three static wall pressures at port 2, 120° apart, were measured on three 60" slack tube water manometers. All wall static pressures were scanned by a Scanivalve Model SSS 48C4BM/124 8 BCD/SLSN 250 using a Statham ±15 psi differential pressure transducer. This signal was recorded on one channel of a S. Sterling Co. 12 channel recorder. Another channel received a signal from a port-positioning sensor in the Scanivalve. Both signals then gave a trace of pressure-position on a TI strip chart recorder on the Sterling recorder rack.

Total temperature of the primary and secondary air flows as well as the temperature of the the air exiting the heater were measured by grounded, fast response iron-constantan thermocouples whose signals were read on Simplytrol pyrometers on the control console.

Pressure transducers were calibrated daily, frequently more than once, against a precision Heise pressure gauge. Thermocouples were calibrated at two temperature points, in an ice bath and in boiling water.

The pressure and mass flows of each run were adjusted for either a constant mass ratio or constant pressure ratio, usually the latter. The secondary mass flow was selected by opening one control valve and selecting a supply pressure.

For a constant pressure ratio run, the secondary total pressure was first calculated from the given pressure ratio and am-

128

bient pressure or expected maximum pressure in the mixing duct. The primary and secondary pressures were adjusted to give this total secondary pressure reading on the manometer ($P_{ambient}$ - $P_o$desired). Heat was added to keep the two air streams at or near 70°F(21°C). Once the temperatures and pressures of the primary and secondary flows were stabilized, a Scanivalve trace was made and data recorded from the control panel, slack tube manometers, and from the X,Y,Y plotter. Primary and secondary pressures were then re-adjusted to give the same total secondary pressure but at a different mass flow ratio.

If a constant mass ratio line was to be run, the procedure was similar. The primary total and secondary supply pressures were adjusted to keep the pen trace on the X,Y,Y plotter following a prescribed constant mass ratio line on the plotter paper.

After a test run, the initial data was transcribed onto data reduction sheets. The Scanivalve tracing was used to obtain a pressure distribution information as well as the maximum pressure inside the mixing section. The X,Y,Y plotter graph gave a trace of total primary pressure (used to calculate the primary mass flow and to determine primary Mach number), secondary supply pressure (used to calculate the secondary mass flow rate), and an independent reading of the secondary total pressure. The slack tube manometer data gave an accurate measurement of the secondary static pressure at the beginning of mixing. This data then could be used in the equations given in the next

129

section to calculate total pressure ratio, mass ratio, primary and secondary Mach numbers and static pressure distribution along the wall of the mixing section.

Mr. Hasinger's report (ref. 10) outlined the basic equations used to analyze the ejector geometries studied. However, the report did not treat cases in which the primary flow further expands outside the nozzle; that is, if the final expansion Mach number is larger than the nozzle design Mach number. In the absence of wall forces outside the nozzle the gain in momentum in the axial direction by the expanding flow simply equals the pressure forces acting on the flow at the nozzle exit. The total axial momentum of the flow after complete expansion is:

$$\dot{m}_p v_p = v_{noz} \dot{m}_p + A_{noz}(P_{noz} - P_p) \tag{1}$$

Using the following basic relations:

$$\dot{m}v = Ap\gamma M^2 \tag{2}$$

$$\dot{m} = \rho A v \tag{3}$$

or with:
$$a = \sqrt{\gamma RT} \tag{4}$$

$$\dot{m} = \frac{Ap M\gamma}{\sqrt{R\gamma T}} \tag{5}$$

one can write

$$\frac{P_{noz}M_{noz} \gamma v_p}{\sqrt{RT_{noz}\gamma}} = P_{noz}\gamma M_{noz}^2 + (P_{noz} - P_p) \tag{6}$$

130

or

$$M_{noz} \; \gamma M_p \sqrt{\frac{T_p}{T_{noz}}} \; = \; \gamma M_{noz}^2 + 1 - \frac{P_p}{P_{noz}} \tag{7}$$

then

$$\frac{P_p}{P_{noz}} \; = \; \gamma M_{noz}^2 + 1 - \gamma M_{noz} M_p \sqrt{\frac{T_p}{T_{noz}}} \tag{8}$$

One can write for the temperature ratio:

$$\frac{T_p}{T_{noz}} = \frac{T_p}{T_{Po}} \; \frac{T_{Po}}{T_{noz}} \tag{9}$$

Since only the kinetic energy of the axial flow component is preserved in this expansion process the adiabatic expansion relations allow one to write:

$$\frac{T_p}{T_{noz}} = \frac{1 + M_p^2 \; \frac{\gamma-1}{2}}{1 + M_{noz}^2 \; \frac{\gamma-1}{2}} \tag{10}$$

Since in the ejector analysis one is interested in the overall pressure ratio of the complete expansion process:

$$\frac{P_p}{P_{Po}} = \frac{P_p}{P_{noz}} \; \frac{P_{noz}}{P_{Po}} \tag{11}$$

$$= \frac{P_p}{P_{noz}} \; (1 + \frac{\gamma-1}{2} M_{noz}^2) \; \frac{\gamma}{\gamma-1} \tag{12}$$

Combining equations (10), (11) and (8):

$$\frac{P_p}{P_{noz}} = \frac{\gamma M_{noz}^2 + 1 - \gamma M_{noz} M_p \sqrt{\dfrac{2+(\gamma-1)M_{noz}^2}{2+(\gamma-1)M_p^2}}}{(1 + \frac{\gamma-1}{2} M_{noz}^2)^{\gamma/\gamma-1}} \tag{13}$$

Equation (13) can be solved for the final flow Mach number of the expansion:

$$M_p^2 = \frac{Z^2}{1 + (M_{noz}^2 - Z^2)(\frac{\gamma-1}{2})} \tag{14}$$

where

$$Z = \frac{1 + \gamma M_{noz}^2 - \dfrac{P_p}{P_{Po}} (1 + \frac{\gamma-1}{2} M_{noz}^2) \frac{\gamma}{\gamma-1}}{\gamma M_{noz}} \tag{15}$$

One can also derive the area ratio ($A_{primary}/A_{secondary}$) for the expansion outside the nozzle. From the continuity law:

$$\rho_{noz}\, v_{noz}\, A_{noz} = \rho_p\, A_p\, v_p \tag{16}$$

and using equation (4) and the equation of state

$$\rho = \frac{p}{RT} \tag{17}$$

then

$$\frac{A_{noz}}{A_p} = \frac{P_p}{P_{noz}} \frac{M_p}{M_{noz}} \sqrt{\frac{T_{noz}}{T_p}} \tag{18}$$

With equation (8), equation (18) can be written as

132

$$\frac{A_{noz}}{A_p} = (\gamma M_{noz}^2 + 1 - \gamma M_{noz}M_p \sqrt{\frac{T_p}{T_{noz}}}) \frac{M_p}{M_{noz}} \sqrt{\frac{T_{noz}}{T_p}} \tag{19}$$

$$= M_p [(\gamma M_{noz} + 1/M_{noz}) \sqrt{\frac{T_{noz}}{T_p}} - \gamma M_p] \tag{20}$$

Using equation (10) yeilds:

$$\frac{A_{noz}}{A_p} = M_p [(\gamma M_{noz} + 1/M_{noz}) \sqrt{\frac{2+(\gamma-1)M_p^2}{2+(\gamma-1)M_{noz}^2}} - \gamma M_p] \tag{21}$$

Since the throat area to exit area ratio of the nozzle is given by the adiabatic relation:

$$\frac{A^*}{A_{noz}} = (\frac{\gamma+1}{2})^{\frac{\gamma+1}{2(\gamma-1)}} M_{noz}(1 + \frac{\gamma-1}{2} M_{noz}^2)^{-\frac{(\gamma+1)}{2(\gamma-1)}} \tag{22}$$

the throat to final expansion area for the off-design flow can be determined from:

$$\frac{A^*}{A_p} = \frac{A_{noz}}{A_p} \frac{A^*}{A_{noz}} \tag{23}$$

For off-design conditions the inlet area ratio of the ejector as defined by the analysis (A_p/A_s) is a variable for a given ejector, depending on the chosen inlet Mach number. For calculating an ejector characteristic, an iterative process is necessary to properly correlate primary Mach number and inlet area ratio.

To demonstrate the influence of an off-design nozzle on the expansion process the area and pressure ratios associated with the two primary nozzles used in the present experiments

133

are plotted in figure 41 as a function of the final expansion

Mach number. For comparison the area and pressure ratio

for the ideal supersonic nozzle are also entered. The plot

shows that the deviations from ideal conditions beyond Mach

numbers 2.7 and 3.2 respectively are at first only slight. How-

ever, say beyond Mach number 3.1 and 3.6 respectively the de-

viations from ideal conditions get out of bound very fast. It

is also obvious that for each nozzle a barrier is reached be-

yond which practically no ejector operation is possible, i.e.,

increasing the primary pressure ratio hardly changes the primary

Mach number. Also for the present ejector geometries the inlet

area ratio increases rapidly to very high values at this point.

d. Constant Area Mixing Studies

Figures 42 & 43 show a comparison of the experimental

performance values for the basic ejector experiment. The curves

shown in this graph represent an ejector performance character-

istic derived in ref. 10 , where the secondary inlet-Mach num-

ber is a function of the primary inlet Mach number for either

a given total pressure ratio or mass flow ratio. In the case

of constant area flow with no subsonic diffuser, the total exit

pressure is equal to the static exit pressure. The analytical

curves in figures 42 & 43 required the following input data, based

on either geometric measurements or assumptions:

Mach 2.7 nozzle:

Geometric inlet area ratio (at the nozzle exit plane)
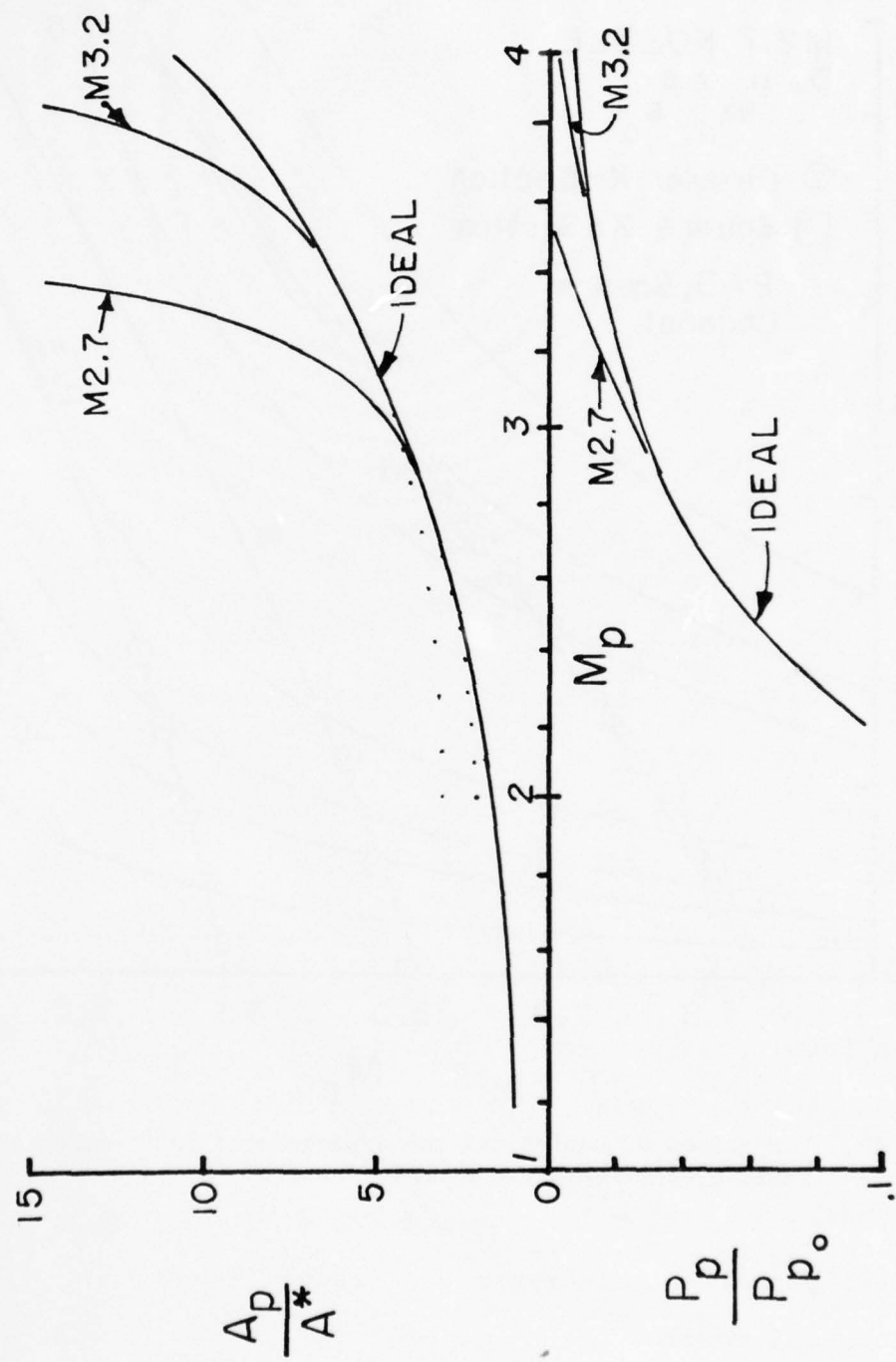
Figure 41. Area expansion ratio and expansion pressure ratio.

135
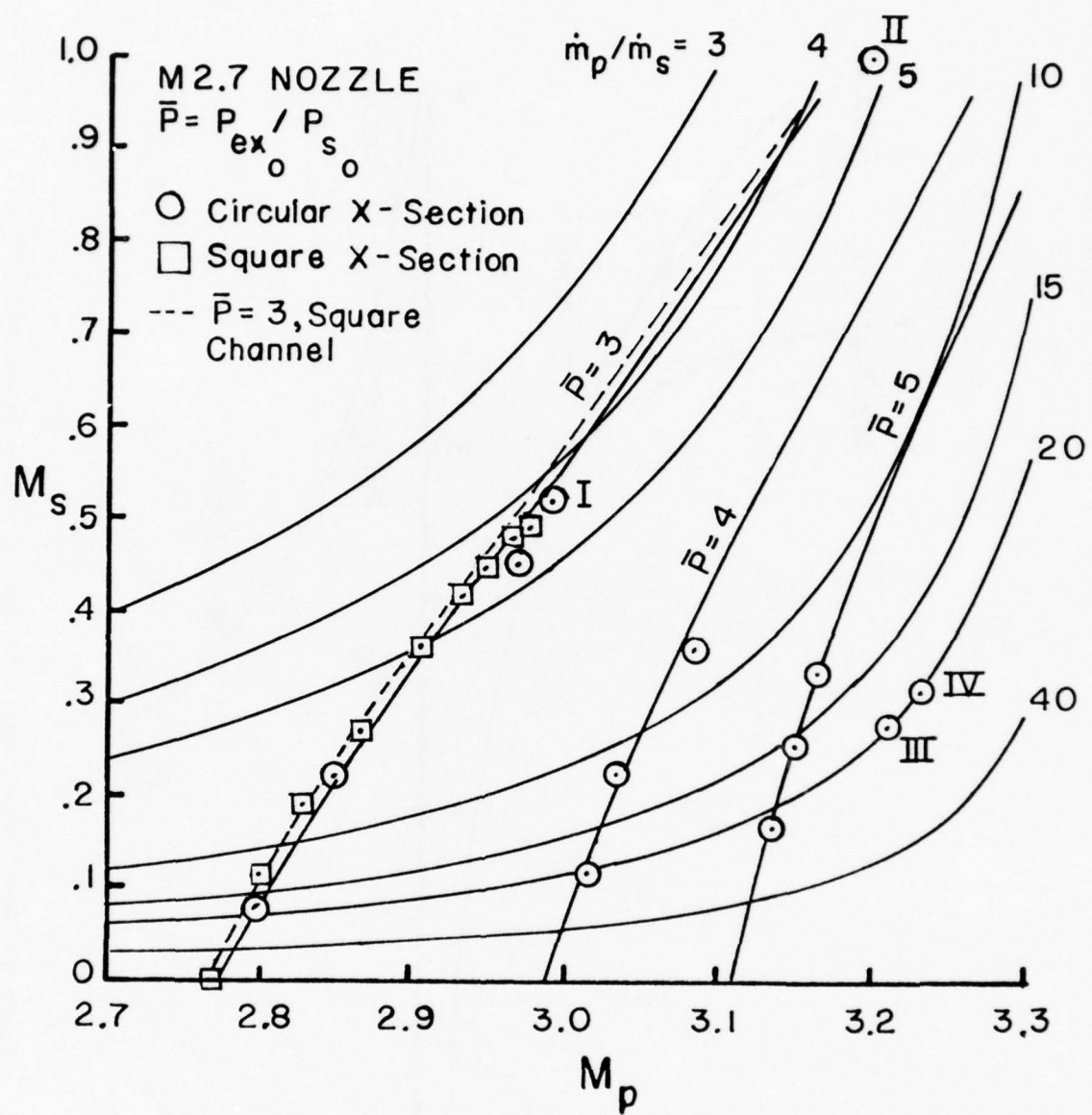
Figure 42. Comparison of analytical and experimental performance of the basic ejector with the Mach 2.7 nozzle.
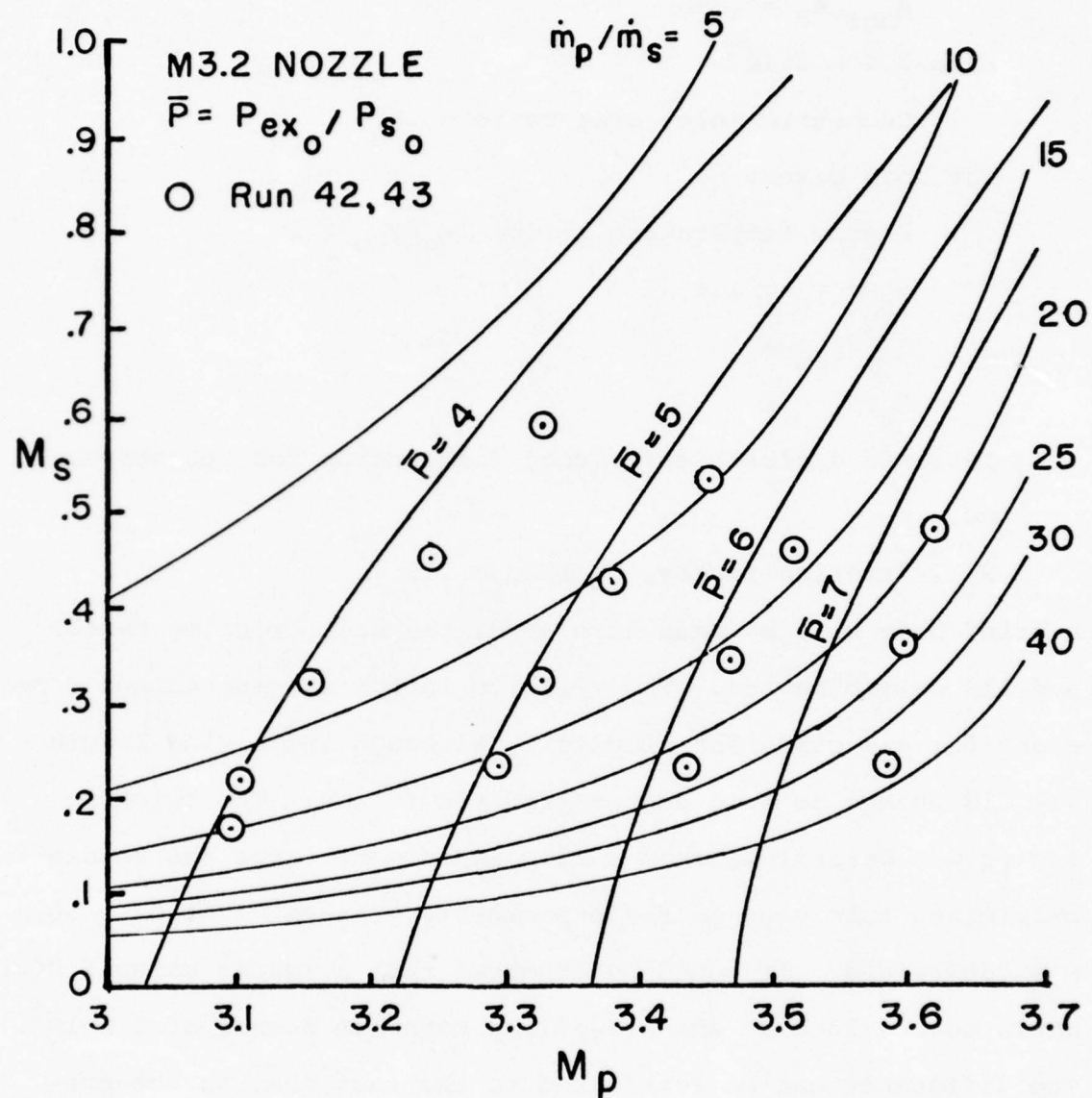
Figure 43. Comparison of analytical and experimental performance of the basic ejector with the Mach 3.2 nozzle.

137

$$A_{noz}/A_s = .285$$

Mach 3.2 nozzle:

Geometric inlet area ratio = .62

For both cases:

Plenum temperature ratio, $T_{p_o}/T_{s_o} = 1$

$\gamma_p = \gamma_s = 1.4$

$C_{p_p}/C_{p_s} = 1$

$R_p/R_s = 1$

Subsonic diffuser efficiency (accounting for its absence) =0.

Wall friction factor, C_f L/2d = .12

A brief note will be made here about the wall friction factor and its determination. The friction factor was maintained constant for all cases for simplicity although the mixing length (L) did change to some degree from run to run. The friction factor was determined from a flow experiment. For the smooth plexiglass tube used in the experiments, the value of C_f = .024 was determined. It would be expected that a lesser value (.003) would be obtained at the prevailing Reynolds number of 3 x 10^5. The difference can be attributed to the fact that in the present determination the flow is not fully developed. Since the flow conditions in the ejector are closer to undeveloped flow than developed flow, the experimentally derived friction coefficient was selected for the analysis. From the experiments it was found that a typical mixing length to tube diameter ratio (L/d) was 10.

138

The continued expansion of the primary flow after it leaves the primary nozzle in case of off-design conditions is accounted for in the analytical program as explained in the analysis section.

The experimental points in figures 42 and 43 have been plotted from primary Mach numbers obtained from measures pressure ratios. The pressure ratio of the ejector was adjusted during the experiments to be within about ±.03 of the values 3, 4,5,6, and 7.

As a further comparison of the analytical and experimental agreement, Table 9 shows the results for non-integral pressure ratios and mass flow ratios. Experimental and analytical values appear to be in satisfactory agreement over the entire range of the experiments. Agreement with the mass flow ratio is better than 1%, and agreement with total pressure ratio is less than 4%. The largest deviations occured near the "popped" mode condition and at a pressure ratio of 7 for the Mach 3.2 nozzle. This variation can be accounted for by the fact that the Mach 3.2 nozzle is operating at a high underexpansion condition. The primary flow is spreading out into the channel considerably. Figure shows that both area ratio and pressure ratio for the Mach 3.2 case is rapidly deviating from ideal behvior, which may also help to explain the deviation from analytical predictions at a pressure ratio of 7.

TABLE 9.

MACH 2.7 NOZZLE - CONSTANT AREA EJECTOR

Run	M_p	M_{s_1}	M_{s_2}†	$\bar{\dot{m}}_{ex}$	$\bar{\dot{m}}_{th}$*	Δ%	$\bar{P}_{ex}$	$\bar{P}_{th}$	Δ%	Remarks
29	2.449	.136	.130	5.607	5.630	.41	2.068	2.053	.39	
A	2.521	.242	.249	3.582	3.577	.14	2.068	2.06	.39	
B	2.884	.239	.241	7.261	7.254	.1	3.111	3.105	.19	
C	3.015	.511	.533	4.696	4.701	.1	3.126	3.220	2.92	
D	3.031	.528	.548	4.776	4.772	.08	3.123	3.277	4.7	Popped Mode
E	3.109	.390	.382	8.595	8.600	.01	4.161	4.232	1.68	
F	3.113	.404	.399	8.427	8.426	.32	4.172	4.234	1.46	
G	3.125	.422	.413	8.453	8.459	.07	4.277	4.303	.60	Popped Mode
H	3.085	.319	.312	9.656	9.647	.09	4.189	4.188	.02	

$\bar{\dot{m}} = \dot{m}_p/\dot{m}_s$; $\bar{P} = P_{ex_o}/P_{s_o}$

† M_{s_2} - calculated from measured pressure ratio

M_{s_1} - calculated from primary Mach number and mass flow ratio

*No diffuser; $C_f \frac{L}{2D} = .12$; $T_{o_p} = T_{o_s} = 295°K$; $\gamma_p = \gamma_s = 1.4$; $d_{ch} = 3.81cm$; $d^*_p = 1cm$;

$d_{exit_p} = 1.795cm$; $M_{exit} = 2.7038$; $t = .9786$; $i = 1.0$.

140

e.   Tapered Mixing Section

Figure 44 compares the experimental results of the optimized tapered ejector with the analytical values for the design total pressure ratio of 5. A series of i-value curves, which are representative of the pressure distribution during mixing, are drawn as the curve parameter. This allows a comparison of i-values found experimentally from the Scanivalve trace for the data given in figure 45 . It is difficult to actually measure i-values from the pressure distributions, but it does appear that for case   5 , the performance point, that i≈0 or very low (almost constant pressure mixing with normal shock recovery). To achieve this value analytically and match the performance of the real ejector would require a t = .77 value. It is possible that mixing starts further down the tube than in the idealized assumption that it begins at the beginning of the taper. This would raise the effective t value from .7 to .77 easily. The identification of the point where mixing begins is difficult to locate experimentally and could easily occur much further downstream in the tube than initially assumed especially in the "popped" mode.

The results of the experimental tests achieved the optimized ejector design goal; in fact it was slightly better. For datum point 5, figure 44 , a total pressure ratio of 5.02 was achieved at a mass flow ratio of 4.4, using the longer supersonic diffuser in this case. Test details are shown in Table 10 on the following page.

141
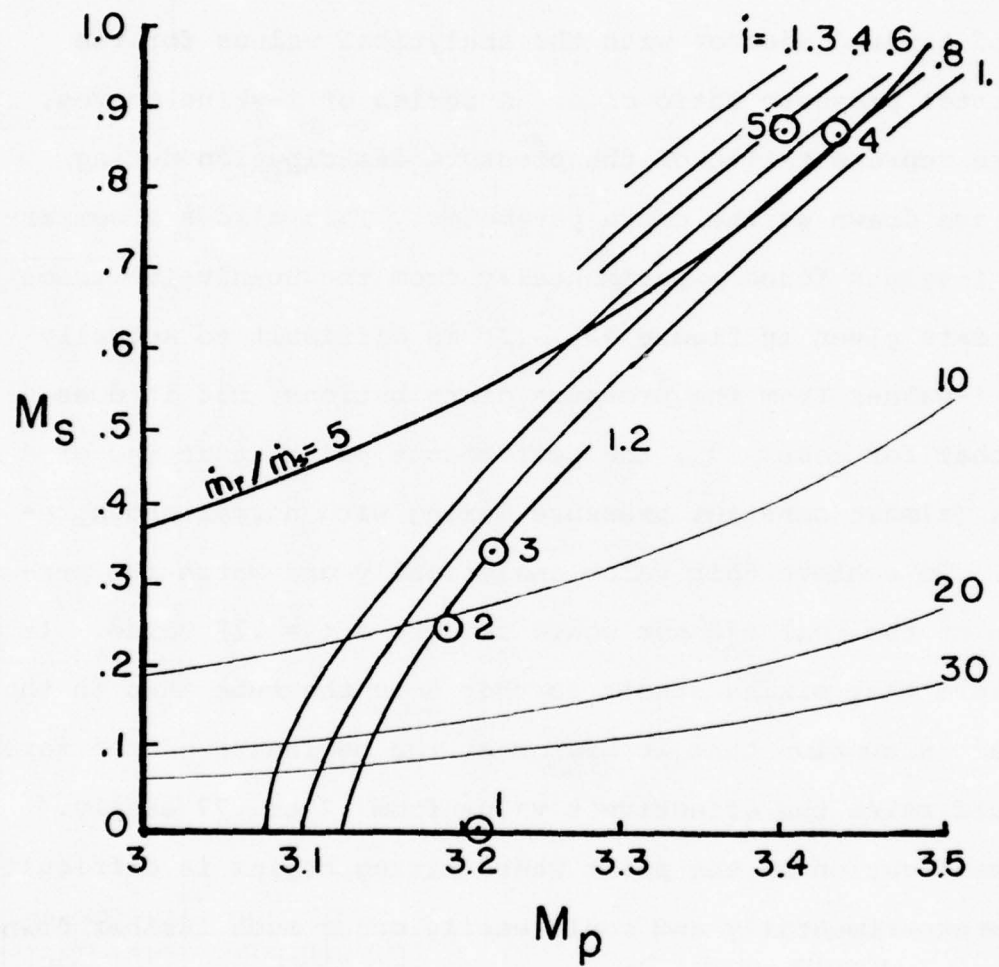
Figure 44. Comparison of the analytical and experimental performance of the optimized ejector at a total pressure ratio of 5.
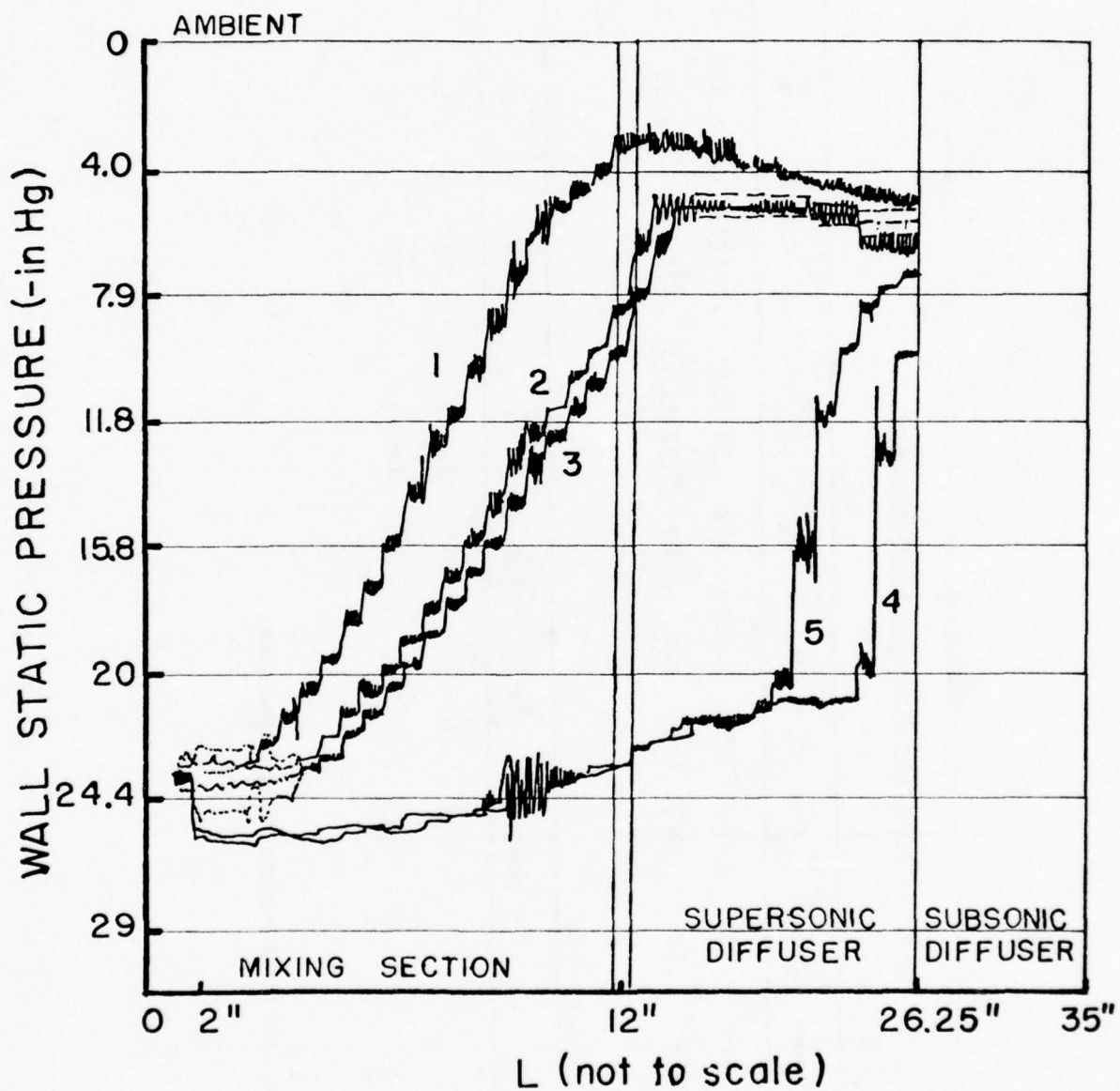
Figure 45. Static pressure distributions along the mixing section and supersonic diffuser of the optimized ejector for the points shown in Figure 44.

143

TABLE 10.

OPTIMIZED EJECTOR TEST RESULTS

Experimental Results

Run	M_{nozzle}	$\frac{A_p}{A_s}$ geo	$\frac{A_p}{A_s}$ act	t	T_o	M_p	M_s	$\frac{\dot{m}_p}{s}$ g/s	$\frac{\dot{m}_s}{s}$ g/s	$\bar{\dot{m}}$	$\bar{p}$
52-C(4)	3.28	.554	.722	.687	70°F	3.432	.882	.34(155)	.071(32.3)	4.788	4.997
52-D(5)	3.28	.554	.68	.687	70°F	3.4	.89	.32(145.3)	.073(33)	4.39	5.02

Initial Design Goal (ref. 70)

A_p/A_s	t	i	η_{poly}	T_o	$C_f\frac{L}{2D}$	M_p	M_c	$\bar{\dot{m}}$	$\bar{p}$
.666	.7	.6	.8	70°F	.07*	3.175	.702	5	5
.632	.7	.6	.8	70°F	.12	3.28	.703	5	5

*Initial assumption for multi-nozzle arrangement.

f.   Square Channel With Constant Area Mixing

An additional study using a square cross sectional
mixing tube was undertaken. The results with the Mach 2.7 noz-
zle were similar to the round mixing tube (see figure 42). The
cross section size is accounted for by calculating an equivalent
diameter tube; that is, the 1.319"(3.335cm) x 1.320"(3.353cm)
is equivalent to a 1.487"(3.782cm) tube diameter. Agreement
with the analytical model was satisfactory.

g.   Pressure Distribution Study

In addition to the performance evaluation, a static
pressure distribution from the Scanivalve trace can be made for
each run. An example of such a pressure-distance trace is shown
in figure 46 for the case of total pressure ratio = 3 and the
Mach 2.7 nozzle with the constant area mixing tube. The pres-
sure rise becomes less steep and occurs at larger X/D values as
the mass flow increases (curves 1,2, and 3). At a particular
point, described in the next section, the flow undergoes a mode
change. The change does not occur at a singular point but in a
very small range of primary pressures as seen in curve 3,4, and
5. The change is often accompanied by an audible change in the
ejector pump noise level. The static pressure distribution shows
that the secondary flow goes sonic, even supersonic (at X/D =
3.5). Mixing behaves as a constant pressure, constant area case,
followed by a rapid increase in pressure to ambient exit pressure
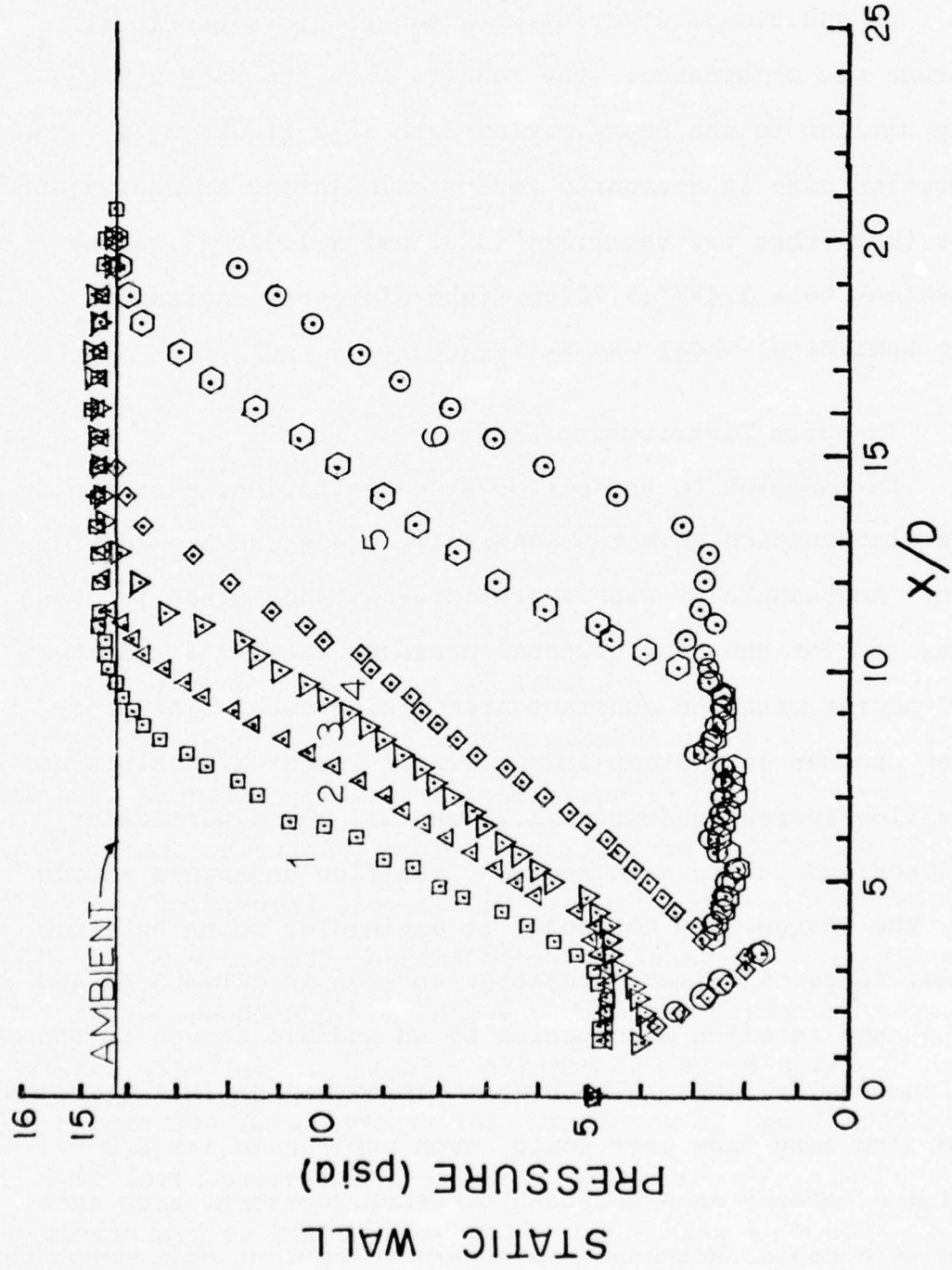
Figure 46. Typical static pressure distribution along the mixing section of the basic ejector for a total pressure ratio of 3, regular and changed mode.

(curves 5 and 6). Further increases in primary pressure pushes
the shock system further down the tube (compare curve 5 and 6).
This behavior was also observed with the Mach 3.2 nozzle, start-
ing at pressure ratios of 4 and higher.

h.   Mixing Mode Change

The change in mixing mode as experienced in the present ex-
periments with constant area mixing for certain operation condi-
tions is characterized by a transition from a rising to a more
or less constant pressure distribution while primary and secon-
dary flow undergo mixing. The beginning of the mode change,
which occurs with either rising primary or secondary Mach number,
is indicated by the appearance of a drop in static pressure at
the beginning of the mixing process. If the mode change is com-
pleted mixing occurs entirely at a pressure lower than the pres-
sure prevailing at the inlet to the mixing section. Figure 45 & 46
show typical pressure distributions for the transition from
normal to changed mode conditions. Though this transition oc-
curs gradually with changing inlet conditions, the range of
ejector operating conditions within which the mode change or at
least certain phases of it are completed is in general very small.
For certain conditions it can occur fast enough to be regarded
as a sudden change, distinctly noticeable in the noise level of
the ejector. The mode change exhibited practically no hysteresis
(in contrast to the case of the optimized ejector).

Analytical considerations allow one to predict the conditions for the occurance of this mode change. The prediction is based on a comparison of the ejector characteristics for constant area mixing with that for constant pressure mixing at given ejector inlet geometry. Figure 47 gives the performance characteristics for the conditions of the experimental ejector with the Mach number 2.7 primary nozzle with constant area mixing replaced by constant pressure mixing, which requires a variable area mixing against the ratio of mixing section exit to inlet area, necessary to accomplish constant pressure mixing (see ref. 10). The plot is made up of curves for constant primary Mach number, secondary Mach number, and mass flow ratio. A point in this curve system fixes given ejector inlet conditions. From the abscissa we can read for given inlet conditions the area reduction ratio "t" of the mixing section needed for constant pressure mixing. In particular we see the inlet conditions, where this reduction ratio becomes unity, i.e., where constant pressure mixing requires a constant cross section area.

If we mark in figure 47 the inlet conditions where the mode change occured in the experiments we are able to check how close the mode change occurs to the line t = 1. This has been done in figure 47 with the two lines I-II and III-IV which correspond to the same designation in figure 42 . Along these lines in figure 47 the mode change occurs with the mass flow ratio kept constant, in one case 4.3 in the other case 2 0. We can

148
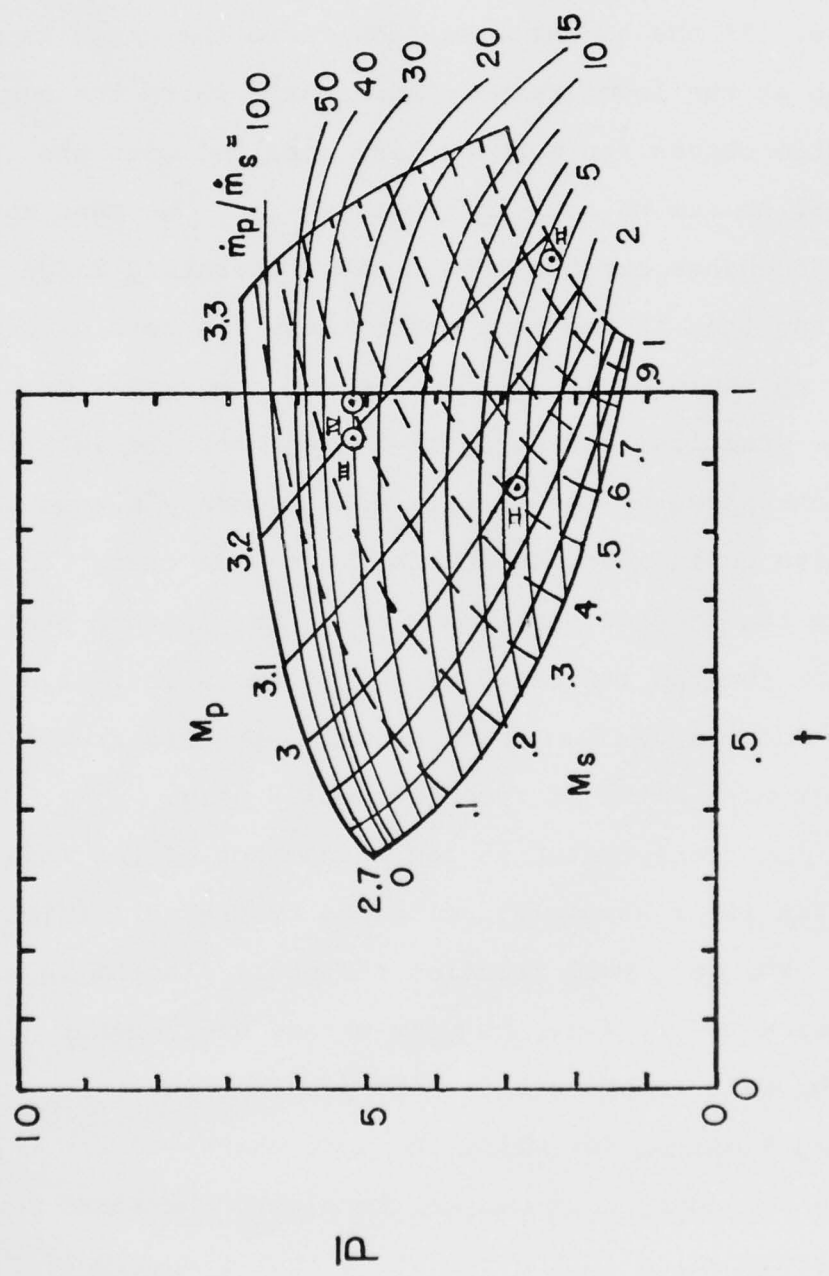
Figure 47. Performance characteristic for constant pressure mixing giving the mixing section area contraction necessary to allow constant area mixing.

149

see that in both cases the mode change occurs near or including the line t = 1. The mode change extends over a different range in each case. At the higher mass flow ratio the range is much shorter than at the lower ratio. Apparently where the constant pressure ratio curves run more or less parallel with the constant ratio curves, as can be seen in figure 47 for the mass ratio 4.3, the mode change extends over a wider operating range for its completion than in the case where these two sets of curves cross under an angle as it is the case for the higher mass ratio.

For the practical operation of the ejector the inlet conditions are controlled by the primary and secondary plenum pressure. To give an indications how fast the mode change occured in operating the ejector the ranges of primary plenum pressure are given for the two indicated cases. At mass ratio 4.3 the mode change occured by raising the primary pressure from 145 to 147 psig, for mass ratio 20 from 156 to 159 psig.

A very important factor in the phenomenon of the mode change is that it is strongly influenced by the wall friction conditions. For zero wall friction the whole diagram in figure 47 falls below t = 1, i.e., no mode change would occur. Evidence for the wall friction influence provided the tests with a square mixing section, for which the mode change occurs earlier (with rising secondary Mach number) than with the round mixing section, corresponding to the condition that a square cross-section is less favorable for the flow than a round one at equal

cross section area.

Under the prevailing conditions the change over to constant
pressure mixing requires supersonic velocity at the end of the
mixing process. Analytically this means that the supersonic
solution of the mixing relations applies (see ref. 10). It
is obvious that due to the supersonic velocities the absolute
wall friction is higher than for the subsonic case. It is in-
herent to the constant area mixing process that the loss due to
wall friction, which causes the coincidence of constant pressure
and constant area mixing in the first place, compensates at the
same time the gain in performance due to constant pressure mixing
i.e., there can be no change in performance due to the mode
change. However, to the degree the supersonic velocity is main-
tained after mixing before supersonic diffusion takes place,
performance deterioration occurs. This actually happens if the
primary Mach number is increased beyond that required to cause
the mode change with the result that the ejector pressure ratio
decreases after the mode change with increasing primary Mach
number (at constant secondary mass flow).

i.   Ejector Efficiency Tests

In conjunction with the ejector performance studies,
efficiency tests on the ejector pump device and on EFD injector
systems was undertaken. The discussion of the tests and results
of experiments with EFD type flow channels is presented in the

151

EFD final report section.

The compression efficiency for ejector pumps was defined in ref. 10 as the adiabatic compression work required to bring the secondary medium to the desired total pressure (p_{ex_O}) to the expansion work provided by the primary medium by expanding it adiabatically from its supply pressure (P_{p_O}) to (P_{ex_O}). It should be noted that this definition is identical to that of Lawson's for an ejector pump.

Figure 48 shows the analytical and experimental results of applying equation 24 to the constant area mixing case powered by the Mach 2.7 primary nozzle. Agreement is excellent for pressure ratios 3,4,and 5. Although it was initially planned to apply Mr. Hasinger's analysis to the EFD injector system, UES was not able to finish these tests at the end of the contract to provide any significant data for comparison.

j.   Conclusions

1.   The analytical technique developed by Mr. S. Hasinger, AFFDL, and as modified for off-design conditions, agrees very satisfactorily with experimental tests conducted by UES on both constant area and constant pressure mixing ejector pumps.

152
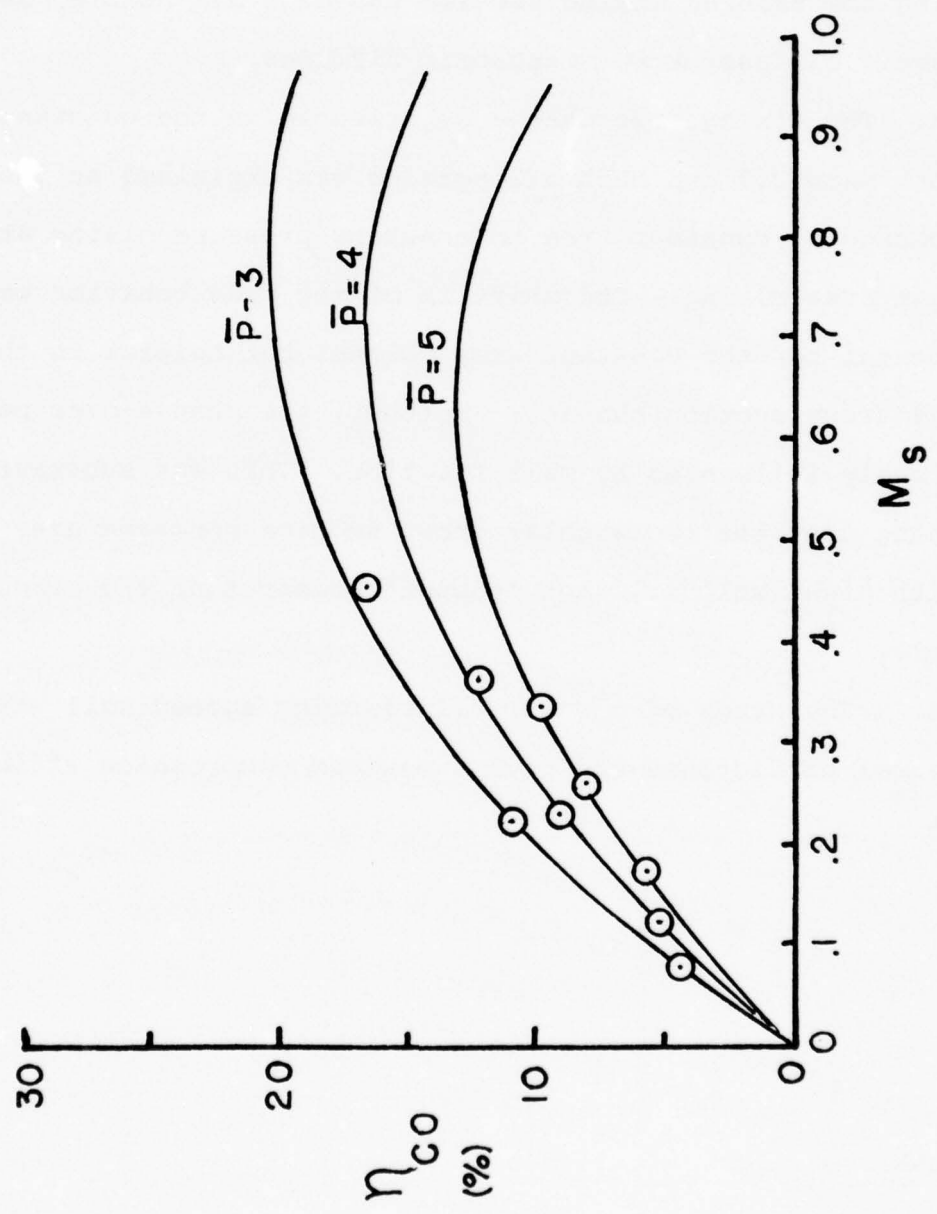
Figure 48. Compression efficiency results for the basic ejector geometry.

2.   For the optimized ejector design, the goal of a total pressure ratio of 5 with mass flow ratio of 5 was net and exceeded using the tapered mixing section and Mach 3.2 nozzle; 30cm supersonic diffuser and40cm subsonic diffuser.

3.   The mixing mode change experienced in the constant area for both Mach 2.7 and Mach 3.2 nozzles was explained on the basis of a change in constant area to constant pressure mixing at constant area mixing. The shift in mixing mode behavior was detrimental for the constant area channel but helpful in the tapered cross section channel. Further, the change-over point is strongly influenced by wall friction. This was substantiated by noting that the rectangular cross section constant area channel with hight wall friction "popped" sooner that the circular channel.

4.   The study of ejector efficiencies agreed well with the analytical predictions and gave a maximum compression efficiency of 22%.

SECTION VI

RADIAL OUTFLOW SUPERSONIC NOZZLE AND DIFFUSER WORK

Work was undertaken by UES to study the fluid dynamics and diffuser problems associated with radial supersonic outflow nozzles. Of interest was the formation of barrel-shock formation and end wall effects in multi-segmented radial outflow nozzles. The primary goal of these investigations was to determine the flow diffusion characteristics and in particular the possibility of achieving normal shock pressure recovery in such systems.

The description of the theory and experimental apparatus is described in ref. 11 . Length to diameter ratios (L/D) up to 2.85, a value of direct application to laser systems, were studied.

Various aspects of flow diffusion in radial outflow nozzle systems were investigated. Results and discussion are reported in ref. 11 and 12 . Although a barrel shock has been observed, pressure measurements indicate that this type of shock provides a much lower pressure recovery than a normal shock. Some type of diffuser should be inserted into the flow to provide the desired pressure recovery.

Further work on supersonic, two-dimensional diffusers was done by Capt. David Miller and Mr. Siegfried Hasinger, AFFDL. Their conclusions are as follows:

"The present diffuser tests show that for supersonic dif-

155

fusers with high aspect ratio rectangular cross sections, energy
redistribution by means of an internal blade system has a very
beneficial effect on the diffusion process. Internal redistri-
bution of kinetic energy might also be applicable in cases where
a supersonic diffuser is subdivided into cells to shorten its
length. In this case diffuser cells located at the periphery
may have to ingest the heavy boundary layer of an approach duct.
These disadvantaged cells could possibly by energized by internal
injection as shown in the present tests in an elementary way."
(ref. 12).

SECTION VII

DIFFUSER DYNAMICS STUDY

The diffuser with significantly better pressure recovery depends on the results of the study of shock-boundary layer interactions and boundary layer growth and control and techniques of shock holding. Normal shocks produce pressure gradients considerably greater than those produced by oblique shocks and intensity the shock boundary layer interaction. Both the exit-flow conditions and performance level of a diffuser are intimately related to the presence or absence of flow separation (or stall) in the diffuser. Regions of separated flow block the flow, cause low pressure recovery, and usually result in severe flow asymmetry, severe unsteadiness or both. To study the internal flow, Dr. Anthony Fiori designed two two-dimensional diffusers which were extensively tested at the water table facility of the Flight Dynamics Laboratory. The water table experiments, which are discussed in the following paragraphs, were recorded on over two dozen films.

1. Normal shock and diamond shock pattern were visualized.

2. The upstream movement of the normal shock was simulated by closing the valve at the downstream side of the diffuser.

3. Shock-boundary layer interactions were visualized.

4. Colored water was injected at the boundary layer to visualize the detachment and reattachment of the internal flow.

5. To eliminate stall, the boundary layer was energized by boundary layer injection under various pressure levels.

6. A second method to eliminate stall, that of boundary layer suction, was also investigated to remove tired, low momentum boundary layer fluid from the walls of the diffuser.

7. After performing half a dozen series of tests it was found that flow did not separate at all and dye injections diffused towards the centre because of the turbulent nature of the flow.

8. To confirm this finding, the flow separation was induced by providing a step at one wall of the diffuser.

9. A series of tests were filmed with steps at four different locations at the internal wall of the diffuser.

PART III

THRUST AUGMENTATION

SECTION I

INTRODUCTION

The objective of this study in Fluid Dynamic Energy
Transfer was to investigate fundamental energy and momentum
exchange processes in order to increase the understanding and
the utility of such processes. The research areas investi-
gated were those of ejectors and ejector processes for both
mass augmentation and thrust augmentation. The specific re-
search tasks which were completed include: 1) Nozzle Test
Facility; 2) Hypermixing and Oscillating Flow Nozzles; 3) The
Thrust Performance and Losses of a Family of Nozzles. All
these areas are discussed in detail in the following.

SECTION II

NOZZLE TEST FACILITY (HIGH BAY)

A.   General Discussion

The greatest degree of precision in measuring the thrust
produced by a nozzle under given conditions can be achieved by
a direct measurement of the nozzle thrust using a rigid but
elastic coupling technique. For this purpose, the upper end
of the 18 foot tube assembly located in the High Bay of Bldg.
450 (shown in figures 49, 50, and 51) was rigidly fastened
to the metal framework of the ceiling of the building. The
longer end of the tube which was welded to a flange was coup-
led to an aluminum chamber 15" long and 15" in diameter. An
internal baffle in the chamber perpendicular to the flow made
an effective stilling chamber. Provisions were made to attach
the nozzles in such a way that the flow direction was parallel
with the horizontal plane and therefore normal to the stainless
steel air supply tube.

The nozzle thrust vector was determined from the electri-
cal output of two load cells which measured forces 90° apart in
a horizontal plane located at 10.04" above the horizontal plane
containing the line of thrust of the calibration nozzle and
24.61" above the horizontal plane containing the line of thrust
of the 2-dimensional test nozzles. Load cells were attached to
a stand made up of Unistrut and fine steel wires ran horizon-
tally from the load cells just barely touching the pulleys to

161
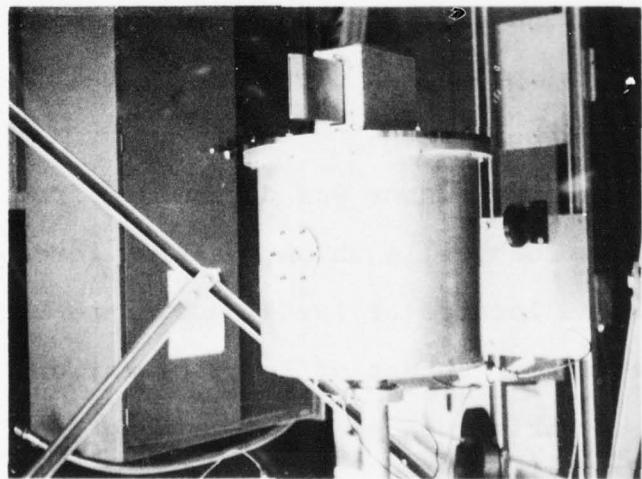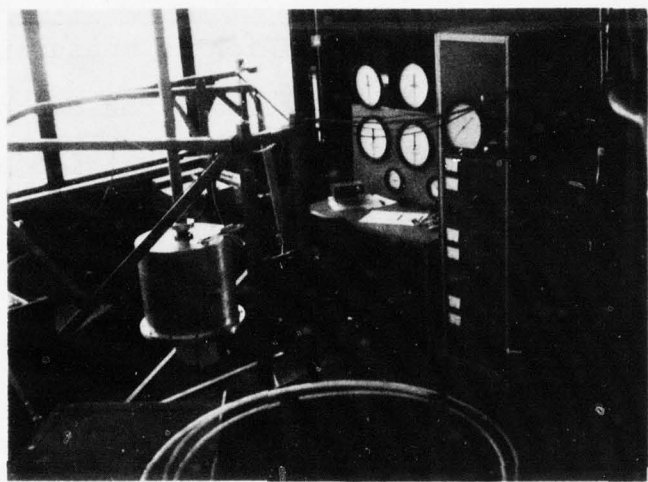
Figure 49. Photographs of facility.
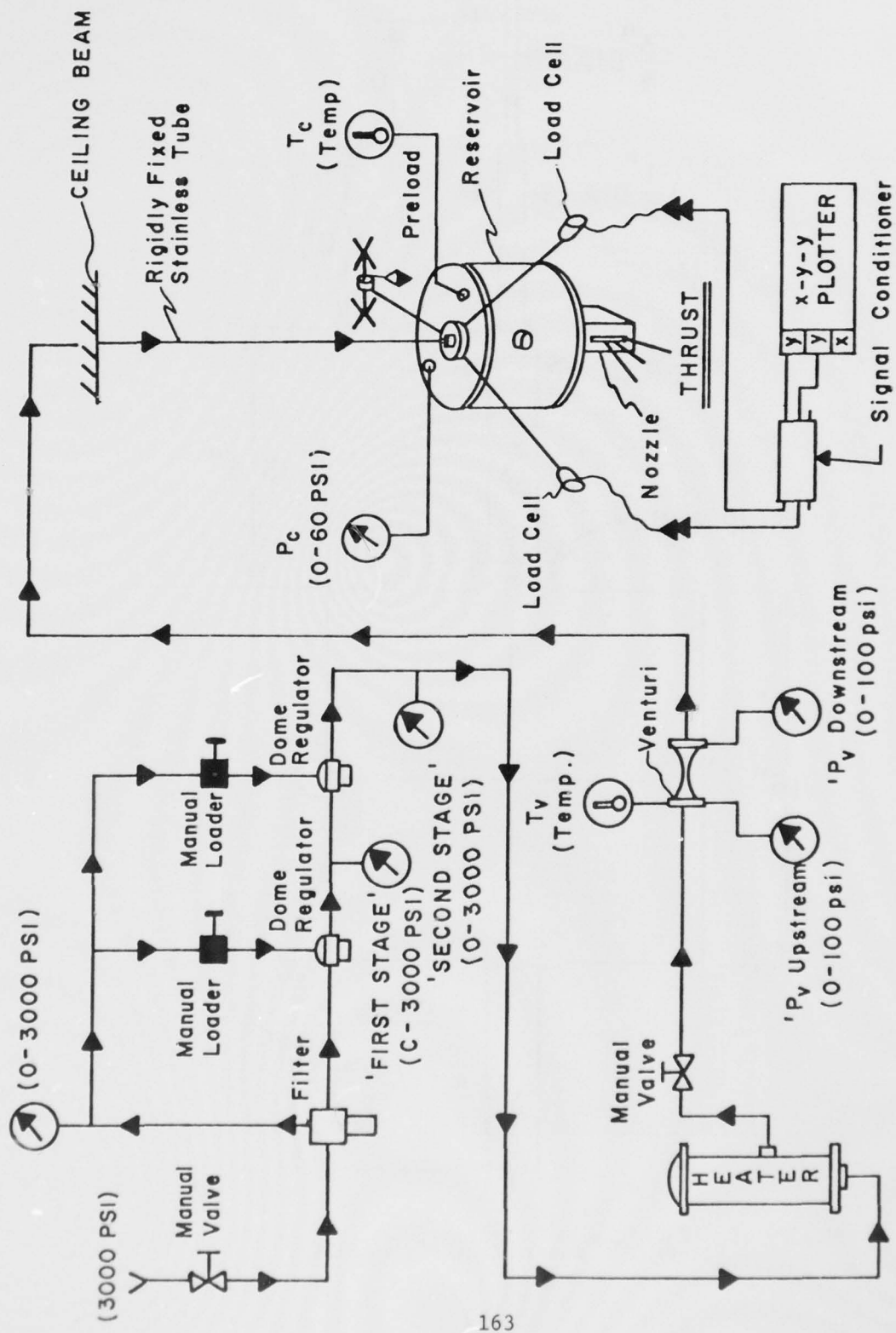
Figure 50. Schematic of nozzle test facility.

163
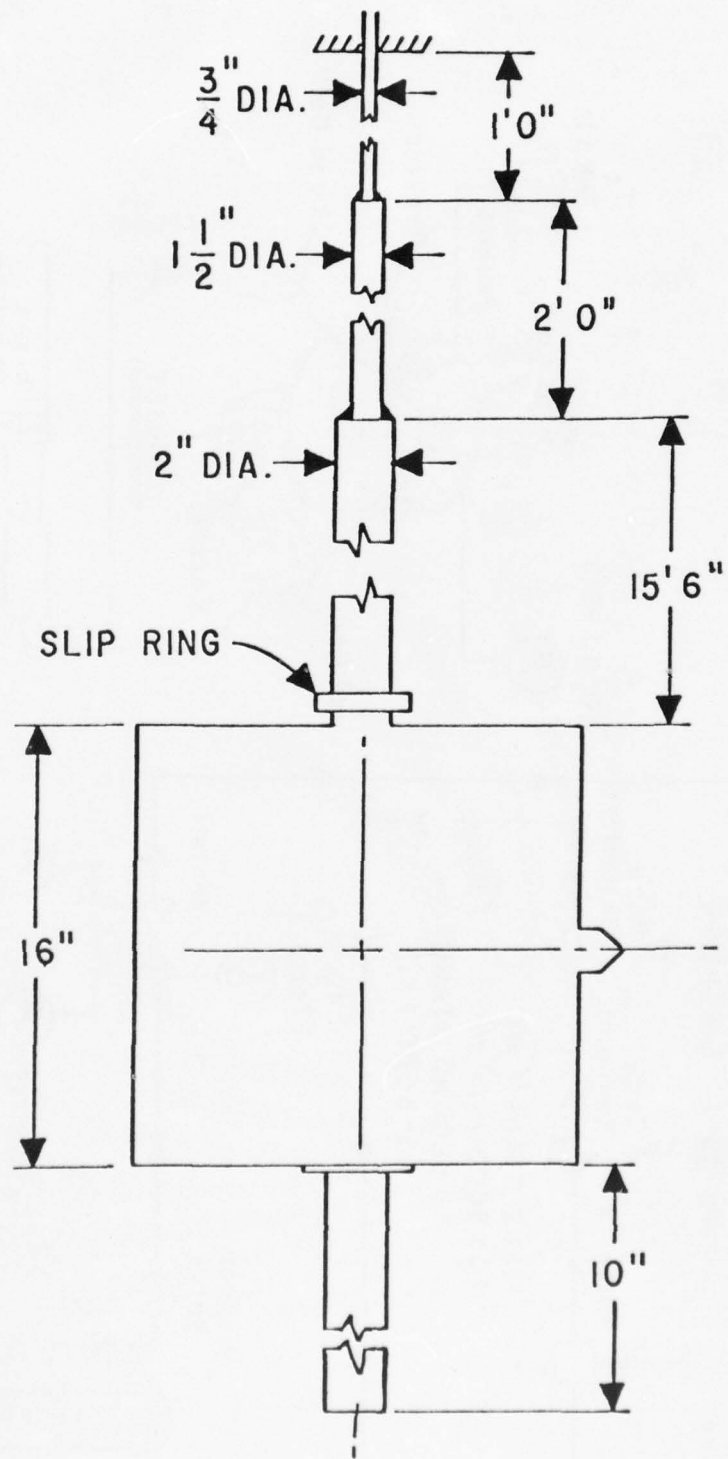
Figure 51. Nozzle test rig assembly.

a ball bearing slip collar around the air supply tube. This
construction assured that the load cell readings would not be
influenced by an eccentrically positioned nozzle. A third
wire ran horizontally from the slip collar to a pulley and was
used for tightening the cables by providing a preload.

The mass flow rate of air to the system was computed from
pressure and temperature measurements from a precalibrated
Venturi meter located some distance upstream of the vertical
tube assembly.

B.   Instrumentation

Two Stathem Model UC3 transducing cells each powered by
Daytronic Model 601B signal conditioners and combined with a
UL4 load cell accessory measured the components of the thrust
vector. The electrical output of each transducer drove one of
the y-axis pens on a Hewlett Packard Model 2FA X,Y,Y plotter,
while the x-axis indicated the excess of the chamber pressure.
The pressure signals were obtained from Stathem Model 399 (0-
15 and 0-50 psi) pressure transducers energized by Elcor Asoply
AQN4 power supplys and these were displayed by an electronic
digital indicator.

Calibration tests were run frequently on the force and
pressure transducing systems which showed linear relationship
within the specified ranges.

C.   Mechanical Properties

Figure 52 schematically represents the test facility reacting to the nozzle thrust P, the weight of the pressure chamber W and a movement M_L at a place where L is applied.

The theoretical relationship between cable tension T and applied load L is derived in the technical report ARL [13] 70-0140 and is given in a simple working formula:

$$\frac{T}{P} = \frac{\frac{3}{2}(\frac{1+h}{a}) - \frac{1}{2}}{1 + \varepsilon}$$

The deflection factor ε is a small number whose value depends explicitly on the material and geometric properties of the wire and the weight distribution of the facility. The relationship between indicated load T and applied load P with values of deflection factor ε are given in figures 53 to 58.

D.   Calibration Procedure

The values of ε were obtained from calibrating the overall force measuring system. Each load cell was first independently calibrated using a pulley and dead weight arrangement. Typical load cell calibrations are shown in figure 59. The system as a whole was calibrated by attaching the load cell cables to the slip ring and adding calibration weights to the pre-load weight hook. Preload signals were usually zeroed with an electrical bias. The linearity of the system is confirmed in figure 60.

166
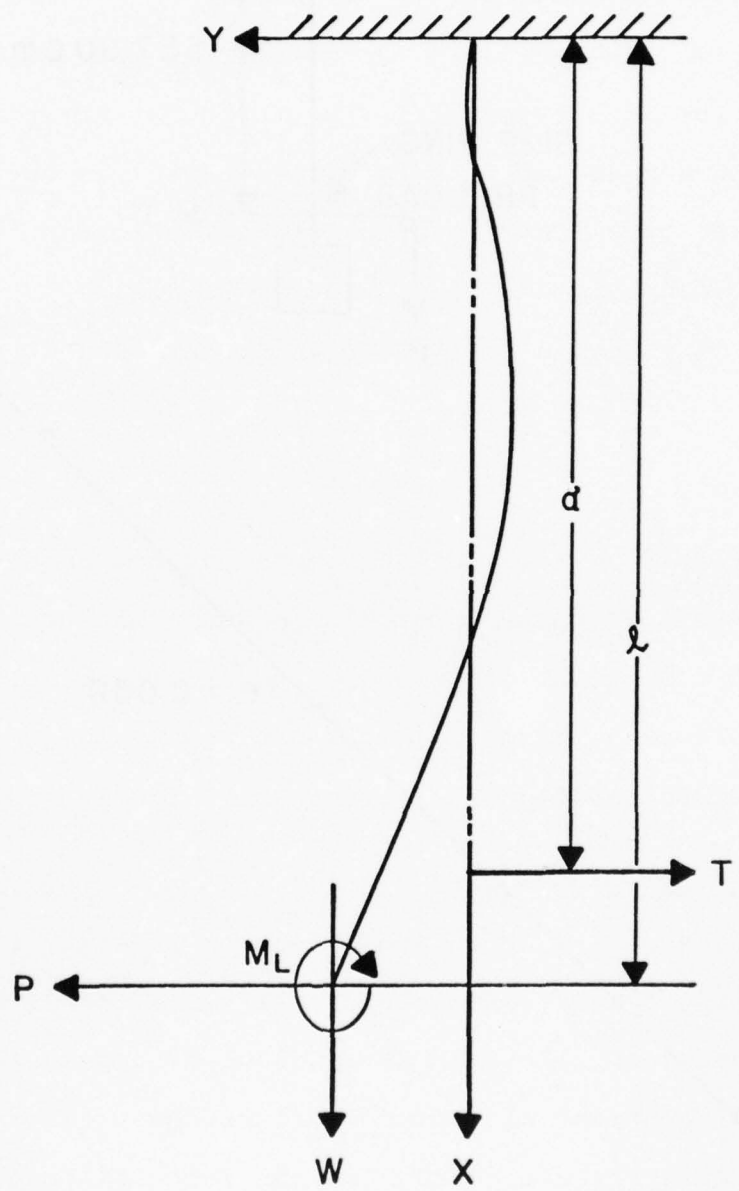
Figure 52. Schematic of applied load and deflections.

167
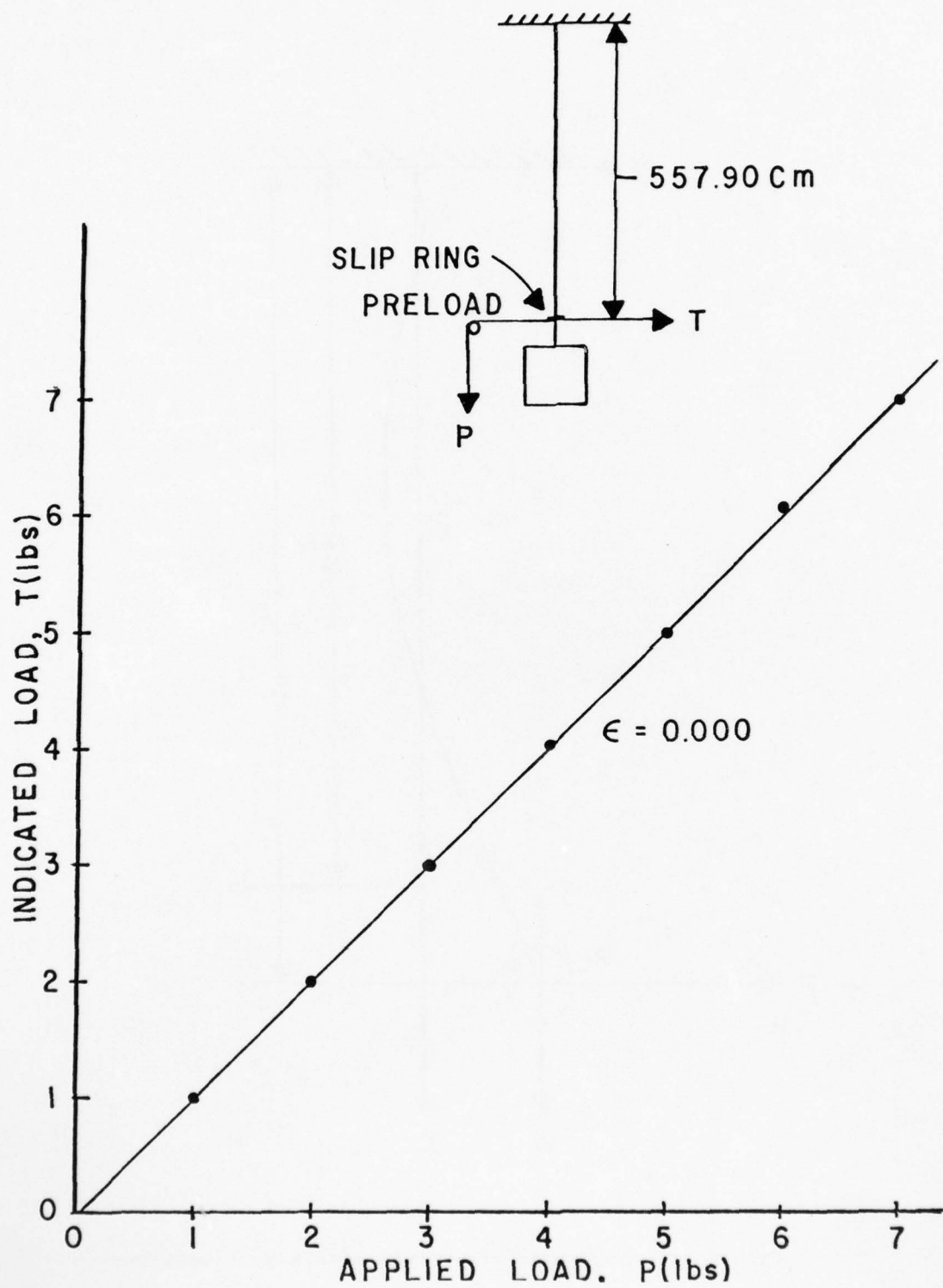
Figure 53. Relation between applied load and recorded loads (loads applied at the plane of load cells).
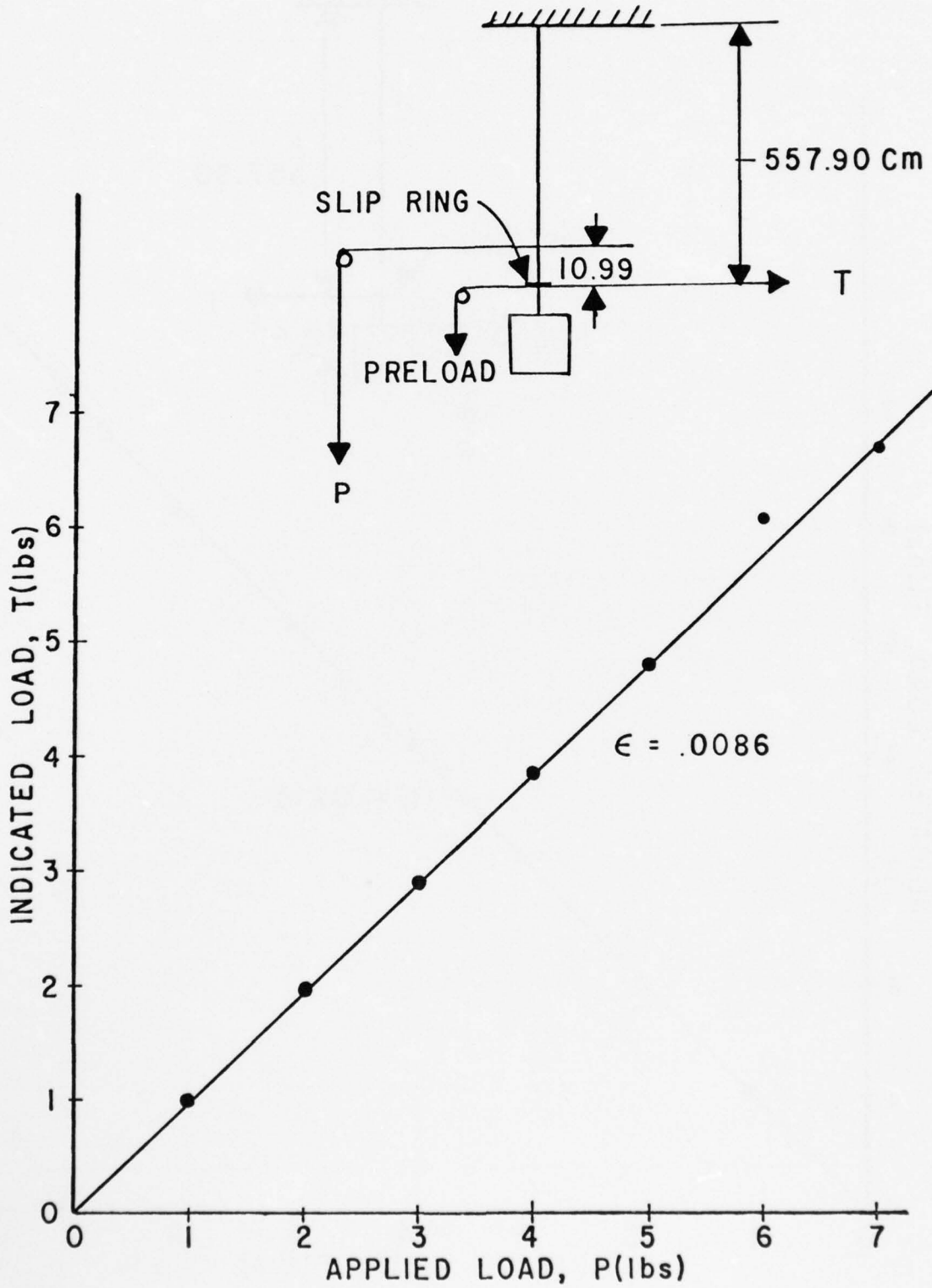
Figure 54. Relation between applied and recorded loads.
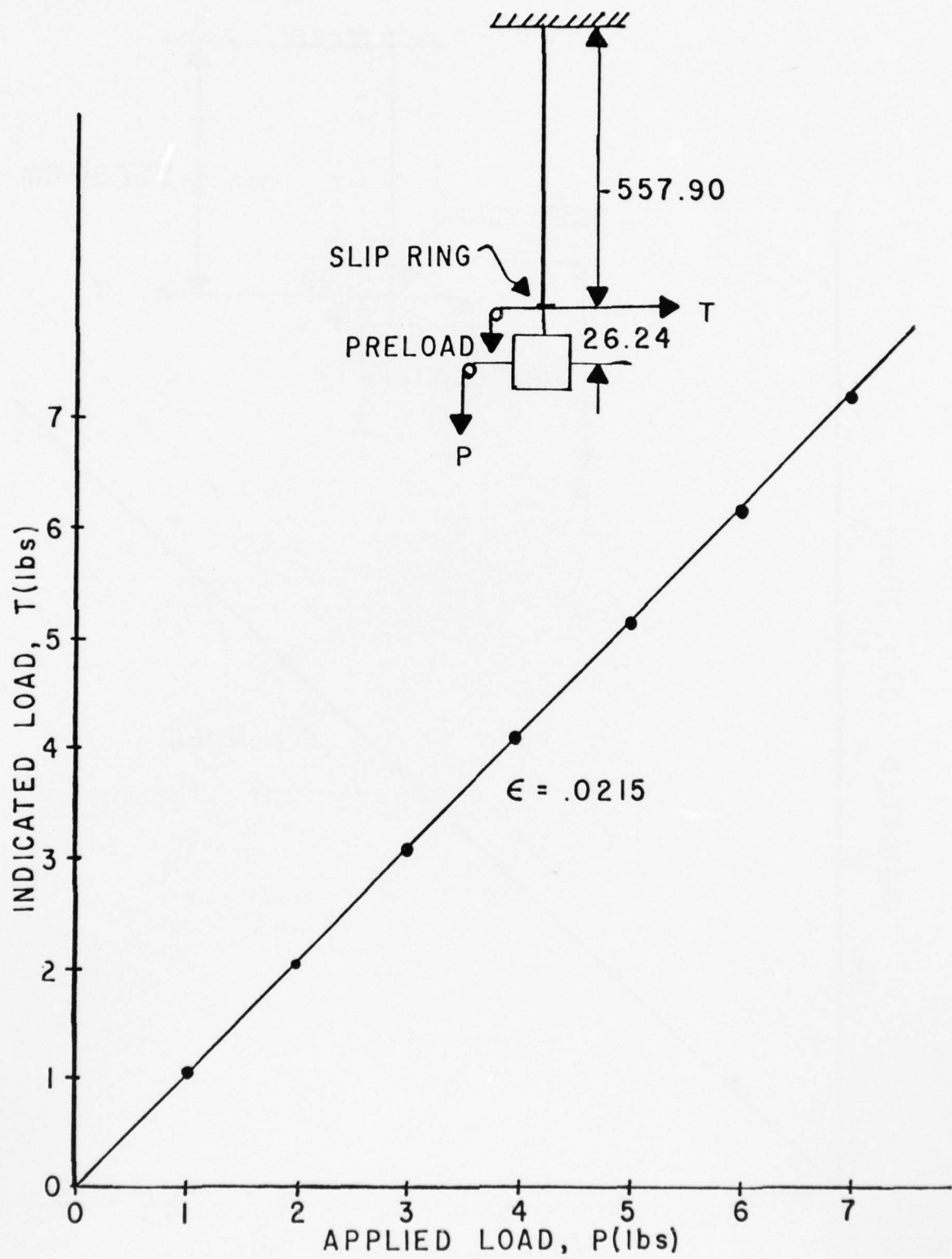
Figure 55. Relation between applied and recorded loads (loads applied at the center of pressure chamber.)
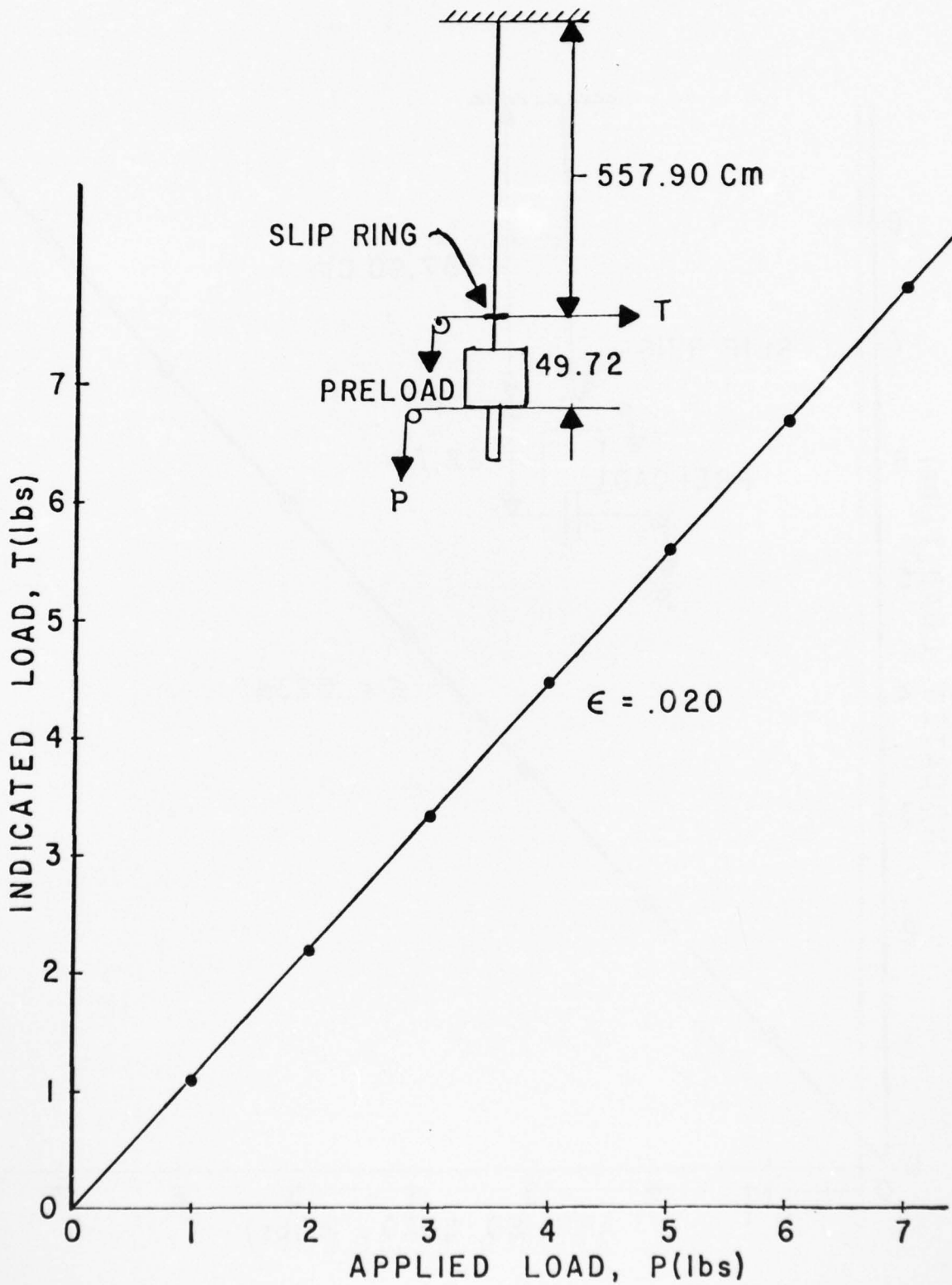
Figure 56. Relation between applied and recorded loads.
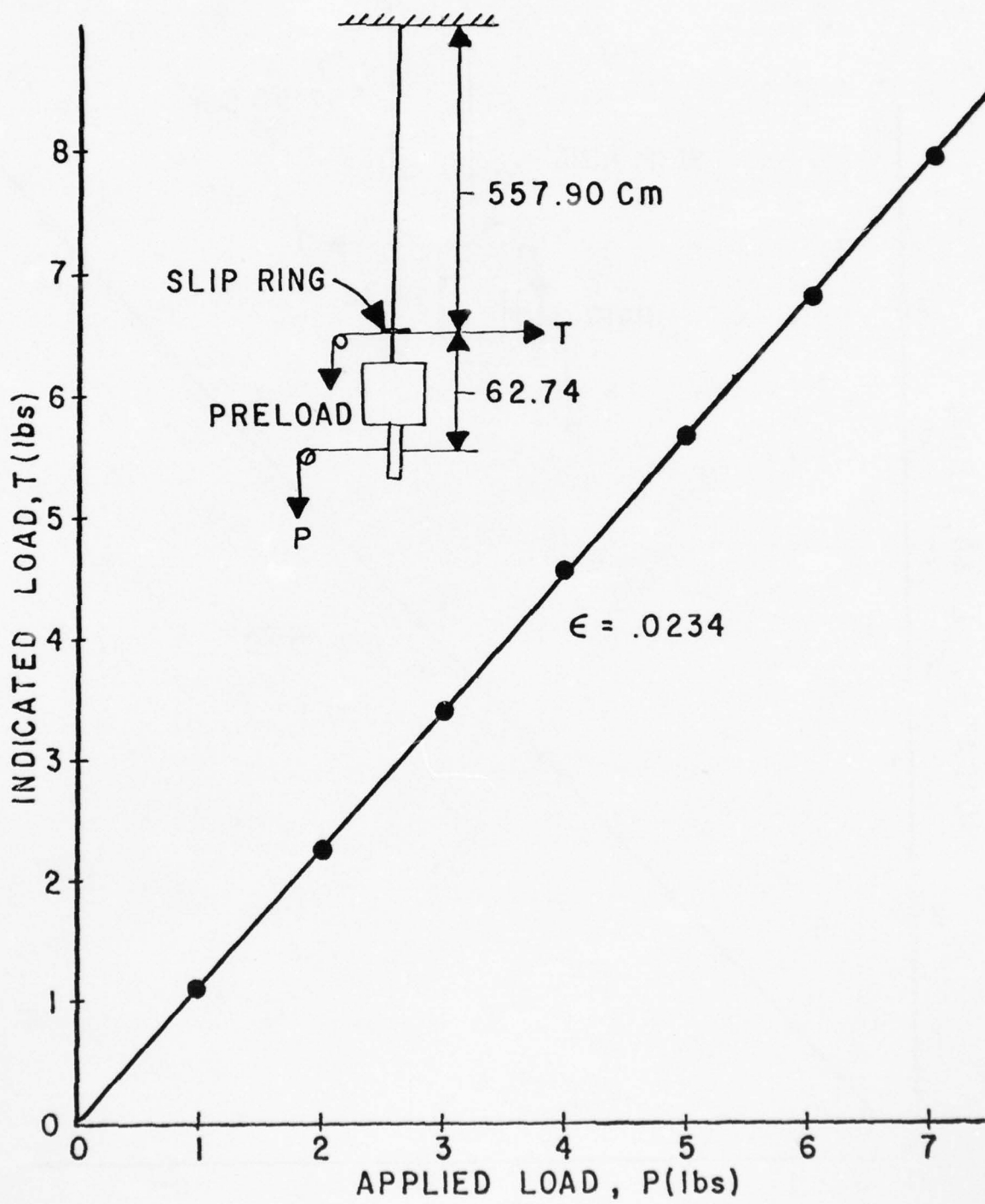
Figure 57. Relation between applied and recorded loads.
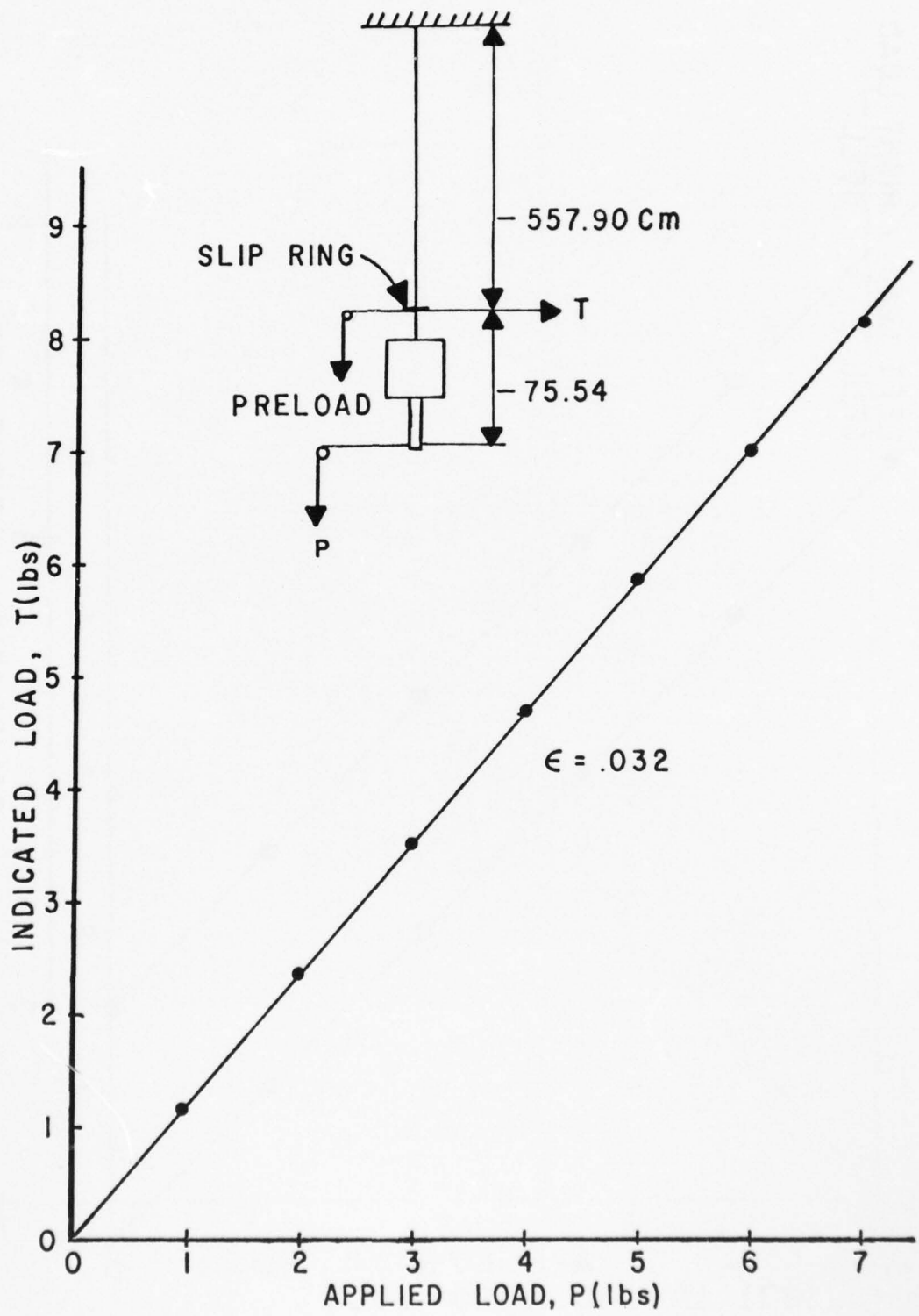
Figure 58. Relation between applied and recorded loads.

173
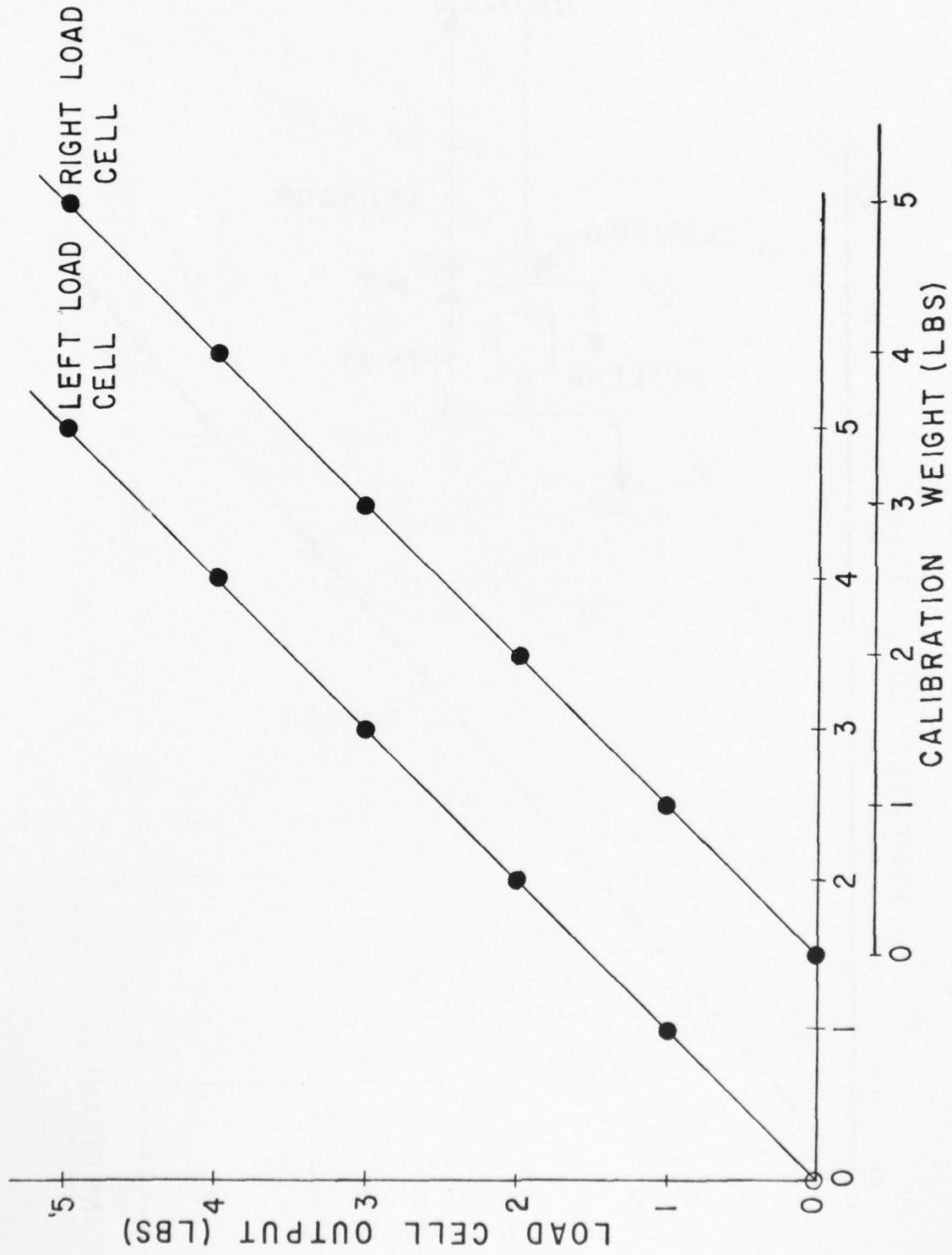
Figure 59. Typical load cell calibration.
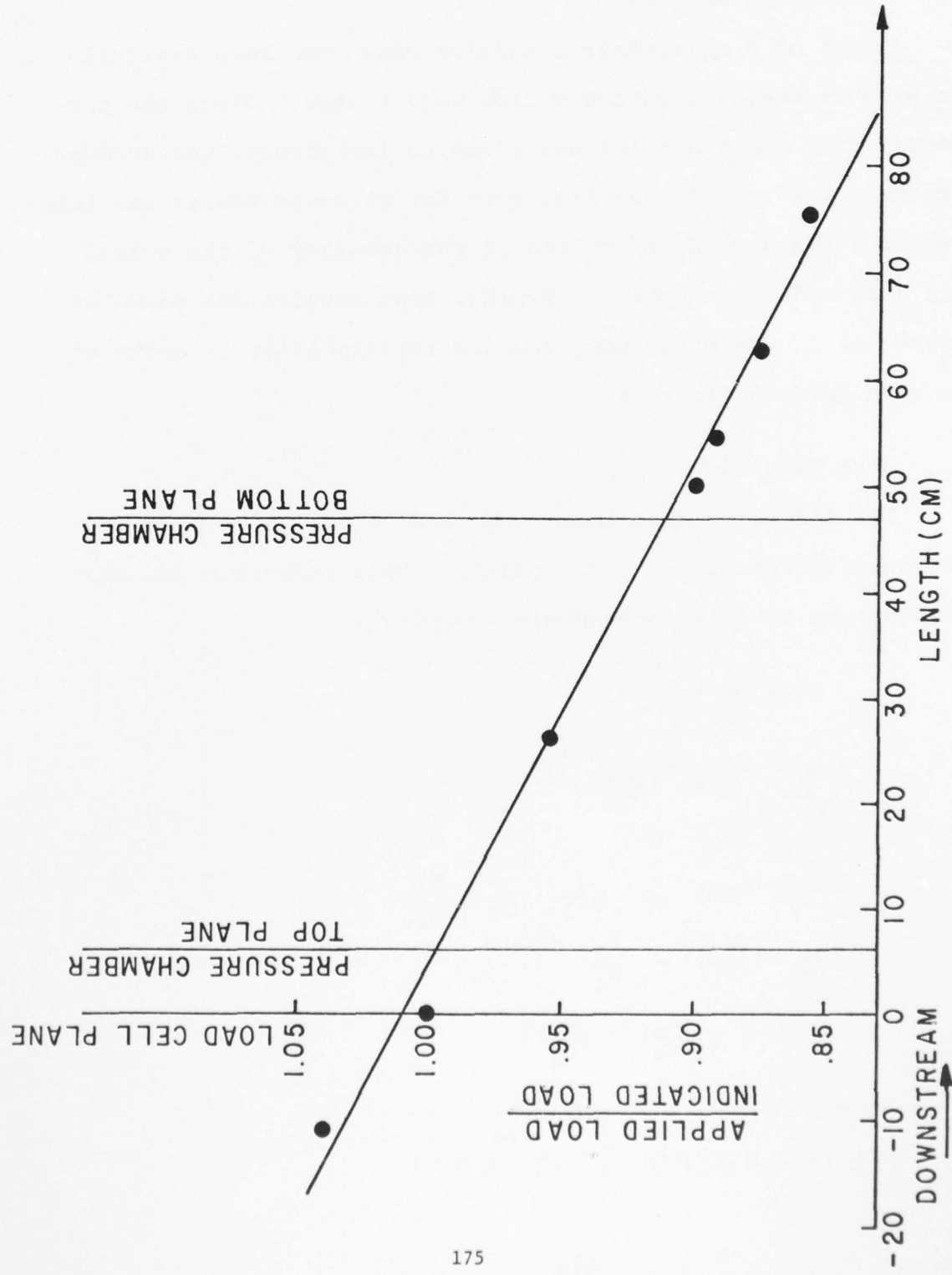
Figure 60. Load cell calibration factor.

E.   Testing of Nozzles

A set of 8 axisymmetric nozzles which had been designed
to produce nearly isentropic flow were tested. Since the per-
formance of these nozzles was close to isentropic, measurement
of their thrust and mass flow rate for given pressures and temp-
eratures was a good indication of the accuracy of the system
and data reduction scheme. Typical test nozzles are shown in
figure 61 . The efficiency and its repeatability is shown to
be very good in figure 62 .

F.   Data Reduction

The following equations were used to evaluate the flow
characteristics of the test nozzles. Data reduction was car-
ried out on Hewlett-Packard mini-computer.

$$PR = \frac{Pc}{Pa} + 1$$

$$A_{eff} = \frac{\dot{m}_a}{(\rho V)_{isen}}$$

$$\dot{m}_a = (\dot{m}_1) \cdot C$$

$$\dot{m}_1 = A_2 P_1 \ \frac{2}{R} \cdot \frac{\gamma}{\gamma - 1} \cdot \frac{1}{Tv} \ \frac{F_1}{F_2}$$

$$F_1 = (\frac{P_2}{P_1})^{\frac{2}{\gamma}} - (\frac{P_2}{P_1})^{\frac{\gamma + 1}{\gamma}}$$

$$F_2 = 1 - (\frac{A_2}{A_1})^4 \cdot (\frac{P_2}{P_1})^{\frac{2}{\gamma}}$$

176

MICROCOPY RESOLUTION TEST CHART
NATIONAL BUREAU OF STANDARDS-1963-A

TYPICAL   CALIBRATION   NOZZLE
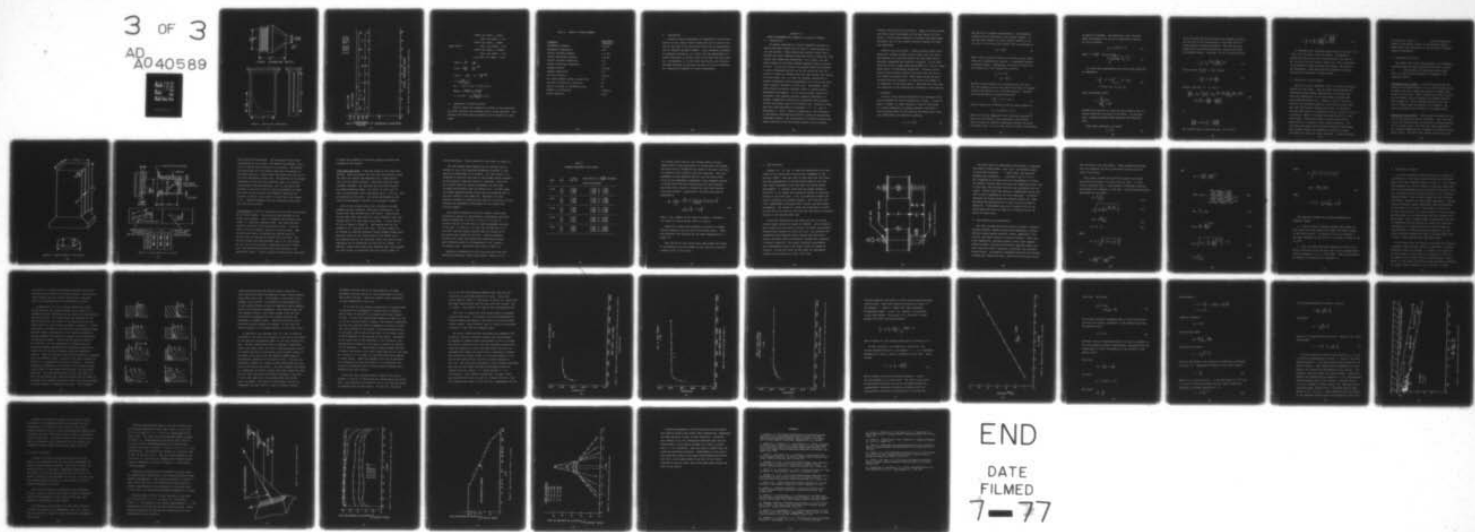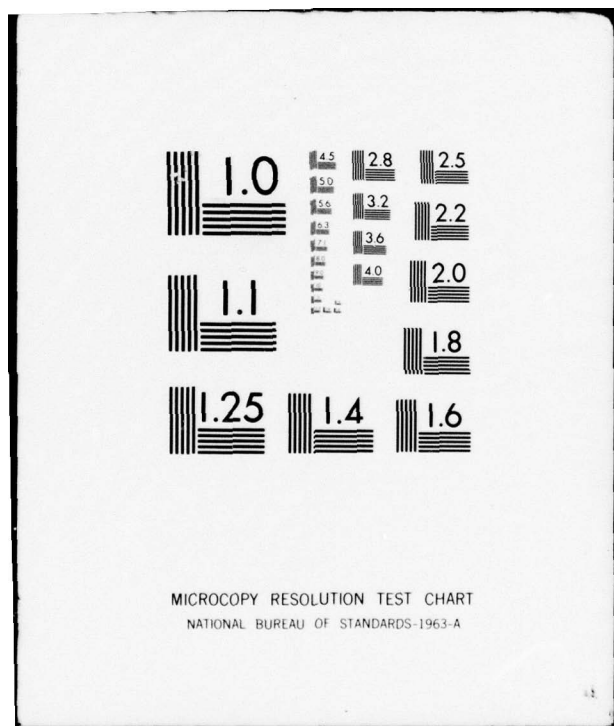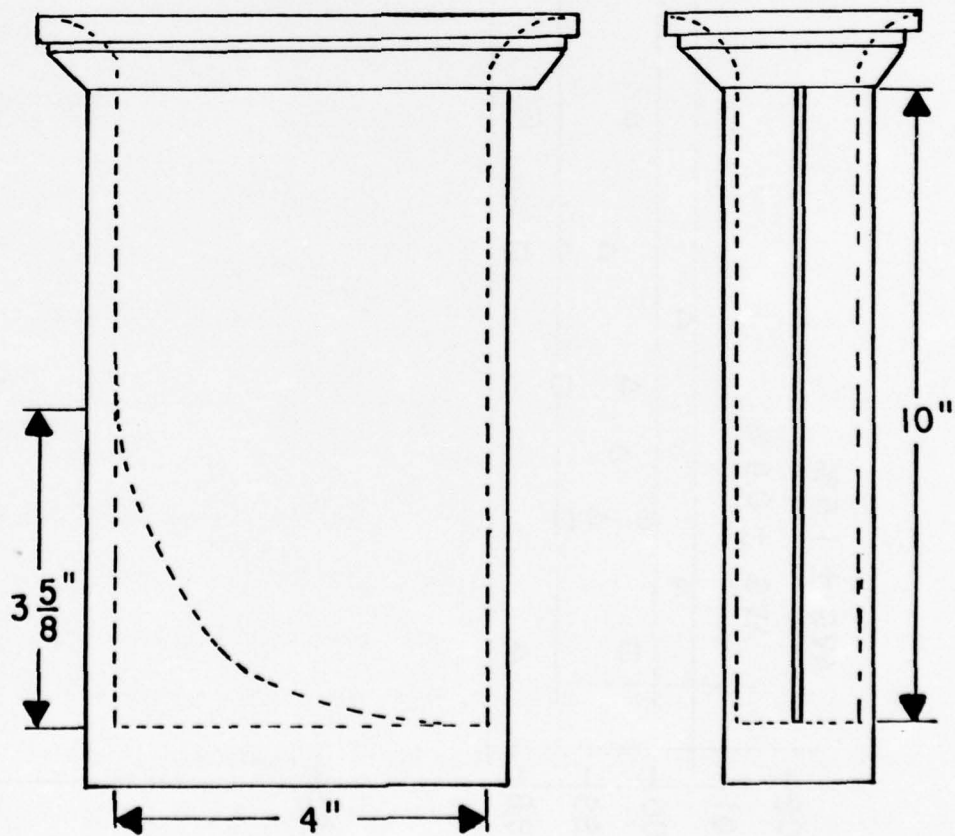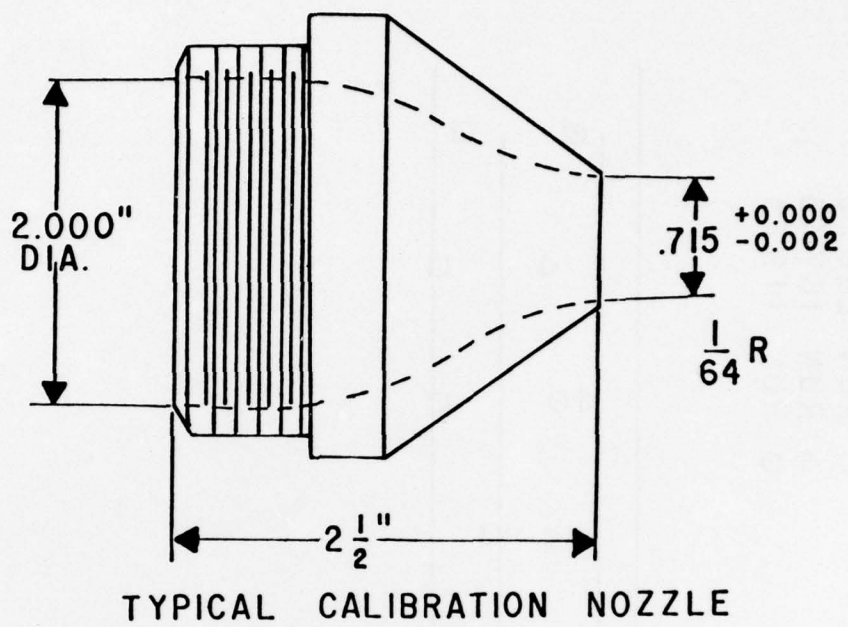
Figure 61.   Typical nozzle configurations.

177
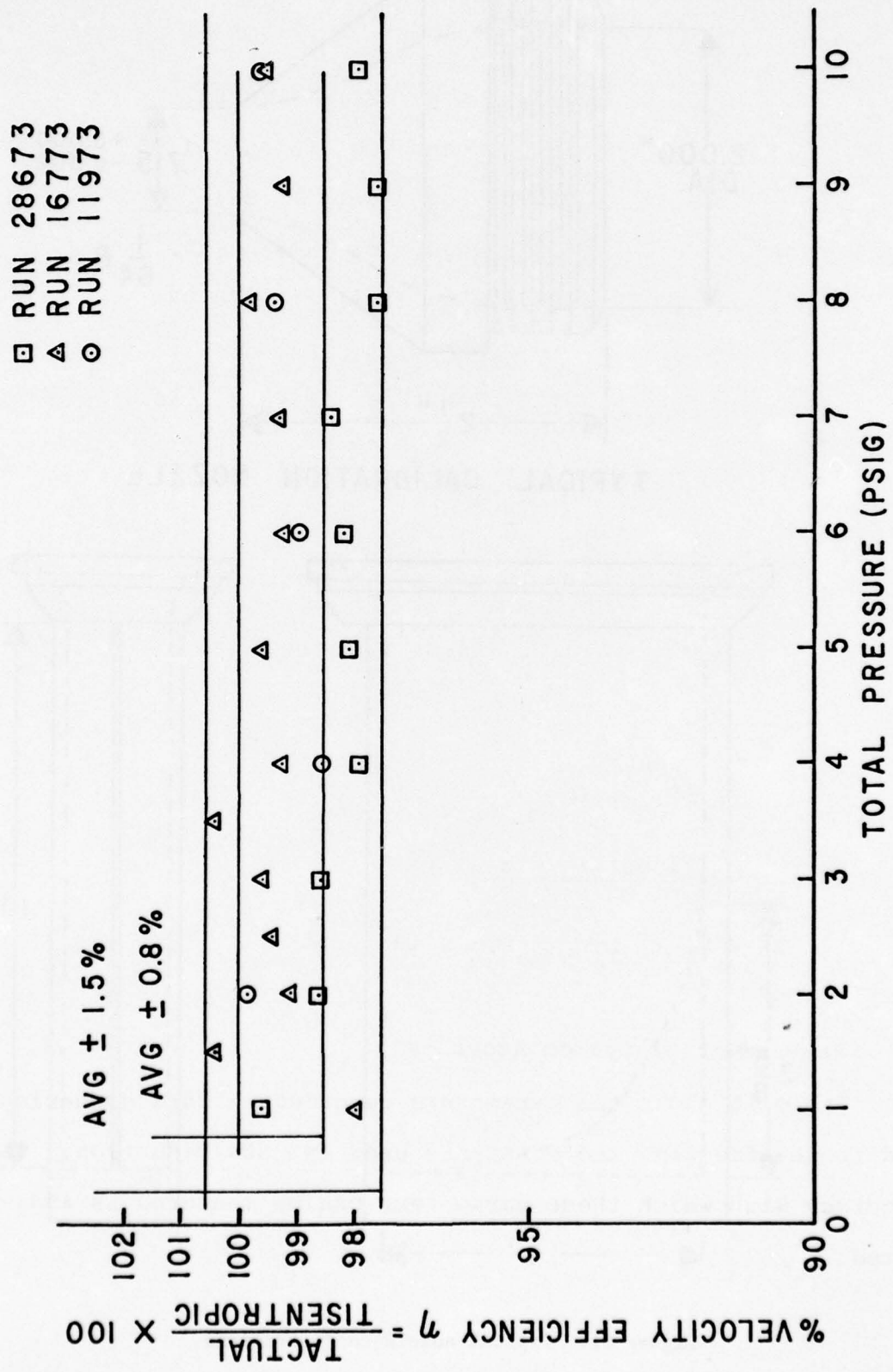
Figure 62. Efficiency repeatability for 1/2 inch diameter standard nozzle.

178

$$C_{NBS} \text{ Venturi} = \begin{cases} .038824 \text{ Log } (RE\#)_v + .82081 \\ \qquad \text{when, Log } (RE\#)_v < 4.95 \\ .025926 \text{ Log } (RE\#)_v + .88467 \\ \qquad \text{when, Log } (RE\#)_v < 5.22 \\ .007895 \text{ Log } (RE\#)_v + .978788 \\ \qquad \text{when, Log } (RE\#)_v < 5.60 \\ 1.023 \text{ when, Log } (RE\#)_v > 5.60 \end{cases}$$

$$(RE\#)_v = (\frac{\dot{m}_1}{\mu}) \cdot (\frac{4}{\pi D_1})$$

$$\rho_{isen} = (\frac{P_a}{RT_C}) \cdot (\frac{P_C}{P_a})^{\frac{\gamma-1}{\gamma}}$$

$$V_{isen} = (\frac{2}{\gamma-1}) \cdot [1 - (\frac{P_a}{P_C})^{\frac{\gamma-1}{\gamma}}]$$

$$\eta = \frac{T_N}{(\dot{m}_a)(V_{isen})}$$

$$T_N = (P_1)^2 + (P_2)^2 + (2P_1 P_2 \cos \theta)$$

$$RE\#/ft = \frac{(V_{isen}) \cdot (\rho_{isen})}{\mu}$$

$$\mu = [2.270] \cdot [\frac{(T_C)^{3/2}}{T_C + 198.6} \times 10^{-8}]$$

G. Assessment of System Accuracy

Table 11 shows the parameters recorded in data gathering and those affecting the constants used in data reduction. The accuracy with which these parameters can be measured is indicated.

179

TABLE 11. ACCURACY OF SYSTEM PARAMETERS

Parameter	Measurement Accuracy
Atmospheric pressure	±.01"Hg
Atmospheric temperature	±1°F
Venturi upstream pressure	±.01 PSI
Venturi downstream pressure	±.01 PSI
Venturi upstream temperature	±1°F
Venturi downstream temperature	±.5%
Chamber pressure	±.01 PSI
Chamber temperature	±1°F
Load cell tension	±.025 lb
Rt. angle between cables to load cells	±.5°
Leveling of cables to load cells	±1°
Thrust of nozzle in horizontal plane	±2°
Weights of calibration	±.0025 lb
Linear dimension	±1/16"

H.   Conclusions

Accurate thrust measurements as suggested by the previous section of this report could be made not only on nozzles, but also on any type of air flow device which can be installed on the 15" diameter pressure chamber. Using reasonable estimates of component accuracies, it is felt that the measurements of nozzle efficiency to within 1-1/2% can be made with this facility. Furthermore, it is felt that this nozzle test facility has been developed to the point at which it can be considered as a laboratory standard for thrust measurements.

SECTION III

THRUST PERFORMANCE AND LOSSES OF A FAMILY OF NOZZLES

A.   Introduction

Of primary importance in thrust augmenting ejectors is
having efficient nozzles that are used to inject primary air
into the ejector. These nozzles must produce thrust with a
minimum loss while remaining light and rigid in order that they
retain their shape when pressurized. As a result, the geo-
metric design of the nozzle becomes important from two points
of view. In the first place, the external walls must present
a clean, aerodynamic profile to the air entrained into the
ejector in order to minimize what have been called inlet losses.
It can be shown (ref. 14)that the marginal degradation of
ejector performance varies approximately on a one-to-one basis
with a marginal increase in inlet loss. Accordingly, every
effort should be made to maintain inlets at nearly perfect
aerodynamic performance. So far as the primary nozzles are
concerned, this suggests external contours reminiscent of
slender, symmetrical airfoils with truncated trailing edges
forming the exhaust area of the primary jets. Nozzles of this
type have been described in references   14 ,   15 , and 16 .
References 14 and 15   permit a comparison of the difference
in performance achieved with nozzles of good and bad external
aerodynamic design. The second point of interest concerns the
losses incurred by the high energy primary flow in passing

182

through the interior of the nozzles. These are nozzle losses,
and lower ejector performance to the same extent as inlet
losses. Nozzle losses diminish as internal flow Mach number
decreases, and for this reason efficient nozzles are thick
and voluminous.

Therein lies the problem: slender nozzles reduce inlet
losses but increase ejector nozzle losses, and vice versa.
The designer of a practical ejector is thus faced with an
important compromise and trade-off situation. In the past
decisions in this regard have been guided by a "rule of thumb",
based solely in engineering experience: internal nozzle
ducts should initially present flow areas that are four or
five times the exhaust area. While some success has been
achieved with this guidance, we cannot help but wonder if
it represents a true design point. Resolving this issue was
the objective of the investigation discussed in this section.

B. Analysis

To do so first required delineating the mechanisms that
tend to degrade the thrust produced by a nozzle. In the ab-
sence of losses, an ideal situation, fluid at exit plane
of a nozzle exhausting to ambient pressure would have a
total pressure equal to that driving the system and a velo-
city determined by the Bernoulli equation,

$$P_T = P_a + \frac{\rho}{2} V_i^2 \qquad (1)$$

when the flow is assumed incompressible. This assumption causes no loss of generality in the present argument. In the real case, however, the total pressure suffers a loss ΔP_T, due to flow turning and friction that may expressed as

$$\Delta P_T = \xi \frac{\rho}{2} V_c^2 \tag{2}$$

where ξ and V_c are mean values of a friction turning coefficient and a characteristic velocity. ξ undoubtedly depends on Reynolds number. Consequently, the real jet issues from the nozzle with a total pressure P_{T_j} given by

$$
\begin{aligned}
P_{T_j} &= P_T - \Delta P_T \\
&= P_T - \xi \frac{\rho}{2} V_c^2
\end{aligned}
\tag{3}
$$

Moreover, because ambient air is entrained into the free jet, the pressure acting on the base of the nozzle is slightly reduced below ambient, say to the mean value p_3. The mass flow rate determines an average velocity $\bar{U}$:

$$\dot{m} = \int_{A_j} \rho \, u \, d \, a = \rho \, \bar{U} \, A_j \tag{4}$$

which we assume can be related to the jet total pressure by

$$P_{T_j} = P_3 + \frac{\rho}{2} (\bar{U}^2 + v^2 + w^2) \tag{5}$$

where the velocity components v and w have been included to allow for the effects of flow seperation or poor design. Their inclusion is especially appropriate because the nozzle of interest (Ref. 14 , 15,16) also turns the primary flow through

184

an angle of 90 degrees. The quantities v and w are both small with respect to $\overline{U}$, and it is convenient to rewrite Eq. (5) as follows:

$$P_{T_j} = P_3 + \frac{\rho}{2} \overline{U}^2 (1 + \delta) \tag{6}$$

where $\delta = \frac{v^2 + w^2}{\overline{U}^2}$. From this follows

$$\overline{U} = \sqrt{\frac{2}{(1 + \delta)\rho} (P_{T_j} - P_3)} \tag{7}$$

To a very close approximation the actual nozzle thrust may be expressed as

$$T = \int_{A_j} \rho \, u^2 \, d \, a + \int_{A_j + A_B} (P_3 - P_a) da \tag{8}$$

$$= \rho \, \overline{U}^2 \, A_j B + (P_3 - P_a) \, (A_j + A_B)$$

where the skewness factor

$$\beta = \frac{\int_{A_j} u^2 \, d \, a}{A_j \left[\int_{A_j} u \, d \, a \right]^2}$$

exceeds unity when the jet velocity profile departs from uniformity across the exit plane of the nozzle. For the most part, β becomes meaningful when separated flow conditions exist.

Under ideal conditions, the thrust

$$T_i = \dot{m} \, V_i \tag{9}$$

185

can be achieved with the active mass flow through the nozzle, and the ratio of the actual thrust to this ideal thrust is a good measure of nozzle performance. The ratio has been called the nozzle thrust efficiency or velocity efficiency by different authors. Using Eqs. (8) and (9) directly gives

$$\eta = \frac{T}{T_i} = \beta \frac{\overline{U}}{V_i} - \frac{\left(P_a - P_3\right)\left(A_B + A_j\right)}{\rho A_j \overline{U} V_i} \tag{10}$$

and by writing $\dfrac{P_a - P_3}{\rho/2 \; \overline{U}^2} = \alpha$ there follows

$$\eta = \frac{\overline{U}}{V_i} \left[\beta - \frac{1}{2} \alpha \left(1 + \frac{A_B}{A_j} \right) \right] \tag{11}$$

However, from Eqs. (7), (3), and (1)

$$\left(\frac{\overline{U}}{V_i}\right)^2 = \frac{1}{1 + \delta} \; \frac{P_{T_j} - P_1}{\rho/2 \; V_1^2} = \frac{1}{1 + \delta} \; \frac{\left(P_T - P_a\right) + \left(P_a - P_3\right) - \xi \frac{\rho}{2} V_c^2}{\rho/2 \; V_1^2}$$

$$= \frac{1}{1 + \delta} \left[1 + \alpha \left(\frac{\overline{U}}{V_i}\right)^2 - \xi \left(\frac{V_c}{V_i}\right)^2 \right] \tag{12}$$

or

$$\left(\frac{\overline{U}}{V_i}\right)^2 = \frac{1}{1 + \delta - \alpha} \left[1 - \xi \left(\frac{V_c}{V_i}\right)^2 \right]$$

The required result follows from Eqs. (11) and (12):

186

$$\eta = \left[\beta - \frac{1}{2} \alpha \left(1 + \frac{A_B}{A_j} \right) \right] \sqrt{\frac{1 - \xi \left(\frac{V_c}{V_i} \right)^2}{1 + \delta - \alpha}} \qquad (13)$$

In reasonably well designed nozzles each of the terms $(\beta - 1)$, α and δ will be small, positive numbers. Consequently, unless the nozzle has a very large base area, the term in Eq. (13) will be very close to unity, and η will be governed by the effects of skin friction and turning. The nozzles and experiments described below were designed to explore the relative influences of these factors.

C. Description of Test Nozzles

The term $\xi (V_c/V_i)^2$ appearing in Eq. (13) was of principal interest to this study. The air supply system feeding the experiments unfortunately operated only at slightly less than room temperature; so we could obtain no significant and deliberate changes in ξ. However, $(V_c/V_i)^2$ can be related by the continuity equation to the ratio of the nozzle exit area and the mean internal flow area. We therefore obtained data across an interesting range of values of $\xi (V_c/V_i)^2$ by testing a family of nozzles with differing exit to flow area ratios. These were molded in three pieces from an epoxy resin in a laborious, slow, manual operation. The fact that each nozzle was distinctly different necessitated very careful molding and assembling practices to insure the absence of leaks and rough junctures. A typical casting

187

can be seen in Figure   63   , and the detailed pro-
cedure of fabrication is given in the following section.
These nozzles were designed by Dr. Brian Quinn of Aerospace
Research Laboratories.

D.   Fabrication of Nozzles

   The fifteen slot nozzles whose geometric and aerodynamic
characteristics have been investigated are shown in Figure
64 .   These nozzles were fabricated from an epoxy
resin, and that detailed procedure is discussed in the
following section.

Preliminary Cavity Casting: A cavity forming mandrel was
placed in the proper position in a 6" x 103/4" molding frame.
An epoxy resin and an appropriate amount of hardener were
poured into the frame. After a proper curing time, the cast-
ing was removed, and any flashings or extraneous material
were trimmed off. The top surface was milled flat, and a
coat of release agent was applied to all surfaces. The
casting and mandrel were returned to the molding frame.

Operational Cavity Halves: Casting resin was poured over the
top of the preliminary casting and mandrel. Care was taken
to pour the required amount of resin and to exclude entrained
air in critical areas. The resin must remain undisturbed
at a constant temperature for a minimum of 12 hours to insure
proper curing. The casting was removed and the two halves
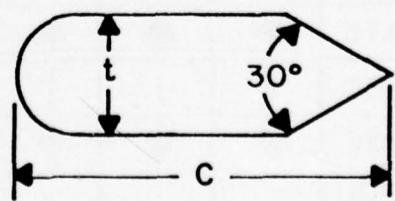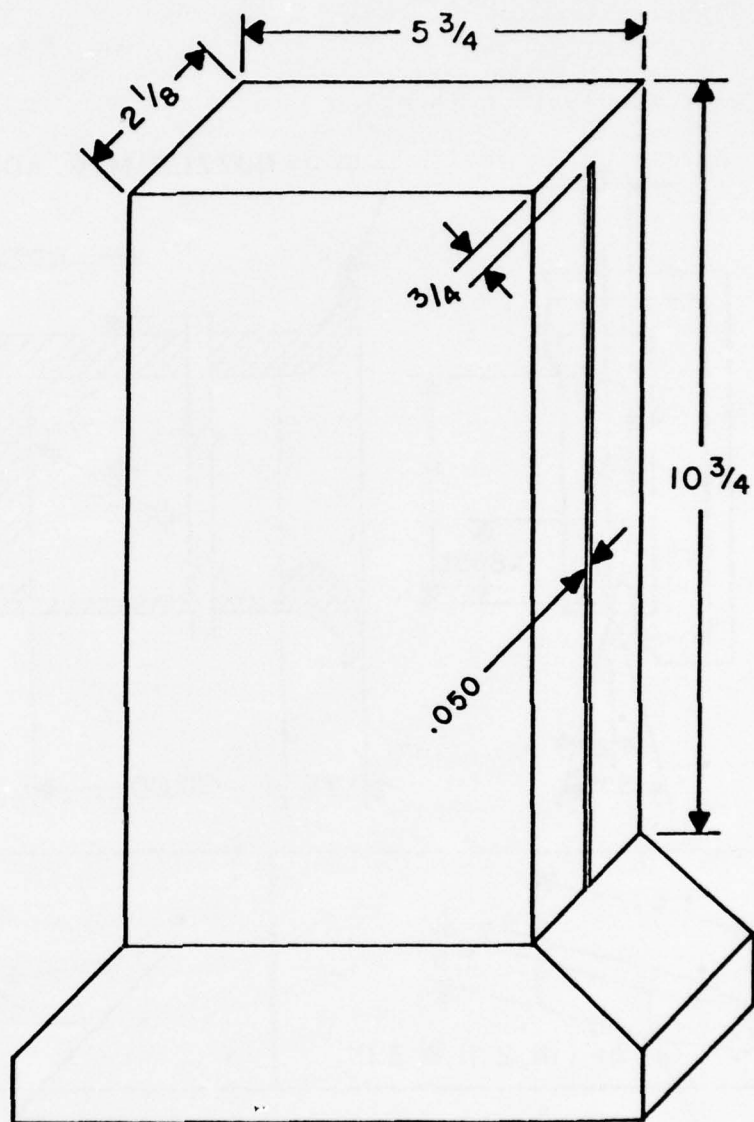
Figure 63.   External geometry of test nozzles.

189
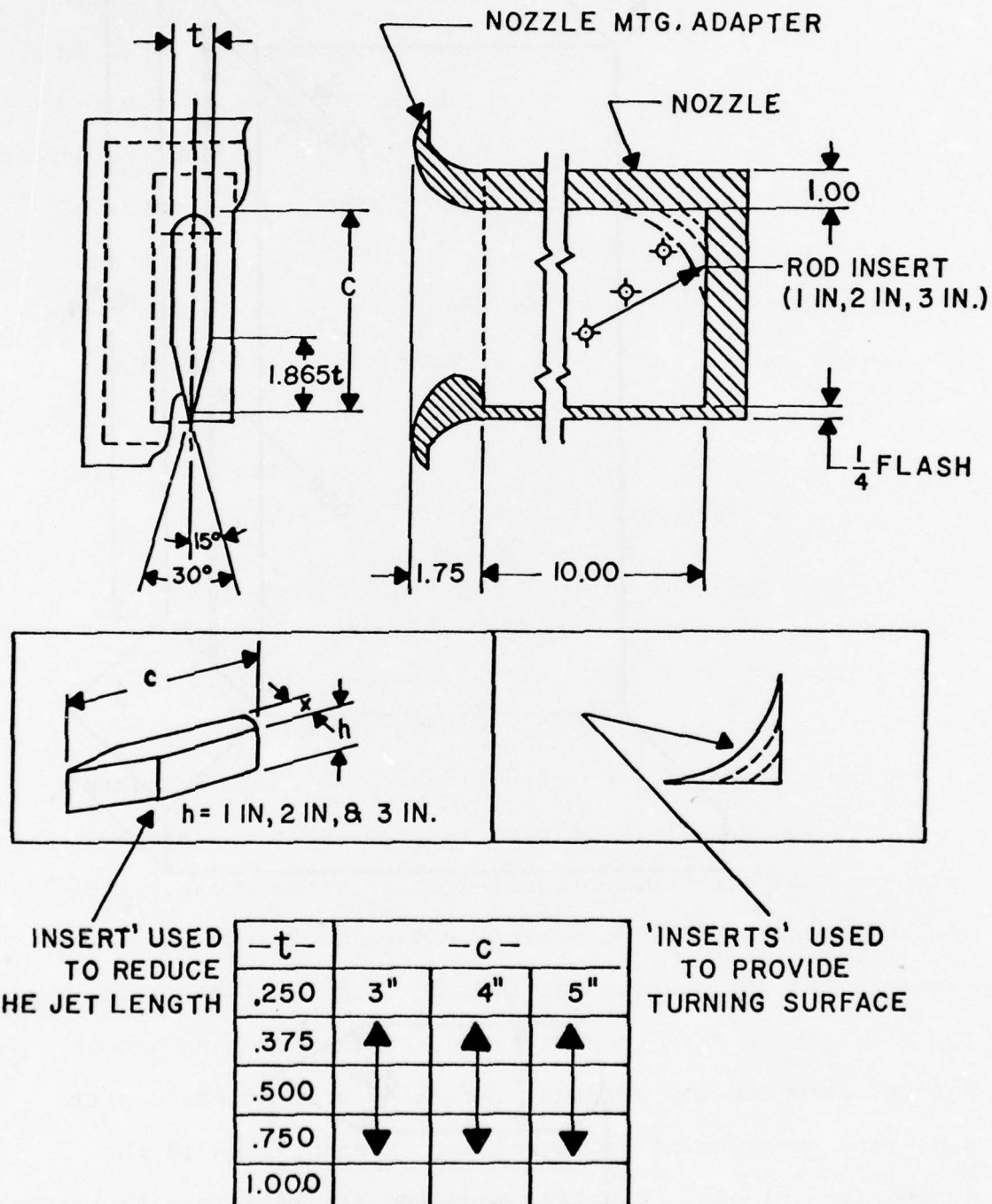
Figure 64. Internal geometry of test nozzles.

190

were carefully broken apart. The operational cavity half was machined on one surface, the mandrel was replaced, and a coat of release agent applied to all surfaces. The casting was placed back into the molding frame with the mandrel in the upper position. Casting resin was poured over the top of the first operational cavity half. The mandrel and the second operational cavity half were similarly made. All outside surfaces were then machined flat. An "O" ring groove was provided in one cavity half to avoid any possible air leaks. The nozzle outlet slot was then formed by machining the material to obtain a slot width of 0.050" and a slot length of 10". Mounting brackets were then fabricated and fitted into both cavity halves.

Inlet Section: A block of sufficient size was cast to fabricate an air inlet mandrel. The block was then machined to the design inlet mandrel. Next, the mandrel was carefully positioned in a specially designed flask. The flask was then filled to the proper level with casting resin. Care was taken to void air bubbles forming in critical areas. When the resin was cured, the mandrel was removed from the casting, and the casting was removed from the flask. The top and flanges were then machined, and an "O" ring groove was cut into the top surface. Mounting bolt holes, center sink, and positioning pin holes were then drilled in the appropriate places. Finally, mounting brackets were fabricated

191

to match the brackets of the cavity section and were then
attached to the casting.

Inlet Area Flow Guide: A dam was placed on the inlet area
section. Resin was poured into the area and allowed to cure.
The block was removed and machined with a tracer device
that gave the proper contours. This piece was later hand
finished, polished and installed into the inlet section.
An aluminum mounting plate, 1/4" thick, 9" wide, and 11"
long, was fabricated, and a rectangular hole, 3 1/4" by 7 1/4",
was machined in the plate. The nozzle was mounted on the
place and subsequently attached to the pressure chamber.

Each of the fifteen nozzles has a different internal
geometry and was therefore, fabricated individually. The
nozzles have been divided into five series. (Each series
has the same inlet area width for three different inlet area
lengths with a 15° cone shape at one end). A cross section
of this is shown in Figure 64. The exhaust slot for all
nozzles is 10" long and 0.050" wide. The slot length can
be reduced by inserting different length elements whose cross
sectional areas are the same as that of the nozzle inlet.
The elements are one, two and three inches long and are used
separately and in combination to vary the slot length. In
addition, corner flow guides with different radii are designed
for each series to investigate the flow turning effect on

nozzle efficiency. These inserts are also shown in Figure 64.

The area through which primary air is injected into an ejector is one of the important parameters involved in estimating the performance of an ejector. For this reason it is necessary to keep the exit area of the primary nozzle constant as the pressure inside the nozzle is increased. Since the slot nozzles were not totally restrained, the exit area expanded significantly from the nominal area. In some cases, the nozzle expansion during testing was so pronounced that it was very visible to the naked eye. Therefore, all data analysis included an effective area that was calculated from the pressure and temperature measurements of the venturi and stilling chamber.

The external geometry of the test nozzles, shown schematically in Figure 63, approximates a rectangular parallelepiped of dimensions 2 1/8 in. x 5 3/4 in. x 10 3/4 in. (54 mm x 146 mm x 273 mm) with a flange arrangement attached to one end. A 0.050 in. (1.27 mm) slot running for 10 in. (25.4 mm) from the flange juncture down the centerline of the narrow face formed the jet exit. Fifteen different internal flow areas were obtained by fabricating nozzles with different values of the dimensions C and t shown in the section view. These have been listed in Table 12.

Additional combinations of flow area and exit area were achieved by machining three filler blocks, (Figure 64) to

TABLE 12

INTERNAL DIMENSIONS OF TEST NOZZLES

t (IN.)	C (IN.)	A FLOW (SQ. IN.)	AREA RATIOS AR = $\frac{A\ FLOW}{A\ JET}$ AVAILABLE USING FILLER BLOCKS		
0.250	3.0	0.6850	1.3700	to	3.4251
	4.0	0.9350	1.8700	to	4.6751
	5.0	1.1850	2.3700	to	5.9251
0.375	3.0	0.9788	1.9576	to	4.8939
	4.0	1.3538	2.7076	to	6.7689
	5.0	1.7288	3.4576	to	8.6439
0.500	3.0	1.2400	2.4801	to	6.2002
	4.0	1.7400	3.4801	to	8.7002
	5.0	2.2400	4.4801	to	11.2002
0.750	3.0	1.6651	3.3302	to	8.3256
	4.0	2.4151	4.8302	to	12.0756
	5.0	3.1651	6.3302	to	15.8256
1.000	3.0	1.9602	3.9204	to	9.8010
	4.0	2.9602	5.9204	to	14.8010
	5.0	3.9602	7.9204	to	19.8010

fit tightly within each of the fifteen nozzle cavities.
These could be used individually or collectively and changed
the area ratio by decreasing the length of the exit slot from
ten inches to four inches in one inch intervals. With this
equipment we were therefore able to vary the nozzle area
ratio by the independent techniques, using different nozzles
to change flow area while maintaining exit area constant
and using filler blocks to change exit area while holding
flow area constant. Analytically, the area ratio may be
expressed as

$$AR = \frac{A_{FLOW}}{A_{JET}} = \frac{t^2 \left[\frac{\pi}{8} - \frac{1}{2} - \frac{1}{2 \tan 15°} + \frac{1}{4 \tan 15°} + \frac{c}{t} \right]}{W(10-h)}$$

$$= \frac{t^2}{W(10-h)} \left(\frac{c}{t} - 1.04029 \right) \tag{14}$$

where t and C depend on the choice of nozzle, h depends on
the choice of filler blocks, and W = 0.050 in.

Additional inserts were available to provide a rounded
turning surface at the far end of the nozzle cavity. These
were machined from aluminum and are shown schematically in
Figure 64.

That portion of each nozzle block that formed the flange
on the exterior was well rounded on the interior to provide
a smooth inlet to the cavity.

195

E. Test Procedure

Figures 65, 49, and 50 show the installation of a test
nozzle in the nozzle test facility and a schematic of the
facility itself. Care was taken to make sure that the nozzle
face was perpendicular to the horizontal plane of the fine
steel wires connected to the load cells for nozzle thrust
measurements. A coplanar third wire was loaded through a
pulley by a 2 lb. weight and maintained tension in the wires
leading to the load cells. A set of calibration weights was
used to calibrate the pressure systems. Each load cell was
first independently calibrated with a pulley and dead weight
arrangement. The system as a whole was calibrated by attach-
ing the load cell cables to the slip ring and adding calibration
weights to the preload weight pan.

Electrical sensitivities and spans were set to present
linear outputs across the ranges of interest. Force readings
were thought to be accurate to within 0.05 pound, and pressure
readings were accurate to within 0.01 psi. All pressure and
temperature data recorded during testing were read from a
digital indicator which was carefully checked and calibrated
at regular intervals. The digital indicator measurements
were consistently found to be linear across the ranges of
interest. During the course of the tests all measurement
systems were calibrated at least once a day.

SLIP RING

PRESSURE CHAMBER

FLOW

16in.

≈11in.

10in.

FLOW
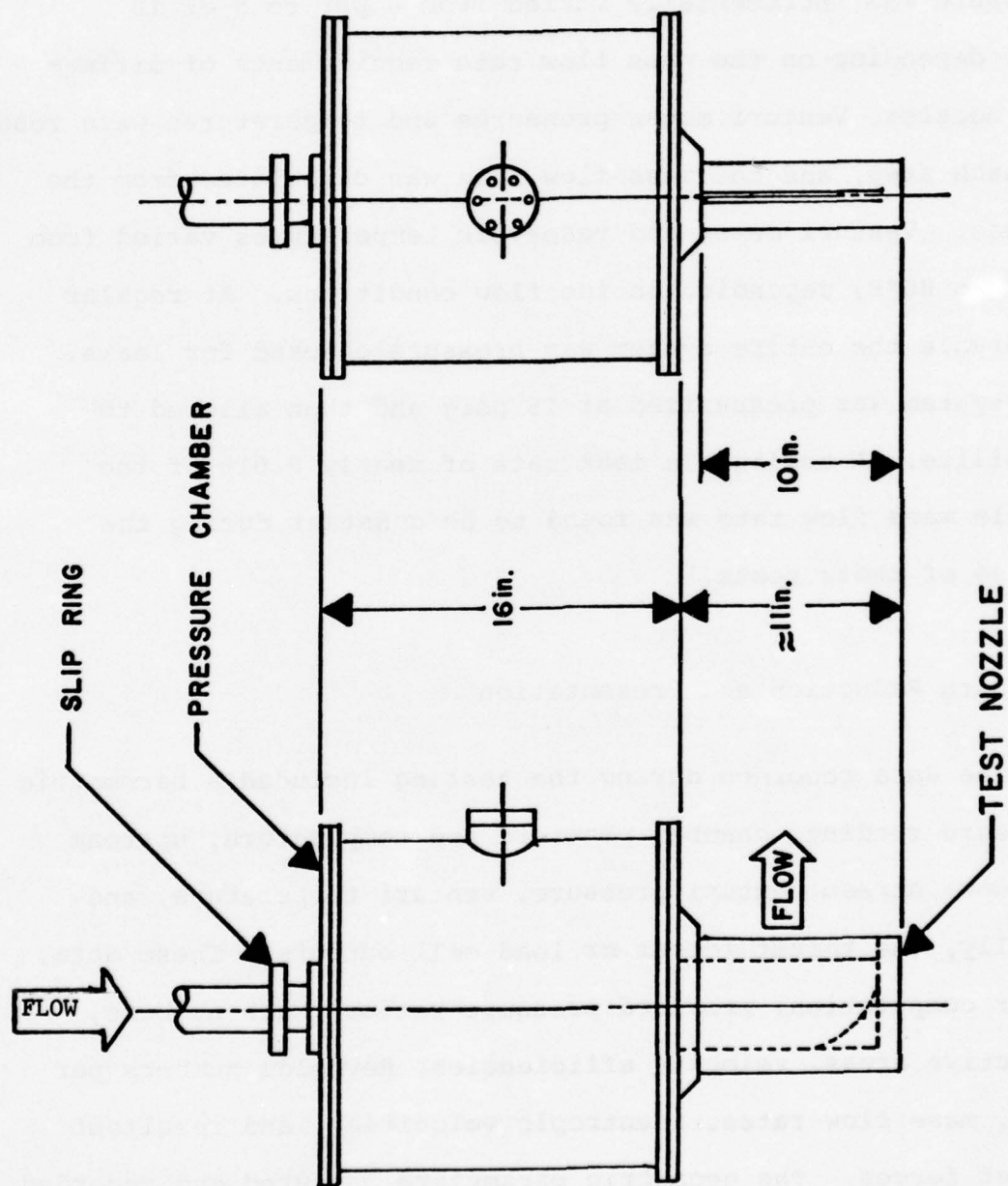
TEST NOZZLE

Figure 65. Test nozzle installation.

The first series of experiments was designed to determine
the effect of Mach number, area ratio, and Reynolds number
on the nozzle efficiency. In these tests, the reservoir
pressure was incrementally varied from 0 psi to 5 or 10
psi, depending on the mass flow rate requirements of differ-
ent nozzles. Venturi meter pressures and temperatures were read
at each step, and the mass flow rate was calculated from the
values. Venturi meter and reservoir temperatures varied from
50°F to 80°F, depending on the flow conditions. At regular
intervals the entire system was pressure checked for leaks.
The system was pressurized at 15 psig and then allowed to
stabilize. A negligible leak rate of nearly 0.01% of the
nozzle mass flow rate was found to be constant during the
course of these tests.

F. Data Reduction and Presentation

The data recorded during the testing included a barometric
pressure reading, chamber pressure and temperature, upsteam
and down stream venturi pressure, venturi temperature, and
finally, the thrust forces or load cell outputs. These data,
after computation, provided pressure ratios, Mach numbers,
effective areas, velocity efficiencies, Reynolds numbers per
foot, mass flow rates, isentropic velocities, and resultant
thrust forces. The geometric parameters measured and recorded
included slot length and width, nozzle inlet and outlet area,

198

and curvature of the flow guides. These parameters provided data for computing the slot length-width ratios and inlet-outlet area ratios.

This report includes the results of nearly two hundred tests with an average of 15 data lines per test. In view of the voluminous data, it was decided to undertake reduction and analysis on a computer, a CDC 6600. The following equations were coded for this task:

$$PR = \frac{P_c + P_a}{P_a} \tag{16}$$

$$M = \sqrt{\frac{2}{\gamma - 1}\left[(PR)^{-\left(\frac{\gamma - 1}{\gamma}\right)} - 1\right]} \tag{17}$$

$$A_{eff} = \frac{\dot{m}_a}{(\rho\, v)_{isen}} \tag{18}$$

$$\dot{m}_a = \dot{m}_1 \cdot C_d \tag{19}$$

where

$$\dot{m}_1 = A_2\, P_1 \sqrt{\frac{2}{R} \cdot \frac{\gamma}{\gamma - 1} \cdot \frac{1}{T_v} \cdot \frac{F_N}{F_D}}$$

and

$$F_N = \left(\frac{P_2}{P_1}\right)^{2/\gamma} - \left(\frac{P_2}{P_1}\right)^{\frac{\gamma + 1}{\gamma}}$$

199

and

$$F_D = 1 - \left(\frac{A_2}{A_1}\right)^2 \cdot \left(\frac{P_2}{P_1}\right)^{2/\gamma}$$

$$C_{d_{Test\ Venturi}} = \begin{array}{l} .13857\ Log(Re)_v + .34472 \\ \quad when,\ Log(Re)_v\ F\ 4.70 \\ .07576\ Log(Re)_v + .639927 \\ \quad when,\ 5.03 > Log(Re)_v > 4.70 \\ .017647\ Log(Re)_v + .932235 \\ \quad when,\ 5.20 > Log(Re)_v > 5.03 \\ 1.024\ when,\ Log(Re)_v > 5.20 \end{array} \qquad (20)$$

$$(Re)_v = \frac{\dot{m}_1}{\mu} \cdot \frac{4}{\pi\ D_1} \qquad (21)$$

$$\rho_{isen} = \frac{P_a}{Rt_c} \cdot \left(\frac{P_c}{P_a}\right)^{\frac{\gamma - 1}{\gamma}} \qquad (22)$$

$$v_{isen} = \sqrt{\frac{2}{\gamma - 1} \cdot \left[1 - \left(\frac{P_a}{P_c}\right)^{\frac{\gamma - 1}{\gamma}}\right]} \cdot a \qquad (23)$$

$$\eta = \frac{T_N}{\dot{m}_a\ (v_{isen})} \qquad (24)$$

200

where

$$T_N = \sqrt{T_1^2 + T_2^2 + (2\, T_1\, T_2\, \cos\theta)}$$

where

$$Re/ft = \frac{v_{isen} \cdot \rho_{isen}}{\mu} \tag{25}$$

where

$$\mu = [2.270] \cdot \left[\frac{t_c^{3/2}}{t_c + 198.6} \times 10^{-8}\right]$$

The computer provided the following combination of graphical output:

1. Plots of nozzle efficiency against Mach number for each nozzle with and without the curved flow guide inserted in the nozzle cavity. In Figures 10 to 14 in reference 17 the sheet parameter is the ratio of the length to width of the jet exit.

2. Plots of nozzle efficiency against the ratio of the cavity inlet area to the jet exit area at four representative levels of pressure; 2, 4, 6, and 8 psig. These are presented as Figures 116 through 145 in reference 17.

G. Discussion of Results

It is not altogether clear from Figures 10 through 114 in reference 17 that thrust efficiency has any real dependence on jet Mach numbers between 0.2 and 0.7. Prior experience suggests not, and the slightly increasing trends apparent in the data obtained from the thinner nozzles with large L to W ratios could be attributed equally to an increasing Reynolds number. Most of these graphs are flat to within one percent, suggesting no Mach number dependence. Some are slightly downward sloping, especially those corresponding to the lower L to W ratios. The graphs of a few of the thicker nozzles with L to W ratios exhibit a slight U-shape, the efficiency at first decreasing and then increasing with Mach number. None of these trends is substantial, but each is repeatable with and without the curved flow guide and consistent in its identification with certain geometric characteristics. These observations suggest to us that nozzle efficiency depends far less on jet Mach number than it does on some characteristic Reynolds number.

For the most part, the effect of providing the flow with a constant radius turning surface is negligible, a maximum difference around two percent. At large L to W ratios, or at least large L, since W was held constant at 0.050 in., the effect of the curved surface is debilitating. As the depth L of the nozzle cavity was reduced through the addition of inserts, small changes, if any, occurred. Further

reductions in L reduced the difference between the results obtained with and without the curved surface. The data provides evidence that the turning surface had a favorable effect on the performance of the shallowest cavities.

An explanation for the interplay between the nozzle cavity depth and the turning surface can be found in the streamline pattern established by the fluid in flowing through the nozzle cavity. One would expect the streamline to be smooth curves that are normal to the nozzle inlet and exit planes similar to the ellipses sketched in Figure 66 . While the explicit structure of the flow will surely depend on some Reynolds number, streamlines A-A will describe boundaries between reversed flow separation regions in the corners and the principal streams. Turning through abrupt corners is not efficient, but the streamlines are smooth and their curvatures promote streamwise and transverse pressure gradients that the sidewall boundary layers can apparently tolerate. When the constant radius turning surface is inserted into the offending corner, as shown in the lower drawings of Figure 66 , a combination of events is possible. Since the curvature of streamline A-A and that of the surface substantially differ at the longest cavity depths, the flow again separates. The dividing streamline is BB, and, while its kinks may be exaggerated, they are possible and are shown to illustrate the secondary separation zones that may be provoked by abrupt changes in streamline curvature. This blockage

203
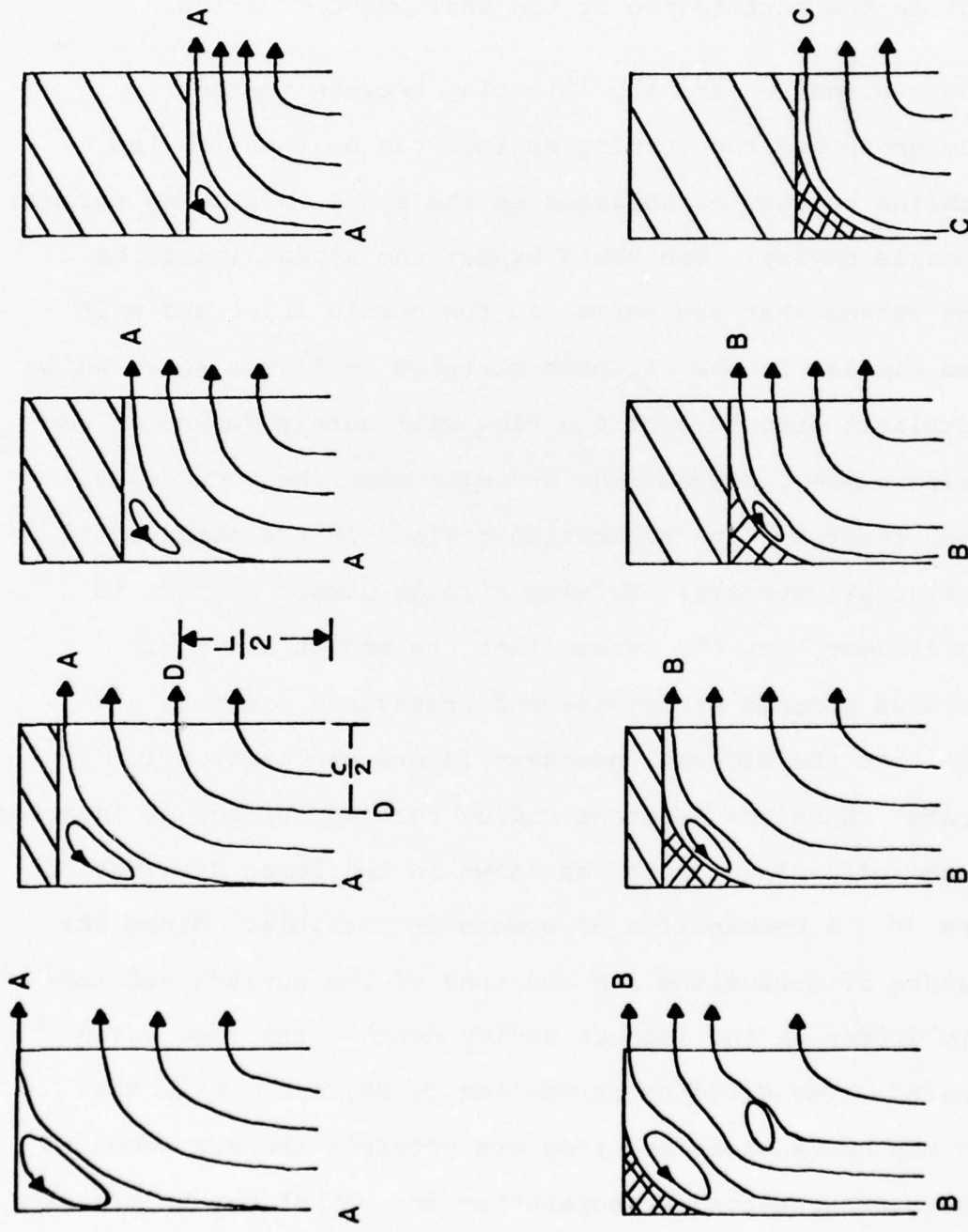
Figure 66. Typical streamline patterns in nozzle blocks with (below) and without (above) turning surface inserts.

causes overvelocities that amplify normal losses due to skin friction and makes the addition of this turning surface worse than none at all. As the depth of the cavity is decreased, the curvature of streamline A-A approaches that of the turning surface so that the separation region becomes smaller and eventually disappears. When inserted into the very shallow cavities, the curved surface turns the flow with relative pressures that are slightly positive and favorable to boundary layers. Velocities are well distributed and friction losses are reduced. In this case the turning surface is a favorable addition to the nozzle block.

In hydraulics, the pressure lost in a turn is normally described by the ratio of the radius of the turn to the radius to the pipe and the Reynolds number of the flow entering the turn. We have insufficient data to undertake a meaningful study along these lines, but such a correlation must certainly include the ratio of the radius of the turning surface to the depth of the cavity and the Reynolds number based on the hydraulic diameter of the nozzle's inlet. The data are sufficient, however, to indicate losses associated with turning the flow within the cavity. The above comments pertaining to a separated flow region suggest that these losses are more akin to those associated with abrupt increases in the area of ducts than they are to those associated with elbows, turns, and bends. The origin of bend losses, it will be remembered, has been tied to a pair of counter rotating

205

streamwise vortices and not to the production of large, transverse vortices similar to those postulated in the present nozzle cavities. These are normally found downstream of rapid expansions in duct size.

If it were not for external constraints, an obvious means of improving the performance of nozzles used in ejectors would consist of providing the nozzles with large internal volumes. In this way internal Mach numbers are kept low, and so too are friction losses. However, the external constraints are real and rigid and tend to compress an ejector's nozzles into flat profiles of low volume. The cross sectional area of the nozzle and the area of the inlet to the nozzle cavity are good measures of the flatness of the nozzle. The effect of the inlet area on the efficiency of our nozzles at four representative pressures can be seen in Figures 116 through 145 in reference 17. These results clearly express the need to design the nozzle's inlet area larger than the jet slot area by a factor of 3, at least, for the efficiency falls sharply at lower values. There also appears to be little incentive for increasing the area ratio above 5, for thereafter the curves are relatively flat, having attained a maximum value determined by other factors.

While data were obtained across a range of area ratio between 1.4 and 20, no one nozzle was tested across the entire span. We arbitrarily selected the 1.00 x 4 for testing across an expanded range of area ratios. To this end, the width

206

of the jet slot was machined somewhat wider than its pre-
vious 0.05 in. and then tested at 2.0 psig. These data
can be found in Figure 67 and again in Figure 68, where they
have been plotted along with the data from the original 1.00
x 4 nozzle. The trend is the same as that discussed earlier.

The 0.375 x 4 nozzle was also tested across an expanded
range of area ratio. In contrast, this was accomplished by
further reducing the depth of the nozzle's cavity with addi-
tional inserts. These results, also at 2 psig, are presented
in Figure 69 and show the expected trend.

The nozzle blocks had been fabricated and assembled very
carefully, and their internal surfaces were quite smooth.
We expected to measure thrust efficiencies of 95% or greater.
The initial results of 85 to 90% were therefore greeted with
alarm and caused us to rerun and recalculate the early ex-
periments many times, but there were no substantial changes.
The problem was finally traced to a suction pressure on the
base of the nozzle block, the term in square brackets in
Eq. (13). The flow survey discussed in the following indicated
that the jet was rather uniformly distributed across the
length of the jet (Figure 73), which implied $\beta \approx 1.0$.
To estimate α, base pressure coefficient, six small holes
were slant-drilled into the base of a nozzle block on a line
that bisected the length of the jet slot. Measurements of the
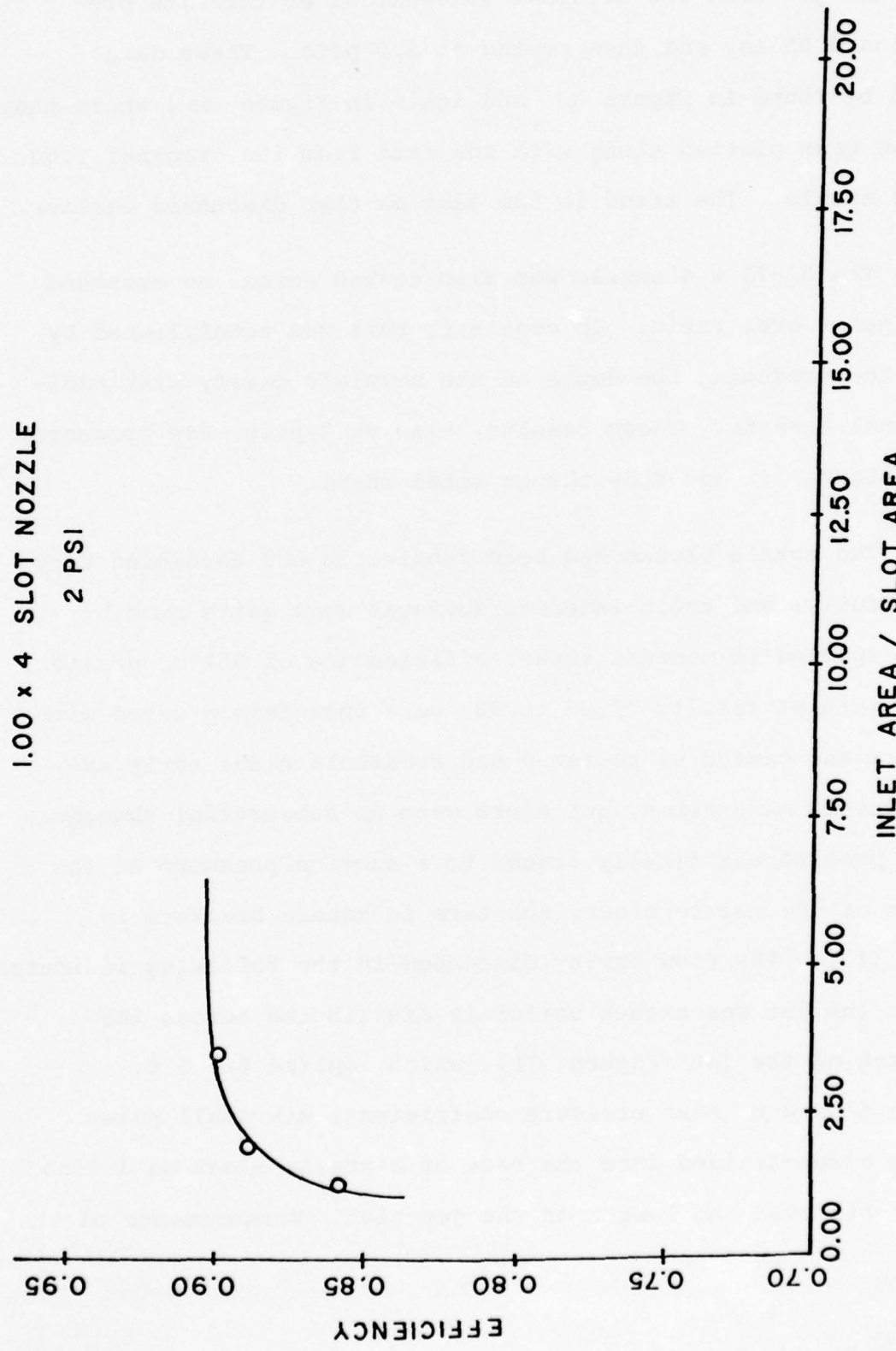
Figure 67. Efficiency as a function of area ratio for 1.00 x 4 Nozzle where exit area is varied by changing slot width.

208

1.00 x 4 SLOT NOZZLE
2 PSI

0.95 0.90 0.85 0.80 0.75 0.70

EFFICIENCY

0.00 2.50 5.00 7.50 10.00 12.50 15.50 17.50 20.00

INLET AREA / SLOT AREA
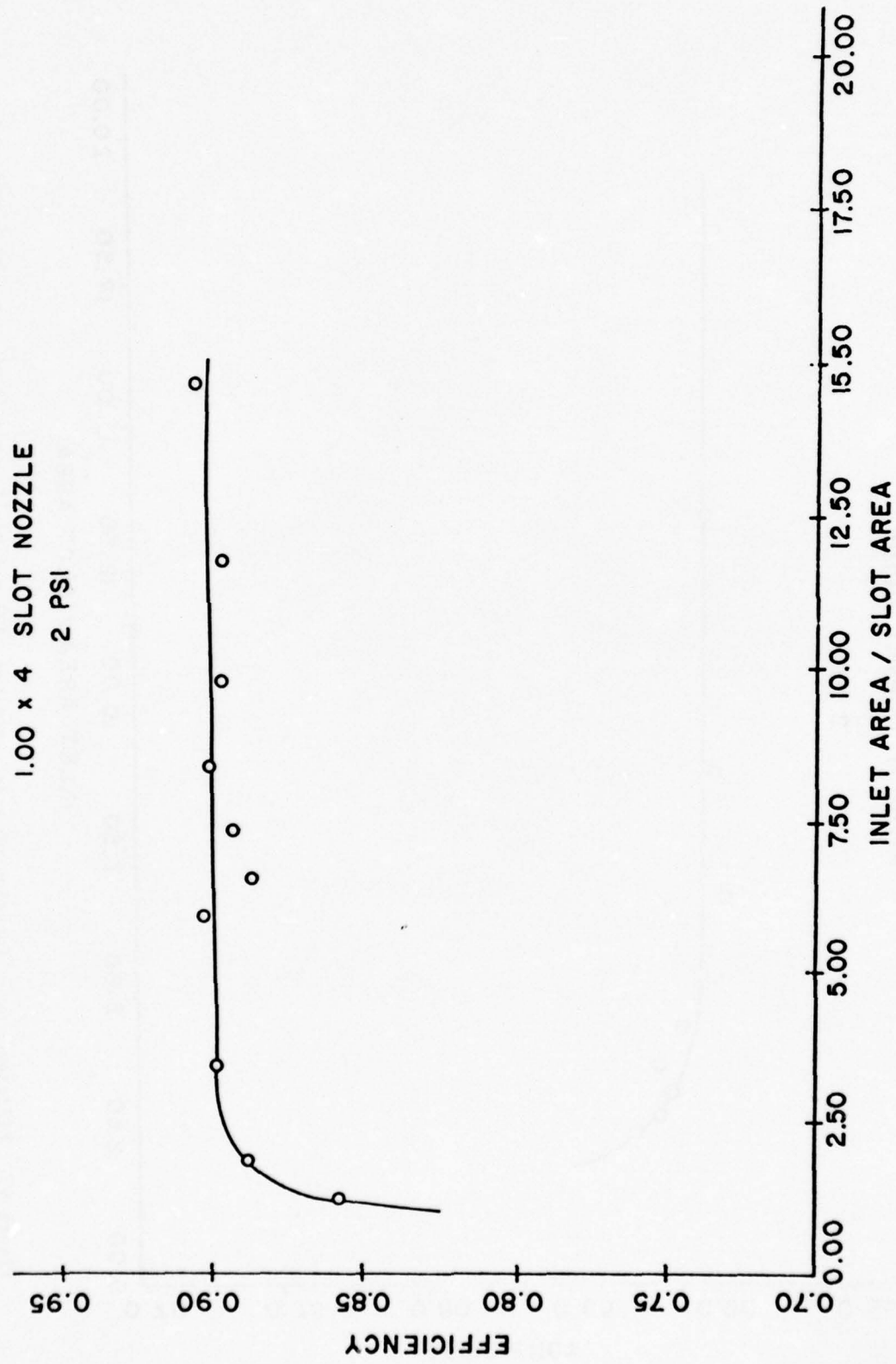
Figure 68. Extension of data shown in Figure 67.

209
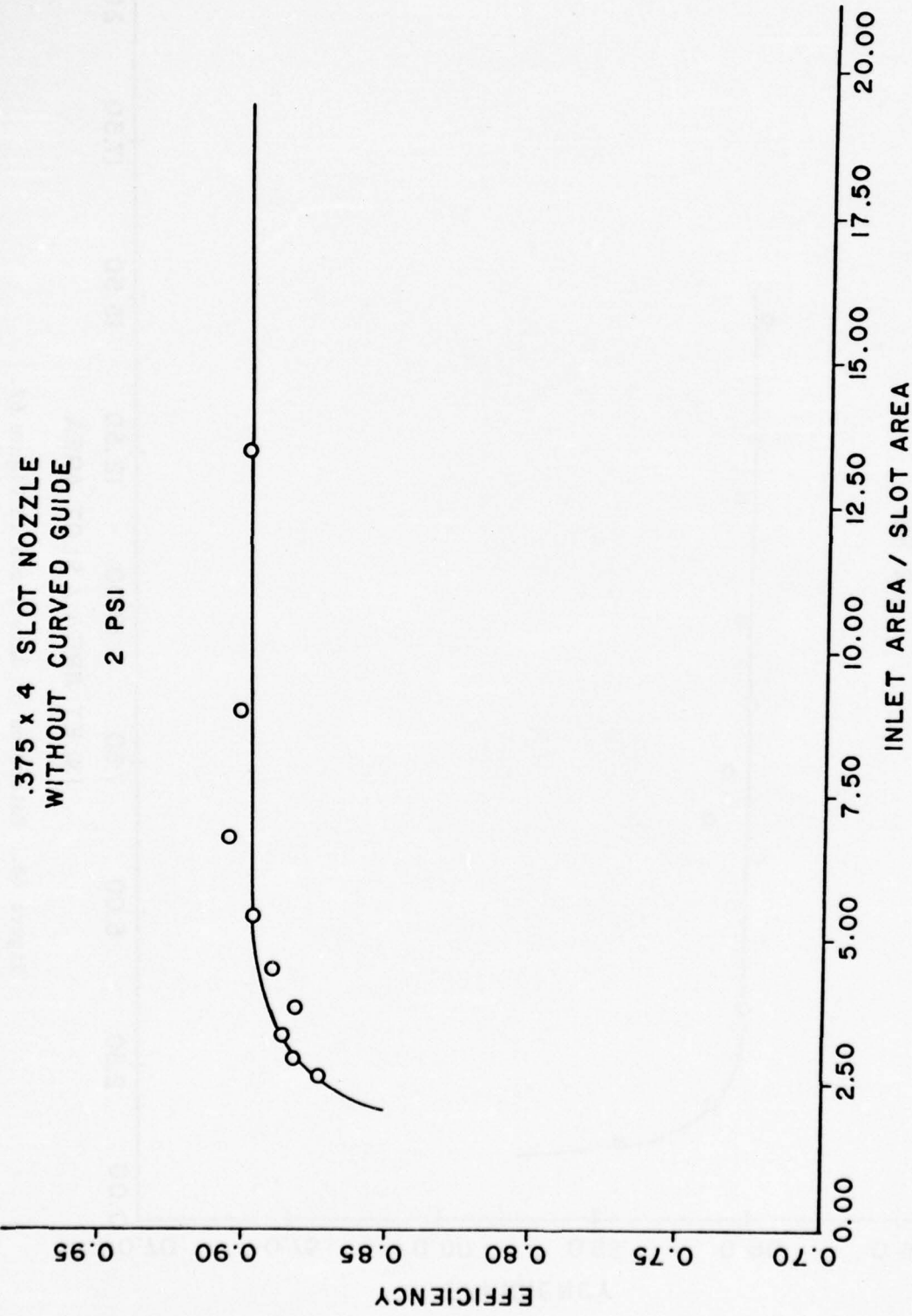
Figure 69. Efficiency as a function of area ratio for .375 x 4 Nozzle where L/W varies from 20 to 200.

six base pressures were made at nozzle total pressures between
1 and 10 psig. Their mean values are plotted in Figure 70
and suggest α = .00212, a number that would ordinarily
be negligibly small. In Eq. (13), however, it multiplies
a very large number. With A_B/A_j = 40, the effect of base
pressure on thrust efficiency becomes:

$$\left[\beta - \frac{1}{2} \alpha \left(1 + \frac{A_B}{A_j} \right) \right] = 1 - \frac{0.00212}{2} \quad (41)$$
$$\simeq .956$$

which accounts for the alarming additional 5% reduction in η.

In what follows it is convenient to square Eq. (13),
use the measured value of $\hat{d}$, and assume $\delta - \alpha \simeq 0$, a reasonable
assumption for given x and the uniformity of the flow. There
follows

$$\eta^2 = .914 \left[1 - \xi \left(\frac{V_c}{V_i} \right)^2 \right] \quad (26)$$

and we inquire into the relationship between $\xi (V_c/V_i)^2$
and the geometry of a given nozzle. The ratio V_c/V_i cannot
be determined explicitly but can be estimated through the
incompressible continuity relation by assuming that the
characteristic flow area is proportional to the entering

211
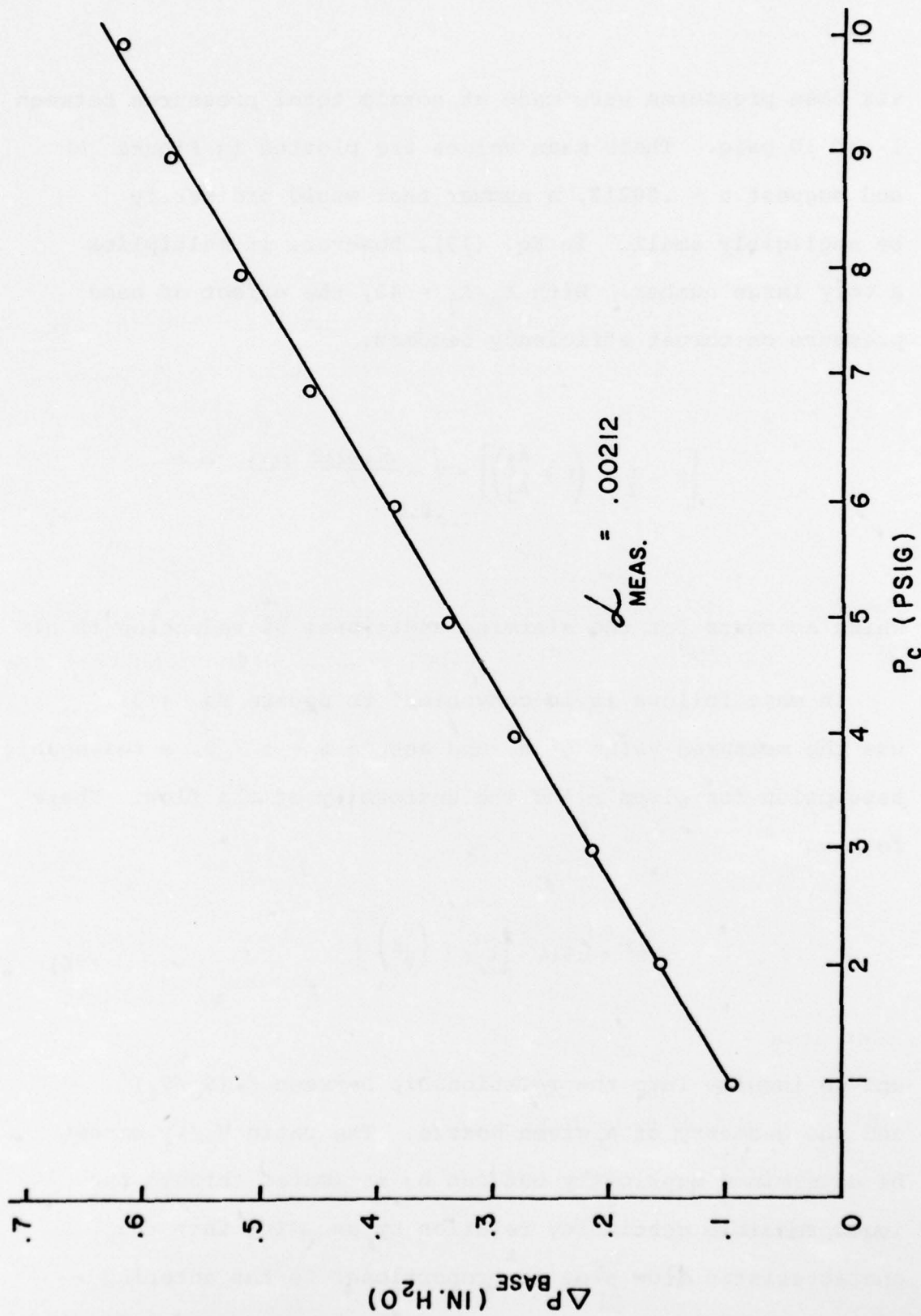
Figure 70. Baseline pressure ratio for .375 x 3 Nozzle.

flow area.   This gives

$$V_c/V_1 = A_j/A_c$$
$$\sim A_j/A_{FLOW} = 1/\mathcal{R} \tag{27}$$

The earlier discussion suggested that at least two factors, friction and turning, contribute to the pressure drop term. We therefore write

$$\xi = \xi_f + \xi_T \tag{28}$$

and admit that our experience permits us only to estimate ξ_f. For this purpose we define characteristic dimensions that are proportional to their counterparts at the entrance to the nozzle cavity:

Flow Area -

$$A_F = t^2 \left(\frac{c}{t} - 1.040 \right)$$

Jet Area -

$$A_j = .05(10-h) = .05 \, L$$

Area Ratio -

$$\mathcal{R} = \frac{A_F}{A_j}$$

Flow Perimeter -

$$\chi = 2C + t \left(\frac{\pi}{2} - 1 + \frac{1}{\sin 15°} - \frac{1}{\tan 15°} \right)$$

$$= 2C + .702 \, t$$

Hydraulic Diameter -

$$D_H = 4 \, A_F / \chi$$

Flow Reynolds Number -

$$Re_F = \left(\frac{\rho \, V}{\mu} \right)_{JET} \frac{D_H}{12 \, AR}$$

Characteristic Length -

$$L_c = .554 \sqrt{C^2 + L^2}$$

which is the length of the elliptical streamline D-D sketched
in Figure 66. Experimental studies of duct flows suggest

$$\xi_f \sim f \frac{L_c}{D_H} \tag{29}$$

where f is a friction factor. In our experiments $9 \times 10^3 < Re_F <
7.2 \times 10^4$, so that the Blasius friction factor formula for
turbulent flow seems appropriate, i.e.,

$$f = .316 \, Re_F^{-1/4} \tag{30}$$

It was found convenient to define a function

$$F = \frac{4}{AR^2} \frac{.316}{Re_F^{1/4}} \frac{L_c}{D_H}$$

from which

$$\xi_f = k \frac{.316}{Re_F^{1/4}} \frac{L_c}{D_H}$$

where k is a proportionality constant. Equation (26) there-fore becomes

$$\eta^2 = .914 \left[1 - \frac{k}{4} F - \frac{1}{AR^2} \xi_T \right] \tag{31}$$

We have arbitratily selected data taken at $p_o = 1.5$ and 5.0 psig for presentation in Figure 71 , where η^2 has been plotted against F. The remaining data were deleted for the sake of clarity. This figure clearly delineates the three factors that reduced the performance of our nozzles: base pressure, friction losses, and turning losses. These data suggest the proportionality constant k = 1.76, approximately, and also suggest that ξ_T/AR^2 attains a limiting value of 0.131 as F exceeds a value of around 0.04. The data points containing small crosses were all obtained with the same nozzle, T x C = 0.25 x 5. Their departure from the pattern of the remaining nozzles cannot be explained at this time.

215

$$F = \frac{4}{AR^2} \cdot \frac{316}{Re_F^{1/4}} \cdot \frac{L_c}{D_H}$$

UPPER LIMIT DUE TO BASE PRESSURE

EQN (31)

$k = 1.76$

$\frac{\xi}{AR} = 0$

TURNING LOSS

η^2

P_o (PSIG)

⊙ — 1.5

△ — 5
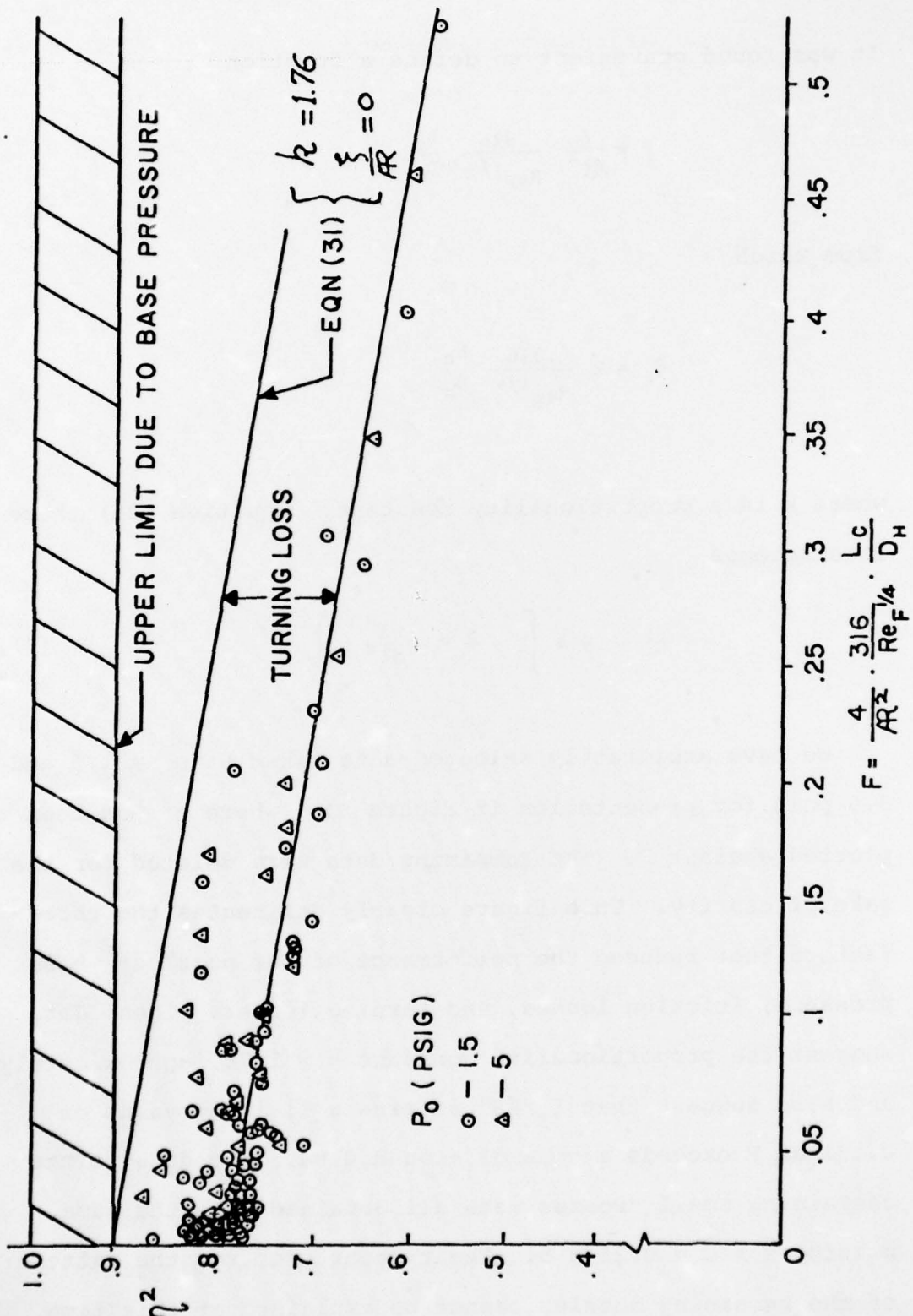
Figure 71. Effect of base pressure, friction, and turning losses.

We hasten to remind the reader that the turning losses discussed in the paragraphs above occur because the flow decelerates as it passes into the cavity of the nozzle. Properly designed nozzles, those whose geometries monotonically accelerate the flow from inlet to exit, would not experience losses of this kind. The nozzles used in the ejector experiments of Reference 14 also turned the flow, but proper area scheduling insured thrust efficiencies greater than 95%.

H.   Nozzle Flow Field

A study of the axis velocity decay rate of 3-D jets leads to the conclusion that the jet can be represented by three relatively distinct regions. The first of these, the potential core, is the region immediately downstream of the nozzle in which the axis velocity has not yet felt the effect of mixing on the boundaries of the jet. The exit velocity remains nearly constant at a value equal to the exit velocity throughout this core.

Once the axis velocity is affected by the boundaries' mixing, a region of decay occurs that is directly dependent upon the exact geometry of the nozzle and has been thus termed the characteristic decay region.

Far downstream of the nozzle all jets tend to exhibit a decay rate typical of an axisymmetric jet. As a result, the third and final region has been labeled the axisymmetric decay region.

217

Velocity profiles were taken in the jets of two of the slot nozzles mentioned in this study (0.375 x 3 and 0.550 x 4) at stations 0.5, 1.2, 3, and 4 cm. downstream of the nozzle exit. The nozzle and jet coordinate system is shown in Figure 72 . Representative profiles of local velocity in the X-Z plane, nondimensionalized by calculated exit velocity, are shown in Figure 73 with x = 0.5, 1, 2, 3, 4 cm consecutively. The profiles are uniform at a velocity close to that of the nozzle exit. The axis velocity decay of the 0.500 inch x 4 inch nozzle is compared with Trentacoste and Sforza's (Reference 18) result in Figure 74 , which shows a near agreement.

Immediately downstream of the potential core and within the characteristic decay region, the velocity profiles become somewhat axisymmetric. This condition persists, as Figure 74 shows, until the end of the characteristic decay region is reached, approximately 25 cm downstream of the nozzle exit. At this point, the flow profiles become axisymmetric in nature.

Profiles taken of the X-Y plane, parallel to the minor axis of the jet at x = 1, 2, 3, and 4 cm., are shown in Figure 75 . The potential core extends approximately x = 1 cm., beyond which the centerline velocity begins to decay. These profiles apparently are similar and representative of two-dimensional free jet profiles.
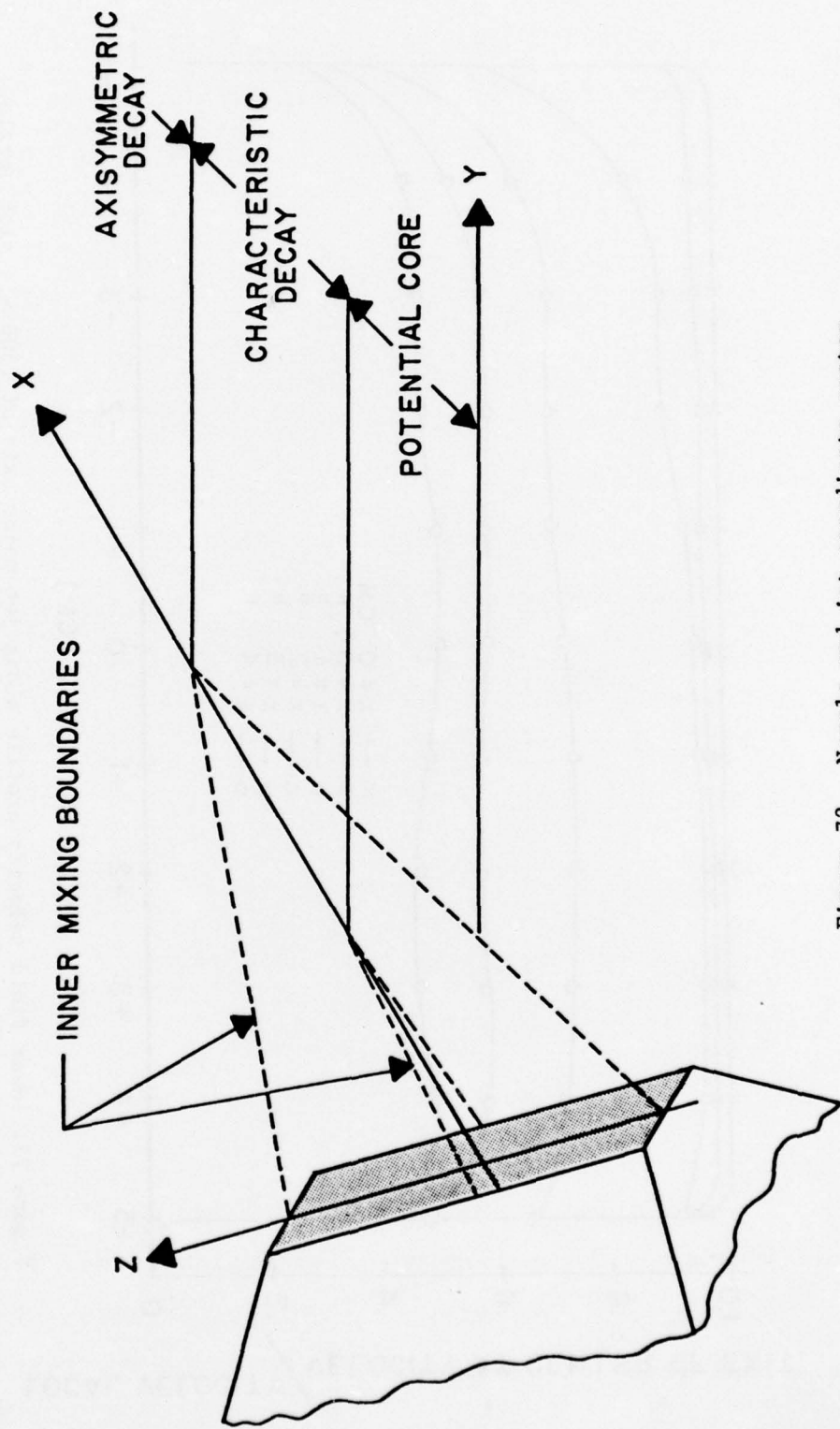
Figure 72. Nozzle and jet coordinate system.
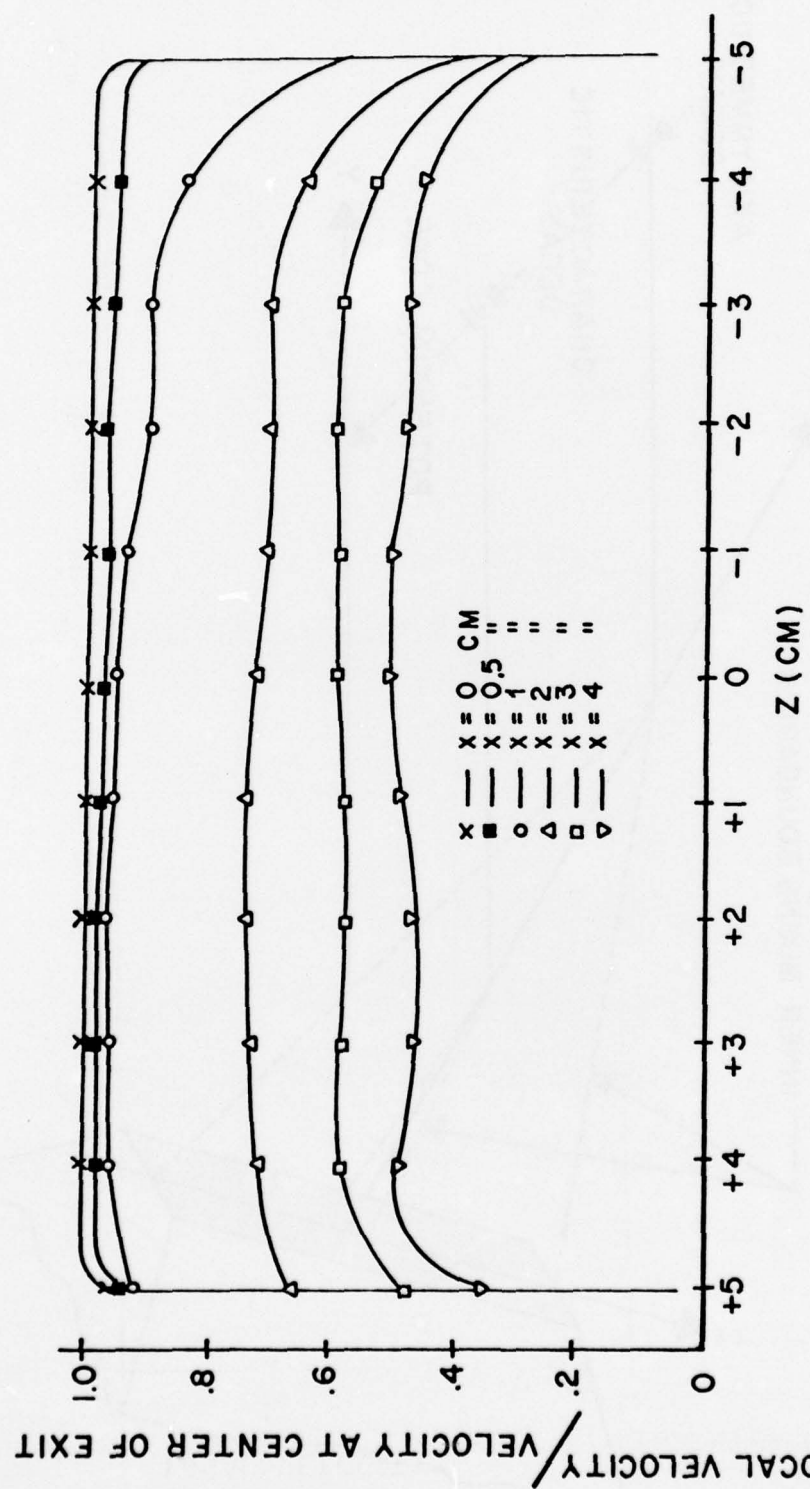
Figure 73. Near field velocity profile along jet major axis of .500 x 4 slot nozzle.

220
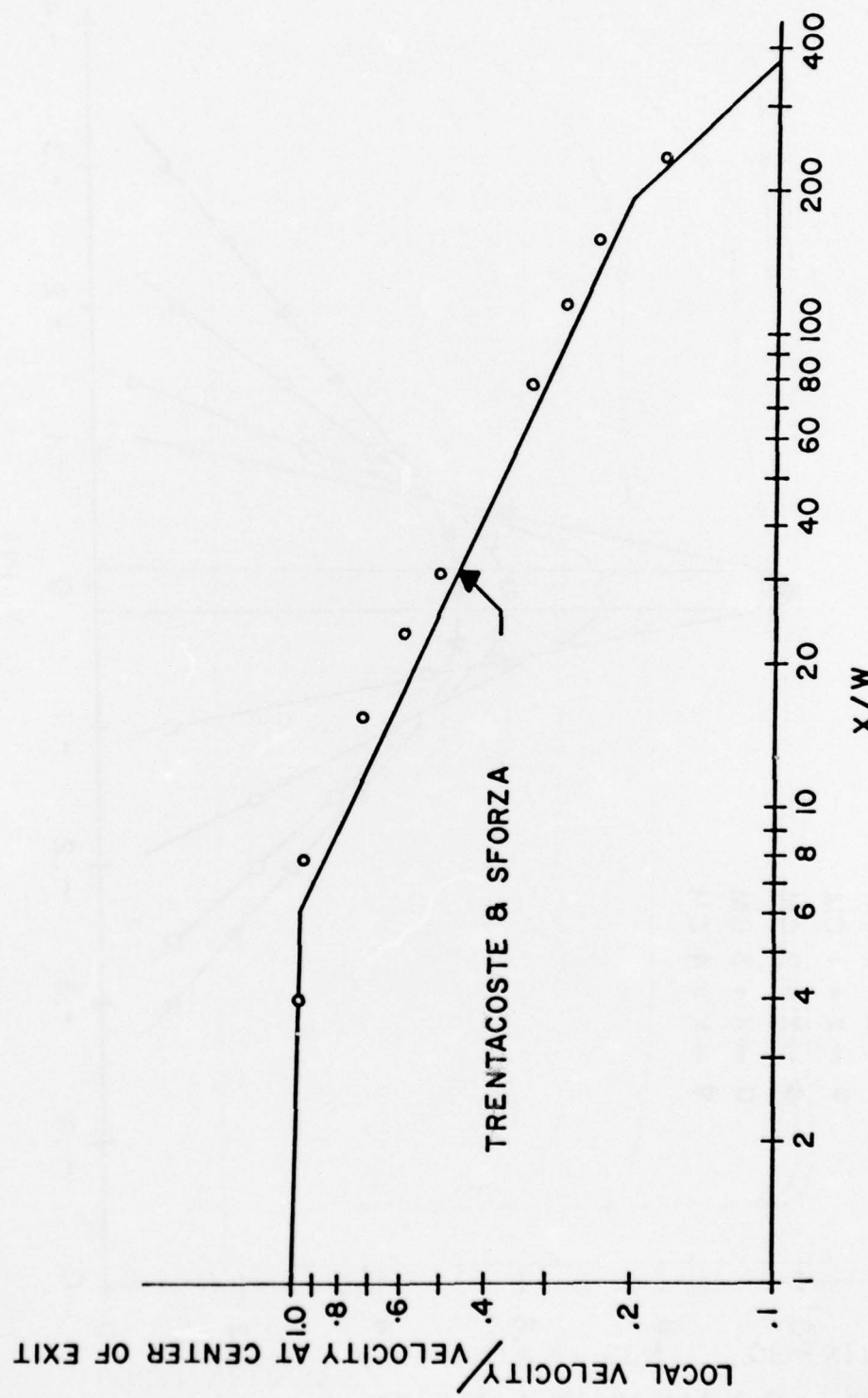
Figure 74. Axis velocity decay of 0.500 x 4 slot nozzle.
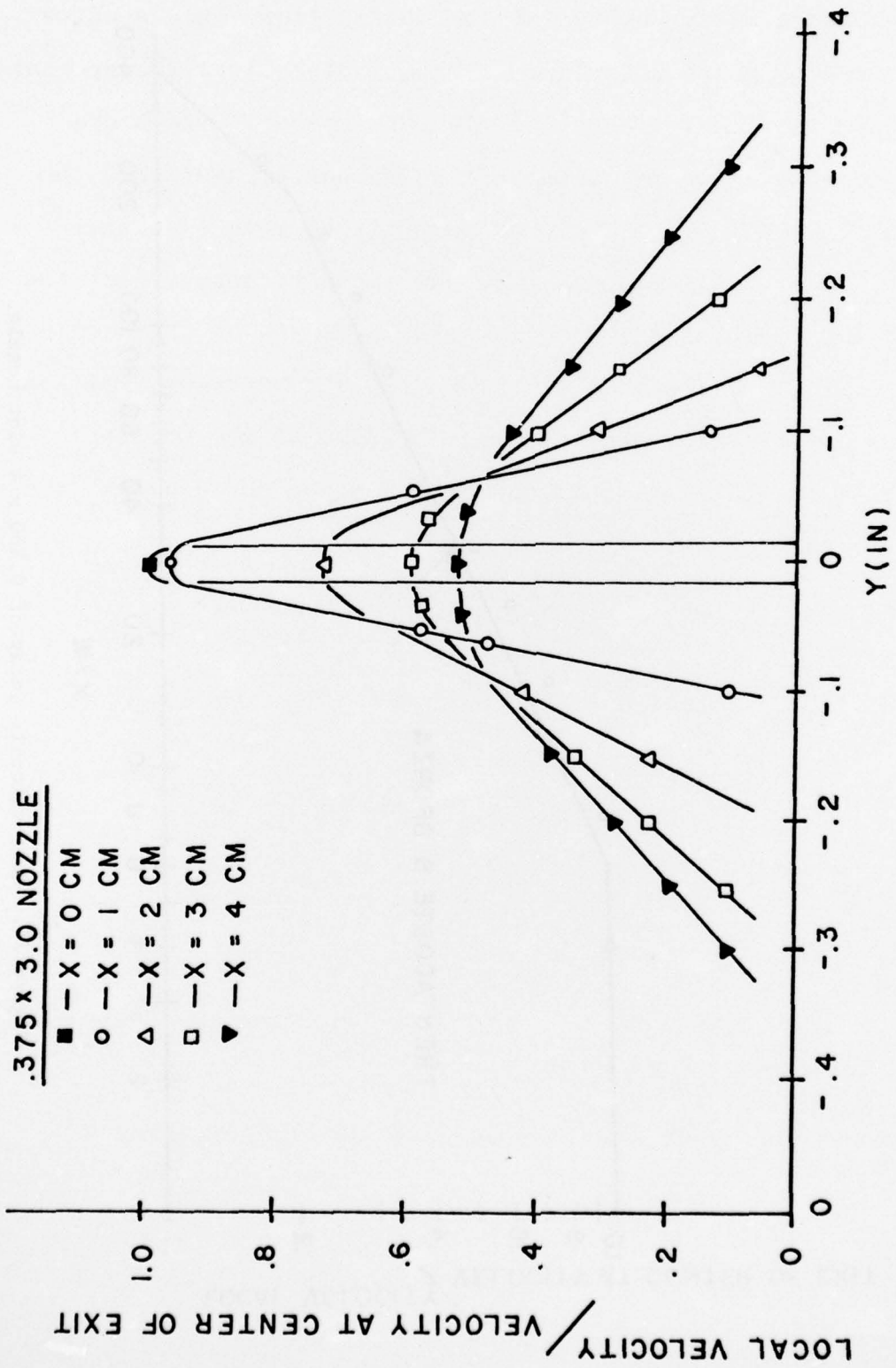
Figure 75. Near field velocity profile along jet minor axis.

Pressure measurements for the nozzle flow field studies were made by using a Kiel probe (that automatically compensated for some variance, if any, of flow direction). The probe was attached to an X-Y transversing mechanism that held the probe firmly in place while allowing it to move in either the X, Y, or Z direction. Care was taken to assure that the probe was positioned correctly. Measurements of the nozzle flow field were taken as the probe moved downstream from the exit slot, as the probe moved up the face of the nozzle centered on the exit slot, and as the probe moved across the face of the nozzle.

REFERENCES

1. Lawson, M. O., "Performance Characteristics of Electrofluid Dynamic Energy Conversion Processes Employing Viscous Coupling," 6th AGARD Combustion and Propulsion Colloquium, Canes; ARL Report 64-73, October 1964, Aerospace Research Laboratories (AGARDograph 81, pp. 539-630).

2. Lawson, M. O., Fretter, E. F., and Griffith, R. W., "Report on Progress in Achieving Direct Conversion of a Major Fraction of Sonic Flow Kinetic Power into Electric Power by Electrofluid Dynamic (EFD) Processes," 9th Intersociety Energy Conversion Engineering Conference, San Francisco, Cal., August 26-30, 1974.

3. Willke, T., and Fretter, E. F., "Description of High Pressure Electrofluid Dynamic Generator," ARL Report 71-0245, Aerospace Research Laboratories, Wright-Patterson AFB, Ohio, October 1971.

4. Huberman, M., et al., "Study on Electrofluid Dynamic Power Generation," Interim Report 23 April 1973 to 22 April 1974, ARL Report 74-0119, Aerospace Research Laboratories, Wright-Patterson AFB, Ohio, October 1974.

5. Fretter, E. F., and Minardi, J., "Effect of Sloped Electrodes on P Times D Parameter for EFD Generators," Report to be published in 1976.

6. Huberman, M., et al., "Study on Electrofluid Dynamic Power Generation," Interim Report 25 April 1974 to 25 April 1975, ARL Report 75-0200, Aerospace Research Laboratories, Wright-Patterson AFB, Ohio, October 1975.

7. Lawson, M. O., "Injector Generator Matching Characteristics," Lecture presented at TRW, Systems, Redondo Beach, Calif., September 11, 1975.

8. Turman, B., "Temperature Dependence of Particulate Erosion," ARL TR 74-0176, Aerospace Research Laboratories, Wright-Patterson AFB, Ohio, December 1974.

9. Johnson, E. G. and Von Ohain, J. P., "Generation of Ultra High Total Enthalph Gases through Multicomponent Flow Techniques", AIAA 10th Aerospace Sciences Meeting, Paper 72-167, ARL 72-1000, as NTIS NO. N72-26247, 1972.

10. Hasinger, Siegfried, "Performance Characteristics of Ejector Devices", ARL TR-75-0205, Final report April 1973-January 1975, Aerospace Research Laboratories, Wright-Patterson AFB, Ohio, 1975.

11. Howard, J. M. and Hasinger, S. H., "Diffusion Characteristics of Large L/D Radial Outflow Nozzle Systems," Laser Digest, AFWL TR-75-229, Air Force Weapons Laboratory, Kirtland AFB, New Mexico, October 1975.

12. Hasinger, S. H. and Miller, D. K., "Two-Dimensional Supersonic Diffuser Experiments", AIAA Journal, Vol. 13, No. 4, pp. 536-538, April 1975

13. Quinn, B., Eastlake, C. N., and Fancher, R. B., "Description of a Nozzle Test Facility", Aerospace Research Laboratories Report, ARL 70-0140, August 1970.

14. Quinn, B., "Compact Ejector Thrust Augmentation", _Journal of Aircraft_, Vol. 10, No. 8, August 1973.

15. Quinn, B., "Experiments with Hypermixing Nozzles in an Area Ration 23 Ejector", Aerospace Research Laboratories Report, ARL 72-0084, AD 752 207, June 1972.

16. Fancher, R. B., "The Performance Characteristics of the 7/10's Nozzles in the Five Foot Single Channel Vertical Ejector", Aerospace Research Laboratories Report, ARL 71-0236, October 1971

17. Quinn, B. and Joshi, K. K., "The Thrust Performance and Losses of a Family of Nozzles, Aerospace Research Laboratories Report, ARL 75-0018, February 1975.

18. Trentacoste, N. and Sforza, P. M., "Further Experimental Results for Three-Dimensional Free Jets", _AIAA Journal_, Vol. 5, May 1967.